NAME	ADDRESS AND AFFILIATION	DATE

ProQuest LLC.
789 East Eisenhower Parkway
P.O. Box 1346
Ann Arbor, MI 48106 – 1346

FACULTY OF ENGINEERING

UNIVERSITY OF GLASGOW

"SUCTION CONDITION: ITS EFFECT ON REFRIGERATION COMPRESSOR PERFORMANCE"

A Thesis presented for

The Degree of Doctor of Philosophy

by

JAMES BROWN, B.Sc., A.R.T.C.

November, 1963.

ABSTRACT

This investigation was carried out to determine the relative importance of the factors affecting volumetric efficiency during the transition from "dry" to "wet" compression when the refrigerant is Freon 12 and the compressor is running at a high speed.

Experimental techniques were developed to measure piston leakage and fluctuating cylinder wall temperatures.

The development of an electrical analogue and a rotating-drum photoformer is described.

This analogue was used to calculate the cyclical heat flow between the cylinder wall and the charge. In addition the performance of non-uniform ladder networks was investigated and the analogue was adapted for various other calculations. These were,

(a) To determine the suitability of thermocouple elements with dissimilar thermal properties to the body whose temperature is being measured.

(b) To determine the effect of irregularities at the thermocouple junction. This took the form of a small "fin" or "lips" on the thermocouple wire, represented by a 2-dimensional network. The investigation showed that when measuring fluctuating temperatures, large errors could be caused by such a "lip" indicating the unsuitability of peening for such purposes.

(c) To investigate the heat transfer between droplets of liquid and an environment of its own vapour when undergoing compression and re-expansion. The effect on volumetric efficiency of the retention of liquid in the cylinder is calculated.

It is concluded that the most important process involved is cyclical heat transfer due to alternate condensation and re-evaporation/

re-evaporation when the cylinder wall temperature falls below the maximum saturation temperature of the vapour. It is shown that "flashing" of entrained liquid has little effect on performance, but that evaporation of this entrainment from the cylinder wall could cause rapid lowering of the cylinder wall temperature.

It is also concluded that liquid deposited on the cylinder walls reduces the rate of condensation on the walls and subsequent re-evaporation.

Piston leakage is shown to have little effect on the performance of the compressor during the change from "wet" to "dry" compression.

SECTION INDEX

(Including certain sub-titles)

SECTION INDEX

(Including certain sub-titles)

APPENDICES

"NOMENCLATURE" prefaces the separate binding of Figures and Graphs.

LIST OF FIGURES & GRAPHS

LIST OF FIGURES & GRAPHS contd.

LIST OF FIGURES & GRAPHS contd.

LIST OF FIGURES & GRAPHS contd.

LIST OF FIGURES & GRAPHS contd.

REVIEW

Work on the cylinder processes involved in a refrigeration compressor was put on a scientific basis by Wirth (35) who carried out a series of tests on an ammonia plant with a view to determining the effect of cylinder wall temperature on the compressor performance. As a result of these researches, he concluded that the drop in volumetric efficiency as the suction superheat was reduced was due to condensation on the cylinder walls during delivery and re-expansion during suction.

Such condensation could occur when the temperature of the cylinder walls or piston crown fell below the saturation vapour temperature at any point of the cycle.

Unfortunately, these experiments did not extend into the wet suction field.

The schematic diagram of fig. 1 is based on Wirth's curves and shows the cylinder processes during one cycle. The curves shown are gas and wall temperatures, exposed surface area and gas temperature and exposed surface area x wall temperature. Heat transfer is caused by the difference between wall and gas temperatures and it will be seen that heat will be given by the gas to the wall during the latter part of the compression delivery and the beginning of re-expansion.

During the remainder of re-expansion and suction, heat is given up to the gas. The amounts of the heat exchange are proportional to the ordinate between curves (3) and (4). This assumes a constant coefficient of heat transfer.

The next experimental investigation was by Smith (29) who devised a liquid flow-meter to measure the mass flow of refrigerant in the circuit. The compressor was a single cylinder unit 4" bore x 6" stroke using ammonia as refrigerant.

The/

The condition at compressor suction was varied from about 0.55 dry to approximately 10°F. superheat by adjustment of the temperature of the brine surrounding the evaporator coils. The flowmeter is shown in fig. 2 and consisted of a cylindrical chamber in which a heating element was enclosed, with provision for measuring temperature rise of the liquid refrigerant by means of copper constantan thermocouples. Heat barriers were provided on each side of the temperature measuring stations to prevent conduction along the pipes. The entire unit was thoroughly lagged to prevent a loss to atmosphere, although the sub-cooled liquid was at a temperature very close to ambient. The check between evaporator mass flow and liquid flow-meter quantity showed agreement within 1%. The circuit diagram of the apparatus is shown in fig. 3 .

The results of this work are shown in the curves of fig. 6 which shows refrigerating effect and coefficients of performance on a basis of dryness fraction. The dryness fraction is derived from the expression -

$$x = \frac{h_x - h_f}{h_g - h_f}$$

where h_x = enthalpy at point under consideration.

h_g = enthalpy at saturation temperature.

h_f = enthalpy of liquid at saturation temperature.

This term was applied even in the superheat field to give a consistent basis on which to plot the results.

These/

These figures show a considerable rise in C.O.P. and R.E. between dryness values of 0.82 and 0.95. No suitable mechanism was fitted to the compressor so that indicated values are not available.

The reason for this substantial rise in efficiency was given as being due to liquid droplets entrained in the suction vapour being unevaporated, or condensation taking place during compression. This "flashed" into vapour during re-expansion thereby reducing the volume of vapour drawn in during suction. Such flashing should be visible on the indicator diagram as a reduction in the index of re-expansion.

Giffen and Newley (13) carried out an investigation, also on an ammonia machine and varied the dryness fraction from about 0.75 dry at suction to 40°F.S.

The flowmeter used by these investigators followed the same general plan as Smith's, but use was made of Beckman thermometers for measurement of temperature rise. The indicator mechanism used by Giffen and Newley was modified from the well-known "Farnborough" design. Instead of a floating diaphragm operating the spark assembly, a light diaphragm clamped around its periphery made or broke contact with a tungsten electrode as the pressure equalised on each side of the diaphragm. The need for clamping the diaphragm will be evident since leakage of air or nitrogen into the circuit must be avoided. The modified pressure unit is shown in fig. 5 .

The rise in performance shown by the curves of fig. 6 is at a higher dryness fraction than determined by Smith. The reason for this difference is due probably to the fact that Smith's figures are based on the evaporator outlet condition while Giffen and Newley estimated the condition at the suction manifold.

A rise in actual volumetric efficiency of 20% was accompanied/

accompanied by a rise in indicated volumetric efficiency of only 5% so that it was assumed that flashing during re-expansion did not in fact account for the entire phenonenon.

The conclusions reached indicated that the reduction in the aspirated volume was caused by re-evaporation during suction of liquid condensed on the walls of the cylinder during compression.

This is in agreement with Wirth's findings.

In a paper by Fuchs, Hoffman and Plank (11) the leakage losses in an ammonia machine were investigated. These tests were carried out using air as working fluid and obtaining the corresponding leakage with ammonia by assuming laminar flow.

It is remarked that no clear dependence on pressure ratio is evident and that leakage is increased at low running speeds. The level of oil in the crankcase was shown to affect results by ±15%.

W.B. Gosney (14) also remarks on the increase in leakage past the piston and valves in a stationary machine over that of a machine while running. During this investigation, a short series of tests showed a depression of the index of re-expansion when the suction vapour was allowed to become wet. This indicates the presence of evaporating liquid during the re-expansion process.

The heat transfer in internal combustion engine cylinders has been considerably investigated. The most important contributions are those of Eichelberg and Elser (9;10) who used sub-surface thermocouples, followed by Oguri (22) who used a true surface thermocouple to measure the heat transfer to the piston of a four stroke spark ignition engine. The work of Overbye et al (23) is notable for the use of a true surface thermocouple of the type developed by Bendersky and similar to that used in the present investigation.

Overbye discovered that there was considerable difficulty in determining/

determining an instantaneous heat transfer rate due to an apparent phase lag between the time when the wall temperature is equal to the gas temperature in the cylinder and the time when the temperature gradient or heat flux is zero. This he attributes to the heat capacity of the fluid. The conditions in the dynamic state existing in the cylinder are probably quite different to those in a steady or a quasi-steady state. The use of the Nusselt equation for instantaneous heat transfer is therefore rather suspect.

In attempting to analyse the process, Overbye considered two models, one of which assumes a mean heat transfer coefficient. Each sinusoidal component of the temperature waveform of the gas produces a surface temperature waveform on the metal, lagging by about 45° for relatively low values of heat transfer coefficient.

Overbye rejects this model as being too idealised and a further model allows for varying heat transfer coefficients and includes with various simplifications, the effects of thermal capacity in the fluid. He arrived at the conclusion that the temperature fluctuations at the surface of the metal should be similar to and in phase with the temperature of the gas at some distance from the surface.

INTRODUCTION

The problem of the effect of suction condition on the performance of refrigeration compressors is akin to the "Missing Quantity" in steam engine practice. The "Missing Quantity" was assumed to be caused by condensation on the cylinder walls during the first part of the stroke and re-evaporation during the latter part of the stroke.

Investigations by Callendar, Nicolson and Mellanby (7) on slow running steam engines revealed heat transfer coefficients of the order of 12,000 BThU/hr.ft.^{2}.°f . during the condensation process. Such coefficients are generally only attained during dropwise condensation and the presence of this mode of condensation in a refrigerating compressor cylinder could cause the remarkable reduction in performance obtained under wet suction operation.

Comparison of theoretical Coefficients of Performance for ammonia and Freon 12 is interesting in that deviation from the reversed Carnot Cycle has less effect on Coefficients of Performance when using F.12 than when using ammonia, due to the lower temperatures at the end of compression. Fig. 7 illustrates this for working limits of 5°F. and 100°F. with the suction condition varied between 0.8 dry and 100° F.S.

The curves are based on 10°F. sub-cooling at condenser outlet, isenthalpic expansion and isentropic compression.

It will be observed that while the C.O.P. for ammonia passes through a maximum value at 0.87 dry, the curve for Freon 12 does not attain a maximum value within the range of the graph.

Although this shows the cycle efficiency to be slightly greater when suction vapour is superheated, the increase in volumetric efficiency of the compressor between wet and dry compression is considerable. Added to the above theoretical increase in C.O.P. this makes the addition of suction line heat exchangers to plants operating on halogenated refrigerants economically worth while.

Exhaustive/

Exhaustive tests on the performance of ammonia compressors in the wet and superheated suction condition have been carried out but little work has been done in this field on small Freon 12 machines. The processes are likely to be very different due to the mutual solubility of Freon 12 with lubricating oil.

It has been shown by McLaren (20) that the suction and discharge valves have little effect on the performance of the compressor over a wide range of operating conditions and the field of investigation has been confined to effects solely engendered by the transition from wet to superheated suction vapour.

Such effects must include actual and indicated volumetric efficiency, cyclical heat transfer and piston leakage.

The use of small domestic compressors for the investigation presented certain problems with regard to size and speed of rotation but the convenient size of these machines for laboratory use, and the lack of experimental data on such machines made this choice desirable.

SECTION 3.

GENERAL OBJECTS OF INVESTIGATION

Due to the widely different characteristics of Freon and ammonia, it appeared that investigations on the lines adopted by Giffen and Newley, but including measurement of the cyclical heat transfer, would yield useful information if carried out on a modern high-speed Freon 12 plant.

To cover as wide a range of operating conditions as possible, a variable speed D.C. motor-driven compressor was chosen, of small size so that ancillary test equipment could be easily manufactured and accommodated.

Since indication of such a small compressor running at speeds in excess of 1000 r.p.m. presented some difficulty, the opportunity was taken of first testing the compressor running on air to develop the indicator mechanism.

Hence the experimental work was carried out with the following objects in view:-

(a) The development of a suitable indicator mechanism.
(b) Development of a Freon 12 test unit suitable for measurement of small mass flows under wet suction conditions.
(c) Measurement of cyclical wall temperature fluctuation.
(d) Measurement of leakage past the piston of the compressor.
(e) Correlation of test results to ascertain the processes involved during wet suction.

SECTION 4.

DESCRIPTION OF APPARATUS

Fig. 8 shows the line diagram of the refrigerant circuit. This will be seen to comprise:- compressor, oil separator, condenser, drier, receiver, precooler, flowmeter and secondary evaporator. The various components are now described in detail.

Compressor and Motor

The compressor is 1" stroke x 1½" bore, single cylinder compressor built by Messrs. L. Sterne & Co., Ltd., of Glasgow. (Fig. 9). The compressor is fitted with automatic valves; both suction and discharge valves being mounted on a valve plate set in the cylinder head.

The suction valve is of the cantilever flapper type and the discharge valve is mounted on a spring-loaded bridge piece which acts as a liquid relief valve.

Fig. 10 shows the valve plate fitted with the discharge reed and spring-loaded bridge piece. The suction reed and the components of the pressure transducers are also shown in this photograph.

The piston is driven by a phosphor-bronze connecting rod runnihg on a cast iron eccentric sheave. The shaft passes through a bellows-packed seal to the driving pulley.

The compressor is directly coupled on to a 0.5 H.P. D.C. compound-wound motor. The carcase is mounted at each end on ball bearings and torque measuring arms of 10½" radius are fitted. Speed control is effected by rheostats in the armature circuit.

An electronic stroboscope is used to check the speed of the motor-compressor.

Leakage Measurement

Fig. 11 shows/

Fig. 11 shows the line diagram of the leakage metering equipment.

The equalising port from crankshaft to suction is sealed by a brass plug and a connection taken to the suction through a valve (A). The line from the crankcase is taken to a cylinder of approximately one half cubic foot capacity (B). This line carries a stop valve (C) and an expansion valve (D) modified to operate as an upstream control valve. Valve (E) isolates the metering cylinder. A mercury manometer (F) with one leg open to atmosphere measures the pressure in the metering cylinder while a differential manometer (G) across the upstream pressure regulator indicates any difference between suction and crankcase pressure. A bypass valve (H) across the regulator valve enables the compressor to be used to evacuate the cylinder, while also allowing the manometer (F) to read suction pressure when the leakage measuring equipment is not in use.

Indicating Mechanism

The development of the indicating mechanism is explained in Appendix II , page 81 .

The unit consists of (a) pressure - transducing element.
(b) phase marker element.
(c) element amplifier.
(d) oscilloscope.
(e) drum camera.

(a) Pressure Transducing Element

The pressure sensitive capacitor is shown in fig. 12 . When placed in the valve plate, the diaphragm is flush with the plate end so does not affect the clearance volume of the compressor. Adequate venting is provided so that air between the disc electrode and the diaphragm has free access to the atmosphere. This was found to be most important and four grooves are cut in the face of the electrode to facillitate this./

this.

A mica disc .001" thick is placed between the electrode and the diaphragm to improve the sensitivity and linearity of the element. The spacing of the electrode is easily modified by a thin washer on the back of the disc electrode.

Any temperature effect on the performance of the element is allowed for by calibrating the element in situ. Fig. 13 shows the alternative element used in certain of the later series of tests to avoid the necessity of opening the cylinder to atmosphere during calibration.

(b). The phase-marker consists of an earthed strip mounted on a fibre disc bolted to the compressor coupling. Along with a similar strip placed in close proximity to the fibre disc, this forms a condenser element which may be placed in parallel with the pressure element and given a well-defined peak on the pressure diagram. In some records the second channel has been used to display the phasing mark.

To enable the phase-marker to be accurately positioned, the fibre disc is graduated in degrees around its periphery. This is also useful for obtaining the T.D.C. of the compressor. The pick-up strip is enclosed in an earthed screen as in fig. 14

(c). The element amplifier is described in Appendix (II) and can be seen in fig. 15 alongside the oscilloscope and the drum camera.

(d). The Cossor double beam D.C. Oscilloscope is a standard commercial model fitted with a 3½" tube with actinic blue trace for photographic purposes.

(e). The drum camera is fitted with a rheostat-controlled universal motor and has a hand-operated shutter. The camera lens has a maximum aperature f1.9 and the record is reduced to 0.696 x oscilloscope screen trace.

The/

The camera incorporates a switch which closes for one revolution of the drum in twenty-five. This is used to brighted the oscilloscope trace and the shutter may be depressed for a considerable time, yet a record will only be taken during the revolution when the beam is brightened. For recording purposes, the time base of the oscilloscope is rendered inoperative and so only a horizontally moving spot is produced on the screen.

The revolving drum applies a uniform linear time base to the record. Record paper is "Ilford" B.P.I. blue-sensitive bromide paper, 59 m.m. wide and unperforated.

Indicator Calibration

This is carried out in the manner described under the heading "Air Circuit Tests", page 85 . Instead of an air supply, dry nitrogen fed through a reducing valve is used as the calibrating pressure source.

To avoid the inconvenience of isolating the compressor from the remainder of the circuit during calibration, the arrangement of fig. 13 was developed. In this, the nitrogen is fed on to the back of the diaphragm and thereby reduces the pressure difference across the diaphragm.

This has the effect of displacing the entire diagram in a direction high to low pressure. When the compressor is running, the calibration is obtained by noting the displacement of the highest point on the diagram while the pressure is gradually increased. A datum pressure is of course required to determine the absolute value of any pressure on the diagram. This is obtained by stopping the compressor and allowing the cantilever valve to fall open by turning the shaft towards O.D.C., when the suction gauge registers the pressure in the cylinder.

The/

The method of calibration described is a development on the lines of the "Farnborough Indicator" and can be used for any electronic indicator requiring frequent calibration. The advantage is that calibration can be carried out while running and at operating temperature, eliminating drift due to temperatur effects.

Oil Separator

Fig. 17 shows a sectional arrangement of the separator. The vapour discharged from the compressor carries oil saturated with Freon. The Freon-oil mixture passes down the column to the electrically heated still in the base, where the Freon is boiled off and passes couterflow with the down-coming mixture. Uncontaminated Freon vapour passes through a small reflux section to the condenser. The temperature of the oil is controlled at 220°F. by adjusting the heat input. A micro-ammeter connected to a thermocouple in the oil indicates the temperature.

A "Pyrex" glass tube is used so that a correct oil level may be maintained by periodically allowing the oil to drain to the compressor sump. The lower end of the unit is well lagged as can be seen from fig. 16 , which also shows the micro-ammeter used for temperature indication.

When the suction vapour condition is very wet it is found that a heater element placed before the separator improves its performance. A further advantage is that vapour to the condenser is superheated and makes control of the condensing pressure much less critical. This heater is a coil wrapped around a 500W. immersion element and well lagged. Control is by a rheostat.

Condenser

This is a concentric tube unit with the water running in contraflow with the Freon which flows inside a $\frac{3}{8}$" o.d. tube.

The/

The condenser is insulated with asbestos sheeting and asbestos cord.

Water flow is controlled by a pressure sensitive valve in the outlet from the condenser and the supply is fed from a constant head tank. The pressure sensitive valve has its sensitive bellows in communication with the discharge line and controls within $\pm$ ½lb/in^2 when equilibrium conditions have been established.

A discharge weir maintains a constant head at outlet. The temperature rise of the cooling water is measured by thermopile and the quantity is measured on a weighbridge. A sightglass is inseted at the condensate outlet to verify that the liquid is subcooled at this point.

A similar sightglass is fitted before the pressure-operated expansion valve.

Drier and Liquid Receiver

These units are as fitted in commercial practice.

Precooler

The precooler is used to ensure that the liquid to the flowmeter is adequately sub-cooled. Cooling water is provided from the same supply tank as the condenser but is not controlled and runs full bore during the test period. A simple shut off valve is provided at the outlet.

Flowmeter

The liquid flowmeter is based on the design adopted by Smith (29). Subcooled Freon enters an insulated tube and is heated by direct contact with an electric heating element whose consumption is measured by a sub-standard wattmeter.

Inlet temperature is measured by thermocouple and the temperature/

temperature rise by a thermopile. Figs. 18 and 18a show the sectional arrangement of the flowmeter and the heat barriers which isolate both the meter from the thermocouple pockets and those latter from the remainder of the circuit. The meter shell is placed in a thermos flask and the thermocouple pockets are lightly insulated with asbestos cord.

Since the liquid entering the meter is approximately at room temperature and adequate heat barriers and thermal insulation are provided, the losses in the flowmeter are negligible.

Evaporator

This is of the secondary fluid type as shown in fig. 19. Previous tests using an evaporator coil directly heated by an electric element showed that control of suction superheat was very difficult due to the low thermal capacity of the dry vapour and the large temperature difference between the heater element and the vapour.

In this unit, the secondary fluid is only slightly warmer than the outgoing (suction) vapour. In addition, estimation of the heat exchange between the shell and the atmosphere is greatly simplified.

As Freon 12 is an excellent insulator, the two 1 K.W. wirewound elements are immersed directly in the secondary fluid and their terminals let out through neoprene-packed tufnol glands. Power input from the D.C. mains is controlled by rheostats and is measured by voltmeter and ammeter. The shell is fitted with a pressure gauge, thermocouple pockets in the vapour space and a sightglass to check the liquid level below the primary coil. The shell is lagged with 3" of granulated cork enclosed in a sheet steel cladding.

Temperature Measurement

All temperatures are measured by copper-constantan thermo-

thermocouples in pockets at the appropriate points in the circuit. These pockets and associated piping are carefully lagged to prevent errors due to difference between pipe and fluid temperatures.

At the compressor suction a thick fibre-joint pad is used to isolate the compressor from the suction line. The pipe temperatures near the suction vapour thermocouple are also measured.

A similar procedure is adopted at the compressor discharge.

These temperatures are measured on a potentiometer fitted with a spot galvanometer for ease and accuracy of measurement. Switching is done by a double-bank switch as shown in fig. 20b. This arrangement avoids any chance of circulating currents due to common paths in the wiring. The individual cold junctions are insulated from each other in a tube of light mineral oil. The tube also contains a thermometer and is placed in a thermos flask of shaved ice and distilled water.

The switch is placed in an insulated box to avoid stray thermal effects and maintain clean contacts.

Measurements are made at the points indicated in fig. 8.

Fluctuating Temperatures.

The measurement of cyclical fluctuating temperatures in the cylinder is described in Section (5) page 22.

Pressure Measurement

Pressures are measured on Bourdon Type gauges at the appropriate points in the circuit. These were calibrated at frequent intervals to maintain accuracy.

Suction pressure may be measured either by pressure gauge or by mercury manometer.

Above pressures of 15lb/in^{2}G. a Bourdon Type gauge is used.

FLUCTUATING TEMPERATURE MEASUREMENT

Measurement of surface temperature was considered to be more practicable than measurements beneath the surface for several reasons.

For a sinusoidal waveform of temperature fluctuation, the temperature range at depth x beneath the surface is given by $t_x = t_s e^{-x\sqrt{\omega/2\alpha}}$

For a complex cyclical fluctuation, the Fourier analysis may be adopted and using ω as the fundamental frequency, the temperature range for any harmonic λ is given by

$$t_x^\lambda = t_s^\lambda e^{-x\sqrt{\frac{\lambda\omega}{2\alpha}}}$$

where t_s^λ is the surface temperature fluctuation for the λ order harmonic.

Fig. 21 shows a curve of $\frac{t_x^\lambda}{t_s^\lambda}$ for several harmonics of the fundamental frequency chosen (750 r.p.m.) for cast iron.

Since it would be difficult accurately to position a thermocouple in the cylinder wall or valve plate of the compressor closer to the surface than .05", the waveform would be considerably damped. This is of course undesirable as the temperature range in the cylinder wall is only a few degrees, even at the surface.

A considerable distortion of the waveform due to unequal harmonic damping must also occur.

Construction of Peened Thermocouples

The simplest temperature measurement element is a thermocouple peened into the surface of the valve plate and led out of the cylinder through a gas tight seal. Since the surface temperature was required, a single thermocouple formed by peening copper and constantan/

constantan wires, separated by a small distance, (.05") was adopted. Lead-out wires electrically insulated from the valve plate surface were taken from the cylinder between two thin joint rings. This construction ensured as far as possible, an isothermal path along the leads and also that the junction actually was on the valve plate surface. The latter is obtained by making the generated E.M.F. between a copper-iron couple added to an iron-constantan couple. Since these junctions are at the same temperature, the E.M.F. is the same as that generated at a single copper-constantan couple.

An isothermal path along the leads assured the temperature at the junction to be the same as that of the remainder of the valve plate.

By using the thinnest practicable wire (40 S.W.G.), combined with the above construction, the temperature was measured with as little disturbance to the gas flow as possible. The construction is shown in fig. 22 .

Measurement

For the recording of a cyclical temperature waveform of a few degrees Fahr. amplitude, the mechanism required a sensitivity of the order of 50 microvolts at frequencies down to the fundamental engine frequency of about 10 cycles/sec.

Such requirements are beyond the scope of ordinary electronic valve amplifiers, which at high gains have a "noise level" considerably in excess of the sensitivity required. It was therefore decided, after several fruitless attempts to construct a suitable high gain, low-noise amplifier, to adopt a step-by-step method as an interim measure.

Joubert Contactor

Fig. 20a shows the circuit diagram of the device which consists of a contact-maker in series with the thermocouple. This is clearly shown on the end of the shaft of the torque-mounted motor in fig. 16 .

The/

The angle of contact of the brushes is easily adjustable.
The angle of contact of the brushes is easily adjustable
and is set by utilizing the contact to short-circuit the input of the indicator mechanism and displaying the waveform on the oscilloscope screen. The brushes and the contact strip are of brass. Similar metals are used to reduce thermal E.M.F. at the contacts to a minimum.

The instananeous E.M.F. generated between the hot and cold junctions is stored in a 20 μF paper condenser placed across the potentiometer terminals. A sensitive spot galvanometer detects any difference between the E.M.F. stored in the condenser and that developed across the potentiometer slide wire.

The mean temperature at the valve plate may be measured by closing the shorting switch across the contactor.

Accuracy of Joubert Contactor

The equivalent circuit of the thermocouple-condenser network is shown in fig. 23 .

In time δT contact is made for $\delta T \cdot \frac{3}{360}$

rise in charge of condenser= $\delta Q_1 = C \delta V_1$

fall in charge of condenser= $\delta Q_2 = C \delta V_2$

rise in charge is by current flow in r with voltage drop $E - V$ $\therefore \delta Q_1 = \frac{E-V}{r} \cdot \frac{\delta T}{120}$

also, fall in charge is by current flow in R with voltage drop V $\therefore \delta Q_2 = \frac{V}{R} \delta T$

nett rise in charge = $C \delta V$

$$= \left(\frac{E-V}{120r} - \frac{V}{R}\right) \cdot \delta T$$

separating variables and integrating,

$$-\log\left\{1 - \frac{V}{E}\left(1 + \frac{120r}{R}\right)\right\} = T\left\{\frac{R+120r}{120rRC}\right\}$$

where T is time to attain voltage from zero charge in condenser.

when $T = \infty$, $\frac{V}{E} = \frac{1}{1 - \frac{120r}{R}}$

but $\frac{120r}{R} = 1.2 \times 10^{-4}$ which is negligible.

i.e./

i.e. voltage across condenser = generated E.M.F.

also, evaluating the equation, $\frac{R+120r}{120CvR} = 8.33$

$\therefore V/E = 1 - e^{-8.33T}$

i.e. the time lag is negligible.

Phasing

The Joubert Contact is coupled to the motor shaft by a dog clutch, and the exact point of contact, related to the compressor cycle is obtained by noting the position of the scale when the shorting pulse coincides with the indicator phasing blip on the oscilloscope.

An oscillogram showing the pulse and phasing blip is illustrated in fig. 24 . These have been offset for clarity. Normally the phasing is checked visually on the oscilloscope screen.

The contact scale is divided into 18 divisions, further subdivided into 2° spacing by an auxiliary scale.

Accuracy of Measurement

Accuracy is not limited by the sensitivity of the potentiometer but by an E.M.F. generated at the contact by friction.

This was limited by using a little paraffin as lubricant and was an almost constant error as shown in fig. 25 (a) which gives curves at various speeds for a thermocouple at steady atmospheric temperature. Figs. 25 (b) and 25 (c) indicate the scatter obtained as the phasing disc is rotated while the speed is held constant.

The scatter of the readings (due to the generated E.M.F. at the contact varying) is seen to be not more than .007 at 500 r.p.m. which corresponds to $0.28^{\circ}F$. Constant difference between true and observed reading is easily allowed for by noting the mean temperature and applying a correction to drop the/

the mean of the observed readings down to the true mean value.

Vacuum-Deposited Thermocouples

While the thermocouples peened into the valve plate gave reasonably satisfactory results, it was felt that some error must be introduced by the disturbance of the surface profile of the plate. Various methods of overcoming this deficiency were attempted without real success, including boring the valve plate from the back to within about .010 in. of the surface and fixing the thermocouple leads in the holes provided.

This was completely unsatisfactory due to the high rotational speeds of the compressor. A more satisfactory solution to the problem was found in vacuum deposition. In this process the junction can be formed by a molecular film of metal bridging two insulated exposed surfaces. The thickness of metal chosen was two thousand Angstroms (.00001 in.) thick. This film is so thin that its effect at any operating speed, including a considerable number of harmonics can be neglected.

This method was successfully used by Bendersky (4) using a vacuum deposited film of nickel one micron thick on an insert probe to measure temperature fluctuations in a gun barrel. The nickel lead was oxydised to insulate it from the surrounding probe. The use of a probe was necessitated by the bulk of the gun barrel. No such limitation exists in the case of the small compressor valve plate.

Several attempts were made to use a nickel wire as a thermocouple element and deposit a film of nickel on the surface of the valve plate but in no case could a reasonable life be obtained. It was found that the only material which had a reasonably long life as a deposit on the valve plate was silver, and the use of a thermocouple element employing silver as the vacuum deposited film was therefore considered.

The arrangement finally adopted consists of an oxidised constantan/

constantan wire cemented into the cast iron valve plate of the compressor. The junction was formed by a film of silver 2000 Å thick. The E.M.F. generated is therefore the sum of the E.M.F.s generated at an iron-silver junction and a silver-constantan junction. Due to the extreme thinness of the film, the temperatures at the junctions may be assumed to be the surface temperatures of the iron and constantan.

In order to ascertain the thermal effects of dissimilarity between the material of the thermocouple wire and the deposited film it was decided to make an investigation utilising the electrical analogue previously described (page 55).

It has been assumed, because of the insulation between the iron and constantan of the thermocouple, that the flow of heat is unidirectional, with no interchange between the iron valve plate and the constantan wire. A simple one dimensional ladder network can therefore be used for the investigation.

The network for the flow of heat through the material with a surface vapour film resistance is shown in fig. 26 .

Amplitude and phase measurements were taken for a wide range of input resistors and for a range of frequencies from 50 cycles/sec. to 5,000 cycles/sec. Only the surface resistor was altered in each test, the same R.C. network being used in each test. The results of the tests can be displayed on a single curve V_s/V_i against $R_i\sqrt{\omega}$. This is derived as shown below:-

applying the equation $$\frac{dV}{dT} = \frac{1}{R_e C_e} \cdot \frac{d^2V}{dx^2}$$

$$\text{as } \frac{dV}{dnT} = \frac{\delta x^2}{n R_s C_s} \cdot \frac{d^2V}{dx^2}$$

for lumped constants, the equation is unaltered/

unaltered so long as $T.\delta x^2$ is unaltered, or $\frac{\delta x^2}{\omega}$ = a constant. (a).

Similarly the distance represented by the surface resistor R_i is $\delta x \, R_i/R_s$ which is unaltered so long as $\delta x R_i$ is a constant. (b).

Combining (a) and (b) we find, for a given analogue network comprising R_s & C_s that the equation is unaltered so long as $R_i\sqrt{\omega}$ is a constant.

Fig. 27 shows the graph of log V_s/V_i plotted against log $R_i\sqrt{\omega}$ for a network in which $R_s = 12K\Omega$; $C_s = \cdot 01\mu F$ for R_i varying from $10K\Omega$ to $1M\Omega$ and ω varying from 50 cycles/sec. to 50,000 cycles/sec.

Application to Temperature Measurement

For a thermal frequency N, $n = N/\omega$

$$\therefore R_s C_s = \frac{\delta x^2}{\alpha} \cdot \frac{N}{\omega}$$

also $R_i \delta x = R_s k/h_f$

giving $$R_i\sqrt{\omega} = \frac{k}{\sqrt{\alpha}} \frac{\sqrt{N}}{h_f} \frac{R_s}{\sqrt{R_s C_s}}$$

With a thermocouple arrangement h_f and N are the same for both elements; the value of $R_i\sqrt{\omega}$ for each material is derived from $\frac{k}{\sqrt{\alpha}}$ for any given condition.

For any material $R_i\sqrt{\omega} = \frac{k}{\sqrt{\alpha}} \cdot \phi$ where $\phi = \frac{\sqrt{N}}{h_f} \frac{R_s}{\sqrt{R_s C_s}}$

$\text{Log} R_i\sqrt{\omega} = \text{Log} C + \text{Log}\phi$ where $C = k/\sqrt{\alpha}$

and $\log (R_i\sqrt{\omega})_a - \log (R_i\sqrt{\omega})_b = \log C_a - \log C_b$

= a constant.

In fig. 28 it will be seen that $\log (V_s/V_i)_a - \log (V_s/V_i)_b = x \tan\theta$

hence $\log \frac{(V_s)_a}{(V_s)_b} = x\tan\theta$, or in thermal units

$\log \left(\frac{t_a}{t_b}\right) = x \tan\theta$ It will be noted that if θ is constant then $\left(t_a/t_b\right)$ is constant. Thus, over the range where the curve of fig. 27 is linear, the relationship between surface temperature fluctuation on one material to the surface temperature fluctuation on another will/

will be constant.

Fig. 29 shows the appropriate values for an iron-constantan couple.

With a silver film forming the junction, the recorded E.M.F. is $(6.95 t_i + 23.6 t_c)\ \mu V/F.$ and fig. 29 shows the sensitivity for such a thermocouple.

This graph shows that within the range $500 < R_i\sqrt{\omega}$ beyond 10^6, the overall thermocouple sensitivity is within ± 5% of the mean value.

These limits correspond to a range of $0 < h < 15{,}000$ at 500 cycles/minute and $0 < h < 150{,}000$ at 50,000 cycles/minute, which covers a sufficient frequency and heat transfer coefficient field for these applications.

Note: h has dimensions B.T.U./hr.ft^{2}F .

Construction of Vacuum Deposited Thermocouples

Four iron-eureka thermocouples were inserted in the valve plate as shown in fig. 30 . An enlarged section shows the method of attachment of the eureka wire in the cylinder. It will be seen that a hole 1/16" dia. is led halfway through the valve plate and is connected up to a smaller hole which breaks through into the cylinder. This hole barely clears the eureka wire which is insulated mainly by an oxide film. The larger hole has negligible effect on the temperature wave since it has been shown that the wave does not penetrate more than 0.1" below the surface.

To ensure complete the insulation of the wires, a coating of shellac was applied and when dry, the wires were coated with "Araldite" thermosetting plastic cement. The coated wire was then carefully pulled through the hole and continuously checked for insulation resistance. Due to the small clearance, this process had to be adopted to ensure that the circuit was not completed within the valve plate. The plate and the attached wires were placed/

placed in an oven at 100°C. until the cement was baked hard. The protruding wires were clipped and the ends filed almost flush with the plate surface. The face was then cleaned with fire emery cloth and the surface dust and grease removed with carbon tetrachloride. A further check on the insulation resistance was made. The valve plate was then inserted in a vacuum deposition chamber and the film of silver 2000 Å thick was deposited on the area around the junctions. Continuity and film resistance was checked before assembly. The thermocouple leads were taken out fibre joints under the cylinder cover as illustrated in the sketch.

The deposition of the metal film was carried out by the staff of the Natural Philosophy department of the Royal College of Science and Technology.

Simultaneously, with this development, further investigations into temperature recording methods were carried out.

It has previously been noted that attempts to construct a high gain, low noise, amplifier suitable for low frequency microvolt inputs had been unsuccessful due to the high noise level in available thermionic circuits. At this time, the Cossor low noise A.C./D.C. battery-operated preamplifier became generally available. This incorporated a new type of low noise factor valve, the O.M.S.C. This seemed to provide a suitable answer to the noise and frequency problem. When the instrument was coupled to the Cossor D.C. oscilloscope No.1049, the valve noise was about 50 microvolts. This seemed to rule out the use of this preamplifier, but it was decided to persevere with the set-up to see whether some correspondence with the Joubert Contact method of temperature recording could be achieved when adequate signals were available.

During this preliminary work, the noise level was noted to be/

be of an almost constant amplitude and even more important, to contain only supersonic frequencies around 50,000 to 100,000 cycles per sec., with practically no low frequency or random components.

It was immediately apparent that a considerable reduction in this noise could be achieved by the use of an ordinary top-cut filter as used in audio work to reduce surface noise on gramophone records. The frequency of the noise signals is so high that a simple capacitor across the output of the pre-amplifier was found to be adequate. The noise level was now of the order of five microvolts without appreciably affecting the thermocouple signal. The response curve for the filter is shown in fig. 31 .

When setting-up the complete temperature recording instrment, complete screening of all components was adopted and a single-earth connection made between each component. Even so, a considerable mains frequency hum level was present. This residual hum was eliminated by the inclusion of a simple hum-bucking arrangement. This could be set to give zero mains frequency signal on the oscilloscope when the thermocouple selector switch was closed.

It will be observed from the records of temperature fluctuation that there is little evidence of hum or noise. It is emphasised that such a high signal/noise ratio can only be achieved by close attention to every detail in the mechanical and electrical layout of the equipment.

The gain of the D.C.-coupled preamplifier and oscilloscope was found to be inadequate. Even A.C.-coupling of the preamplifier did not give a signal of a suitable amplitude, although the noise level was still of a very low order. Since the pre-amplifier was now A.C. coupled, it was no advantage to use a D.C. oscilloscope. The Cossor A.C. oscilloscope No.1035 was pressed into service. The gain of this instrument is four

times/

times as great as that of the No.1049, in the maximum sensitivity setting. With this arrangement signals of 15 peak-to-peak could easily be detected and measured. The noise level of about 5 μV amplitude, was considered satisfactory.

Calibration is carried out by means of a mains signal of known amplitude.

A series of tests using this equipment was carried out.

Correlation between the Joubert Contactor and the electronic recorder was not achieved. It seemed likely that some deficiency existed in the recording chain. The thermocouple itself was common to both systems and there was little possibility of a partial failure of the contactor. The error was obviously due to amplitude and phase distortion in the A.C. coupling networks. Time-constant checks were therefore made on the equipment and gave a value of 12.12 m.s. Such a small time-constant obviously must produce considerable distortion in the temperature wave at frequencies of 10-20 cycles/sec.

The presence of such a short time-constant was surprising in this oscilloscope since it had been designed for ordinary audio work and in previous use had been noted to give a flat response within 3 d.b. to 5 cycles/sec. Investigation of the circuit showed the gain control to be in the form of a negative feedback loop on the first valve of the Y.I. amplifier. On normal gains, feedback maintains the response adequately but on maximum gain the feedback is removed and the time-constant consequently is reduced. Verification of this was given by reducing the gain of the oscilloscope by 3 x . This gave an improved time-constant of 36.4.m.secs., which is three times that obtained at the maximum gain position.

Correction of temperature traces to allow for short time-constant was carried out as follows:-

The coupling networks may be considered as a single R-C coupled system. (fig. 32 a).

In /

In time δT ; V_1 rises δV_1 and $V_2 - \delta V_2$
charge on C increases by $C[\delta V_1 - \delta V_2]$
charge passed through $R = \frac{V_2}{R} \delta T$

hence $$C \delta V_1 - \delta V_2 = \frac{V_2}{R} \delta T$$

$$C \frac{\delta V_1}{\delta T} - C \frac{\delta V_2}{\delta T} = \frac{V_2}{R}$$

expressing as infinite differentials,

$$\frac{\delta V_1}{\delta T} - \frac{d V_2}{d T} = \frac{V_2}{RC}$$

i.e.

$$\frac{\delta V_1}{\delta T} = \frac{d V_2}{d T} + \frac{V_2}{\tau} \qquad \tau = \text{time constant}$$

integrating,

$$V_1 = V_2 + \int V_2 \, d T + (\text{a constant.})$$

i.e. input voltage = output voltage +(area of output voltage/time diagram) x $1/\tau$ + a constant.

The scale of the integral curve is m.n.h. units of area and when multiplied by $1/\tau$ gives the added fraction.

For convenience, therefore, the scale of (integral $\propto 1/\tau$) should be the same as the ordinate scale,

$$\therefore h = \tau/m$$

i.e. the polar distance for integration = τ/m

Fig. 33 illustrates a typical correction process. In this case, at 600 r.p.m. 9" = 1 rev. = 1/10th sec.

$$m = 1/90 \text{ sec/in.}$$

$$1/\tau = 82.6 \text{ /sec}$$

$$\therefore h = 1.09 \text{ in.}$$

The integration constant is obviously the shift in the zero of the trace due to the added integral.

i.e. Constant = mean height of integral curve.

Evaluation of Time-Constant

This was carried out experimentally as shown in fig. 34a.

A/

A step function of 150μV was applied at the input of the preamplifier using dry battery and a potential divider.

The keying action was utilized to trigger the oscilloscope time base so that a single keyed pulse was recorded, the camera shutter being held open. A 50 ~ timing pulse was displayed on the second beam which also served as the zero line for the exponential decay trace. (Fig. 35a)

In later series of tests, the short time constant of the oscilloscope was eliminated by introducing a further stage of amplification between the pre-amplifier and the oscilloscope.

This amplifier was quite stable and was directly connected to the output of the pre-amplifier. The output of this stage of amplification fed into the D.C. oscilloscope through a time constant of 50 m.s. The correction of this time constant was quite simple and a passive network of the type shown in fig. 34b was introduced between the photoformer and the ladder network when the diagrams were being analysed. The response of the correction network to a square wave which has been passed through a differentiating network is shown in fig. 35b. The time constant of this network is chosen to correspond to the compressor speed.

Two-Dimensional Analogue for Extended Surface

When fixing a thermocouple wire for measurement of surface temperature, it is not possible to be certain that the wire has a perfectly sharp cylindrical edge or that the hole has a perfectly sharp edge. It is therefore conceivable that the thermoelectric effects generated between the vacuum-deposited film and the wire extended surface could have an appreciable effect on the accuracy of the readings obtained from the thermocouple, especiall at high frequencies.

To obtain some idea of the magnitude of the errors which might be involved, a two-dimensional network representing a sectio of the thermocouple wire with attached "fin" was constructed. The block diagram of the network is shown in fig. 36 . The condensers at the nodes of the network are all .01μF. and the unit of resistance is taken as 10K. On this basis, the block is 20 units wide and 53 units deep. The "fin" is represented in depth by 1 unit of resistance i.e. 10 K. and one unit of capacitance i.e. .01μ F. and in width it can be represented by either 17.1 K. with 2 x .01μ F. condensers or 12 K.Ω with 1 x .01μ F. capacitance. The network is fed along the top edge through variable resistances from a variable-frequency oscillator. These resistances represent the vapour film resistance and the effect of the "fin" is noted by taking the difference in voltage between surface at the finned end of the network and at each of the other surface junctions. This gives an accurate reading of the voltage at each of the surface junctions and the extremely high input impedance of the difference amplifier ensures that the measuring probe has no effect on the conditions in the network. The network is shown in fig. 37 & 76 b.

In each case, the time scale multiplier "n" has been chosen so that the "fin" is .001" deep and either .0011" wide or .0019" wide/

wide depending on the circuit. The oscillator frequency was varied from 5 cycles/sec. to 5000 cycles/sec. with surface resistors being varied from 125 K.ohm to 22.7 M.ohm.

The possible errors involved are presented as the excess of the temperature at the tip of the "fin" (where the E.M.F. is generated) over the temperature of the bulk of the wire surface. The range of heat transfer coefficients is approximately from 80 to 14,000 BTU/hr.ft.^{2o}F.

The graphs 38, 39, 40, 41, show that the existence of a small "lip" or "fin" on the thermocouple wire or on the edge of the hole in which the wire is inserted can cause appreciable errors in the recorded temperature. These errors can extend over the entire range of frequencies met with in engine and compressor work and some account must be taken of the possibility of such errors in the assessment of the accuracy of the results obtained from experimental work.

Doubling the width of the "fin" has the effect of approximately doubling the error. In fig. 41 it will be seen that as the frequency is taken to a very high value, the error passes through a maximum value and then gradually falls. This is due to the reduction in the penetration of the wave into the wire. When the penetration approaches the depth of the fin, the error will tend towards zero.

From the above it is clear that the accuracy of the surface thermocouple is limited by the degree to which the edges of the elements of the thermocouple are distorted.

The use of peened thermocouples for measurement of fluctuating temperatures is therefore, to say the least, suspect.

TEST PROCEDURE

The following procedure is that adopted after the fitting of automatic controls when the machine was run continuously in order to eliminate, as far as possible, transient conditions in the circuit. These comprised,

(a) electrical cut-outs to shut-down the circuit in case of failure.

(b) controls to maintain steady conditions in the plant.

The circuit diagram of the electrical cut-outs is shown in fig. 42 . Controls fitted to assist in steady running included a modulating valve controlling the cooling water to maintain constant discharge temperature and a feedback-controlled motor to keep the speed at the desired value.

When the plant is running continuously, two tests are run per day and the actual readings taken before eight in the morning and before eight in the evening in order to have the advantage of steady voltage conditions.

The test commences, after the leakage readings of the previous test have been taken, with the opening of the equalising valve and the shutting off of all heaters. The shorting switch on the L.P. cut-off is closed and the condenser water turned to full flow. The evaporator outlet and inlet valves are closed and this causes the compressor to draw a vacuum in the measuring cylinder.

When this is sufficient for the purposes of the test, the cylinder valve is closed and the refrigeration circuit opened again. This operation should take less than 10 minutes. The condenser is returned to automatic control and when the L.P. cut-out has closed, the shorting switch across it is opened.

The calorimeter heat input is adjusted to the desired level and the oil heater and flowmeter switched on.

The/

The plant is now run for about an hour during which time the expansion valve setting and the condenser water flow are adjusted to give the desired test conditions. When conditions have steadied down and the oil is maintaining a steady low level in the separator the plant is left to run under automatic control for a period of at least eight hours.

After this period, the power pack, oscillator and oscilloscope are switched on and allowed to warm up while the oscilloscope camera is loaded and the refrigerant circuit conditions checked. The condenser water is switched to flow through a glass orifice column which indicates whether the automatic water valve has modulated to give the correct constant flow or whether this has not been possible, perhaps due to variations in speed. If conditions are satisfactory, the collection of condenser water for weighing is started and this proceeds while the temperatures, pressures and other readings are noted. A valuable indication of the degree of thermal equilibrium is given by the oscilloscope trace which will drift due to very slight changes in cylinder head temperatures. Readings are duplicated to ensure that equilibrium has been established.

When these readings have been obtained, the pressure and "Farnborough" diagrams are photographed and the trace is calibrated by introducing nitrogen pressure above the capacitor diaphram and photographing the deflected trace at successive pressure increments.

Fluctuating Temperatures in Valve Plate

The phasing contactor is clipped into place and the thermocouple circuit switched so that fluctuating temperatures may be read. The signal from the contactor is fed into the pressure trace and the two "blips" aligned for phasing purposes. The wire to the pressure element is then disconnected and temperature readings/

readings taken at every 20° of crank rotation. To guard against the effects of slight changes in cylinder head temperature, the mean temperatures are frequently noted in a separate column, giving an indication of the time element involved in the readings.

After the introduction of electronic recording equipment for temperature measurement, the temperature traces were photographed on the oscilloscope along with calibration traces.

Piston Leakage

The following operations refer to the apparatus shown in fig. 11 . The crankcase pressure control valve (D) is now set to the estimated position for the expected leakage and the differential manometer opened. The evacuated cylinder (B) is now opened and gas flows into it from the suction line. The equalising valve (A) is closed and the gas flowing into the cylinder must come from the crankcase. Slight adjustments are made to the control valve to bring the differential manometer to its original reading and when this is steady, readings of mercury height at each minute are taken on the other manometer. This gives the rate of increase of pressure in the cylinder from which the rate of leakage can be calculated. When the pressure in the cylinder has risen sufficiently for the rate to be established, the equalising valve is opened and another test is commenced by shutting off the heaters and drawing a vacuum in the cylinder.

Note.

Leakage vapour normally finds its way back into the suction line but when this vapour is removed for measurement there is an increased draw-off from the evaporator and condenser while the flow into the condenser is unaltered. This may be seen from fig. 43 . This tends to lower the evaporator and condenser pressures which must be countered by increasing the evaporator heat input and reducing the water supply to the condenser. The former is achieved manually but the condenser modulating valve successfully maintains the discharge pressure.

VOLUMETRIC EFFICIENCY

REDUCTION OF RESULTS

When suction vapour is superheated, the mass flow may be determined from either the enthalpy balance across the Calorimeter or from the liquid mass flowmeter.

When the suction vapour is wet, the condition at suction is inferred from the enthalpy rise across the evaporator in conjunction with the mass flow determined solely by the liquid mass flowmeter.

Due to the concentric-tube construction of the condenser and the small mass flows encountered, the condenser method of mass flow determination was not used. This was due to the comparatively large heat leakage from the condenser which was impossible to calibrate since the position at which sub-cooling occured varied from test to test. The readings from the condenser - especially the rate of water flow were nevertheless a useful guide to equilibrium conditions in the system.

Thermodynamic properties of Freon 12 were obtained from "Properties of Commonly Used Refrigerants" (3) and these were plotted on a base of dryness fraction and superheat so that the best basis in which to plot the results could be found.

For continuity in all curves, increments of entropy, specific volume and enthalpy should be uniform in the change from the wet to the superheated field.

i.e. $\left(\frac{\partial F}{\partial \varphi}\right)_{\phi} = \left(\frac{\partial F}{\partial \varphi}\right)_{h} = \left(\frac{\partial F}{\partial \varphi}\right)_{v}$ where F = degree of superheat.

In fact, these equalities are not realized but the variation is sufficiently small to be ignored.

e.g. at 15°F. saturation temperature,

$\left(\frac{\partial F}{\partial \varphi}\right)_{\phi} = 522$ °F/Unit of dryness.

$\left(\frac{\partial F}{\partial \varphi}\right)_{h} = 473$ °F/Unit of dryness.

$\left(\frac{\partial F}{\partial \varphi}\right)_{v} = 438$ °F/Unit of dryness.

The best basis on which to construct all curves is therefore with 438°F ≡ 1 unit of dryness since specific volume is the property primarily concerned with volumetric efficiency. Volumetric Efficiency is defined as,

$$\frac{\text{Aspirated volume at conditions at suction manifold}}{\text{Swept volume of compressor.}}$$

Indicated Volumetric Efficiency is defined as,

$$\frac{\text{Length of suction pressure intercept on P-V diagram}}{\text{Swept volume of compressor.}}$$

The form taken by the volumetric efficiency curves, (figs. 44 to 46) is similar in each case. The rising characteristic of the curves as the suction dryness approaches 0.85 corresponds with the previous work by Smith and Giffen and Newley. The absence of a maximum in these graphs even with over 100°F. superheated at the suction is surprising although the increase is quite small with superheat greater than 30°F.

It will be seen that in the superheat field, the most suitable speed is 750 rev./min. whereas when air is the working fluid (Appendix III) no maximum is apparent. The incidence of wet compression favours the higher speed of rotation.

The valve plate temperature (figs. 47 to 49) shows similar characteristics, rising slowly as the suction quality is raised and then rising much more steeply as the discharge vapour becomes superheated.

It is surprising that the discharge vapour superheats down to such low suction qualities (fig. 51). This cannot be totally ascribed to steady state heat transfer since with a low discharge temperature, (fig. 68) the superheat exists down to 0.6 dry. It is significant that the slope of the discharge vapour curve continuously rises until well into the superheat field, whereas steady-state heat transfer would produce/

produce a curve of continuously falling slope.

Fig.52 shows that the temperature difference across the valve plate does not vary greatly. Hence the heat transfer to the vapour as it passes through the compressor, must also be sensibly constant.

An alternative explanation lies in an inefficiency in the compression process which increases the work of compression. Change of suction condition makes little difference to the indicator diagrams, in fact the scatter of results due to variation in oil level made such diagrams of little value.

The fall in volumetric efficiency must therefore be due principally to actions not apparent from the indicator card. These will occur during suction and discharge when changes in density have little effect on the indicator card.

In the analysis of the indicator diagrams, the suction pressure intercept is difficult to determine and although the "Farnborough" Indicator assisted in obtaining this intercept, considerable scatter could occur due to the action being affected by oil on the diaphragm.

This is particularly apparent on the curve for 1000 rev./min. on fig.50. Under these conditions the splash lubrication causes considerable oil carry-over into the discharge line. In this connection it was apparent that the oil carry-over was much greater when the suction condition was wet than when it was highly superheated. It was impossible to obtain quantitive results since the slightest alteration in oil level in the sump had a great effect in the amount of oil carried over. This quantity in any case was never more than about 1.5×10^{-3}lb./min. and even if 50% saturated with Freon could account for only $.75 \times 10^{-3}$lb./min. of the capacity of the compressor.

The method of analysing the pressure diagrams will be seen from/

from fig. 102 in which the pressure-time diagram is set out and divided into strips 10° apart. The pressures are obtained from the oscillograms shown in fig. 101 in which calibration traces are superimposed at 20 lb./in.^{2} intervals. The trace from the "Farnborough" element also carries the phasing mark. The indicator diagram, on a volume basis is shown on fig. 103 .

It will be seen that closure of the suction valve occurs some 35° after B.D.C. It was realized that some blow-back must occur to cause closure of the valve and work on this was carried out by Pearson (26) using this compressor and its associated test equipment.

PISTON LEAKAGE
REDUCTION OF RESULTS

The leakage rate is obtained by measuring the rise of pressure in the cylinder with respect to time, assuming isothermal conditions in the measuring cylinder.

$$P.V. = W.R.T.$$

$$\frac{dP}{d\tau} = \frac{dw}{d} R \frac{T}{\upsilon}$$

$$\frac{dw}{d\tau} = \frac{\upsilon}{RT} \cdot \frac{dP}{d\tau} = C \frac{dp}{dt}$$

P, from the manometer, is graphed in inches Hg to a base of time in minutes.

The validity of any set of readings is automatically checked by their approximation to a straight line. If the rate of leakage is not constant then the gradient of the line will vary. By using the modified expansion valve to maintain a constant mean pressure in the crankcase, it was possible to produce results that showed no progressive deviation from a straight line.

A typical curve for rise of pressure in the metering cylinder is shown in fig. 53 and the leakage rate is calculated as shown below:

$C = \frac{V}{RT}$ where V = volume of cylinder (.4375 ft. ^{3})
R = gas constant for F.12 (11.7 lb.ft/^{o}F. lb)
T = mean temperature of vapour.
h = pressure (in. Hg.)

$$\frac{dw}{d\tau} = \frac{144 \times .4375 \times .49}{11.7 \times 560} \times \frac{dh}{d\tau}$$

From fig. 53 $\frac{dh}{d\tau}$ = 2.56 in.Hg./Min.

$$\frac{dw}{d\tau} = 4.71 \times 10^{-3} \times 2.56$$

= .0121 lb/min. leakage flow

Accuracy of Results/

Accuracy of Results

The method of estimating piston leakage was designed to give an error of less than 5% in the Freon 12 tests where flow quantities of about .015 lb/min. were expected.

It is reasonable to assume that the timing of readings was carried out to an accuracy of .01 minutes and that the height of the mercury column could be read to within 0.1 of an inch. The normal duration of a leakage run was 8 minutes during which time the manometer reading would rise to approximately 25" Hg. These figures give an estimated error of 0.5% indicating that the main source of error is likely to be incorrect control of crankcase pressure. The differential manometer between sump and suction (G. fig. 11) showed that the modified expansion valve controlled the crankcase pressure to $\pm$ 0.25" Hg. Assuming a mean differential pressure of 10 lb/in^2 and a linear relationship between leakage and M.D.P. this gives rise to a possible error of $\pm$ 1.5%.

Thus it can be seen that the theoretical error is within the 5% set as the standard required for useful results.

The normal deviation of experimental points from the mean straight line is considerably less than 0.1 inch in a line rising to 5" giving an observed error of about 2%.

Comments on Results

The results of the tests using both Freon 12 and air as the working fluids are shown in figs. 54 to 56 . In analysing the results the standardised curves of fig. 57 were drawn. These enable the mean pressure differences between the cylinder and the crankcase to be deduced from a knowledge of the suction and delivery pressures of the compressor.

This mean pressure has been termed "Mean Differential Pressure" since it is calculated on a time basis.

That is, "Mean Differential Pressure" (M.D.P.) = $\int \frac{P d\tau}{\tau} = \int \frac{P d\theta}{\theta}$

These curves were constructed from theoretical pressure/crank angle diagrams assuming isentropic compression and have been constructed for both Freon 12 and air. Using the standardised M.D.P. curves, and assuming that the leakage is laminar, a curve of theoretical piston leakage has been prepared. This is shown in fig. 58 . This curve indicates that the piston leakage will increase with increasing suction pressure up to high suction pressure. This increase in leakage has been noted by Fuchs, Hoffmann and Klank (11) and also by Lorentzen (19).

The variation of piston leakage with speed is quite small within the practical speed range of the compressor. Values of piston leakage under static conditions have not been given, since (1) static tests are quite meaningless as the normal oil film would quickly be washed away,

(2) the effects of side thrust on the piston would not be obtained.

The inadequacy of static tests has already been noted by Gosney (14).

It/

It will be noted that the reduction in piston leakage with increasing speed is greater when Freon 12 is the working fluid than when air is the working fluid. This would seem to indicate the importance of the oil film presented to the soluble refrigerant. It would appear that the increase of speed reduces the dilution of the oil film by the refrigerant.

Piston Leakage/Suction Enthalpy (fig. 54)

The curve of leakage against suction enthalpy shows a slightly increasing characteristic in the range 0.5 - 0.8 dry followed by a relatively sharp decrease between 0.8 and 1.0 dry. In the dry field the leakage appears to be approximately constant.

The increased leakage at about 0.9 dry is presumably due to the dilution of the oil film by condensation on the cylinder walls. The apparent slight decrease in leakage at suction conditions below 0.8 dry may be a temperature effect.

The leakage rate appears more stable in the superheat field. Increased specific volume will tend to reduce the leakage but this will be counteracted by the greatly reduced thickness and viscosity of the oil film.

Leakage/Suction Enthalpy at Various Pressures

These curves display the form observed in the curves of fig. 55 .

It is noticeable that high suction pressures produce increases in the leakage rate. This is in agreement with the curve of theoretical piston leakage. (fig. 58).

The leakage of vapour past the piston is about 5% of the mass flow of refrigerant in the compressor. Hence, even although there is a 30% increase of leakage in the transition from "dry" to "wet" compression, it is clear that the effect on the volumetric efficiency of the compressor is slight. A 30% variation in leakage/

leakage rate produces about 1.5% variation in volumetric efficiency.

Comparison of Air and Freon 12 Leakage

In comparing the leakage of air, which is immiscible with the lubricating oil, with that of Freon 12, which is miscible with the lubricating oil, use has been made of the M.D.P. curves. The experimentally determined leakage past the piston has been plotted against mean differential pressure. This is shown in fig. 59 . The linear nature of these curves indicates that the flow past the piston is viscous in nature.

Assuming a viscous leak, we have, $\frac{m}{\Delta P} = K\frac{\rho}{\mu}$

By experiment, we know that $\frac{m}{\Delta P}$ for Freon is approximately twice the $\frac{m}{\Delta P}$ value for air. (fig. 59)

For air under the test conditions, $\rho = .075$ lb/ft.^{3}

$\mu = .0175$ c.p.

$$\frac{m}{\Delta P} = K \times \frac{.075}{.0175} = \underline{4.3\ K}$$

For Freon 12 under the test conditions,

(a) assuming it leaks as a vapour, $\rho = .558$ lb/ft.^{3}

$\mu = .01$ c.p.

$$\frac{m}{\Delta P} = K \times \frac{.588}{.012} = \underline{49\ K}$$

(b) assuming it leaks as a liquid, $\rho = 84$ lb/ft.^{3}

$\mu = 0.29$

$$\frac{m}{\Delta P} = K \times \frac{84}{.29} = \underline{290\ K}$$

Assumptions (a) and (b) do not yield solutions which are of the same order as the experimental results.

(c) An alternative assumption is that the greater part of the Freon 12/

Freon 12 leaks past the piston as a solution in the oil film on the cylinder wall.

The mean dilution of the oil film cannot easily be calculated but considering the large surface areas involved solutions of as much as 50% Freon are possible.

In the case of a 50% solution under test conditions,

$$\rho = 70 \text{ lb/ft.}^3$$

$$\mu = 4 \text{ c.p. (A.S.R.E. Data Book, 1949, p.309).}$$

$$\frac{m}{\Delta p} = K \times .5 \times \frac{70}{4} = \underline{8.75 \text{ K.}}$$

The result produced by assumption (c) is of the same order as the experimental result.

Conclusions

(1) The leakage of Freon 12 past the piston is probably laminar flow dissolved or partly dissolved in the oil film on the cylinder wall.

(2) For all practical pressure ratios, the piston leakage will be increased if the suction pressure is raised.

(3) Piston leakage does not vary greatly with speed, thus the loss of volumetric efficiency due to this leakage is much greater at low speeds.

(4) Piston leakage is greatest under "wet" conditions reaching a maximum at about 0.8 dry and falling to an almost constant figure in the superheat field.

(5) The alteration in leakage of refrigerant past the piston during the transition from "dry" to "wet" compression is slight and does not make a significant contribution to the reduction in the volumetric efficiency for the compressor during such transition.

TEMPERATURE GRADIENT IN VALVE PLATE

From a knowledge of the surface temperature fluctuations of the valve plate during the cycle, the cyclical heat exchange between the vapour and the plate may be obtained.

Steady state heat exchange is allowed for in the normal fashion.

If the heat flow is assured to be normal to the surface then the periodic heat flow may be found by carrying out a Fourier analysis of the temperature fluctuation.

For the λ harmonic, the temperature gradient at the surface is given by :

$$\frac{dt}{dx} \; t_s^{\lambda} \sqrt{\frac{\lambda\omega}{2\alpha}} \; (\sin \lambda\omega\tau + \cos \lambda\omega\tau)$$

where ω is the fundamental frequency.

From this it will be seen that higher order harmonics in the temperature waveform have a large effect on the heat transfer and cannot be neglected in the analysis.

This involves considerable labour in the calculation of the temperature gradient and as an alternative, a relaxation method and an electrical analogue have been used in the present investigation.

Relaxation Pattern

Figs. 60 (a) and (b) show curves of temperature with respect to time and depth in plate.

The mean temperature gradient at time τ is given approximately by $\frac{dt}{d\tau} = (t_4 - t_2)/2\delta\tau$

and the mean temperature gradient at depth x by $\frac{dt}{dx} = (t_1 - t_1)/2\delta x$

Rate of change of the above gradient is $\frac{d^2t}{dx^2} = (t_1 + t_3 - 2t_0)/\delta x^2$

Therefore, for heat transfer through the walls in one plane, the Fourier equation may be applied in the form $\alpha \frac{d^2t}{dx^2} = \frac{dt}{d\tau}$

and using the above approximations, is $\frac{\alpha}{\delta x^2}(t_1 + t_3 - 2t_0) = (t_4 - t_2)/2\delta\tau$

Hence/

Hence choosing $2\alpha\delta T = \delta x^2$
this equation becomes $T_1 + T_2 + T_3 - T_4 - 2T_0 = 0$
If the equation is not satisfied, then $T_1 + T_2 + T_3 - T_4 - 2T_0 = r$
where r is the residual at T_0 .

This can be applied to a suitable relaxation pattern as shown in fig. 60c .

The pattern has time as one axis and depth in the cylinder wall, as the other. Each time interval is taken as a suitable crank-angle rotation and the depth " δx " is of the value to satisfy the equation.

The numerical values at each node show the corrections to be made in the residuals when the value T_0 is increased by +1.
e.g. when considering equilibrium at T_2
an increase of +1 at position T_0
reduces the residual by 1, since the
equation for position T_2 is $T_5 + T_6 + T_7 - T_0 - 2T_2 = r_2$

Hence, choosing the largest residual and reducing it to zero by increasing the temperature at that node by half the amount of the residual, the true temperature at a particular node may be obtained.

The temperatures at the various nodes are assumed at the mean temperature of the surface and the residuals calculated and inserted as shown in fig. 60c .

Since the time scale is continuous, values at 360° immediately precede values at 20° in the pattern.

When the process is carried in the direction x sufficiently that the residuals are unimportant, the temperature gradient at the surface may be calculated by advancing the pattern in the direction $-x$ to obtain the temperature gradient at the surface.

The/

The use of this relaxation technique was adequate for the calculation of temperature gradients due to temperature fluctuations not containing high harmonics.

Such is the case when the Joubert Contactor is used to record the temperature since the scatter of results due to expansion valve "hunting" precludes the plotting of closely-spaced temperatures. This technique was used by the author (6) before the electronic recording equipment was developed.

The higher resolution of the electronic system of temperature recording requires such refinement of the relaxation "net" as to render the process excessively laborious.

Electrical Analogue

The development of the electrical analogue is described in Section 10 .

Temperature gradient and cyclical heat flow are derived as follows:

From the temperature fluctuation curves and its calibration, the scale of the temperature fluctuation curve can be obtained, and when processed through the analogue, the scale for the temperature gradient curve is obtained by considering the constants of the analogue and the amplification of the various amplifiers in the circuit.

For a speed of 1000 rev./min., $R_s = 12 \times 10^3 \Omega$

$\delta x^2 = n R_s C_s \alpha$ $C_s = .01 \mu F$

$= 1.04 \times 10^{-7} ft^2$ $n = \frac{100}{1000 \times 60}$

$\alpha = .52 ft^2/hr$

Temperature gradient scale on oscilloscope

$$= \frac{\text{Scale of Temperature Fluctuation Curve}}{\left(\text{Gain of } \frac{\text{Gradient Channel}}{\text{Temperature Channel}}\right) \times (\text{gain of difference amplifier})}$$

$= S\ ^{o}F/cm.$

Temperature gradient $= \frac{S \times y}{\Delta}$ where y = ordinate of gradient curve.

Δ = distance represented by first resistor in network.

Cyclical/

Cyclical heat flow = $\int kA \frac{dT}{dx}$ where A = area of cylinder wall exposed to vapour.

$= kA$ x area of temperature gradient diagram.

In this calculation A has been assumed to be approximately equal to 2 x valve plate surface.

Comments on Results (Presentation)

Graphs of "Reduction of Volumetric Efficiency" due to cyclical heat transfer are shown in figs. 65 to 68 .

This presentation is possible since it has been stated (page 42) that the major causes of reduced performances occur during suction and discharge.

The heat flow during suction will result in an increase in the volume of vapour in the cylinder with consequent reduction in volumetric efficiency.

An approximate value can be obtained if the process is assumed to occur at constant pressure.

The increase in volume/unit heat transfer will depend on whether (a) liquid is being evaporated or (b) vapour is being superheated.

In the section on volumetric efficiency (page 40) it was shown that $\left(\frac{\partial F}{\partial q}\right)_v = \left(\frac{\partial F}{\partial q}\right)_h$ constant in both the wet and

i shown that

s i.e. $\frac{\text{Increase of volume}}{\text{Increase of enthalpy}}$ i

The mean values for this ratio are,

.0233 ft.^{3}/B.T.U. at 5°F.

.0183 ft.^{3}/B.T.U. at 15°F.

.0144 ft.^{3}/B.T.U. at 30°F.

And at 5°F. the percentage increase in volume of vapour in cylinder = $\frac{.0233 \times \text{heat transfer/cycle}}{\text{cylinder volume}} \times 100$

$= 2.28 \times 10^3$% per B.T.U. heat transfer.

Specimen temperature gradient oscillograms are shown in figs. 62b and 63 .

The figures for heat transfer are necessarily approximate since they are based on readings from a single thermocouple.

Comments

It will be seen that the general form assumed by the curves of reduction of volumetric efficiency is similar in each case, namely a rapid increase in loss of volumetric efficiency as the suction vapour becomes wet followed by a flattening out or fall as the wetness is further reduced.

Fig. 61 shows the change in the temperature fluctuation as the wetness is increased and fig. 64 shows the reduction in temperature fluctuation when the wetness is such that the discharge vapour is no longer superheated.

The form of these Reduction in Volumetric Efficiency curves is therefore dependent on whether the discharge vapour is wet or superheated. The presence of liquid in the discharge must interfere with the condensation on the valve plate. This is most probably due to a liquid film being deposited in addition to the condensation.

It is doubtful if this occurs at the same condition on all points on the cylinder surface although eventually the process must carry to the entire cylinder.

The shape of the volumetric efficiency curves is now quite capable of explanation, that is, a rapid fall in performance as the quality is lowered, followed by a less rapid fall corresponding to the gradual increase in condensed liquid on the surfaces of the cylinder wall.

The existence of this condensed film is clearly indicated by fig. 49 in which the valve plate temperature falls rapidly as the suction vapour condition for 30°F. saturation temperature is made very wet.

ELECTRICAL ANALOGUE

It has already been stated that a considerable number of harmonics must be allowed for in the calculation of the cyclical heat transfer. The method of estimating the temperature gradient by means of a relaxation pattern, while a practical method, is not very suitable when a large number of calculations are required. This is due to the relatively slow rate of convergence of residuals.

It was therefore deemed worth while to investigate the construction of a computing mechanism to calculate these temperature gradients. An electrical analogue method seemed the most attractive and the use of a photoformer to provide the cyclical voltage waveform was decided upon.

The use of electrical analogues involving photoformers has of course been common for some time for the study of servo-mechanism problems, as shown by Korn and Korn (16). The use of analogue methods for transient heat flow has however been restricted mainly to the simple cases of step function and sinusoidal boundary conditions.

V. Paschkis and H.P. Baker (24) describe a method of R.C. networks based on finite differences as in the graphical methods of Schmidt (27). Examples are given both for one and two dimensional cases with step-functions and sinusoidal conditions and also for steady state conditions.

An analogue described by Lawson (18) made use of an electronically generated exponential waveform to feed an iterated network. In his analytical work, Lawson suggested that for a prescribed accuracy of the first section of a network, the length of subsequent sections can vary in direct proportion to the distance from the surface.

Such an arrangement was decided upon, but since the accuracy

was/

was difficult to calculate, a method similar to that adopted by Stevenson and Mitalas (32) was used to ascertain this, both in regard to the amplitude and phase-shift of the current flow pattern. This was expedited by the use of a decade oscillator and a transfer function analyser in conjunction with a transfer function resolver.

Fig. 69 shows the amplitude of sinusoidal waves penetrating from the surface of the material for various frequencies and for the network arrangements shown in fig. 70 . Fig. 71 shows the phasing of the current, i.e. the flow, at the surface for different networks. It will be seen that there can be considerable divergence from the theoretical 45° phase-shift and that where the lumping is not uniform, divergence is very great. The graph "c" shows the best arrangement between the frequency limits of 100 cycles/sec. and 2000 cycles/sec., giving 20 harmonics. This is considered to be of sufficient range to suit the equipment used in the measurement of temperature fluctuation. The shapes of the curves are indicated by the presence of small networks with short time constants in "d" and "e" giving a hump at high frequencies and the presence in all cases of a long time constant network at the end of the chain, giving emphasis to the low frequencies. The effect on the amplitude of the heat flow is not so great as on the phase-shift as can be seen from fig. 72 in which reasonable agreement is obtained with all the arrangements shown, up to quite high frequencies.

The use of non-regular networks where the current flow rather than the temperature pattern is required must therefore be preceded by a careful theoretical or experimental analysis of the system. It is convenient that at the higher frequencies where the phase-shift is smaller than 45° the amplitude is also lower than the theoretical. Hence the higher harmonics will automatically disappear. The photoformer used in the actual analogue has a noise filter fitted, which limits the output of the photoformer to about 30 harmonics.

The/

The feedback photoformer using an opaque mask, as described by Sunstein (33) was used to provide non-sinusoidal cyclical voltage variations as input functions for a direct electrical analogue by S.E. Isakoff (15).

The purpose of the analogue was to measure the performance of pulsation dampers at the outlet from reciprocating compressors.

The first arrangement adopted was as shown in fig. 73 . A photo-multiplier cell was acted upon by reflected light transmitted through a narrow slot from a uniform light source by way of a rotating drum. The drum carried a matt white surface on which was affixed a black trace whose width was proportional to the temperature fluctuation. The voltage variation on the photocell anode was amplified and fed at a low impedance to an analogue chain. This arrangement was reasonably satisfactory but suffered from several defects as noted under:-

(a) the relative reflectivity of the black and white paper had to be accurately controlled.

(b) the linearity of the phototube cathode was assumed to be adequate.

(c) the light source was assumed to be completely uniform.

Variations in any of these factors obviously must detract from the accuracy of the method and although reasonable initial success was achieved it was eventually decided to replace the reflected light source with a direct light source.

This arrangement incorporates the more usual type of photo-former circuit using the photocell as an error-indicating device to position a cathode ray. It was further considered desirable to preserve the rotating drum feature of the original machine/

machine, since adjustment of the time base trace of an oscilloscope to scan a mask is an exacting operation which incidentally introduces a fly-back period and the possibility of non-linearity in the time base sweep.

The rotating drum was therefore replaced by a perspex cylinder on to which an opaque (black) paper trace could be affixed in the same manner as before omitting, of course, the white backing sheet. The light spot is reflected on to the photocell by a mirror-lens system as shown in the block diagram of fig. 74 . The output of the phototube feeds a D.C. push-pull amplifier coupled to the cathode ray tube deflection plates. The signal is taken from one of these plates.

Design of the feed-back amplifier was found to be rather difficult due to the large scanning voltages necessary on the cathode ray tube, which was run on a fairly high E.H.T. voltage to give a sharp spot. A further difficulty which was not recognised until a considerable number of different amplifier designs had been tried and discarded was the tendency of the feed-back loop to be unstable due to excessive gain.and long time constant. (Fig.75)

The long time constant of the loop was almost entirely due to the unsatisfactory photoscanning tube used in the first arrangement. This was an ACR 10 (green) fluorescence tube and proved to have a time constant of 4·26 m.s. It is thus apparent that the spot will not faithfully follow the trace at writing speeds above 50 cycles/sec. The tube time constant exhibits itself as a delay mainly in the decay of the spot and not in its appearance. (Fig. 75)

Hence on a forward stroke in which the spot is tending to be covered, the trace is followed accurately but when the trace uncovers the spot, although the plate potential correctly deflects the spot, its afterglow causes further deflection, giving/

giving a completely distorted trace.

The accuracy of the instrument is therefore limited by loop instability and tube frequency response.

The instability displayed itself as distortion of the trace which was marked as a slight overshoot at commencement and complete unrecognisability under the gain at first adopted. After the cause of this distortion was recognised, the solution was comparatively simple, being the reduction of the cathode potential on the photocell. The high scanning voltages were attained by using S.P.61 valves which are high-slope, high-current pentodes. These were connected in a long-tailed-pair arrangement with shift facilities on the "dead" grid. This necessitated the use of a negative voltage supply to maintain the input grid at the level of the phototube anode.

The relevant photographs and circuit diagrams for the photoformer and its associated power supplies are shown in figs. 76 to 78 . It will be observed from fig. 77 that the output from the photo-former is by a cathode follower stage. This is employed to provide a low impedance source for the analogue network. The use of such low impedance cathode followers has been adopted for associated circuitry in the analogue.

Since the analogue is used to determine temperature gradient, the quantity to be measured is the current flow into the transmission line representing the cylinder wall. The current flow can be conveniently measured by noting the voltage drop across the first resistor in the line, which is proportional to current flow. The most essential part of the analogue apparatus, assuming the input voltage to be available, therefore becomes the voltage difference measuring equipment.

Differential Amplifier

The/

Differential Amplifier

The requirements here are strict linearity of output with input over a wide frequency range.

These have been adequately met in the unit shown in fig. 78 .

This is based on a well known audio-frequency phase splitting stage first developed for medical research purposes in U.S.A. and later the basis of several well known "High - Fidelity" amplifier designs.

The cross-coupling between the first and second double valves, provided heavy negative feedback and adequately compensates for slight assymmetry in the valves and components. The output can be taken from either final valve anode since the signals at these points are exactly equal, but in phase opposition.

Balancing is carried out by adjustment of the cathode potentiometer in the cathode-follower input sections. Equal signals applied to both inputs (by strapping them together) give zero output when the circuit is properly balanced.

Analogue for Radial Flow in Spheres

The accuracy of lumping in an electric circuit representing heat flow in cylindrical and spherical body is discussed by Paschkis and Heisler (24) and the values of resistors and capacitors used are determined from the physical dimensions of the cylinders and spheres. It therefore follows that the networks are not uniform. This is satisfactory for dealing with temperature distribution but when one considers temperature gradient and heat flow it has been found for flow through a slab (Fig.71) that the effect of non-uniformity in the network is very considerable when phase relationships are considered. In dealing with spheres, therefore, it is probably more accurate to use the transformation $U = Tr$ and treat the system as a linear network.

In the problem of heat flow to a sphere with a fluctuating temperature on the surface, the boundary conditions on the linear network/

network must be such that at the centre, r=0, the value of U must also be zero. Hence this end of the network will be at earth potential.

For the determination of temperature gradients we require the values $\frac{dt}{dr}$ and by differentiation of U=tr we get the expression $\frac{dt}{dr} = \frac{1}{r}\left[\frac{dU}{dr} - \frac{U}{r}\right]$

and considering the gradient at the surface and using finite increments we get $\left(\frac{dt}{dr}\right)_s = \frac{1}{r_s \Delta r}\left[U_s \times \frac{r_\Delta}{r_s} - U_\Delta\right]$

and in the electrical terms of a lumped network

$$\left(\frac{dV}{dr}\right)_s = \frac{1}{r_s \Delta r}\left[V_s \times \frac{R_\Delta}{R_s} - V_\Delta\right]$$

Referring to the circuit diagram for the analogue, fig. 79, it will be seen that the fraction of the input voltage $V_s \cdot R_\Delta/R_s$ can be taken off by a potentiometer across the input of the network and that the required difference $\left[V_s \cdot \frac{R_\Delta}{R_s} - V_\Delta\right]$ can be obtained by using the differential amplifier as for a linear network. It has been found that the proportion of the input voltage must be picked off with extreme accuracy. This is facilitated by the fact that if a direct current is fed to the input of the network, the proportion of the input given by R_Δ/R_s will be at the same potential as the first iterated point on the network. A micro-ammeter placed across these two points on the potentiometer to be accurately found. enables the setting

To complete the investigation on the suitability of the analogue shown, sinusoidal inputs were applied at the surface of the chosen analogue chain (i.e. arrangement C,) for varying frequencies. Amplitude and phase-shift down the chain were noted, and are shown in figs. 80 and 81. Theoretical curves are shown for comparison. Similar curves have been drawn for the network simulating radial heat flow in spheres. These are shown in figs. 82 to 85.

It/

It will be observed that the amplitude relationships are much more closely followed than the phase relationships and it is these phase relationships which are the limiting factor in the use of passive networks. This has been pointed out by Stevenson and Mitalas although their remarks referred to uniform networks. It will also be seen from fig. 81 that the use of non-uniform networks can give very considerable phase distortion, although the amplitude relationships are adequately matched for a considerable frequency range. Hence if a complex waveform is applied to the surface of the network, then it is important that a considerable length of uniform network be placed at the beginning of the chain if phase distortion of the current of heat flow waveform at the surface and subsequently down the chain is to be avoided. In such cases, it is probable that the use of an active uniform network would give better results. It will be seen from the above investigation that the most suitable fundamental frequency for the input waveform to the photo-former is about 100 cycles per second.

This corresponds to four diagrams on the drum trace when the drum is rotated at 1500 revs. per minute. This value is chosen since a synchronous motor running at 1500 rev./min. was fitted to the photo-former. The use of a synchronous motor enables a very steady trace to be shown on the cathode ray tube since any 50 cycles/sec. interference or hum will itself be stationary on the tube and synchronisation of the trace for photography is simplified.

ELECTRICAL ANALOGUE

BASIC FORMULAE

For 1-dimensional heat flow in an infinite slab,

$$\frac{d\tau}{d\tau} = \alpha \frac{d^2\tau}{dx^2}$$

and for current flow in an infinite cable with zero inductance,

$$\frac{dV}{d\tau} = \frac{1}{R_e C_e} \frac{d^2V}{dx^2}$$

These are analogous if $\alpha = \frac{1}{R_e C_e}$ and $\tau_t = \tau_e$

but a change in time scale is possible if $n = \tau_t/\tau_e$ is introduced.

Also by writing $R_e = R_s/\delta x$

and $C_e = C_s/\delta x$

we may write $\frac{dV}{dn\tau_e} = \frac{\delta x^2}{R_s C_s} \cdot \frac{d^2V}{dx^2}$

Hence $\delta x^2 = \alpha n R_s C_s$

and $\tau_t = n\tau_e$

or for sinusoidal components,

$nN = \omega$ where N = Thermal frequency
ω = electrical frequency

For a film resistance represented by R_i',

film thickness = k/h_f

Distance represented by $R_i' = \frac{R_i}{R_s}\delta x$

$$R_i = kR_s/h_f \delta x$$

Formulae Used in Constructing Theoretical Curves

(A) For temperature at any depth in an infinite slab, due to cyclically varying surface temperature, $\tau = \tau_s e^{-x\sqrt{N/2\alpha}}$

or electrically, $V = V_s e^{-\frac{x}{\delta x}\sqrt{\omega R_s C_s/2}}$

Phase/

Phase lag of waveform, $\psi = x\sqrt{N/2\alpha}$

or electrically, $\psi = \frac{x}{\delta x}\sqrt{\frac{\omega R_s C_s}{2}}$

Temperature gradient at surface is given by,

$\left(\frac{dt}{dx}\right)_s = t_s\sqrt{\frac{\omega}{\alpha}}$ or electrically, $\frac{dV}{dx}_s = \frac{V_s}{\delta x}\sqrt{\omega R_s C_s}$

Phase displacement = 45°.

(B) For radial heat flow in a sphere, with cyclically varying surface temperature, graphs are plotted on to a base,

Ratio $\frac{\text{Radius}}{\text{Outer Radius}}$

or $\phi = \sqrt{\frac{\pi \nu_s^2}{\alpha T}}$ (Thermal)

$\phi = \frac{\nu_s}{\delta x}\sqrt{\frac{\omega R_s C_s}{2}}$ (Electrical)

Amplitude at any radius is derived from,

$$\frac{U}{U_s} = \frac{\sinh (1+i)\phi \, \nu/\nu_s}{\sinh (1+i)\phi}$$ where $U = t\nu$

and

$$\frac{t}{t_s} = \frac{\nu_s U}{U_s \nu} = \frac{\nu_s \sinh(1+i)\phi \, \nu/\nu_s}{\nu \sinh(1+i)\phi}$$

$= V/V_s$ (Electrical)

Phase lag of waveform is given by,

$\psi = \text{Arg.} \sinh (1+i)\phi \, \nu/\nu_s$

Temperature gradient at surface,

$$\left(\frac{dt}{d\nu}\right)_s = \frac{t_s}{\nu_s}\left[\frac{(1+i)\phi \cosh 1+i\phi}{\sinh(1+i)\phi} - 1\right]$$

$= (dV/dv)_s$ (Electrical)

Phase displacement of gradient curve is given by,

$$\psi = \text{Arg.}\left[\frac{(1+i)\phi \cosh(1+i)\phi}{\sinh(1+i)\phi} - 1\right]$$

EVAPORATION OF ENTRAINED DROPLETS

In a compressor running at high speed it cannot reasonably be assumed that liquid induced into the cylinder during a wet suction process will be evaporated before the end of the delivery stroke. This has previously been suggested by Smith (29).

The size of droplet is difficult to estimate but in the discussion which follows, droplet sizes of 25, 50 and 80 microns have been assumed as representing a reasonable distribution of droplet diameter.

The process of heat transfer between the liquid and the surrounding vapour will occur by evaporation, condensation and sensible heat exchange. These are illustrated in fig. 86

Diagram "A" shows the vapour transferring heat through a superheated film and since the surface temperature of the droplets is lower than the saturation temperature of the vapour, condensation is taking place. The heat being transferred at the interface to the droplets will comprise,

(a) the sensible heat of the superheated vapour $(t_v - \pi)h_f$

(b) the latent heat of condensation λh

This heat absorbtion by the droplets must be equal to the heat transfer at the surface given by $-k\frac{dt}{dv}$

Diagram "B" shows the droplets evaporating into the vapour stream. In this case, the λ is positive but if we examine the general expression for the interchange at the surface of the drop $(t_v - \pi)h_f + \lambda h + k\frac{dt}{dv} = 0$ we see that for evaporation, i.e. a negative value of λ, $\frac{dt}{dv}$ can be positive or negative, depending on the value of $(t_v - \pi)h_f$

With condensation, however, the value of $\frac{dt}{dv}$ will always be negative. This is illustrated in diagram "C". This shows a negative temperature gradient at the surface gradually reducing to zero, with condensation or evaporation taking place depending on/

on whether $(T_v - T)h_s$ is less than, or greater than $\frac{dT}{dv}$. The lower diagram, "D" shows the corresponding growth and decay of the drop size.

It has been indicated by G. Brown (5) that the temperature of a droplet in contact with its vapour, is defined almost exactly by the saturation temperature of the vapour. To check on this, the condensation coefficients of Freon 12 under varying conditions of pressure and superheat were evaluated by the method of Silver (28). Fig.87 shows these condensation coeffieients. A typical estimation of λ gives a value of about 1% of the vapour superheat which is quite negligible. From the above, it is clear that the surface temperature of droplets existing during a compression cycle can be estimated with reasonable accuracy from the indicator diagram. This is done by taking the saturation temperature corresponding to the pressure. Knowing this surface temperature fluctuation, it is possible to calculate the surface temperature gradient necessary to maintain the temperature pattern.

In order to determine whether condensation or evaporation is taking place, it is necessary to know the vapour film coefficient. This is extremely difficult to calculate, but an approximation has been made as shown below. This calculation is subject to various simplifying assumptions including:

(a) The droplets are assumed to enter the cylinder without swirl. this has been shown by Alcock (/) to be correct for cylinders and pistons of the kind used in the compressor.

(b) It is assumed that compression of vapour continues in an isentropic fashion as though no heat exchange was undertaken with the droplets. The amount of superheat actually existing in the vapour will therefore be less than that assumed in the calculation.

(c) The gas velocity through the suction valve is assumed to be proportional/

(c) proportional to the ratio of piston area to valve port area.

Relative velocity between the vapour and a liquid droplet is determined by considering the drag force and inertia force acting on the droplet. This drag force has been determined from the settling speed of the sphere in the vapour. The velocity of a droplet of liquid entering during the suction stroke can therefore be determined throughout the compression and delivery stroke. Fig. 88 shows the velocity of droplets at various points during the compression stroke. These curves are drawn to a base of the point of admission of the droplet during the suction stroke.

The mean height of these curves gives the mean velocity of droplets during the compression and discharge stroke. Curves of mean velocity are shown in fig. 89 . for 25, 50 and 80 microns diameter droplets.

Knowledge of these velocities enables the heat transfer coefficient between the liquid and vapour to be calculated. These are made on the Nusselt - Reynolds relations, shown on fig. 90 . Below Re=1000, the expression $Nu = 2 + \cdot 6(R_e)^{\cdot 5}$ is used and above Re=1000, the expression $Nu = \cdot 33(R_e)^{\cdot 6}$

The Prandtl number has not been introduced into the Nusselt-Reynolds expression since for Freon 12 vapour under conditions obtaining, the Prandtl number is sufficiently near unity for this to be neglected.

The electrical analogue was that used to determine the accuracy of lumping for radial heat flow in spheres (page 60). The input however, was provided by the photoformer and comprised a saturation temperature curve for "wet" compression (suction dryness 0.7; saturation temperature at suction 5°F; saturation temperature at discharge 100°F, speed 750 r.p.m.). To simulate conditions/

conditions in the cylinder as closely as possible, the trace inserted on the photoformer drum consisted of one cycle of temperature excursion, followed by one cycle at suction temperature. This ensured that the condensers in the network were fully discharged at the beginning of compression, as would of course occur in the compressor cylinder where droplets at the beginning of compression would be at a constant temperature equal to the suction temperature. The time required to cause the condensers in the analogue chain to be fully discharged was checked by applying a step function to the input of the chain and noting the time taken for the last condenser in the chain to reach equilibrium conditions. This was greatest in the case of the network comprising 51 K. resistors and was about 3 m.s. (fig. 79).

Since the system is in a steady state for one half revolution of the drum i.e. 20 m.s. it may be assumed that the condensers are fully discharged at the beginning of compression.

When the steady phase before compression is not allowed, the alteration in the temperature gradient is seen by comparing figs. 91a and 91b. The oscillograms for the temperature gradients are shown in fig. 92 and the diagrams on fig. 93 show the temperature gradients with calculated values of heat transfer through the vapour film superimposed. These diagrams correspond to Diagram "C" of fig. 86 .

In each case it will be seen that during the first part of the cycle the temperature gradient curve is above the heat transfer curve. This means that condensation is occuring on the surface of the droplets. During discharge and re-expansion the heat transfer exceeds the temperature gradient and evaporation is therefore occuring. On the assumption that the size of the droplet is unaltered, the figures of Table A have been calculated.

TABLE A

Droplet Dia. (inch)	Evaporation after T.D.C. (%)	Condensation on drop up to T.D.C. (%)
.001	33.7	10.3
.002	36.3	14.8
.003	45.5	1.0

These figures indicate that during compression and discharge the droplet is virtually unchanged in size and that during the re-expansion stroke about 30% of the droplet is evaporated. If it is assumed that all the droplets remain in the clearance space then the reduction in volumetric efficiency due to the "flashing" of these droplets can easily be calculated. The curves of fig. 94 show the reduction in volumetric efficiency based on the above assumption. As the suction vapour condition becomes progressively wetter, the degree of superheat during compression will be reduced. Increased condensation on the droplets will result from the fall in sensible heat transfer from the vapour and a reduction in the "flashing" during re-expansion will also occur.

The effect of variation in compressor speed was investigated by modifying the speed of the rotating drum of the photoformer to determine the temperature gradient at the surface of the droplets Fig. 95 shows the values of temperature gradient and Nusselt Number drawn on a basis of speed ratio.

It will be seen that the rate of increase of Nusselt Number is greater than the rate of increase of heat transfer coefficient so that the condensation during compression will be reduced and the evaporation during re-expansion will be increased, as the compressor speed is raised.

The/

The variation in these quantities is not, however, considerable, and since at the higher velocities the drop size distribution is probably considerably modified, it would appear that the values calculated for 750 rev./min. can be applied over a wide range of speeds.

Drop sizes outwith the range considered (.001" - .003" dia.) have similar characteristics unless (a) the drops are very large, or (b) the drops are very small.

(a) Very large drops will, by their inertia, impinge on the walls of the cylinder and form a film without rebounding. This has been shown by Garner (12) to apply for droplets of up to 200 μ (.008") diameter striking a baffle plate.

(b) Very small droplets are probably completely evaporated during the latter part of the compression and discharge stroke. This is indicated by the following approximate calculation.

Heat Transfer to Very Small Droplets

If it is assumed that there is no relative motion between the droplets and the vapour, then Nu = 2.

It is further assumed, as before, that the heat transfer through the vapour film is the controlling factor and that means transfer will proceed at a higher rate than this.

To simplify calculation, the process is confined to a droplet which is (1) at a uniform temperature equal to saturation temperature.

(2) in a constant environment 20°F. superheated.

(3) the duration of the process corresponds to the discharge stroke of the compressor at 750 rev./min. (50°).

$$Nu = 2 = h \frac{d}{k}$$

$$\text{Rate of evaporation of droplet} = \frac{\text{Total Heat Transfer}}{\text{Latent Heat}}$$

i.e. rate of evaporation of droplet $= \frac{h A \Theta}{L}$

$$= - \frac{dw}{dt}$$

$$\frac{dw}{dt} = - \frac{4 \pi \Theta r^2 k}{r L} \qquad (h = \frac{2k}{d}) \quad (a = 4 \pi r^2)$$

also $W = V\rho = \frac{4 \pi r^3 \rho}{3}$

$$\frac{dw}{dr} = 4 \pi r^2 \rho$$

now $\frac{dr}{dt} = \frac{dr}{dw} \cdot \frac{dw}{dt}$

$$\frac{dr}{dt} = - \frac{\Theta k}{r L \rho}$$

or $dt = - \frac{Lr\rho}{k\Theta} dr$

$$t = + \frac{Lr^2\rho}{2\Theta k} \Big|_o^r$$ for complete evaporation.

$3.13 \times 10^{-6} = 2.89 \times 10^4 \, r^2$ for the conditions assumed.

$r = 1.04 \times 10^{-5}$ ft.

Droplet diameter = $\underline{0.25 \times 10^{-3} \text{ in.}}$

i.e. droplets below this size are completely evaporated.

This estimate is probably high since no account has been taken of the thermal capacity of the droplet or of surface tension at the vapour-liquid interface. The effect of surface tension can be considered by using the method of Laine (17) to estimate the surface tension for Freon 12 at the conditions assumed. This is low (approx. 10 dyne/cm.) so that the pressure across the interface is small with only .456 lb./in.^{2} for a .001 in. dia. droplet.

However/

However, as the droplet is evaporated, the increase in pressure could become significant. Assuming the effect to be important, when the pressure difference corresponds to half of the vapour superheat (about 19 lb./in.^{2}) the droplet diameter is then 2.4×10^{-5}in.

Droplets reduced to this size even from 5×10^{-5}in. (1μ) have lost 90% of their mass so that the effect of surface tension may be ignored in all cases.

Note:- The distribution of droplet diameter, in the first instance is determined by the mode of evaporation in the calorimeter as investigated by Newitt (21).

The size distribution is further modified by the "baffle" action of the suction valve reed. The impingement, spreading and tearing off which occurs at the valve results in a mixture of large and small droplets, quite independent of the distribution at the compressor suction manifold.

Examination of the graphs of indicated volumetric efficiency which would reflect increase in the volume of the expanded vapour shows that the reduction in indicated volumetric efficiency is quite small and therefore the assumptions which have been made are obviously not correct. It is improbable that all of the liquid would remain in the clearance space, even when the suction vapour is almost dry. Certainly when the dryness fraction falls below about .8 the discharge vapour is wet.

Garner (12) investigated the action of baffles on the liquid particles and it is probable that a considerable amount of the liquid impinging on the valve plate and piston surfaces spreads as a thin film and does not leave with the vapour at all.

This liquid film on the cylinder wall would of course reduce the condensation which takes place when the mean temperature of the cylinder wall is less than the temperature corresponding to the saturation pressure of the vapour. This is reflected in the cyclical temperature fluctuations on the cylinder wall which show/

show a reduction when the discharge temperature falls to the saturation temperature at discharge, indicating the presence of liquid in the discharge stream and possibly an extensive amount of liquid on the cylinder surfaces. This has been discussed on page 54 .

GENERAL CONCLUSIONS AND COMMENTS

The development of a satisfactory analogue for the analysis of cyclical heat flow problems has been described. The investigation of the accuracy of passive networks indicated the desirability of a uniform section at the input end of the network to avoid serious errors due to phase distortion of current flow. This is contrary to a suggestion by Lawson (18) probably referring only to voltage, that lumps of varying length be placed at the input.

The processes affecting the transition from superheated suction to wet suction have been analysed and the following have been inferred:

1) Piston leakage has little effect on the volumetric efficiency during the transition.
2) The effect of valve leakage was not measured, but the small change in leakage past the piston suggests that the action of the valves will be similarly affected by change of suction condition.
3) Droplets entering with the vapour at suction may exist and even grow during compression but the existence of free droplets is limited and liquid which remains in the cylinder spreads on the cylinder walls to be evaporated, in part, during the suction stroke, causing rapid fall in cylinder wall temperature.
4) The principal cause of inferior performance during wet compression is cyclical heat transfer between cylinder wall and charge, the reduction in volumetric efficiency due to this being approximately calculated from cyclical temperature fluctuation at the cylinder wall.

Calculation of heat transfer coefficients has not been included since, as Overbye (23) stated, negative values of heat/

heat transfer coefficient are obtained.

This was found by the author to be very pronounced when the suction vapour was wet and condensation or evaporation was taking place.

Overbye contended that the assumption of quasi-steady state heat transfer was unjustifiable due to thermal capacity in the fluid. This was supported by Annand (2) and is in line with the author's findings.

The electrical analogue described has been modified to analyse the flow of air in the lung and is the subject of a paper by the author (8).

Development of the equipment to allow for non-linearity in airway resistance and compliance is being carried out.

ACKNOWLEDGMENTS

The research was carried out in the Laboratories of the Mechanical, Civil and Chemical Engineering, Department of the Royal College of Science and Technology.

The author would like to thank Professor A.S.T. Thomson for the provision of these facilities and the interest which he and Professors A.W. Scott and J.C. Orkney showed in this work.

Mr. W.B. McHutchison provided much helpful assistance in the design of the photoformer and thanks are due to him and other members of the staff for encouragement and practical assistance in the preparation of this thesis.

In conclusion the author would like to thank the technicians of the department, especially Mr. C.W. Richardson, who gave such enthusiastic and patient assistance.

APPENDIX 1.

BIBLIOGRAPHY

Ref.No.		
1	Alcock, J.F.	"Air Swirl in Oil Engines" Proc. I.Mech.E. Vol.128, 1934. p.123.
2	Annand, W.J.D.	"Heat Transfer in the Cylinders of Reciprocating Internal Combustion Engine". I.Mech.E. (Thermodynamics & Fluid Mechanics Group) 1963.
3	No Author	"Properties of Commonly-used Refrigerants" Air Conditioning & Refrigerating Machinery Association, Inc.
4	Bendersky, D.	"A Special Thermocouple for Measuring Transient Temperatures" Mech.Eng. N.Y. 1953, Vol.75, p.117.
5	Brown, G.	"Heat Transmission by Condensation of Steam on a Spray of Water". General Discussion on Heat Transfer, I.Mech.E., London, 1951.
6	Brown, J.	"Cyclical Heat Interchanges Between Charge & Cylinder in a Refrigerating Compressor Operating on Freon 12" General Discussion on Heat Transfer, I. Mech.E., London, 1951.
7	Callander, H.L. & Nicolson, J.T.	"Condensation of Steam in Steam Engines & its Measurement" Engineering, Vol.64, p.481, 1897.
8	Campbell, D. & Brown, J.	"Electrical Analogue of the Lung" British Journal of Anaesthetics, Nov. 1963.
9	Eichelberg, O.	"Zeitlicher Verlauf der Warmenbertragung in Dieselmotor" Geb.Ing.Wes. H.300 (1928) p.61-66.
10	Elser, K.	"Der Instationare Warmenbergang in Dieselmotoren" Mitt.15 Inst.Thermodyn Verbrennungsmotorenbau, E.T.H.Zurich, 1954.
11	Fuchs, R., Hoffmann E. & Plank, R.	"Tests with a High Speed Six Cylinder Ammonia Compressor". Z.d. V.D.I.1940, Vol.84 No.16, p.265.

BIBLIOGRAPHY, Contd.

Ref.No.		
12	Garner, F.H. et al	"The Size Distribution & Entrainment of Droplets" Transactions of Inst. Chem. Eng. Vol.32, 1954.
13	Giffen, E. & Newley, E.F.	"Refrigerator Performance, An Investigation into Volumetric Efficiency" Proc. I.Mech.E. 1940, Vol.143, p.227.
14	Gosney, W.D.	"An Analysis of the Factor Affecting Performance of Small Compressors" Proc. I. Refrig. 1952-53.
15	Isakoff, S.E.	"Analysis of Unsteady Fluid Flow, Using Direct Electrical Analogues" Ind. & Engineering Chemistry, Vol.47, 1955, p.413.
16	Korn & Korn	"Electronic Analogue Computers" (McGraw Hill) 1942.
17	Laine, P.	"Surface Tension of Freons" Report No.129, Section 55, 4th International Congress on Industrial Heating, Paris, 1952.
18	Lawson, D.I. & McGuire, J.H.	"Solution of Transient Heat Flow Problem by Analogous Electrical Networks" Proc. (A) I. Mech.E. Vol.167, No.3, 1953 p. 246.
19	Lorentzen, G.	"Leveringsgrad og Virkringsgrad for Kjølekompressorer" Fiskeridirektoratet, Bergen, 1949.
19a	----------	"Performance of Automatic Compressor Valves" Proc. 9th Int. Congress of Refrigeration p.3, 1955.
20	McLaren, J.F.T.	"Valve Behaviour & the Performance of Small Compressors" Proc. I. Refrig., 1954.
21	Newitt, D.M. et al	Liquid Entrainment. "The Mechanism of Drop Formation from Gas on Vapour Bubble Transactions of Inst.Chem.Eng. Vol. 32 1954.

BIBLIOGRAPHY, Contd.

Ref.No.		
22	Oguri, T.	"On the Coefficient of Heat Transfer Between Gases & Cylinder Walls of the Spark-Ignition Engine" Bull.Jap. Soc. Mech.Eng. 1960, Vol.3, p.363.
23	Overbye, V.D. et al	"Unsteady Heat Transfer in Engines" Trans. of Soc. Automat. Eng. N.Y. 1961, Vol.69, p.461.
24	Paschkis V, & Baker, H.D.	"Heat Transfer Analogue" Trans. A.S.M.E. Vol.64, p.105, 1942.
25	Paschkis V. & Heisler, M.P.	"The Accuracy of Measurements in Lumped R-C Cable Circuits as used in the Study of Transient Heat Flow". Trans. Amer. Inst. Elect.Engineers, Vol.63 p.165, 1944.
26	Pearson, S.F.	"Component Losses in Refrigeration Compressors" Thesis for Ph.D. Glasgow, 1957.
27	Schmidt, E.	"Thermodynamics" 1949, p.428. Oxford University Press.
28	Silver, R.S.	"Heat Transfer Coefficients in Surface Condensers". Engineering, Vol.161, 1946.
29	Smith, E.C.	"Determination of Mass Flow in a Vapour Compression Refrigerator" Thesis for Ph.D. London, 1934.
30	Smith, H.J.	"Effect of Piston/Bore Clearance in Small Refrigeration Compressors" Proc. Inst. Mech.E 1961, Vol.175, No.22.
31	Sneeden, J.B.C.	"Introduction to Internal Combustion Engineering" Longmans, 1938, p.226.
32	Stevenson, D.G. & Mitalas, G.P.	"Lumping Errors of Analog Circuits for Heat Flow through a Homogeneous Slab" International Developments in Heat Transfer, A.S.M.E.,A.I.C.E.,I.Mech.E. and I.Chem.E. Boulder, Colorado and London. (Repeated) 1961.

BIBLIOGRAPHY, Contd.

Ref.No.		
33	Sunstein, D.E.	"Photo-electric Waveform Generator" Electronics, Vol.22, p.100, Feb. 1949.
34	No Author	"Temperature - its Measurement & Control in Science & Industry". American Inst. of Physics, 1941.
35	Wirth, G.	"The Influence of Cylinder Wall Temperature on the Performance of a Refrigerating Compressor". Zeitschrift fur die Gesamte Kalte-Industrie, Vol.40, No.9, Sept.1933 p.138-44.

INDICATING MECHANISM

For successful indication of a refrigeration compressor, the mechanism should satisfy the following requirements:-

(a) independence of pressure waveform frequency.
(b) calibration by a static pressure.
(c) insensitivity to change in temperature.
(d) sealed against leakage of vapour from cylinder.
(e) modification of clearance volume small or zero.
(f) simple and reliable construction.

The above requirements eliminate the mechanical indicator due to its poor frequency response and large clearance requirements. The modified "Farnborough" indicator as used by Giffen and Newley (13) is worthy of consideration, but in the case of a 1½" diameter cylinder with minimum clearance, a more compact pressure transducer is desirable.

This points to some type of electronic indicator and to facilitate machining, a small condenser type of pressure transducer is capable of satisfying the above requirements.

To accommodate zero and low pressure indications, a high frequency modulated carrier wave principle may be employed.

Following the above principles, the indicating mechanism described below was designed and built.

Electronic Circuitry

Fig. 96 shows the circuit and block diagrams of the signal transducing unit or Element Amplifier.

The block diagram shows the oscillator and amplifier feeding two identical channels comprising buffer amplifier input stage, biassing section and demodulator. The output is fed to a double-beam Cossor D.C. oscilloscope.

The circuit diagram shows a series-valve stabilised power pack supplying H.T. as 270 V. to the entire unit. Such a pack reduces ripple to the minimum and assists in maintaining the frequency/

frequency stability of the oscillator. A Colpitts electron-coupled oscillator supplied a small R.F. carrier output at 1.6 Mc/s. to a tuned amplifier. This frequency is used since being an intermediate frequency for broadcast radio receivers, tuned transformers of high quality can easily be obtained.

The pentode buffer amplifiers were found to be necessary to prevent common capacitances in the two channels feeding signals from one channel into the other.

The input section consists of a coil, variable condenser, the pressure transducing elements and associated cable.

This is followed by a biassing section which removes any unwanted carrier by operating an amplifier under class "C" conditions. This is necessary, since under certain circumstances the modulation is only a small percentage of the carrier voltage. Variable bias is obtained from a potentiometer across the H.T. supply. The mode of operation is illustrated in fig. 97 .

The output signal is passed to a diode rectifier followed by a network to remove any trace of ripple introduced in the H.T. supply. This was found to be barely necessary in the final layout of the unit.

The micro-ammeter shown is useful for setting-up purposes and enables the trace to be set on the screen of the oscilloscope with the minimum of difficulty.

Modulation

The carrier voltage is amplitude modulated in the input section by varying the impedance of the circuit and thereby altering the voltage across it.

Fig. 98 (a) shows the buffer amplifier and input section in skeleton form, and fig. 98 (b) shows the simplified equivalent circuit. In this, the coupling of the transformer is assumed to be perfect.

voltage $V = \mu E_g \frac{Z}{R_a + Z} = \mu E_g \left(\frac{1}{R_a/Z + 1} \right)$

where Z = impedance of series parallel network r, L & C

hence $V = \mu E_g \left[\frac{1}{\left(\frac{R_a}{r + i\omega L}\right)(1 + i r \omega C - \omega^2 L C) + 1} \right]$

simplifying to

$$V = \frac{K}{A - BC}$$ where K, A and B are constants.

$K = (r + i\omega L)\mu E_g / R_a$

$A = (1 + i\omega L + r) R_a$

$B = (\omega^2 L - i\omega r)$

For maximum rate of change of voltage with change in capacity dV/dC should be maximum.

i.e. $KB/(A-BC)^2$ is maximum

and since only C is variable,

dV/dC is maximum when $(A - BC)$ is minimum.

$1 + \frac{i\omega L + r}{R_a} - (\omega^2 L - i\omega r)C$ is minimum.

Separating Real and Unreal parts,

minimum when $1 - \omega^2 L C = 0$ (r/R_a negligible)

which is resonance for the input circuit.

Hence the variable capacitor is adjusted so that the circuit is near resonance to give maximum sensitivity.

In normal use, the operating condition is somewhat off resonance to maintain the calibration as linear as possible.

The effect of frequency drift is similar to that of variation in capacity and causes a change in the impedance of the input section which alters the output voltage. Frequency stability is therefore of first importance.

For a small change in capacitance, the change in voltage may be assumed as almost linear, since $V = \frac{K}{A - BC}$ and for a small increase in C equal to δC,

$$\delta V \simeq \frac{K B \delta C}{[A - B C]^2}$$

i.e. δV is proportional to δC.

In the pressure transducer element, the movement is small compared with the gap between the pin and the diaphragm, so that/

that the change in capacitance is almost proportional to change in pressure.

thus:-

capacity of element = $\frac{k}{x^2}$ where x is distance between plates of element.

displacement due to pressure = mp

hence for a pressure p the capacity becomes, $k/(x-mp)^2$

or, the change in capacity = $2mpk/x^3$

which is proportional to p.

i.e. <u>the change is pressure is approximately proportional to the change in voltage at the output of the unit</u>.

The indicating mechanism described proved to be extremely sensitive and provided a "warming-up" time of about two hours was allowed, the stability of the equipment was adequate. To improve stability, the use of crystal-controlled oscillators was considered. Since this involved a complete re-design of the equipment, opportunity was taken to employ the most modern electronic techniques.

The rather simple circuit shown in fig. 99 was evolved. Two such pieces of equipment were of course required and to avoid interaction the crystal-controlled oscillators were set at slightly different frequencies. The response of the unit to a suddenly switched-in capacitor is shown in fig. 100. This response shows an excellent zero-frequency and high frequency characteristic.

APPENDIX 111.

AIR CIRCUIT TESTS

It was decided to carry out a series of tests on the compressor using air and the working fluid. The purpose of the tests was two-fold:

(a) as a means of developing a suitable indicating mechanism.

(b) to observe the characteristics of the compressor over a range of speeds.

It was early evident that available methods of measuring the air flow were inadequate for the small quantities delivered by the compressor.

Orifices form a convenient and accurate method of steady flow measurement but the flow through the smallest standard orifice (0.25 in. dia.) was insufficient to exceed the critical Reynolds Number for the orifice, as well as giving a quite inadequate head on the manometer.

A range of sharp-edged orifices of small diameter operating over suitable ranges was therefore constructed and being outwith standard dimensions were calibrated individually.

The method of calibration is outlined and curves of coefficient of discharge are included in fig. 117&118.

The orifices were calibrated in the approach tube used during the tests to maintain accuracy.

Summary

After using the test layout to develop the indicating mechanism described under its own heading, the following series of tests were carried out on the compressor:-

(a) constant speed and suction pressure - varying pressure ratio.

(b) constant suction pressure and pressure ratio - varying speed.

(c) constant speed and pressure ratio-varying suction pressure.

Actual/

Actual and indicated performances are measured and illustrated on the various graphs.

Descriptions of the apparatus, test procedure and reduction are appended along with sample calculations.

Complete sets of readings etc., are not included but are illustrated in graphical form.

It can be stated also that the compressor is a standard production model, designed to run at 600 r.p.m. and as can be seen from its performance, was exceedingly efficient even at speeds of 1750 r.p.m., though the balance of the reciprocating masses left something to be desired at such a speed.

This was remedied to a great extent before the series of tests on the refrigeration circuit was carried out.

Apparatus

Fig. 106 shows the line diagram of the apparatus.

The compressor and indicator mechanism are as used in the refrigeration tests.

The suction manifold enables the pressure of the suction gas to be controlled either by throttling the main suction valve or by applying high pressure air from the large tank shown. Connections from the suction and discharge service valves to the auxiliary compressor are used in calibrating the indicating mechanism.

Flow measuring equipment and its calibration are described at the end of this appendix.

Suction and discharge temperatures and pressure are measured by thermocouples and calibrated Bourden-type pressure gauges. Vacuum is measured by a mercury manometer.

Test Procedure

During tests at atmospheric suction pressure, the main suction valve was kept wide open except during pressure element calibration. The discharge pressure is adjusted by the throttling valve/

valve at the approach tube inlet.

When steady conditions obtain, readings are taken simultaneously and then an indicator diagram recorded on the drum camera. The compressor is immediately stopped and atmospheric pressure obtained in the compressor by closing the discharge service valve and moving the piston to B.D.C. when the suction reed valve falls open and renders the cylinder open to atmosphere.

The correctness of this was checked by connecting the cylinder of a similar compressor to a pressure gauge. It was observed also that the suction gauge recorded the cylinder pressure even when a high pressure was maintained on the compressor discharge. This is utilized to obtain a datum line on the diagram when the compressor is in the refrigeration test circuit.

This datum is recorded on the indicator diagrams and the camera is removed from the oscilloscope when air from the pressure tank is admitted to the cylinder and corresponding readings of suction pressure (equal to cylinder pressure) and spot deflection on the oscilloscope screen are noted.

A great deal of time cannot be allowed for readings, as due to the high adiabatic constant of air compared to Freon 12, considerable cylinder heating takes place.

Where suction pressures are above atmospheric, the main suction valve is partially closed, suction gas being provided from the high pressure supply tank whose compressor is run continuously. Excess discharge from this compressor is passed to atmosphere through the main suction valve which acts as a suction pressure regulator. Calibration is carried out as in the previous case.

For sub-atmospheric suction pressures, throttling of the supply to the manifold enables the desired condition to be attained. The calibration procedure is slightly varied for sub-atmospheric pressures, since these must be supplied from a/

a vacuum source.

To maintain the suction reed value open, the byepass valve across the suction and discharge service valves is opened. This byepass connection is across the pressure tappings and when the service valves are closed still maintain contact with the compressor head. The suction connection of the service air compressor provided a convenient source of vacuum when partially closed.

A small "Farnborough" type element was ultimately constructed, as shown in fig. 105 so that a datum could be obtained without disturbing running conditions. The back-pressure port was put into connection with the suction manifold so that the points on the cycle where suction pressure was attained could be shown. This element was used in later tests both with air and with refrigerant. In this instance, the drum camera was dispensed with and the Cossor 35 m.m. camera was used in its place. The oscilloscope therefore displays on one channel the pressure diagram and the other channel the datum pressure diagram, together with a phase-mark. This datum pressure element was used in conjunction with the indicator element described on page 17 and shown in fig. 13 . Since this element is calibrated by means of a back-pressure and the datum is properly phased by the "Farnborough" element it will be seen that calibration can be carried out while the compressor is running. Photographs of the apparatus are shown in figs. 104, 107, 108 .

Leakage Measurement

Leakage past the piston is measured in the same manner as for the refrigeration compressor, using the same apparatus for the purpose.

Cyclical Temperature Measurements

Measurements of cyclical temperature fluctuations on the valve plate when air was used as a working fluid, was not possible/

possible while the Joubert contact was in use, due to the transient nature of the air tests. It was possible, however, to take such measurements when electronic recording by means of the Cossor preamplifier and oscilloscope was adopted.

Comments on Results

The results of these tests are shown on the graphs, figs. 109 to 114.

The graphs of actual performance are interesting in that the volumetric efficiency on a basis of speed does not show a maximum value even at 1750 r.p.m. while below 750 r.p.m. the performance falls off considerably.

Indicated volumetric efficiency is almost constant over the entire speed range.

The curves drawn on a basis of pressure ratio show the falling off in performance as the pressure ratio is increased.

On a basis of suction pressure a maximum is attained. This is reached, because at low pressures, losses in the valves due to blow-by and inertia are increased, while at high pressure, the leakage due to large pressure difference across the piston and valves becomes important.

Indicated performance shows a slight rise as the suction pressure is increased.

Indicated power curves, as taken from the indicator diagrams, are in excess of the power requirements for adiabatic compression. This is due in part to the large pressure drop across the discharge valve and also to leakage effects.

Leakage figures are discussed in conjunction with the results for leakage of refrigerant (page 48).

Orifice Calibration

The sharp-edged orifices are based on B.S.S. 1042-1934 but due to the small diameter, these were calibrated individually and the calibration rig utilized the apparatus of fig. 115 . This shows a small compression unit feeding air to a pressure tank fitted with a pressure gauge.

This tank is connected by a very short length of pipe to the control valve and approach tube. The approach tube is 4ft. long and $3\frac{1}{2}$" diameter with an upstream pressure tap conforming to B.S. recommendations at $3\frac{3}{4}$" from the orifice. The downstream side of the orifice is open to atmosphere.

The arrangement from the control valve is therefore the same as in the compressor test unit.

Theory

If air is discharged from a tank in an isothermal manner, the rate of flow is derived from the general gas law, $pv = wRT$,

rate of flow $\frac{dw}{dT} = \frac{d}{dT} \cdot \frac{pV}{RT}$

$\frac{v}{RT} \cdot \frac{dp}{dT}$

i.e. the rate of pressure drop is proportional to the mass flow.

Theoretical flow through the orifice is obtained by using the formula derived by Sneeden (31).

Theoretical flow:

$$\frac{dw}{dT} = \cdot 164\, d^2 \left(\frac{Ph}{T}\right) \text{lb/sec.}$$

where P is the pressure at the orifice throat.

T is the temperature at th orifice.

h is the manometer head.

d is the orifice diameter.

Note: P is lb/in^2 absolute

d is inches.

And co-efficient of discharge = $\frac{\text{Actual Flow}}{\text{Theoretical Flow}}$

Reynolds/

Reynolds Number for the orifice flow is given by the expression in B.S.S. 1042-1934.

$$Re = \frac{L}{1583 d \mu}$$

where L in flow in lb/hr.
d is diameter in inches
μ is viscosity in lb.sec/ft

Procedure

The volume of the tank and pipe to the control valve was obtained by carefully weighing the tank empty and when filled with water. After coupling up to the control valve and approach tube, the circuit was leak-checked and the tank charged to 100lb/in^{2}G. and the control valve opened to allow air to flow through the orific under a head of about 30in H_2O.

Corresponding readings of pressure, orifice head and time were taken at convenient intervals.

For each orifice, a series of 4 tests was run and a sample set of readings along with an appropriate analysis is given below.

The graph of manometer head to a base of time is plotted as in fig. 116 . and the corresponding values of dp/dT obtained by utilizing the Newton-Gregor formula.

$$\Delta T \frac{dp}{dT} = \nabla U_0 + \frac{1}{2}\nabla^2 U_0 - \frac{1}{3}\nabla^3 U_0 + \cdots$$

$$\Delta T \frac{dp}{dT} = \Delta U_0 - \frac{1}{2}\Delta^2 U_0 + \frac{1}{3}\Delta^3 U_0 - \cdots$$

where ∇U_0 etc., are successive differences.

The values of dp/dT obtained from this calculation are also plotted on the curve of fig. 116 .

From these two curves corresponding values of manometer head "h" and dp/dT are taken.

The mean values of dp/dT for a series of tests are estimated and the coefficient of discharge of the orifice calculated.

The/

The curves of fig. 117 show the coefficients of discharge for each orifice on a basis of manometer head and fig. 118 shows these on a basis of Reynolds' Number.

CALIBRATION TESTS

As already stated, pressure gauges were calibrated at frequent intervals to ensure accuracy and similar procedure was adopted for the thermocouples and the evaporator unit. The flowmeter used in the main body of tests was not capable of being calibrated since the element was directly immersed in the refrigerant. Cross checking with the evaporator when the suction vapour was superheated showed the mass flow to be within 2% of each other. This was assumed to be satisfactory.

A short series of tests was carried out using a flowmeter incorporating a "Pyrotenax" element inserted in a "Pyrex" glass tube and this particular flowmeter was calibrated using water, as shown below.

Calibration of Flowmeter

In order to calibrate the flowmeter, the arrangement of fig. 19 was adopted. The water was supplied from a constant head tank and the output to the flowmeter finely adjusted by a needle control valve. The water leaving the flowmeter passed through a glass orifice tank with a very finely drawn jet so that the flow of water could be observed at all times. This was found to be necessary, since the slightest variation in the resistance characteristic of the flowmeter could cause a wide variation in the flow of water, even although this was supplied by a constant head tank. The incorporation of the little orifice tank enabled continuous adjustment of the control valve to be made and the mean level of liquid in the orifice tank was always maintained within plus or minus .5 c.m. of 60 c.m.

To carry out the calibration, the flow was maintained constant and the power input adjusted to give a suitable rise in water temperature. Conditions were allowed to settle for at least four hours before readings were taken. These were repeated at 15 minute intervals over the period of an hour to ensure complete/

complete stability. The results of these tests are shown in the table below:

Run No.	Electrical Heat Input	Water Temp. rise	Water (c.c./min)	Loss %
1	2.208	16.44	64.2	- 0.10
2	2.209	10.87	92.2	+ 0.04
3	2.228	8.18	122.1	+ 1.40
4	1.069	16.25	30.4	+ 1.00

The greatest loss is 1.4% and the scatter of results is such that the losses in the flowmeter have been ignored since even although an efficient oil separator has been inserted in the refrigeration circuit, it must be assumed that some oil will circulate. The degree of uncertainty due to this factor is probably greater than the degree of inaccuracy in the meter itself.

Evaporator Calibration

This was carried out in the simple manner as described in B.S.S. 3122:1959, para.13. The ambient temperature was the mean of four thermometers placed around the evaporator and the electrical heat input arranged to give a temperature rise of about 25°F. After steady conditions had been achieved, readings were taken at half-hourly intervals and the mean of these values are shown in the table below:

Ambient Temperature °F.	Shell Temperature °F.	Electrical Heat Input BTU/Min.	Leakage Coefficient BTU/Min.°F.
69.3	93.6	0.499	0.0205

Thermocouple Calibration

Thermocouples were calibrated by means of melting ice and steam at atmospheric pressure. The calibration curves were constructed from tables in "Temperature - its Measurement and Control in Science and Industry", (34) using a deviation constant.

SUCTION CONDITION: ITS EFFECT ON REFRIGERATOR COMPRESSOR PERFORMANCE

SUMMARY OF THESIS

Presented to the University of Glasgow
for the degree of Doctor of Philosophy

by

JAMES BROWN, B.Sc., A.R.C.S.T.

November, 1968.

SUMMARY

The investigation was carried out to determine the relativ importance of the factors affecting volumetric efficiency during the transition from "wet" to "dry" compression, when the refrigerant is Freon 12 and the compressor running at high speed.

Experimental techniques were developed to measure piston leakage and the fluctuating cylinder wall temperatures. The development of an electrical analogue and rotating drum photo-former is described.

Piston leakage was measured by noting the rate of pressure rise in a cylinder connected to the sump of the compressor, while the pressure in the sump was maintained constant. The increase in leakage as the vapour condition at the suction of the compressor was taken from the superheated field to the wet field was calculated. Although the leakage increased by abou 30% during transition, the total leakage was so small that the effect on the volumetric efficiency was itself quite negligibl Leakage past the piston of miscible refrigerant was compared w the leakage past the piston when the working fluid was air and it was concluded that the diluting effect of the refrigerant o the lubricating oil had a decisive effect on the pattern of leakage flow.

To measure the cyclical heat flow between the vapour and the cylinder wall, a true surface thermocouple was used. Due to practical difficulties in maintaining a nickel film across the thermocouple elements, recourse had to be made to constant as the thermocouple element. This was set in the compressor valve plate. The considerable difference between the thermal diffusivities of the valve plate material (cast-iron) and the constantan wire required that a careful investigation be made of the characteristics of such an arrangement. By using an electrical/

electrical analogue of the thermocouple it is shown that this thermocouple may be used over a wide range of frequencies and heat transfer coefficients.

A 2-dimensional electrical analogue was also used to investigate the effect of irregularities at the junction of a thermocouple when used to measure fluctuating temperatures. This investigation showed that large errors were possible and indicated the unsuitability of "peened" thermocouples for such purposes.

The development of a suitable photoformer and electrical analogue network to simulate the heat flow through the cylinder wall was carried out. Frequency limits on passive electrical analogue networks used to determine heat flow, as opposed to temperature distribution, have been noted. The inaccuracies due to phase distortion in non-uniform networks are measured an an analogue to simulate the radial flow of heat in a sphere wa constructed using a uniform network. In this case the transformation U = tr was adopted and the temperature gradient was measured directly from the analogue.

Calculation of the heat flow to liquid droplets entrained in the suction vapour showed that during the compression proces condensation could occur on the surface of the droplet, but that during the latter part of the discharge period and during the re-expansion that evaporation takes place. It was conclud that since the indicated volumetric efficiency of the compresso did not vary greatly as the suction enthalpy was reduced, liqui in the cylinder at the end of the discharge stroke was mostly deposited as a film of the cylinder wall. Deposition of such liquid from the vapour reduced the rate of condensation and subsequent re-evaporation.

Figures of heat transfer coefficient between vapour and the cylinder wall have not been included in the thesis since it was/

was found that negative coefficients were obtained at certain points in the stroke. This corresponds to work carried out on internal combustion engines, from which it was deduced that a quasi-steady state heat transfer coefficient is invalid for transient heat transfer. This was assumed to be due to the thermal capacity of the fluid.

NOMENCLATURE

A	Area
C_e	Capacitance/unit length
C_s	Capacitance/section
d	Diameter
H	Enthalpy
h	Head, Condensation coefficient
h_f	Vapour film coefficient
k	Thermal Conductivity
L	Flow, Inductance, Latent Heat
N	Frequency (Thermal)
n	Time scale multiplier
p	Pressure
Q	Charge on Condenser
R	Gas Constant, Resistance
Re	Resistance/unit length
R_s	Resistance/section
R_i	Input Resistance
r	Radius, Resistance
s	Scale Factor
T	Temperature (abs.)
t	Temperature
t_s	Surface temperature
V	Specific volume, Voltage

NOMENCLATURE

V_s	Surface Voltage
V_i	Input Voltage
W	Weight
x	Distance
y	Ordinate

GREEK SYMBOLS

α	Thermal diffusivity
Δ	Distance represented by measuring resistor
θ	Temperature difference
λ	Temperature drop across condensing film, Order of Harmonic
μ	Viscosity; Amplification factor of valve
π	Saturation temperature, 3.1415 ...
ρ	Specific weight
τ	Time, Time Constant, Period
ϕ	Entropy, $\sqrt{\frac{\pi v_s^2}{\alpha \tau}}$
ψ	Phase displacement

DIMENSIONLESS PARAMETERS

Nu	Nusselt Number
Pr	Prandtl Number
Re	Reynolds Number

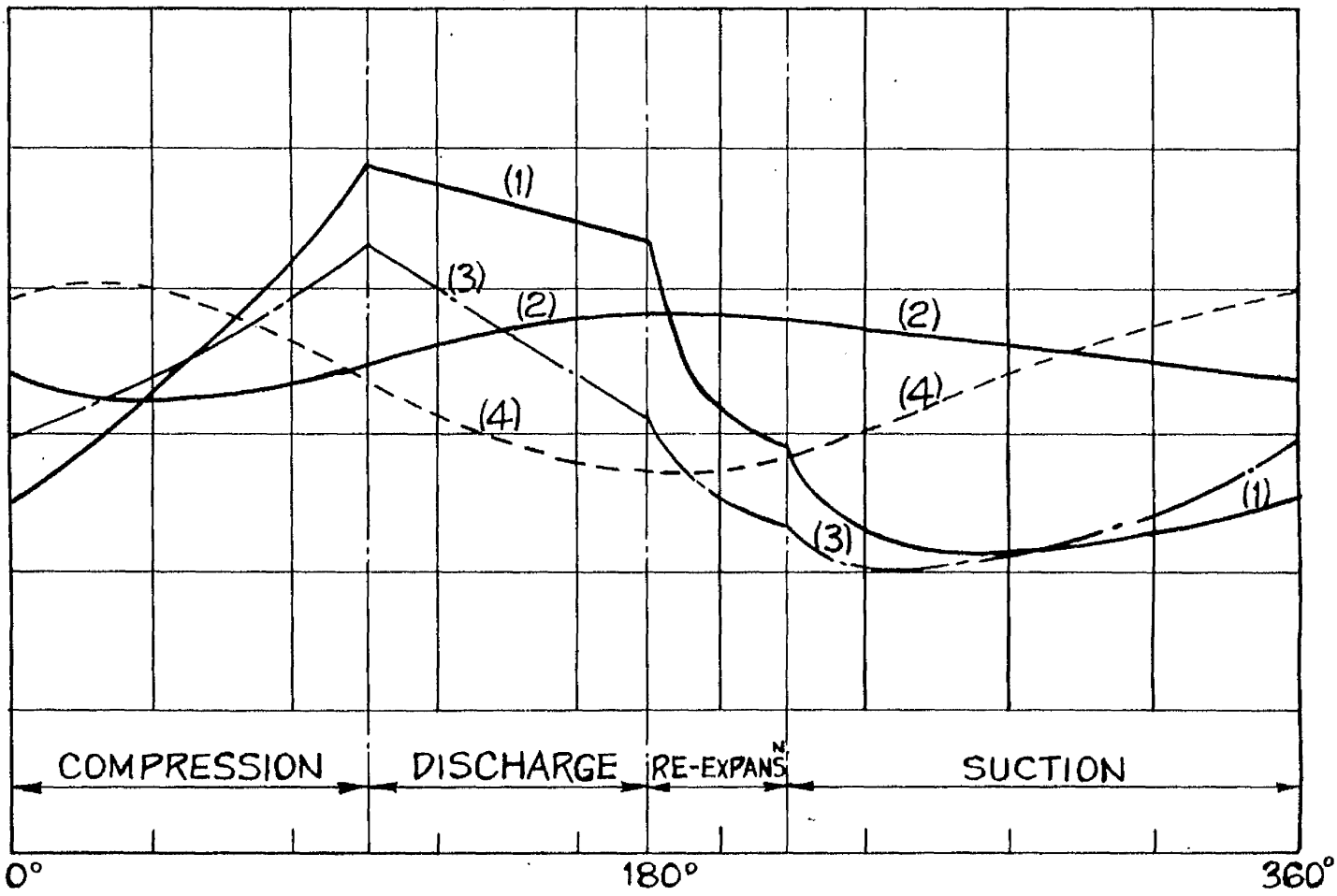

WIRTH :-

DIAGRAM SCHEMATIC ONLY

CURVE NOTATION

(1) GAS TEMPERATURE

(2) MEAN WALL TEMPERATURE

(3) EXPOSED SURFACE x GAS TEMPERATURE

(4) EXPOSED SURFACE x MEAN WALL TEMPERATURE

CYLINDER WALL TEMPERATURE CURVES FIG. 1.

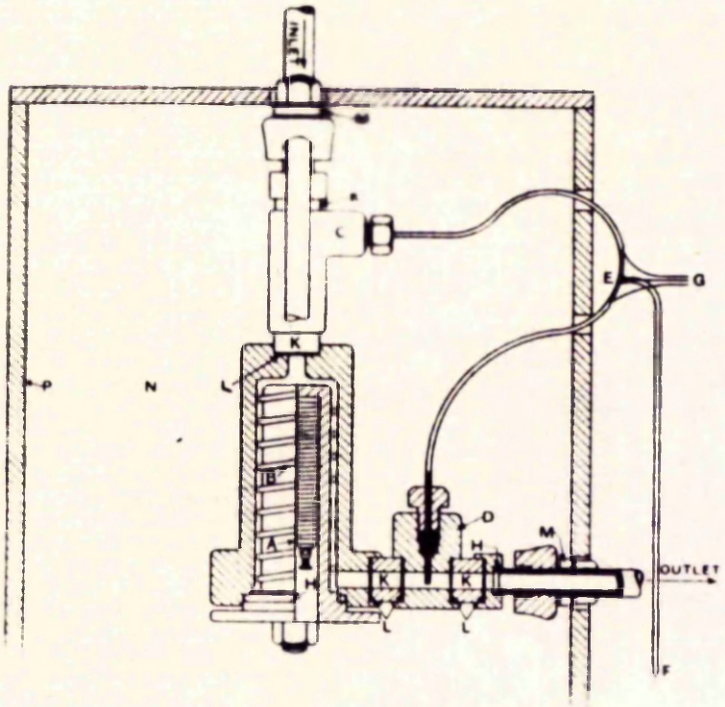

MASS FLOW METER (SMITH) Fig.2.

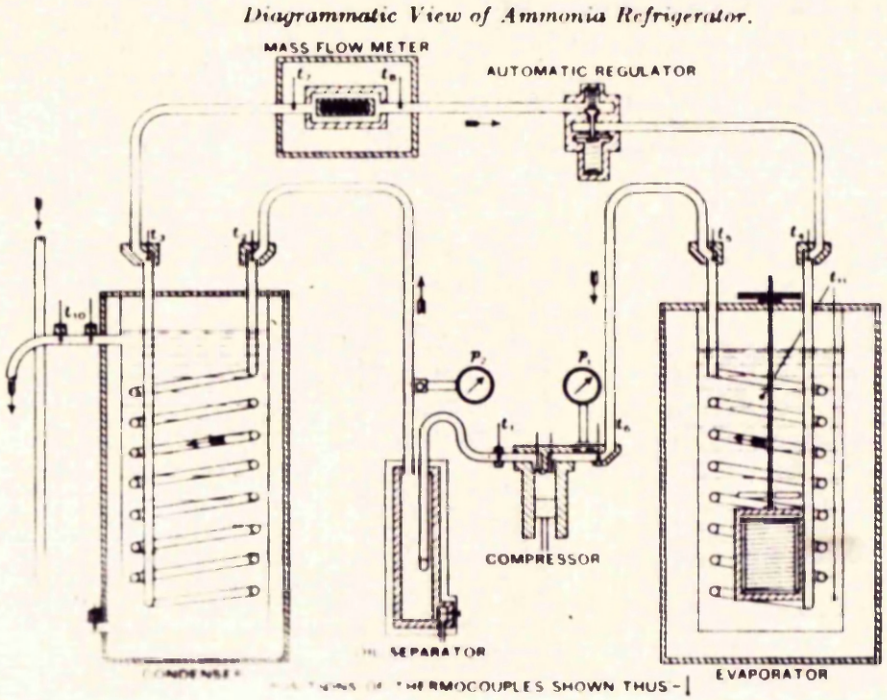

REFRIGERATOR CIRCUIT DIAGRAM (SMITH) Fig.3.

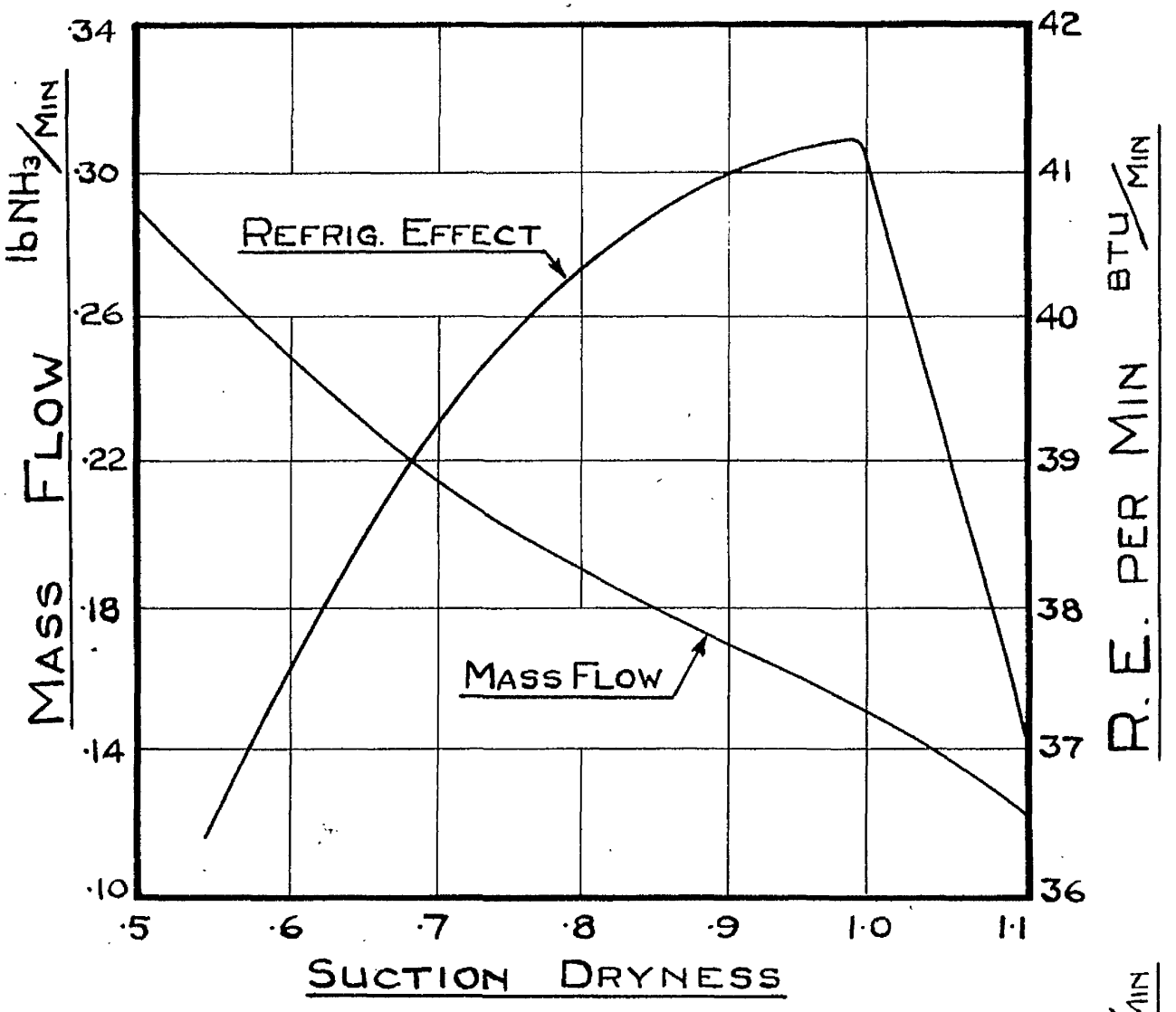

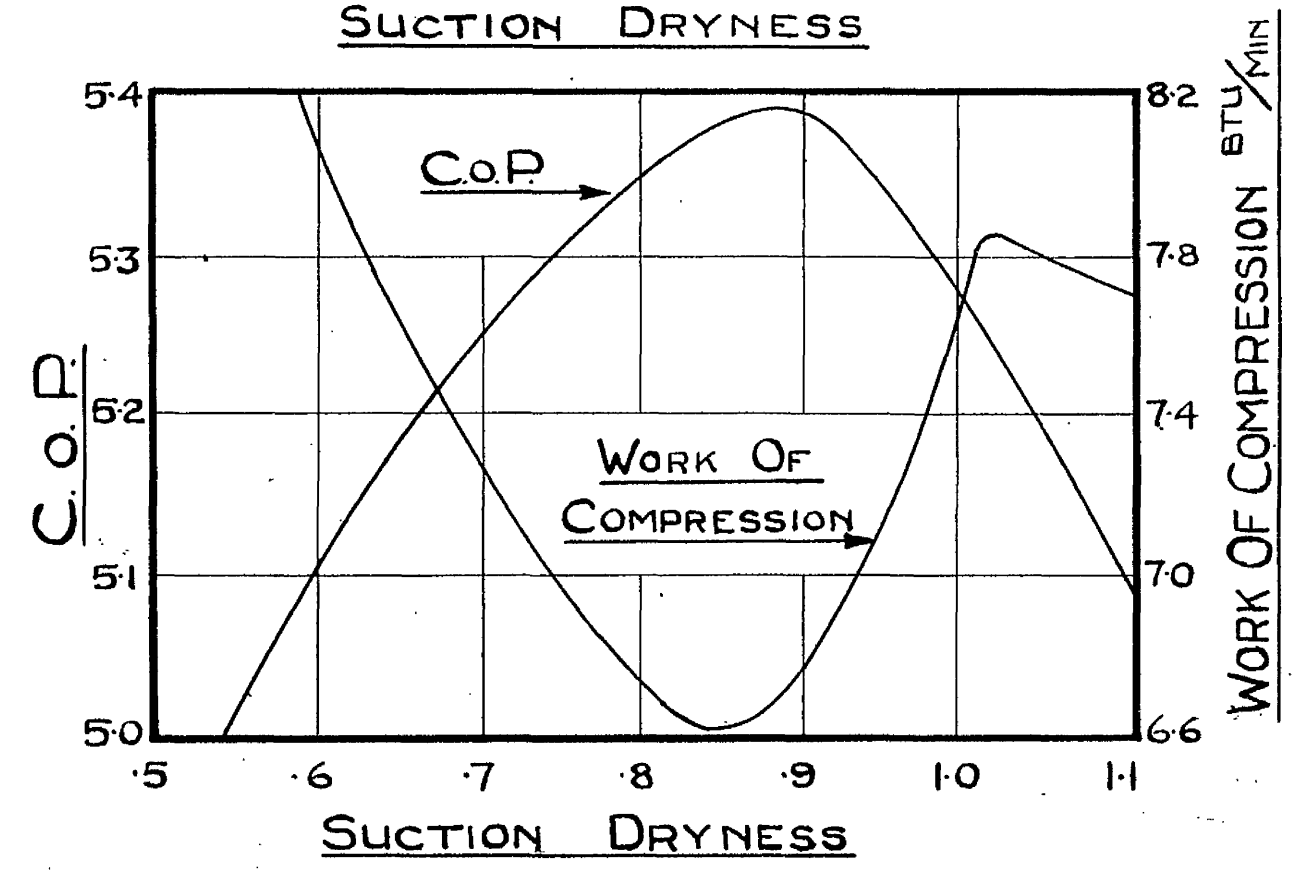

Theoretical Performance on NH_3

— Smith

Fig. No. 4

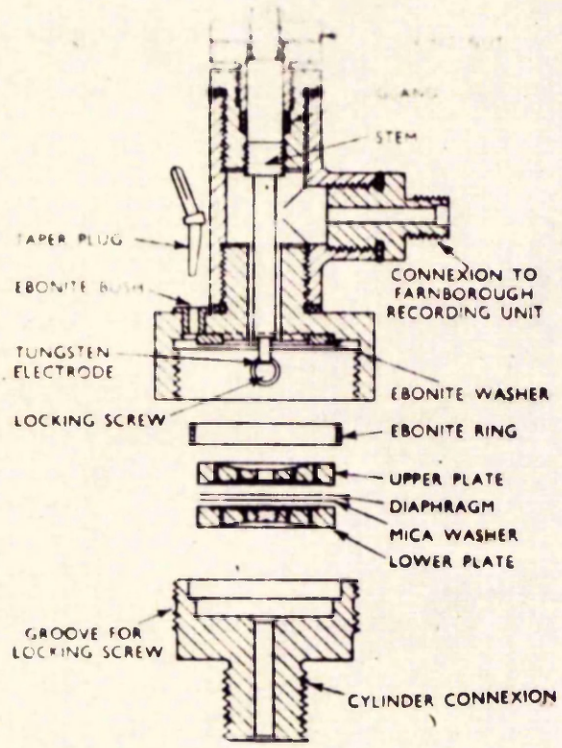

PRESSURE INDICATING UNIT (GIFFEN & NEWLEY) Fig.5.

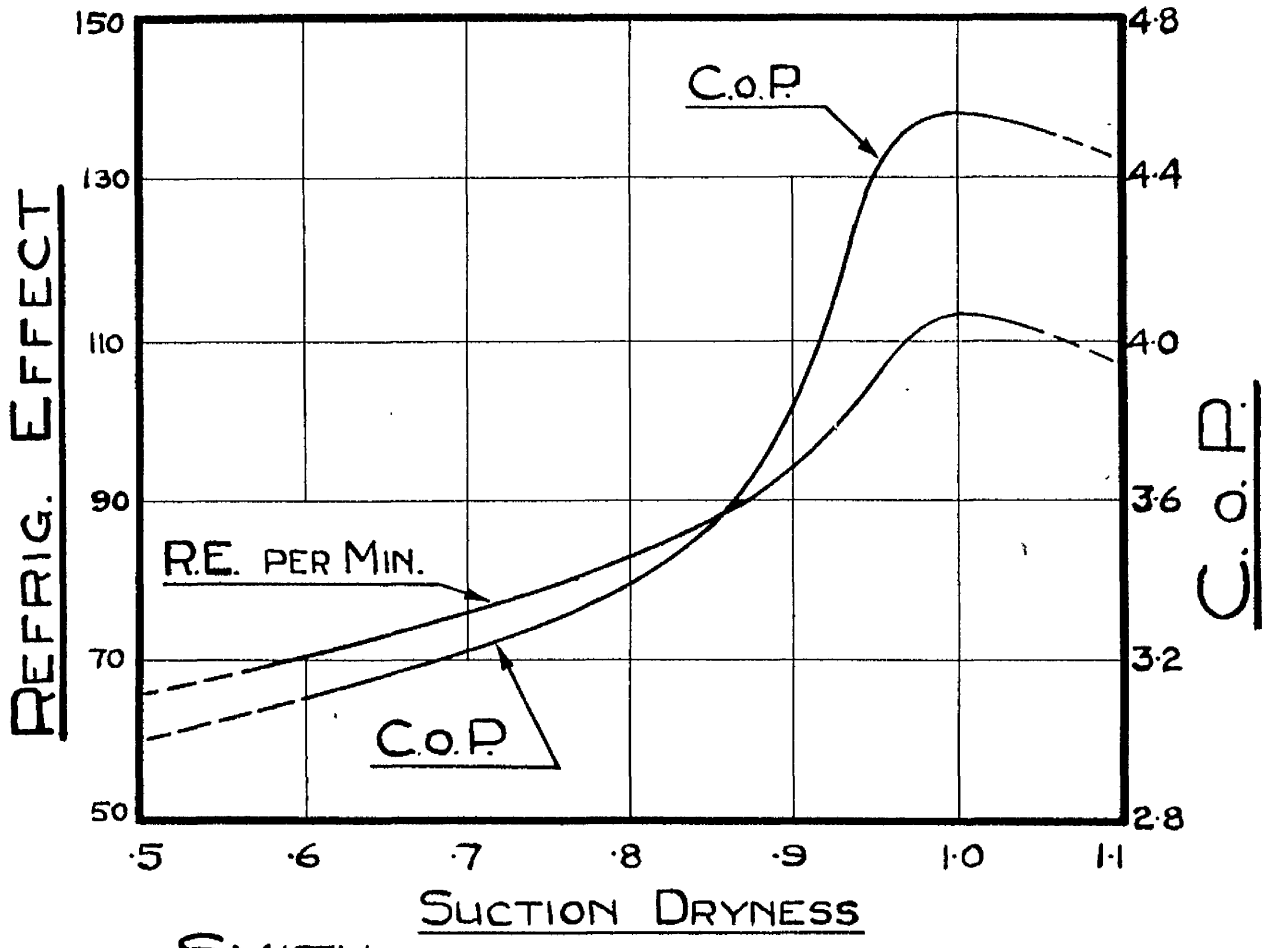

— SMITH

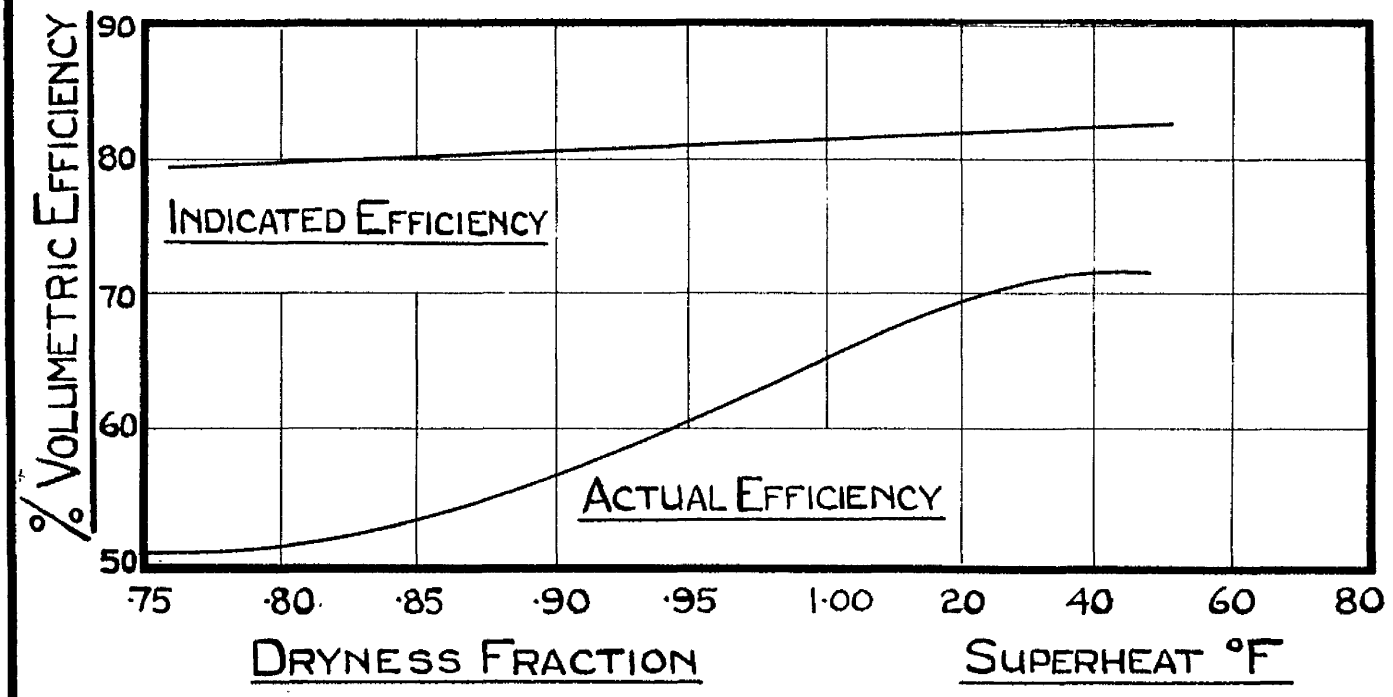

— GIFFEN & NEWLEY

ACTUAL PERFORMANCES.

FIG. No. 6

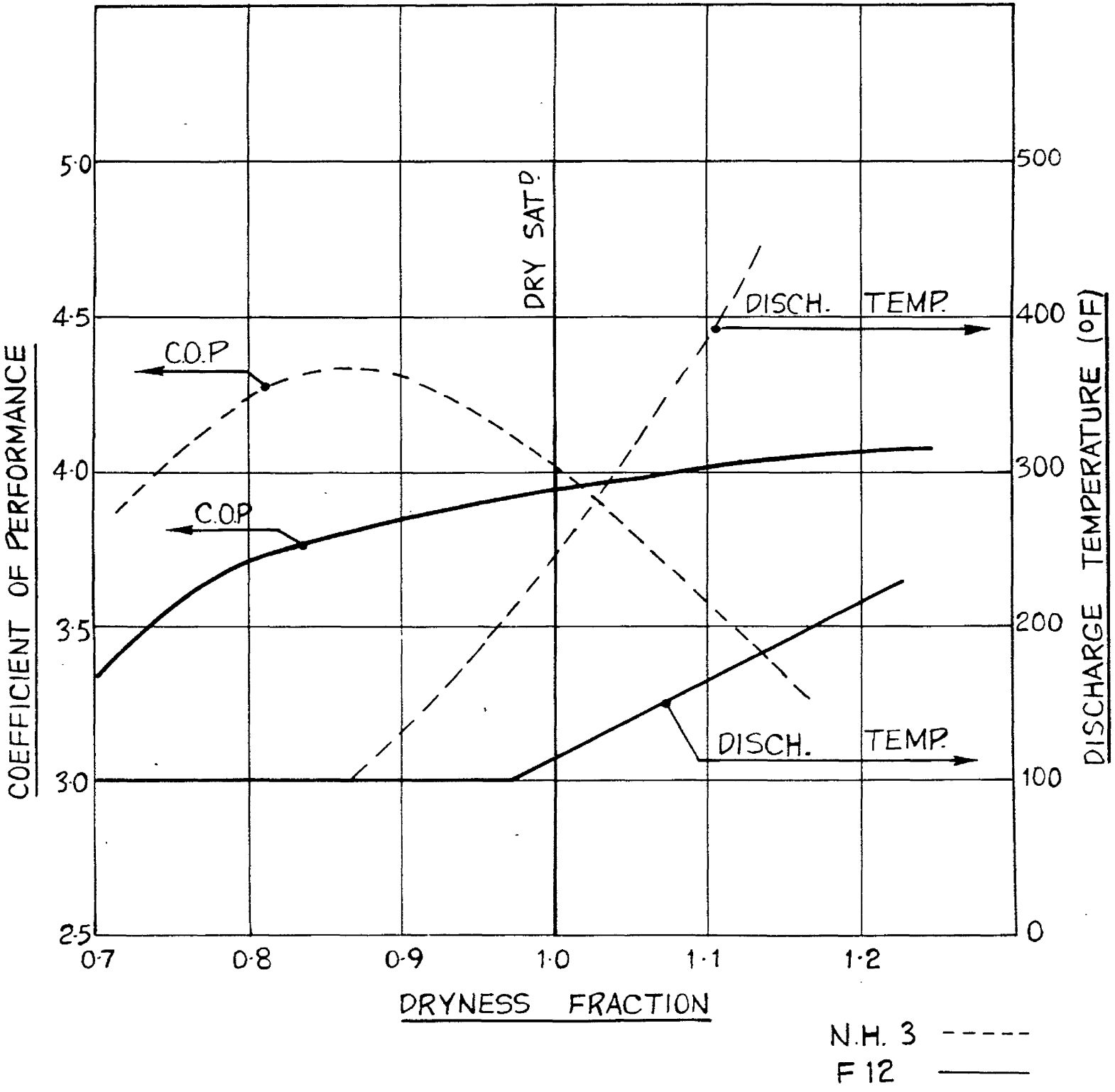

COMPARISON OF AMMONIA AND FREON 12 FIG. 7

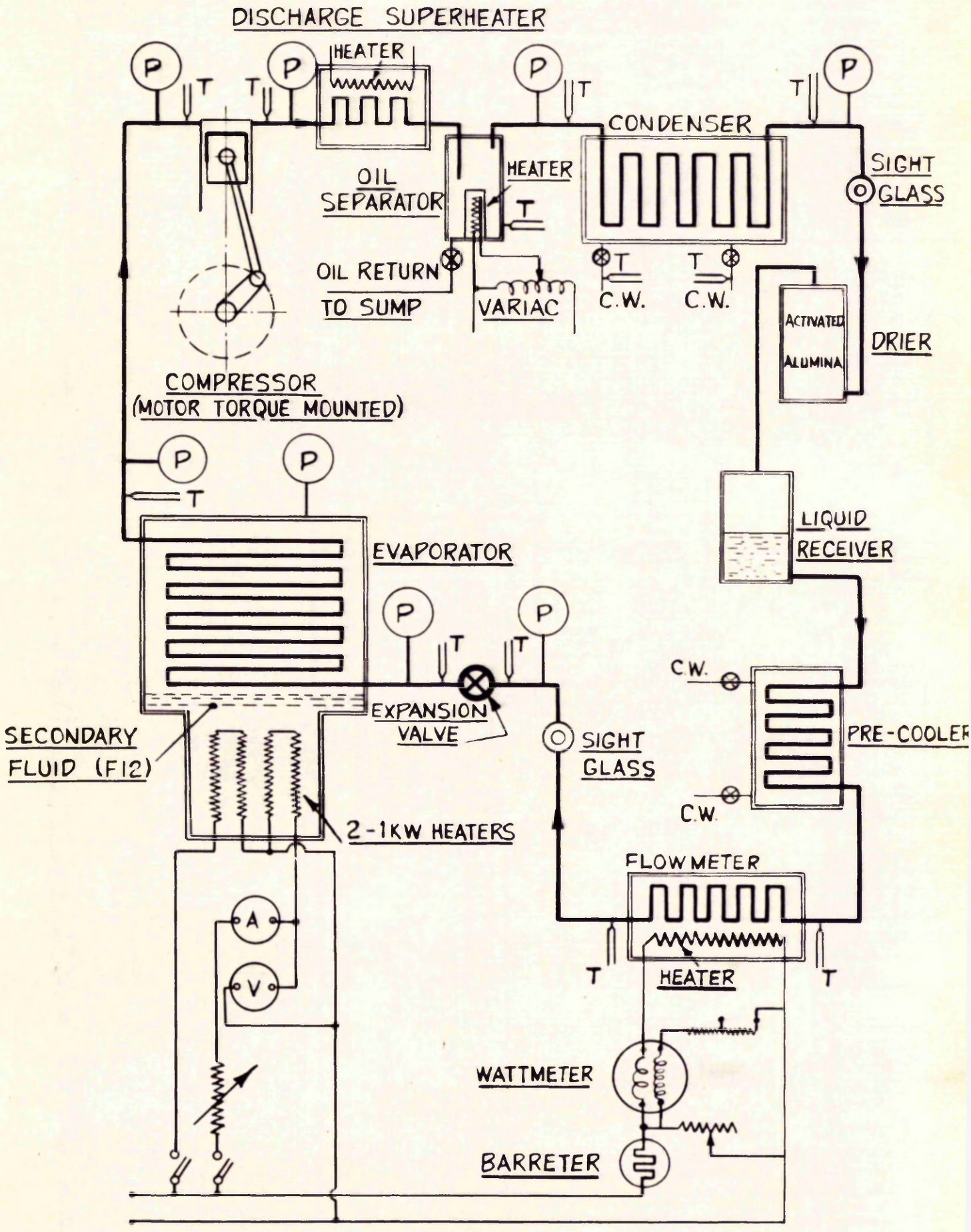

REFRIGERATOR CIRCUIT DIAGRAM

FIG.8

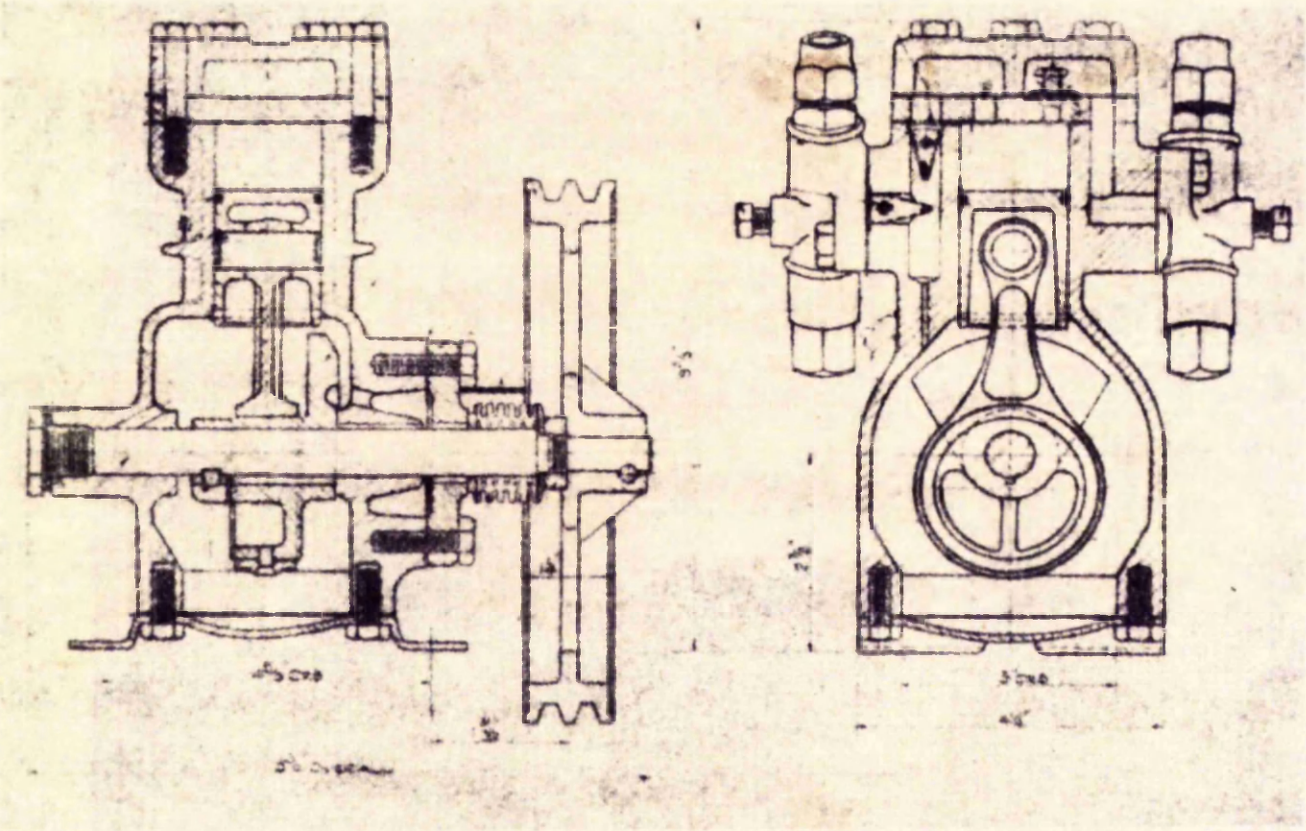

CROSS-SECTIONAL VIEW OF THE COMPRESSOR Fig. 9.

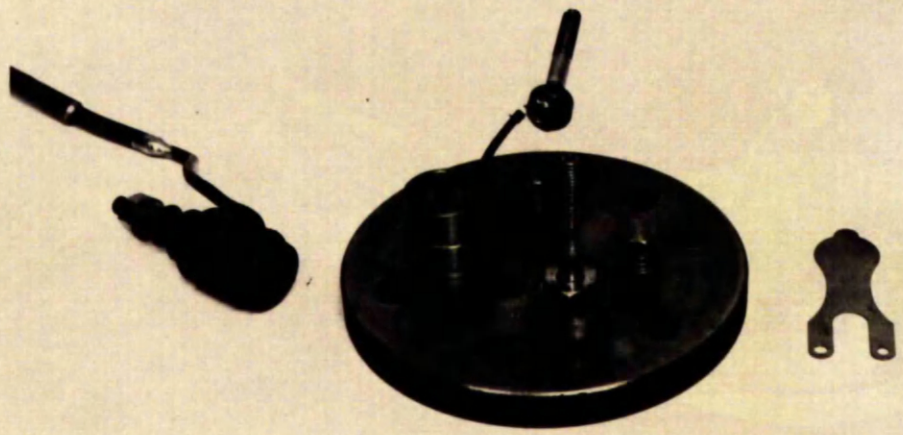

VALVE PLATE SHOWING PRESSURE ELEMENTS & SUCTION REED

Fig. 10.

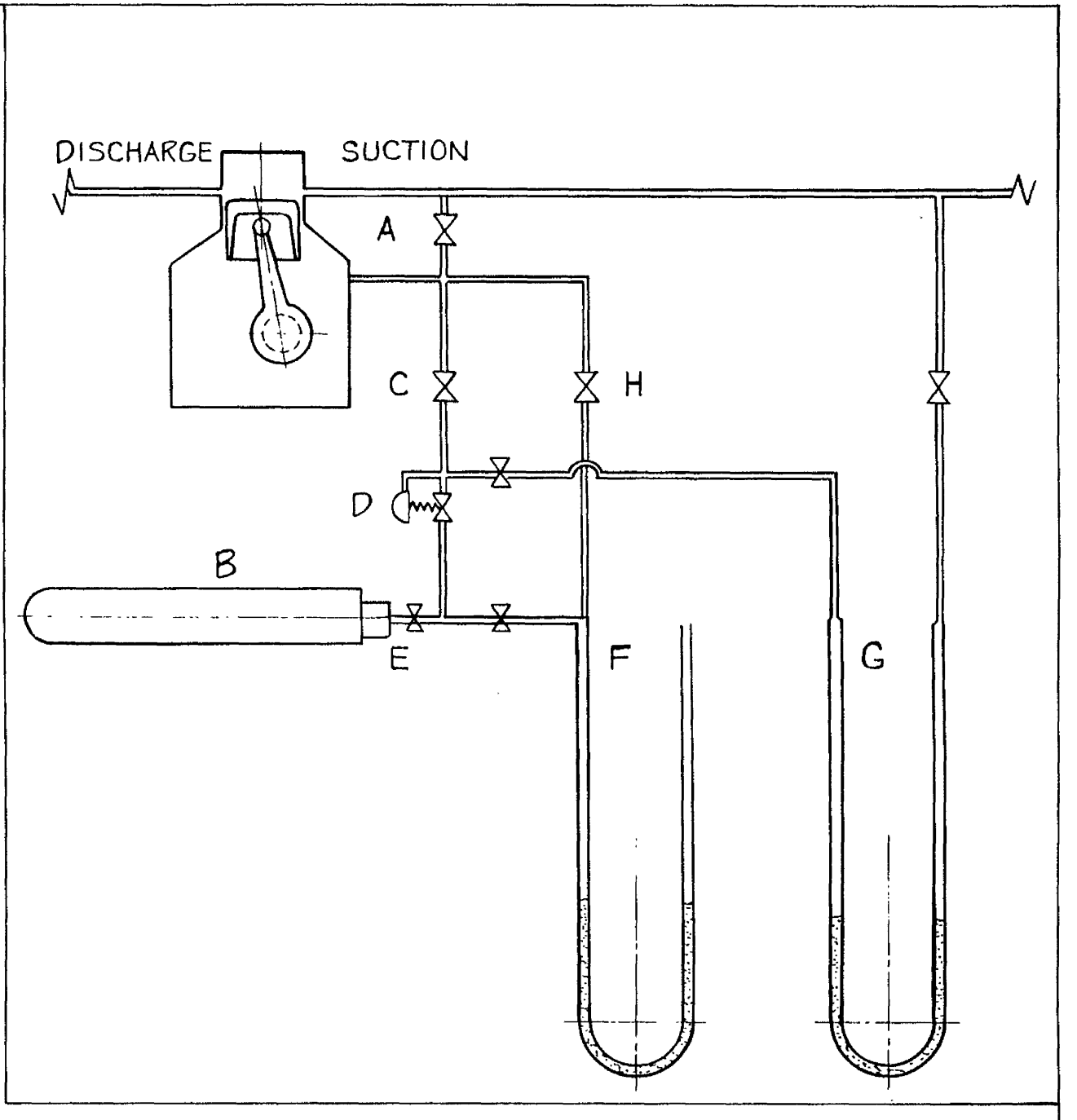

PISTON LEAKAGE MEASURING CIRCUIT

FIG. 11

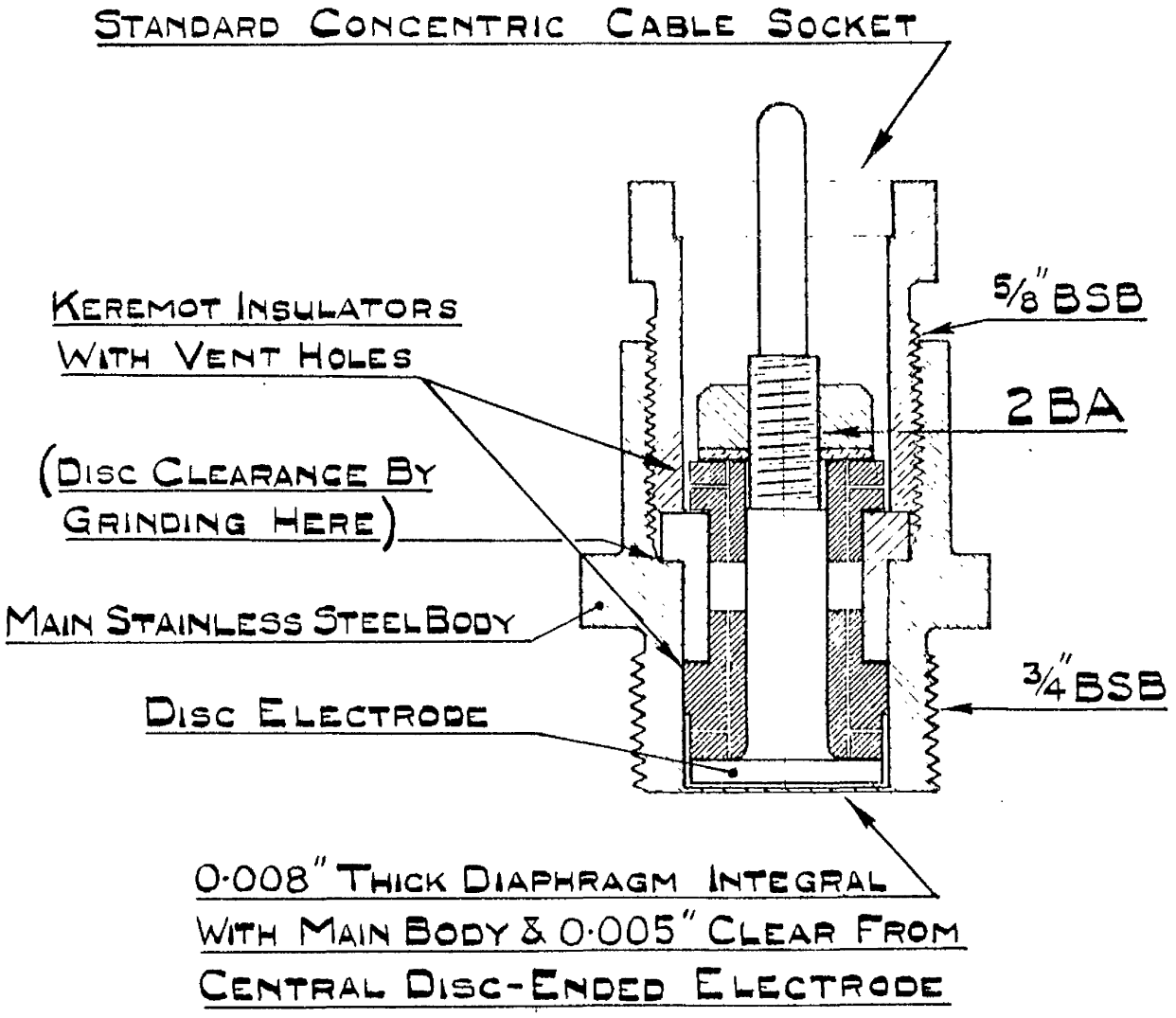

PRESSURE SENSITIVE ELEMENT

(CAPACITOR-TRANSDUCER)

TWICE FULL SIZE

FIG. NO. 12

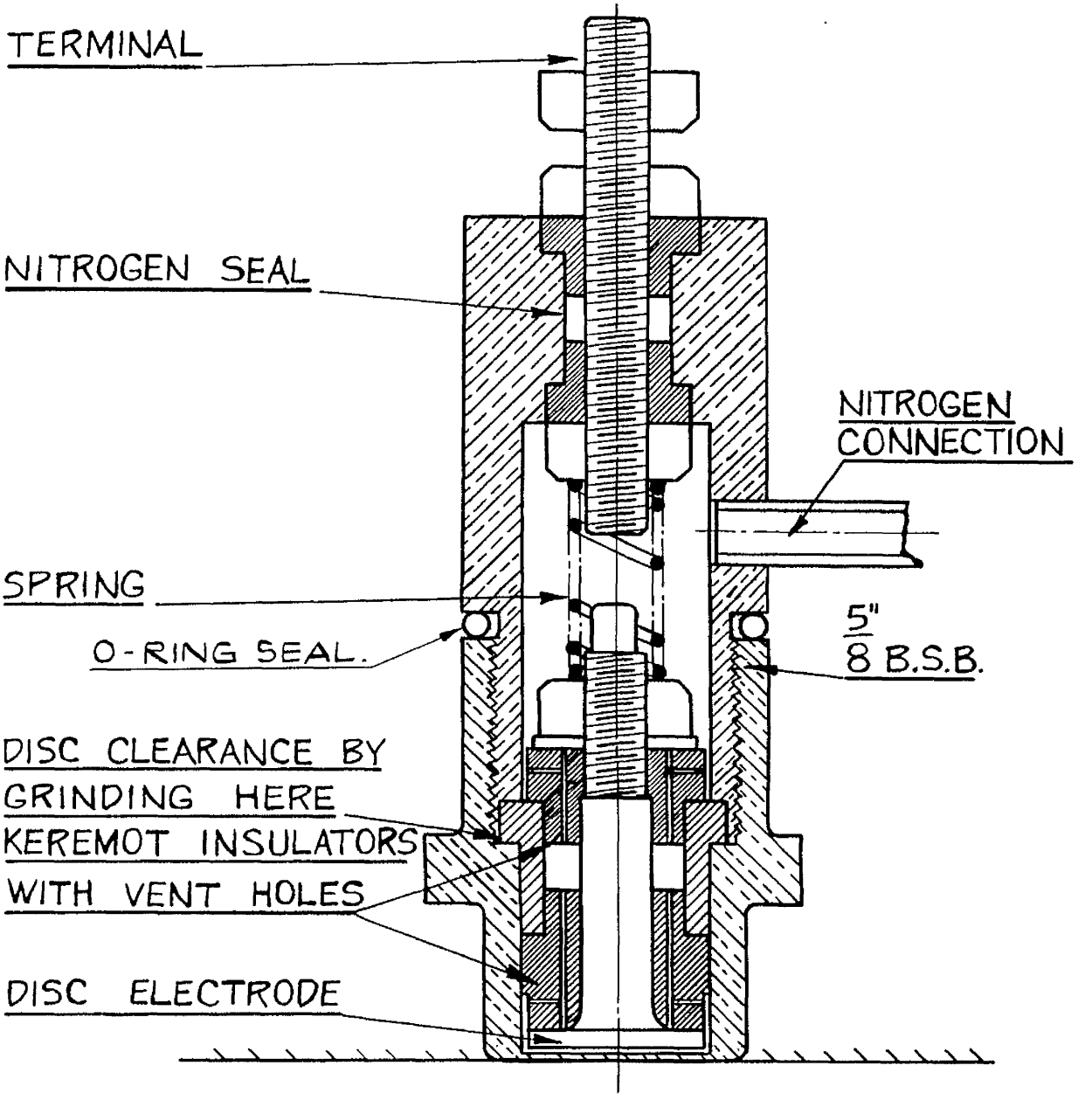

0·015" THICK DIAPHRAGM INTEGRAL WITH MAIN BODY

PRESSURE SENSITIVE ELEMENT

(CAPACITOR - TRANSDUCER)

SCALE:- TWICE FULL SIZE

FIG. 13

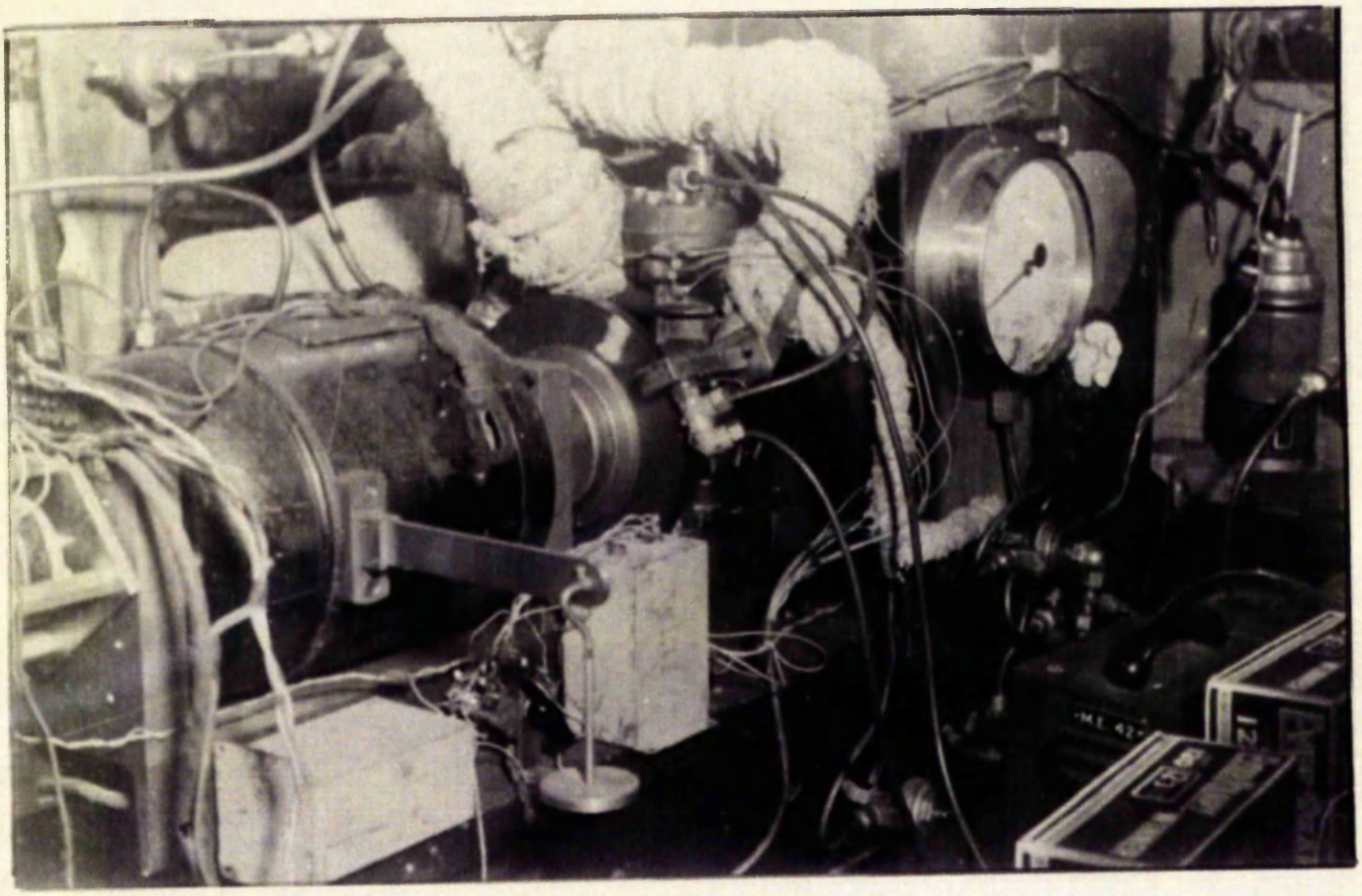

VIEW OF MOTOR COMPRESSOR UNIT. Fig. 14.

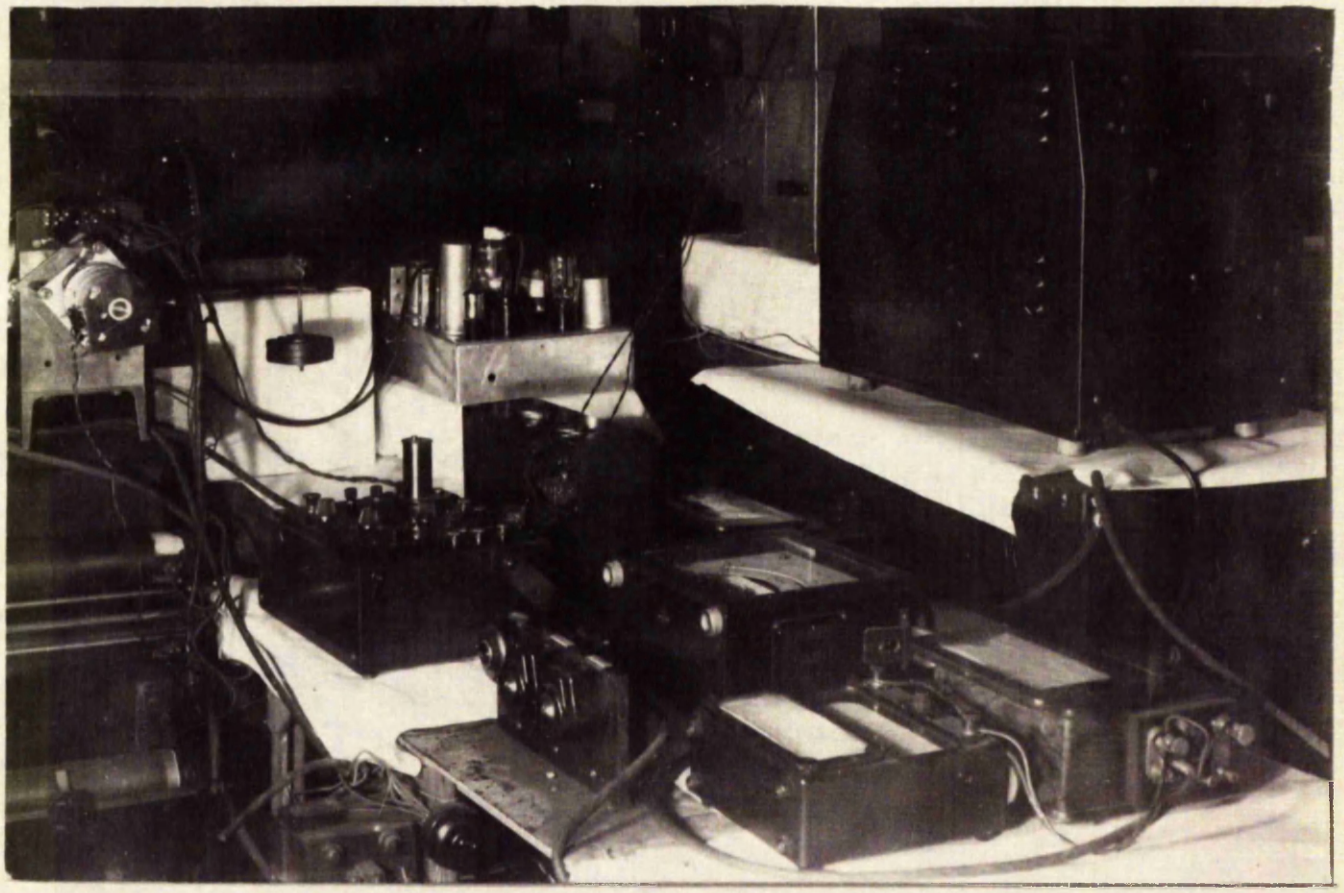

VIEW OF ELECTRICAL MEASURING EQUIPMENT

Fig. 15.

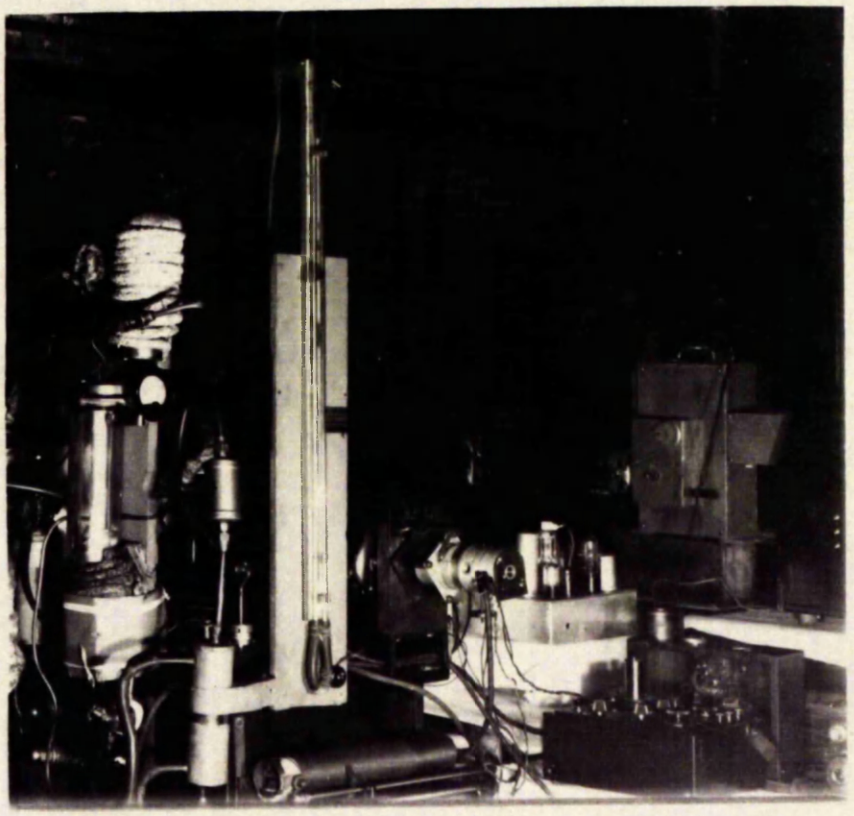

FREON/OIL SEPARATOR Fig. 16.

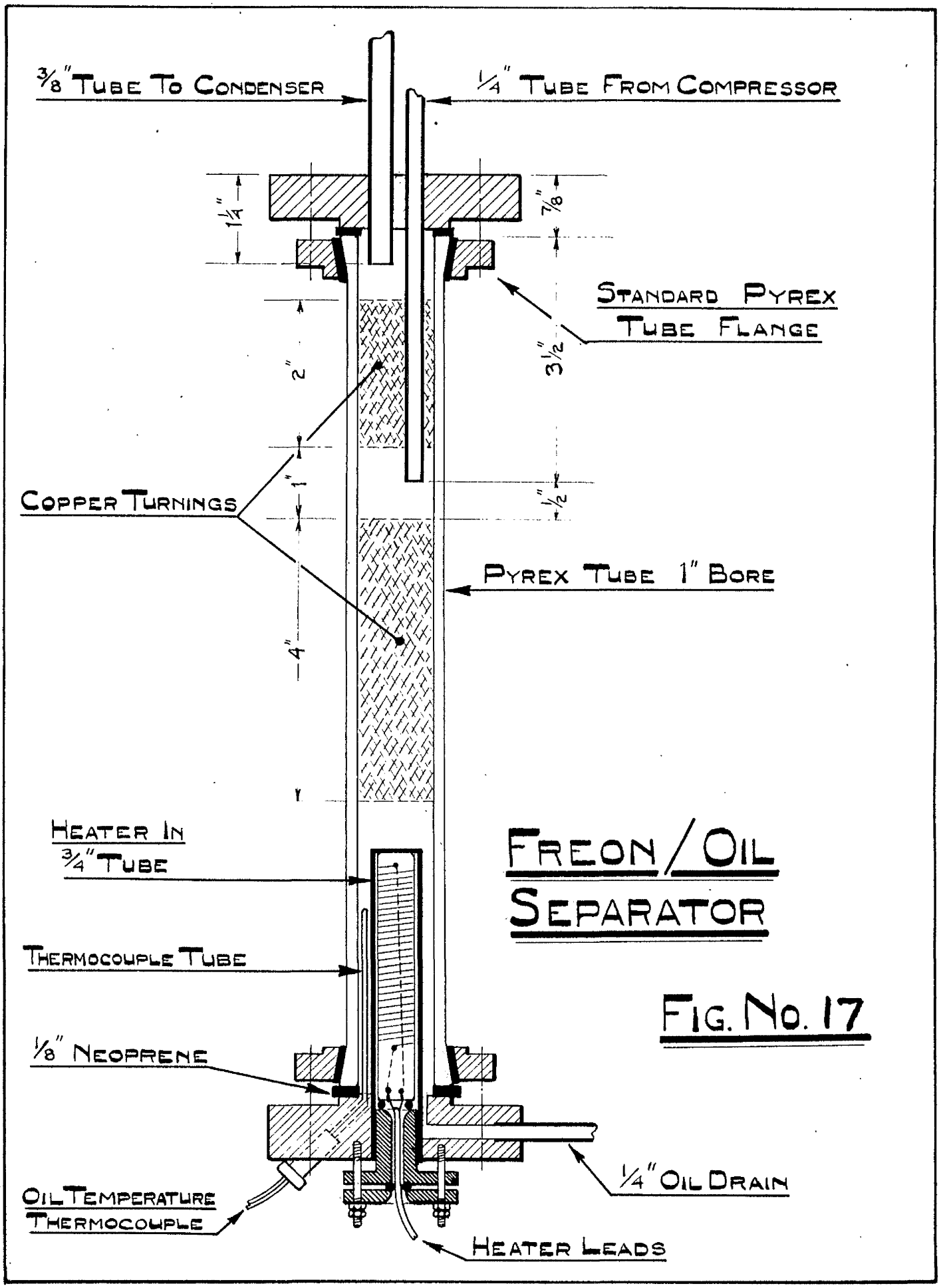
3/8" Tube To Condenser
1/4" Tube From Compressor
1 1/4"
7/8"
Standard Pyrex Tube Flange
3 1/2"
2"
1"
1/2"
Copper Turnings
Pyrex Tube 1" Bore
4"
Heater In 3/4" Tube
Freon/Oil Separator
Thermocouple Tube
Fig. No. 17
1/8" Neoprene
1/4" Oil Drain
Oil Temperature Thermocouple
Heater Leads

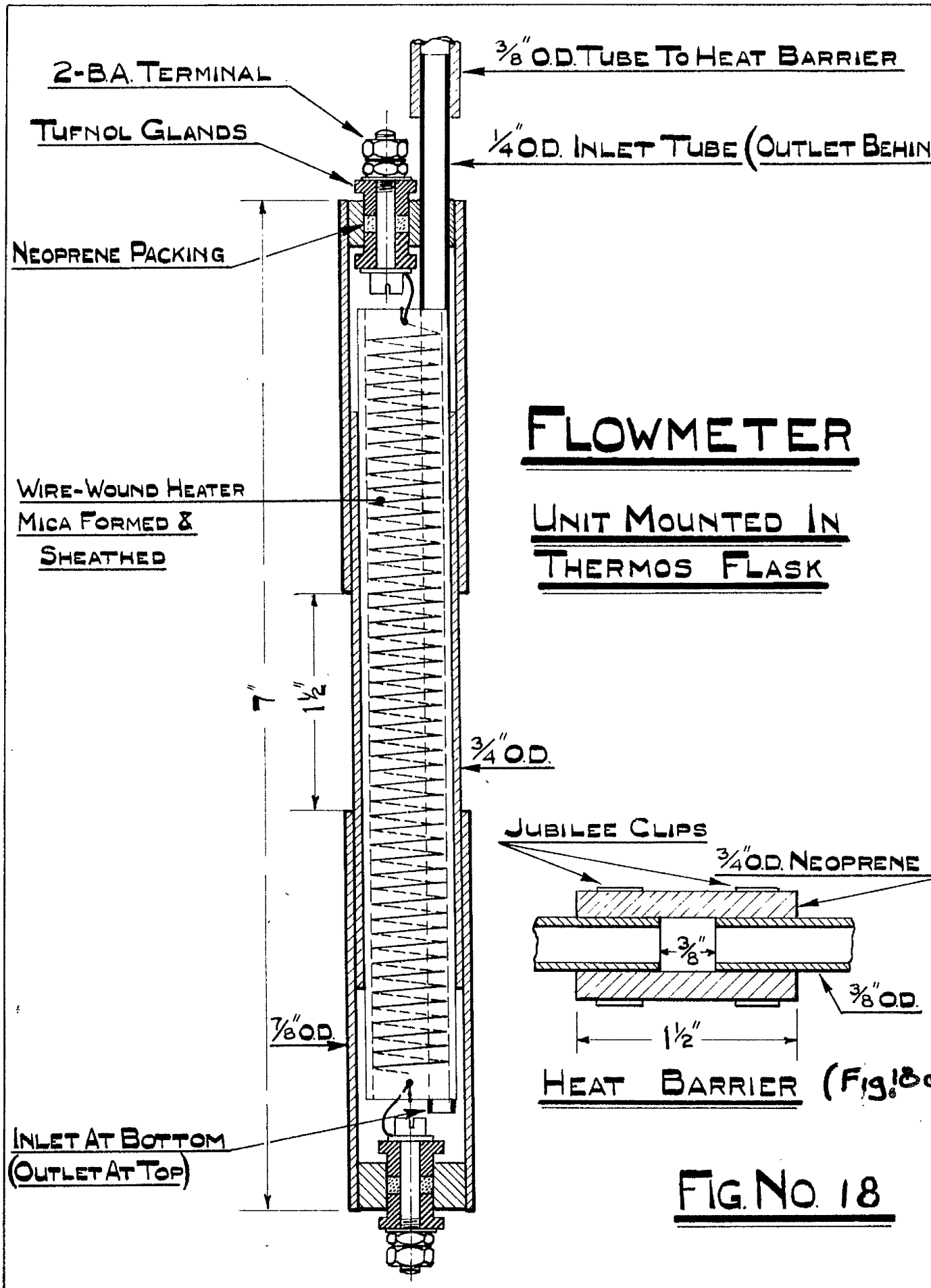

FLOWMETER

UNIT MOUNTED IN THERMOS FLASK

FIG. NO. 18

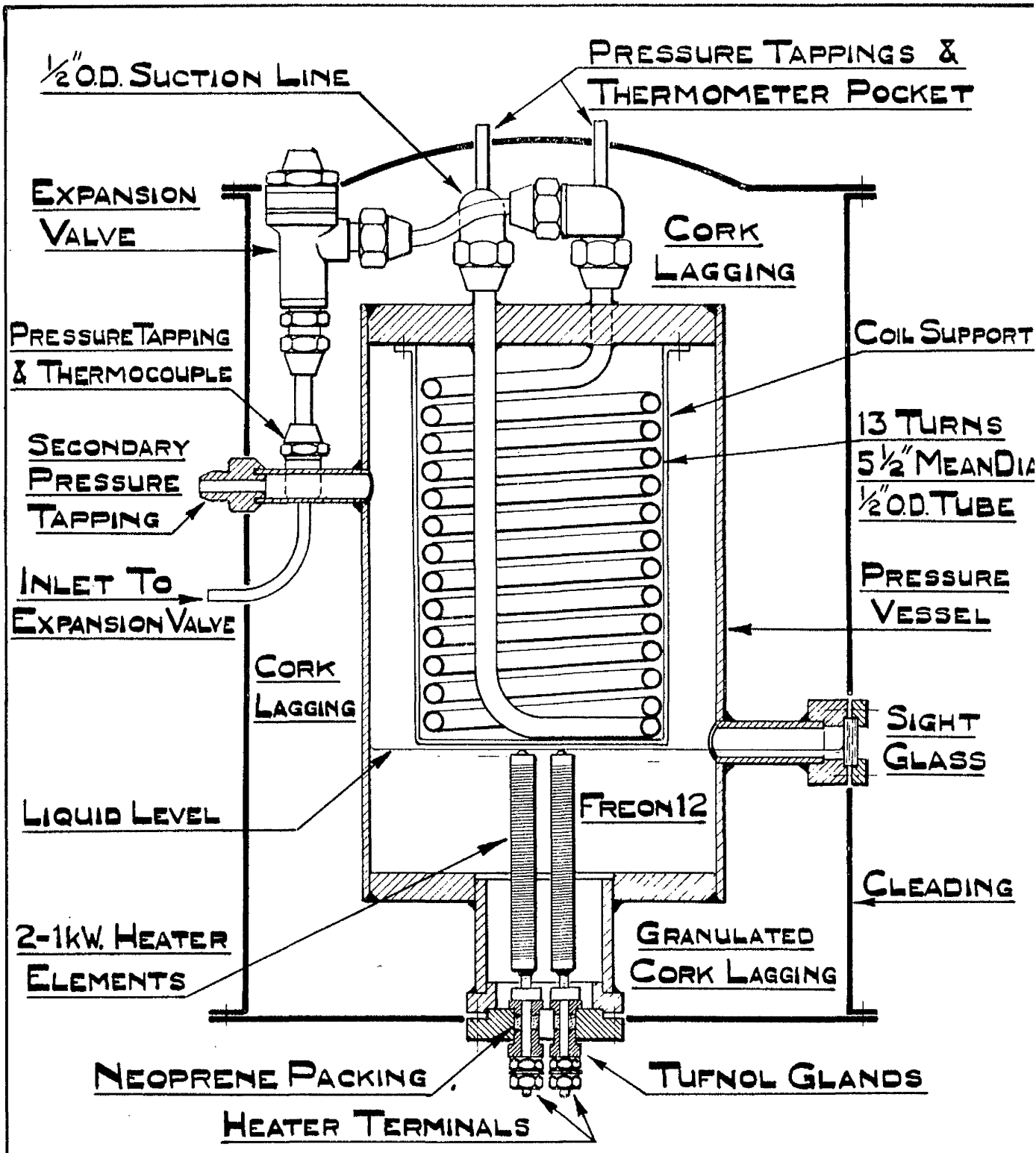

Secondary Fluid Type Calorimeter

Fig. No. 19

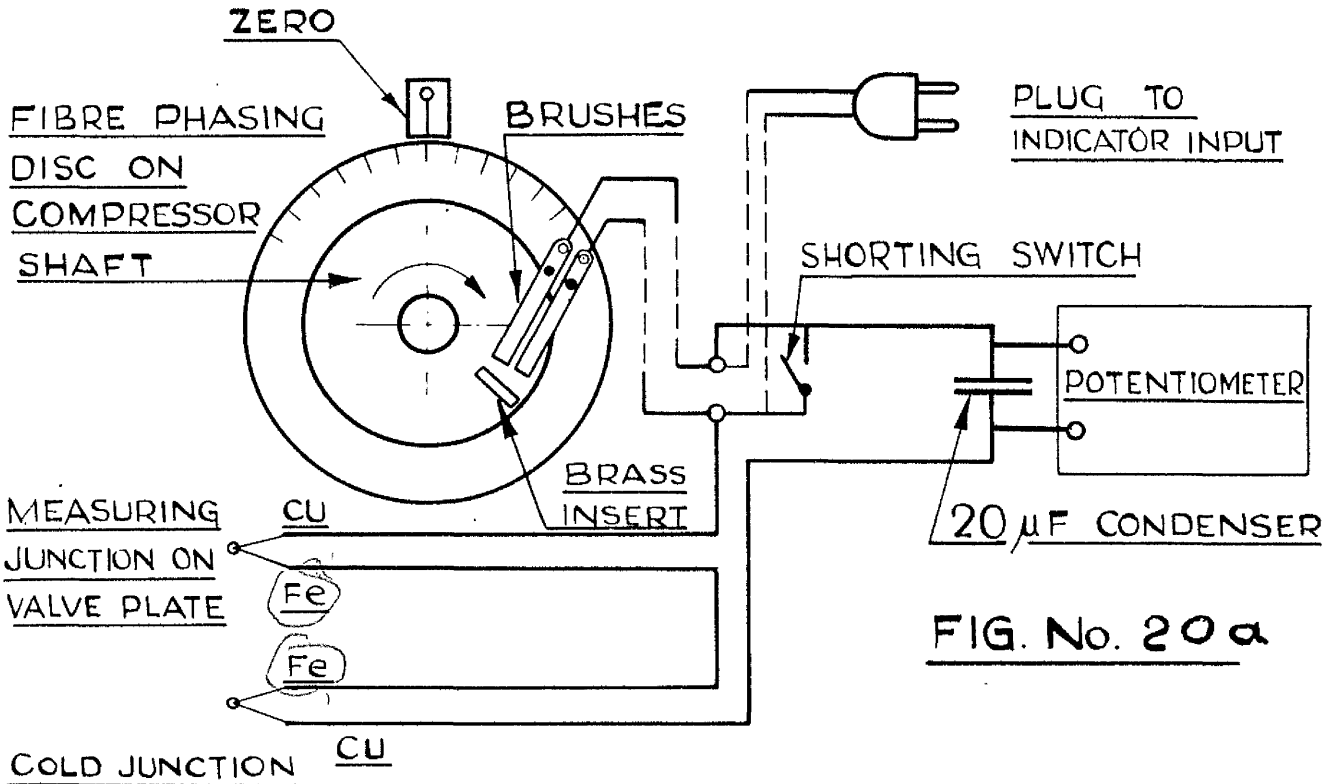

FIG. No. 20a

JOUBERT CONTACT & CIRCUIT FOR FLUCTUATING TEMPERATURE MEASUREMENTS

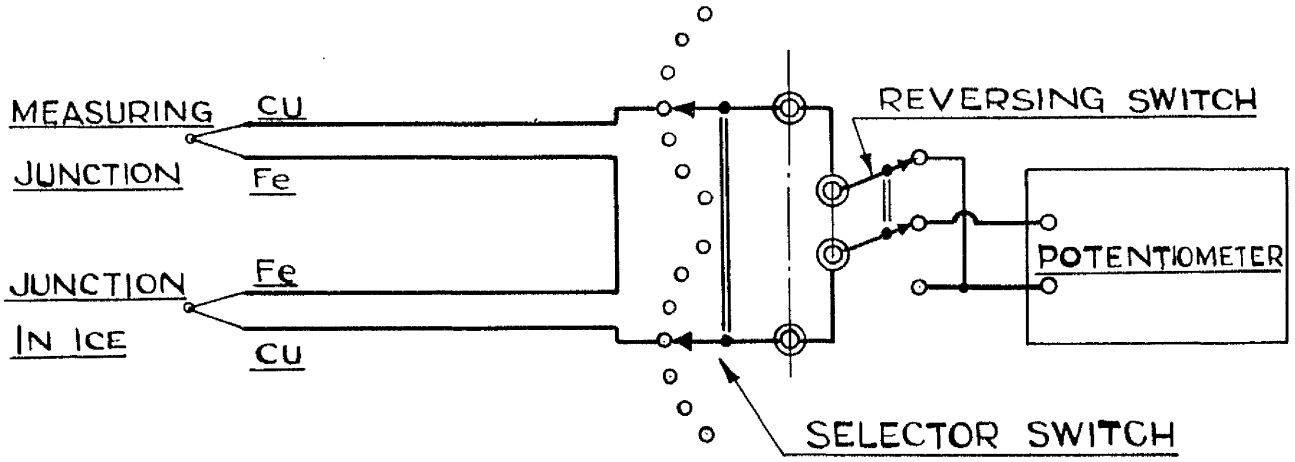

THERMOCOUPLE SELECTOR

FIG. No. 20b

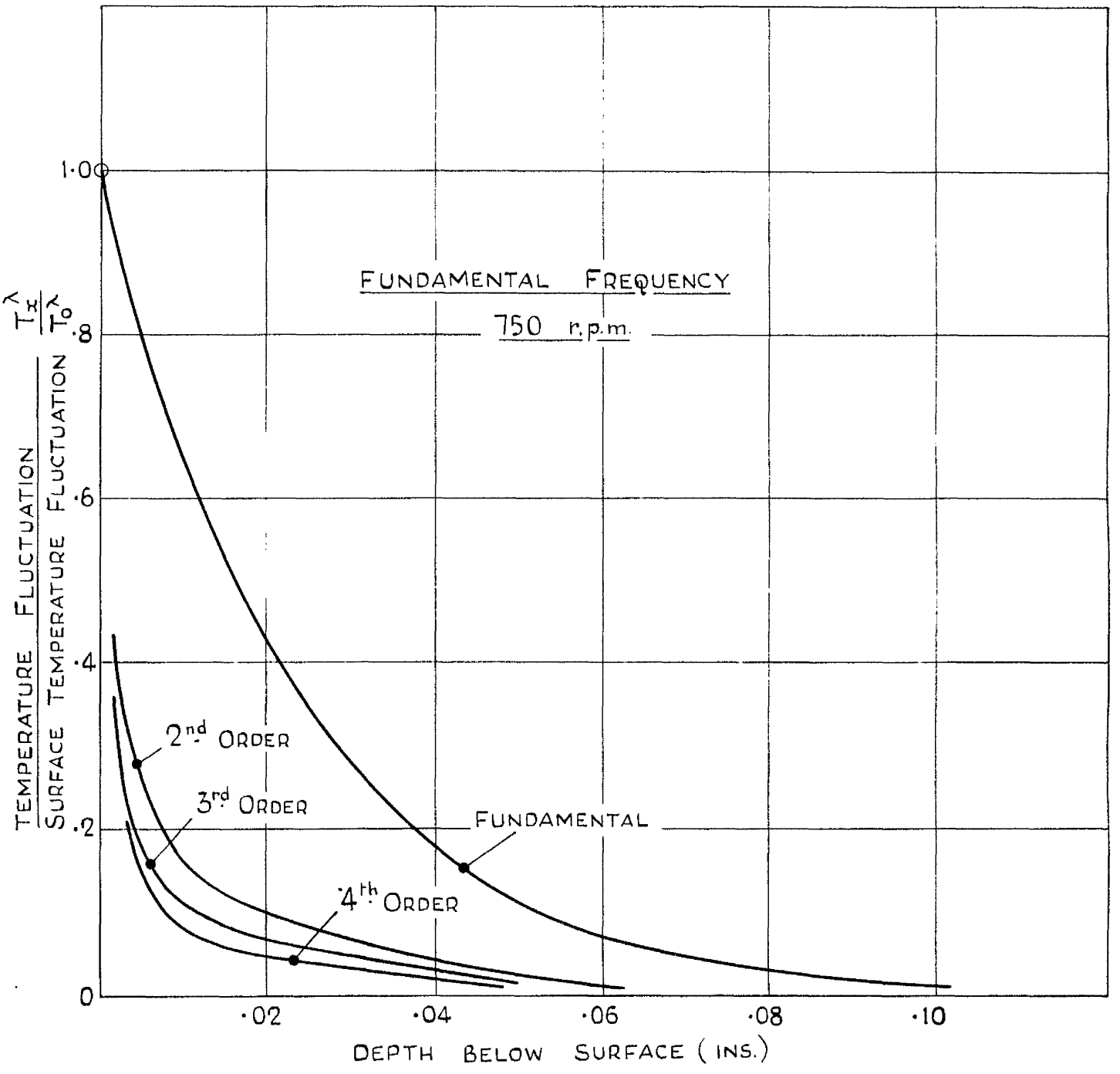

CYCLICAL TEMPERATURE FLUCTUATION AT VARIOUS DEPTHS IN CAST IRON PLATE

FIG. Nº 21

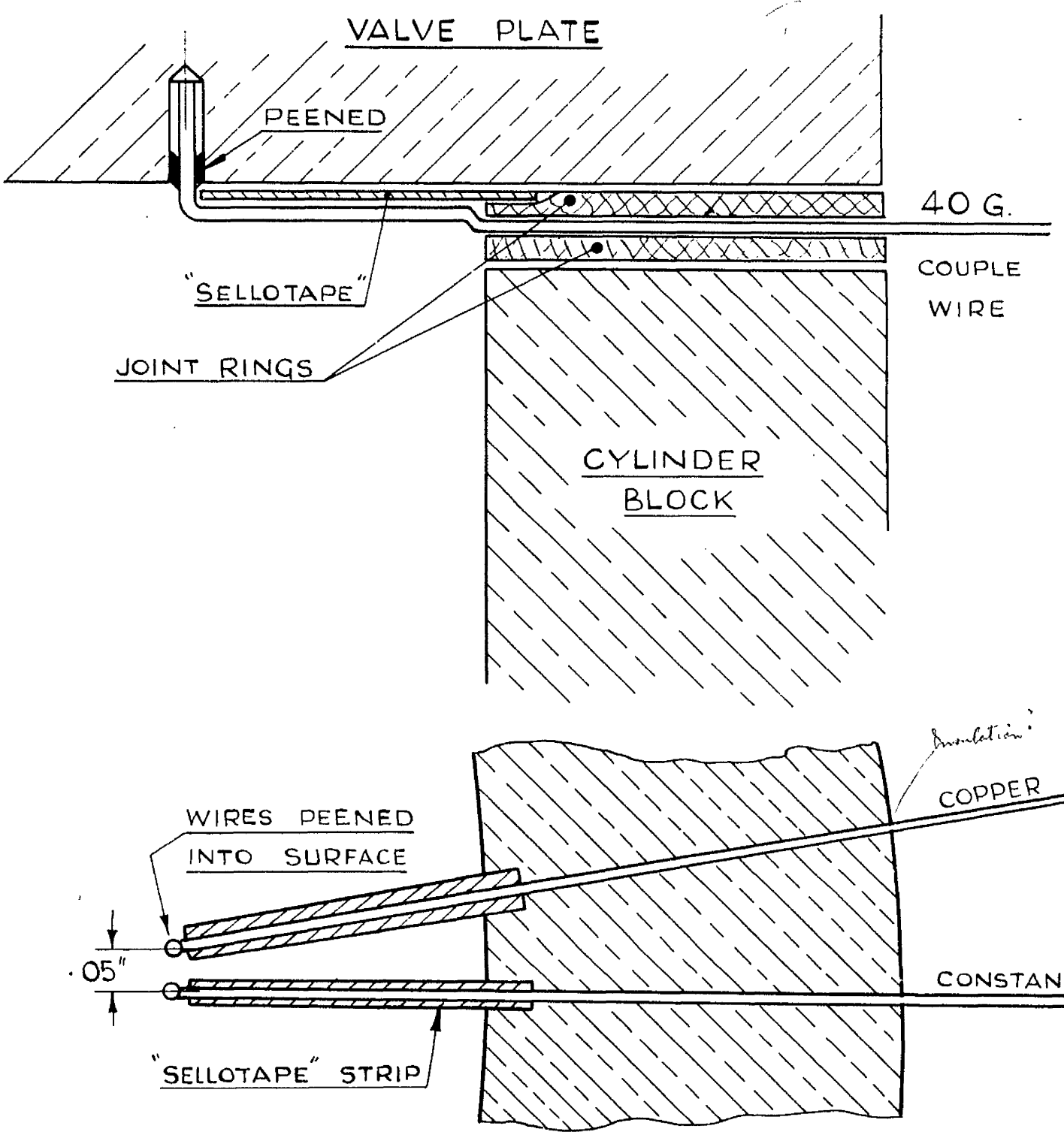

VALVE PLATE THERMOCOUPLE

FIG. No. 22

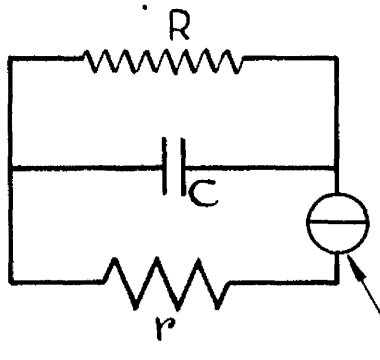

$R > 50$ Meg. Ω

$C = 20\ \mu F$

$r < 50\ \Omega$

EQUIVALENT CIRCUIT OF FLUCTUATING TEMPERATURE MEASURING DEVICE

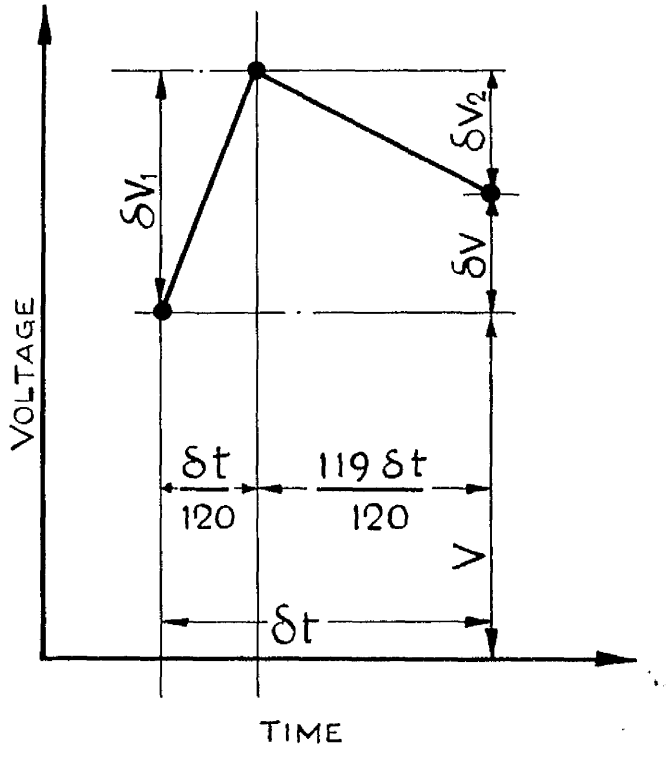

VOLTAGES DURING CYCLE

FIG. Nº 23

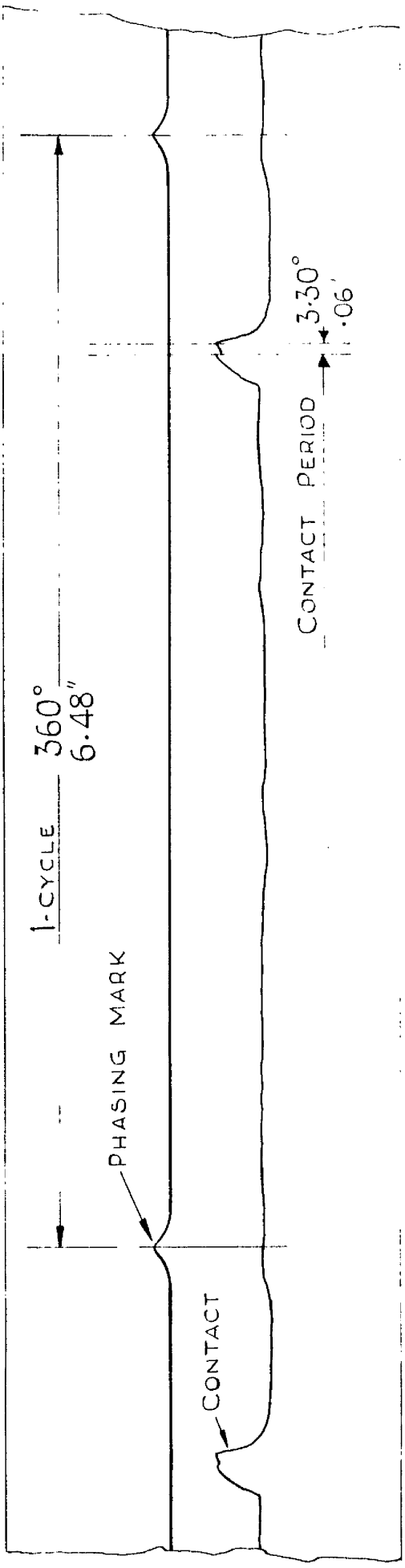

PHASING DIAGRAM FOR
THERMOCOUPLE CONTACTOR

FIG. Nº 24

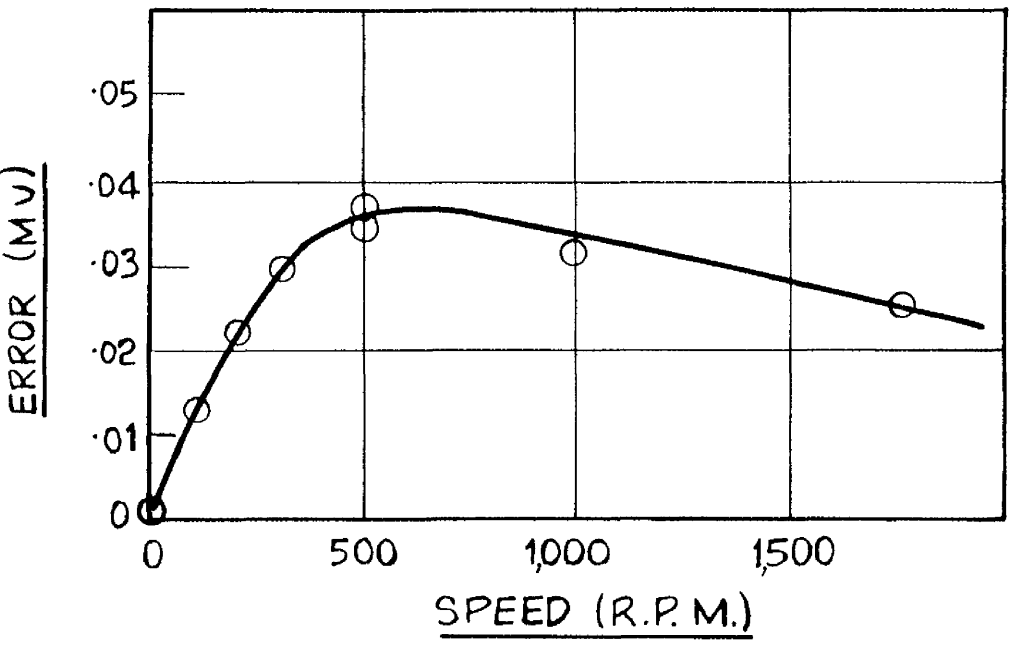

JOUBERT CONTACTOR

VARIATION OF ERROR WITH SPEED

(MEAN POTENTIAL 0·453 Mv)

FIG. A

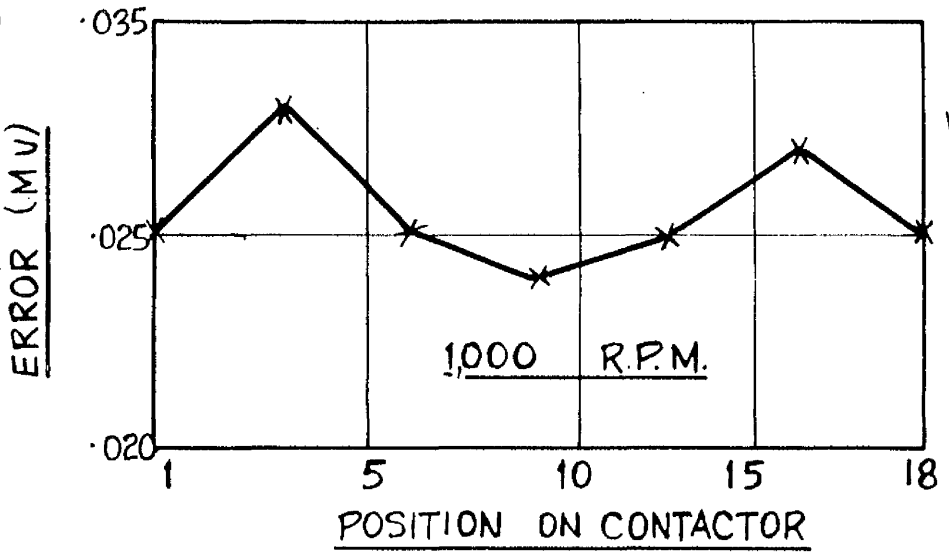

JOUBERT CONTACTOR

VARIATION OF ERROR WITH POSITION

(MEAN POTENTIAL 0·485 Mv)

FIG. B

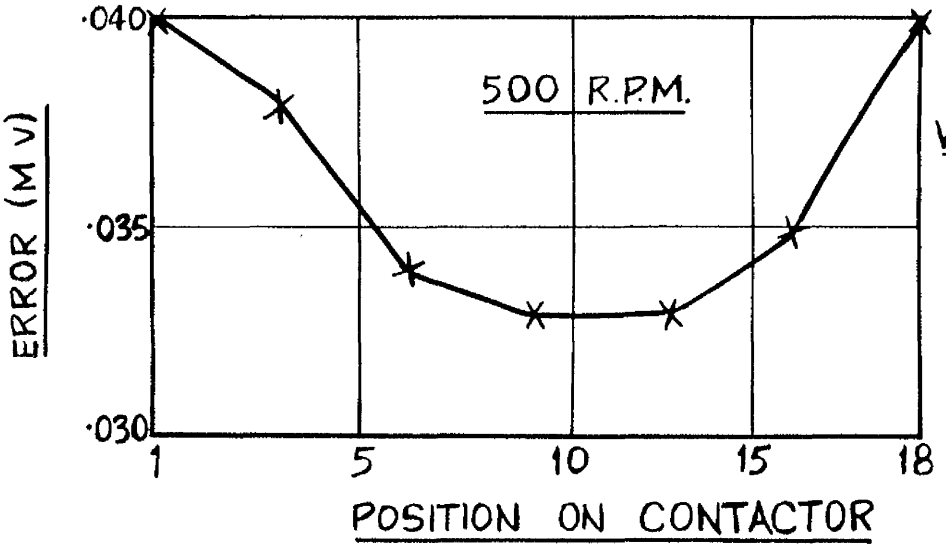

JOUBERT CONTACTOR

VARIATION OF ERROR WITH POSITION

(MEAN POTENTIAL 0·485 Mv)

FIG. C

FIG. 25

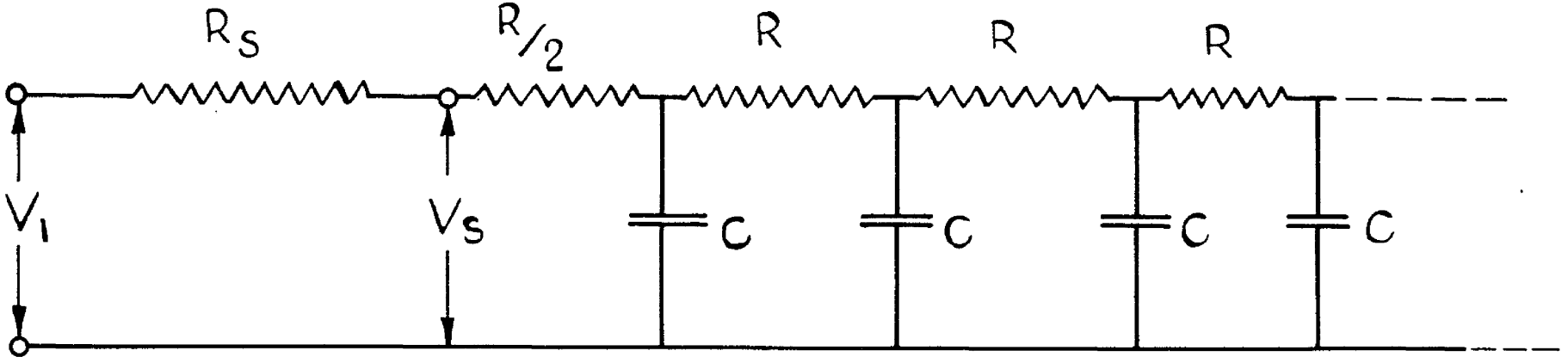

LADDER NETWORK FOR SURFACE THERMOCOUPLE

FIG. 26

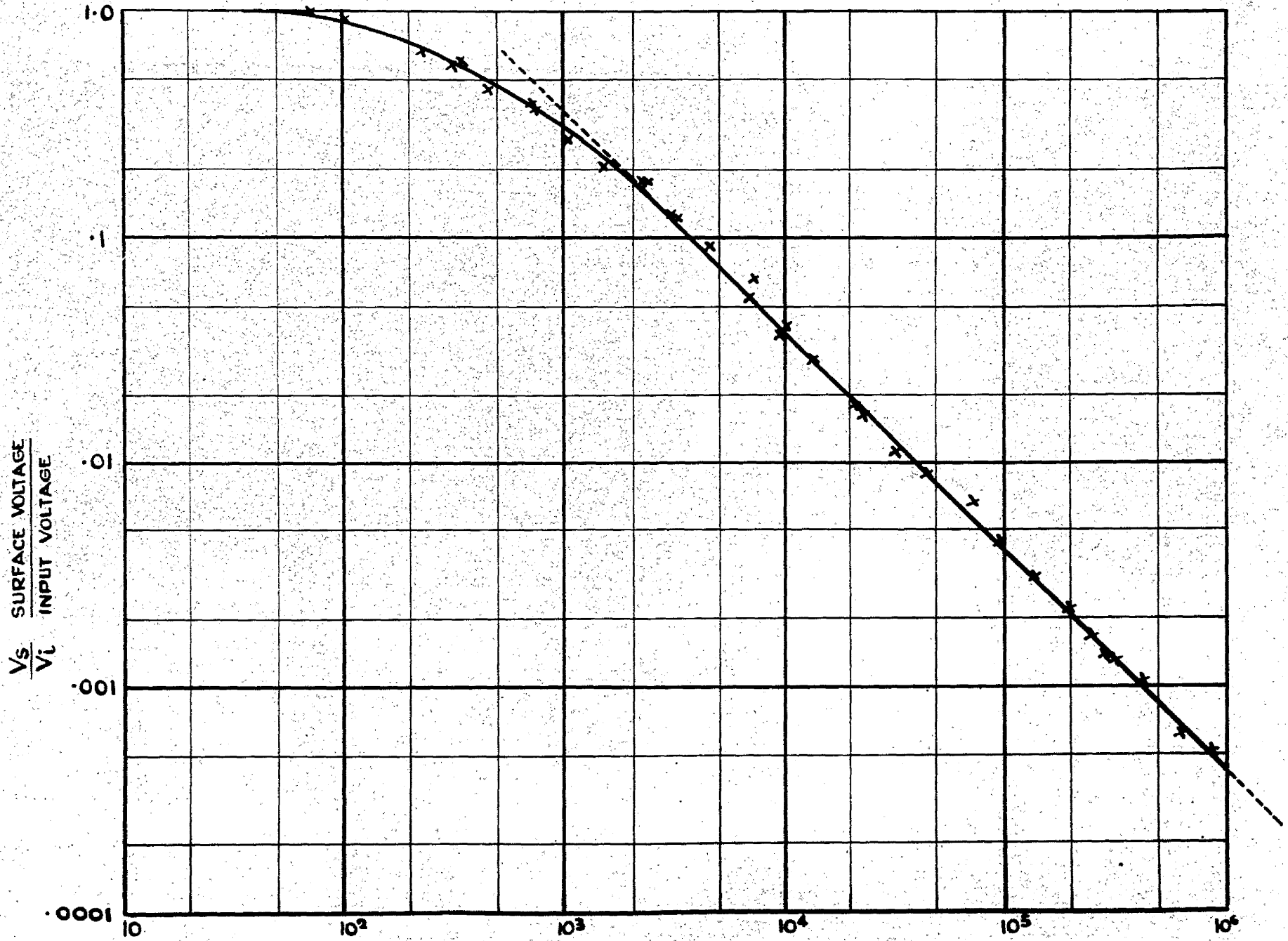
1·0
·1
·01
·001
·0001
$\frac{V_S}{V_i}$ SURFACE VOLTAGE / INPUT VOLTAGE
10
10^2
10^3
10^4
10^5
10^6
$R_i\sqrt{\omega}$ KΩ - [CYCLES/SEC]$^{1/2}$

FIG. 27.

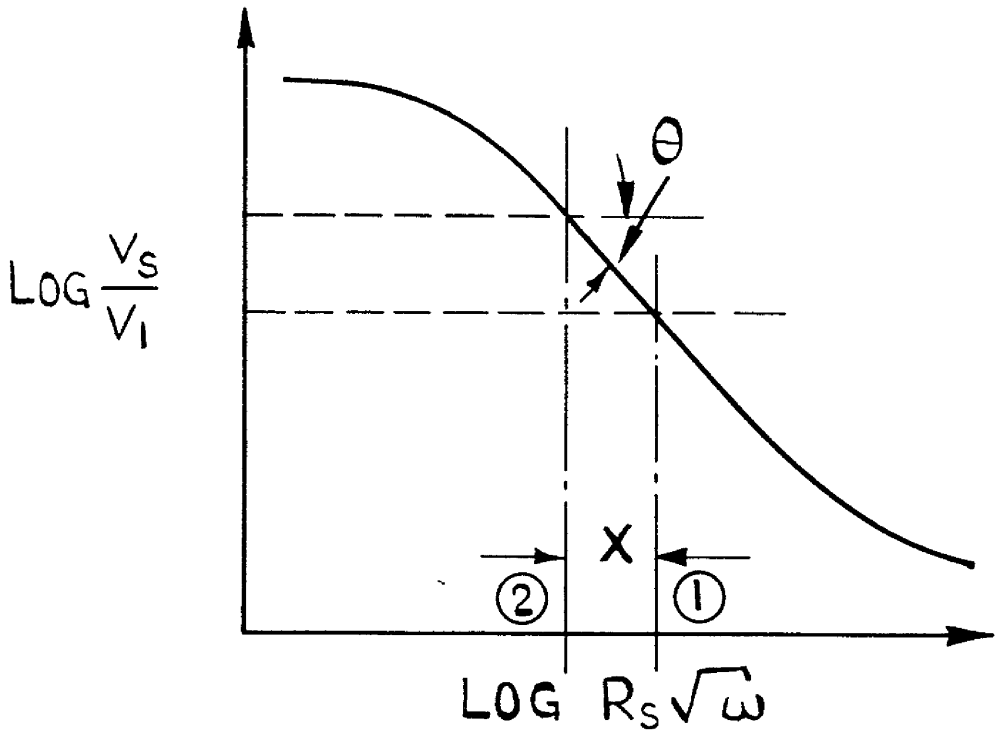

FIG.28.

THERMOCOUPLE SENSITIVITY - μV/°F
30
25
20
15
10
5
0
THERMOCOUPLE SENSITIVITY
Ti/Tc
1.0
.8
.6
.4
.2
0
10
10²
10³
10⁴
10⁵
10⁶
Ri √ω K Ω [CYCLES/SEC]½
Ti TEMPERATURE FLUCTUATION AT SURFACE OF CAST IRON
Tc TEMPERATURE FLUCTUATION AT SURFACE OF CONSTANTAN

FIG 29

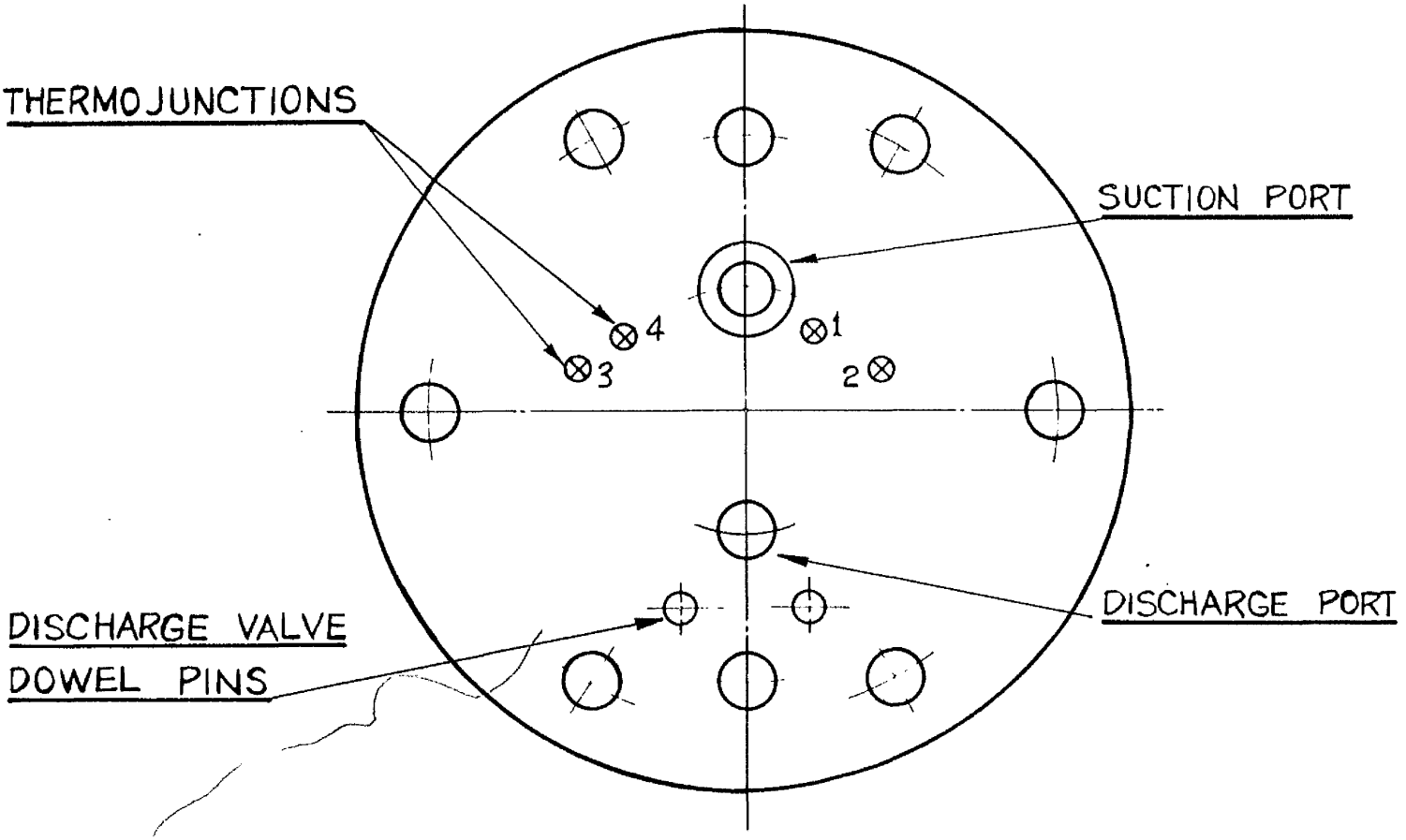

VALVE PLATE (FULL SIZE)

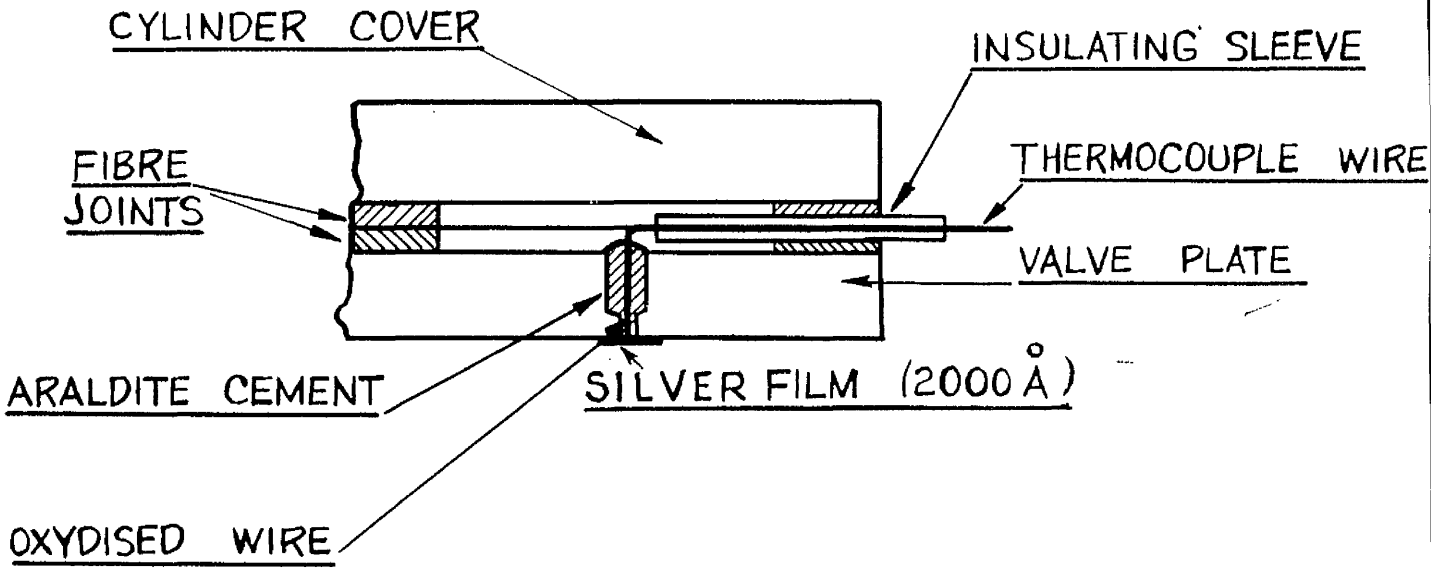

THERMOCOUPLE INSULATION

FIG. 30

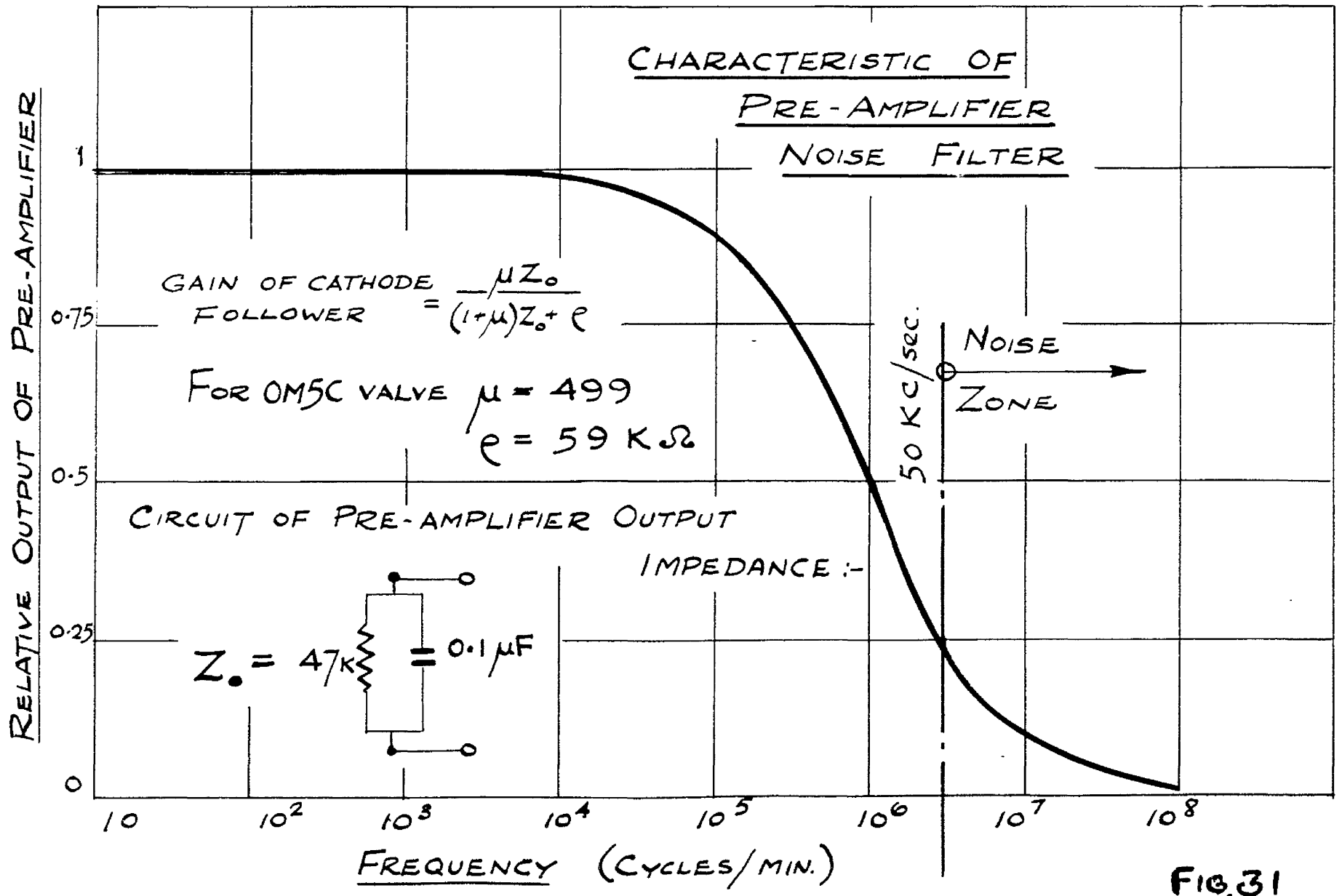
CHARACTERISTIC OF
PRE-AMPLIFIER
NOISE FILTER
RELATIVE OUTPUT OF PRE-AMPLIFIER
1
0·75
0·5
0·25
0
GAIN OF CATHODE FOLLOWER = μZ₀ / (1+μ)Z₀ + ρ
FOR 0M5C VALVE μ = 499
ρ = 59 KΩ
50 KC/SEC.
NOISE ZONE
CIRCUIT OF PRE-AMPLIFIER OUTPUT IMPEDANCE :-
Z₀ = 47K
0·1 μF
10
10²
10³
10⁴
10⁵
10⁶
10⁷
10⁸
FREQUENCY (CYCLES/MIN.)

FIG. 31

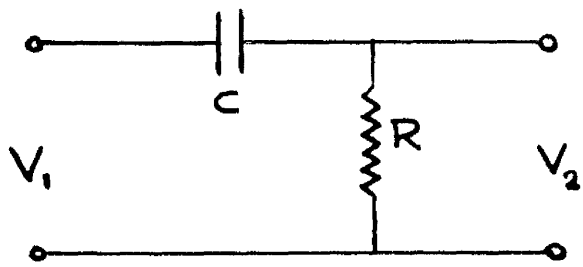

COUPLING NETWORK

FIG 32 a

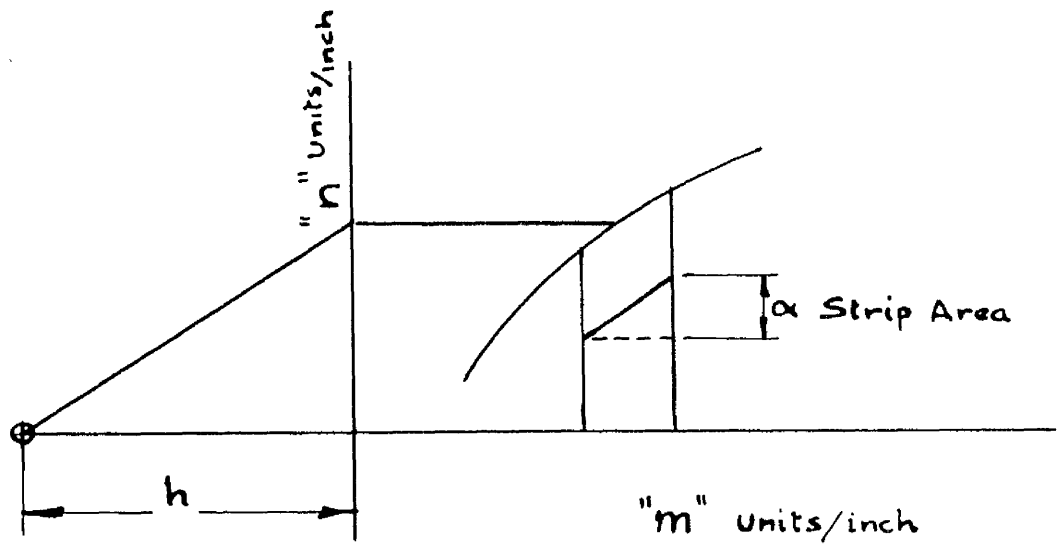

GRAPHICAL INTEGRATION PROCESS

FIG 32 b

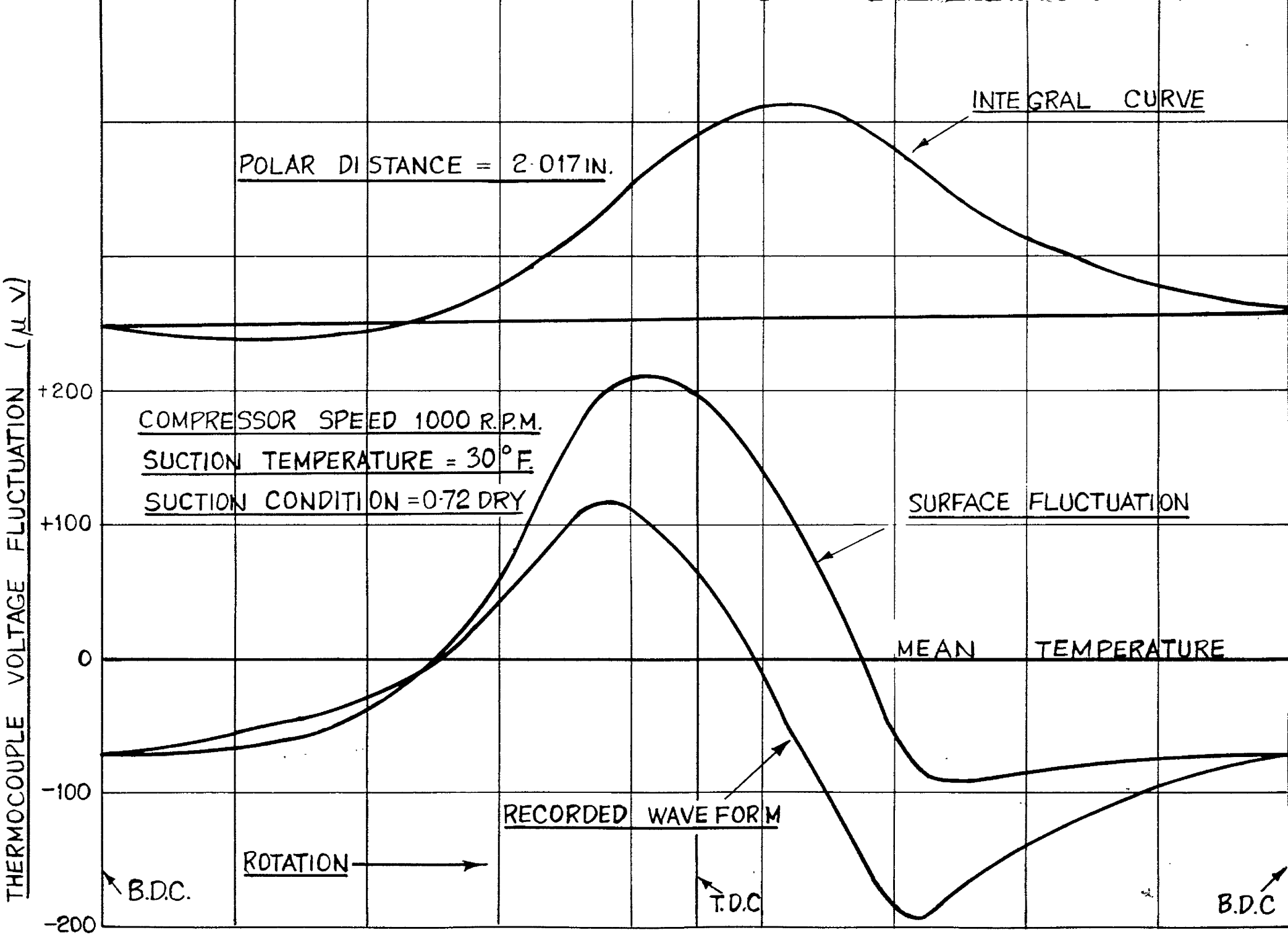

CORRECTION OF TEMPERATURE FLUCTUATION RECORD FIG. 33

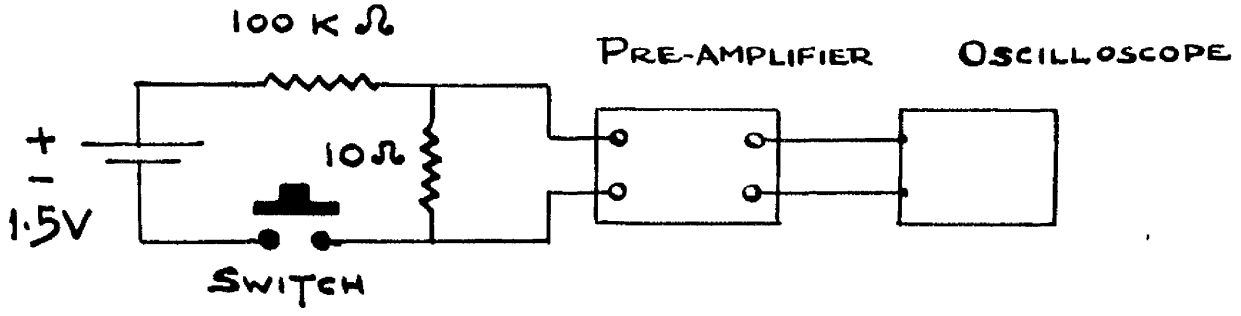

EVALUATION OF TIME CONSTANT

FIG 34 a

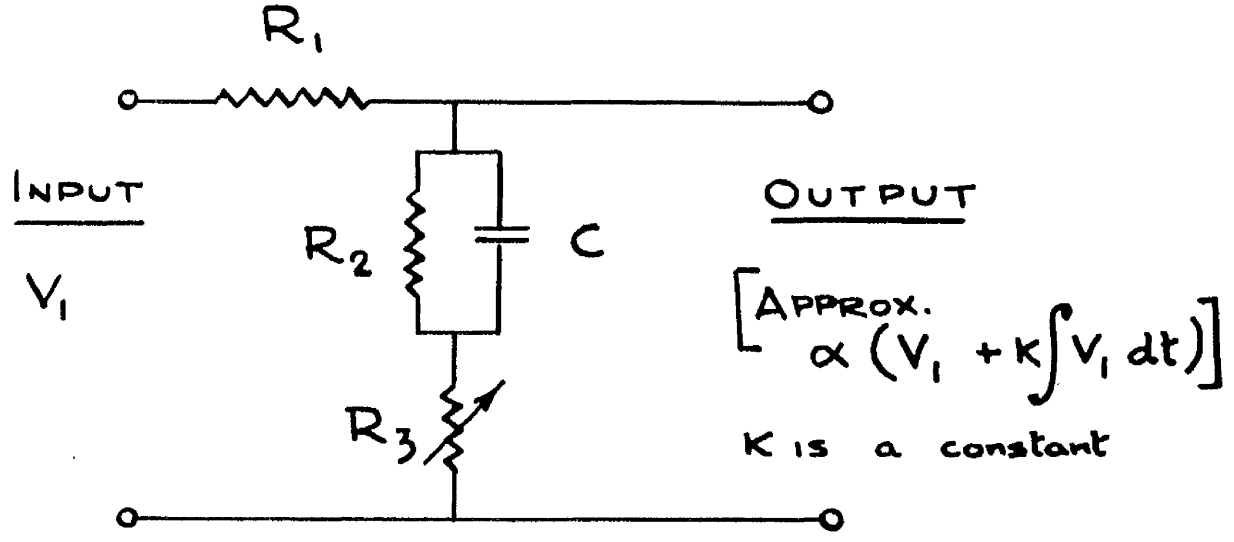

CORRECTION NETWORK

FIG 34 b

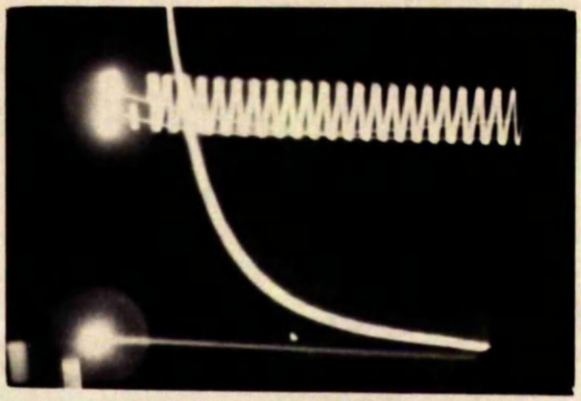

EXPONENTIAL DECAY TRACE, Fig.35a.

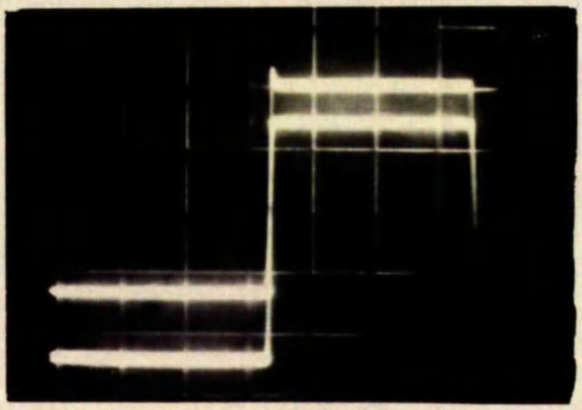

Response at
1000 rev./min.

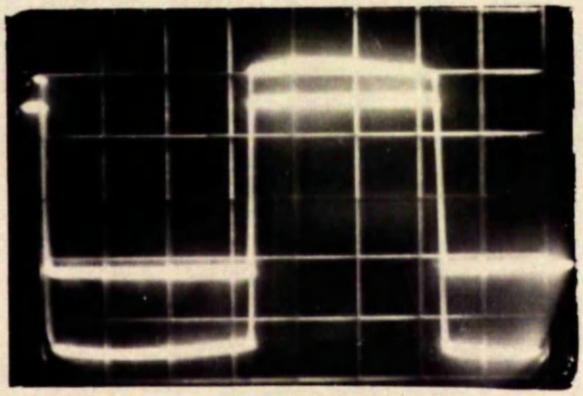

Response at
500 rev./min.

RESPONSE OF PASSIVE CORRECTION NETWORK, Fig.35b.

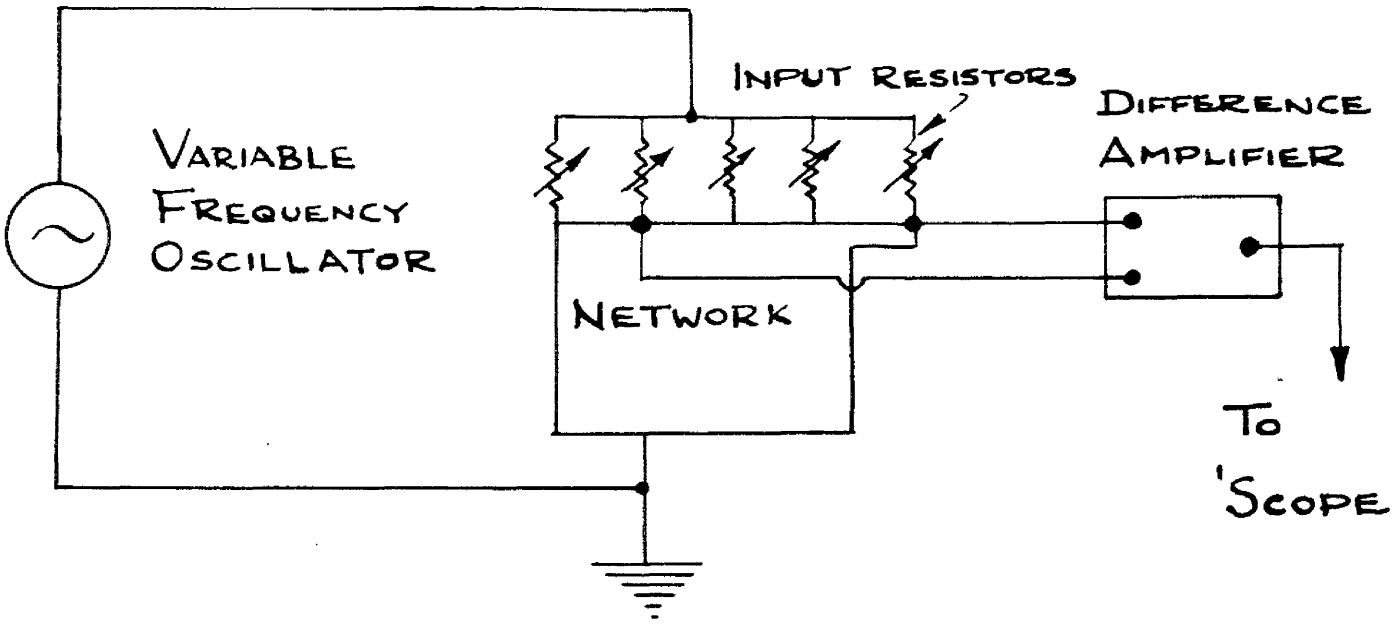

BLOCK DIAGRAM OF 2-DIMENSIONAL ANALOGUE

FIG NO. 36

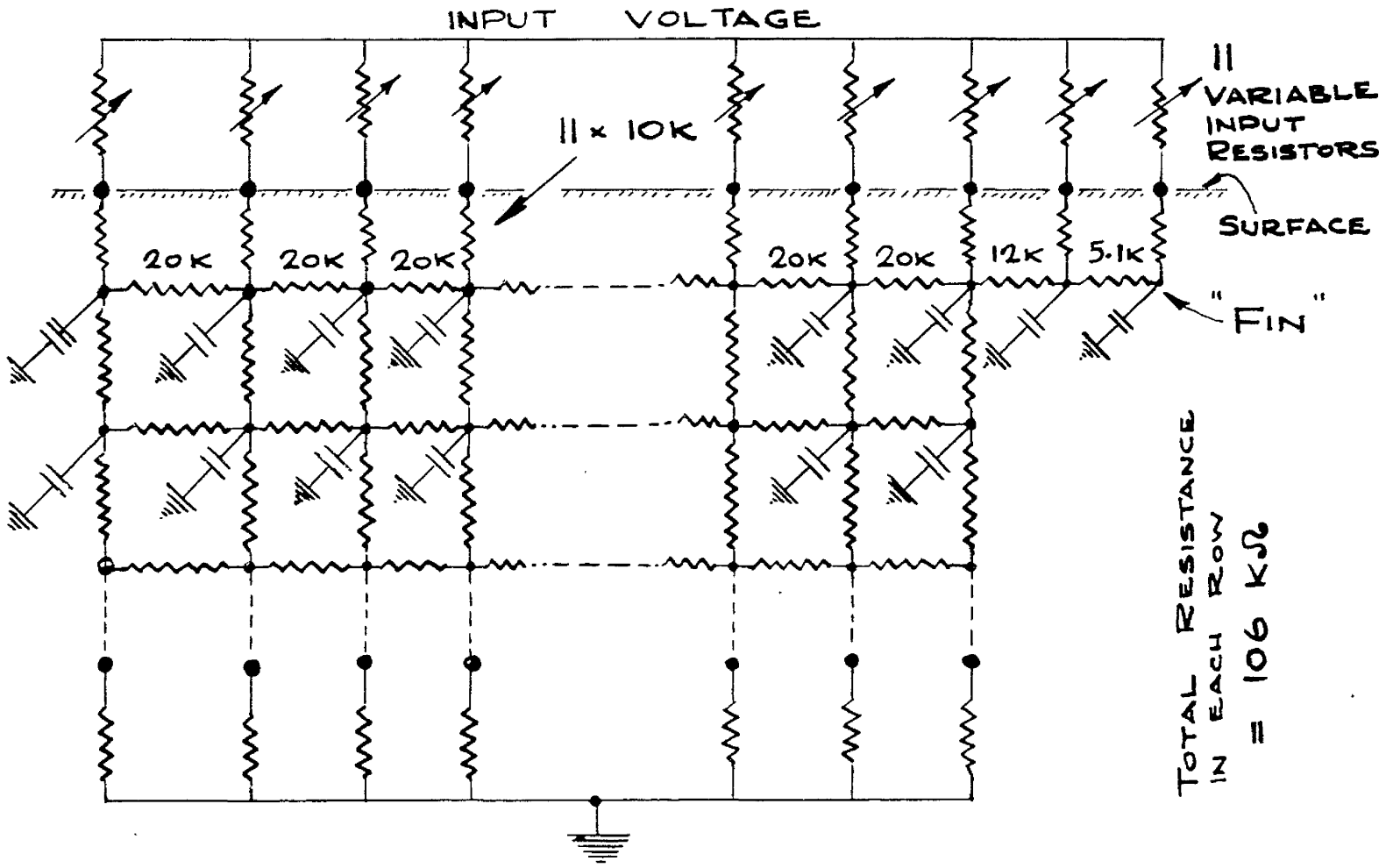

CONDENSER AT EACH NODE = 0.01 μF

NETWORK FOR 2-DIMENSIONAL ANALOGUE

FIG. No 37

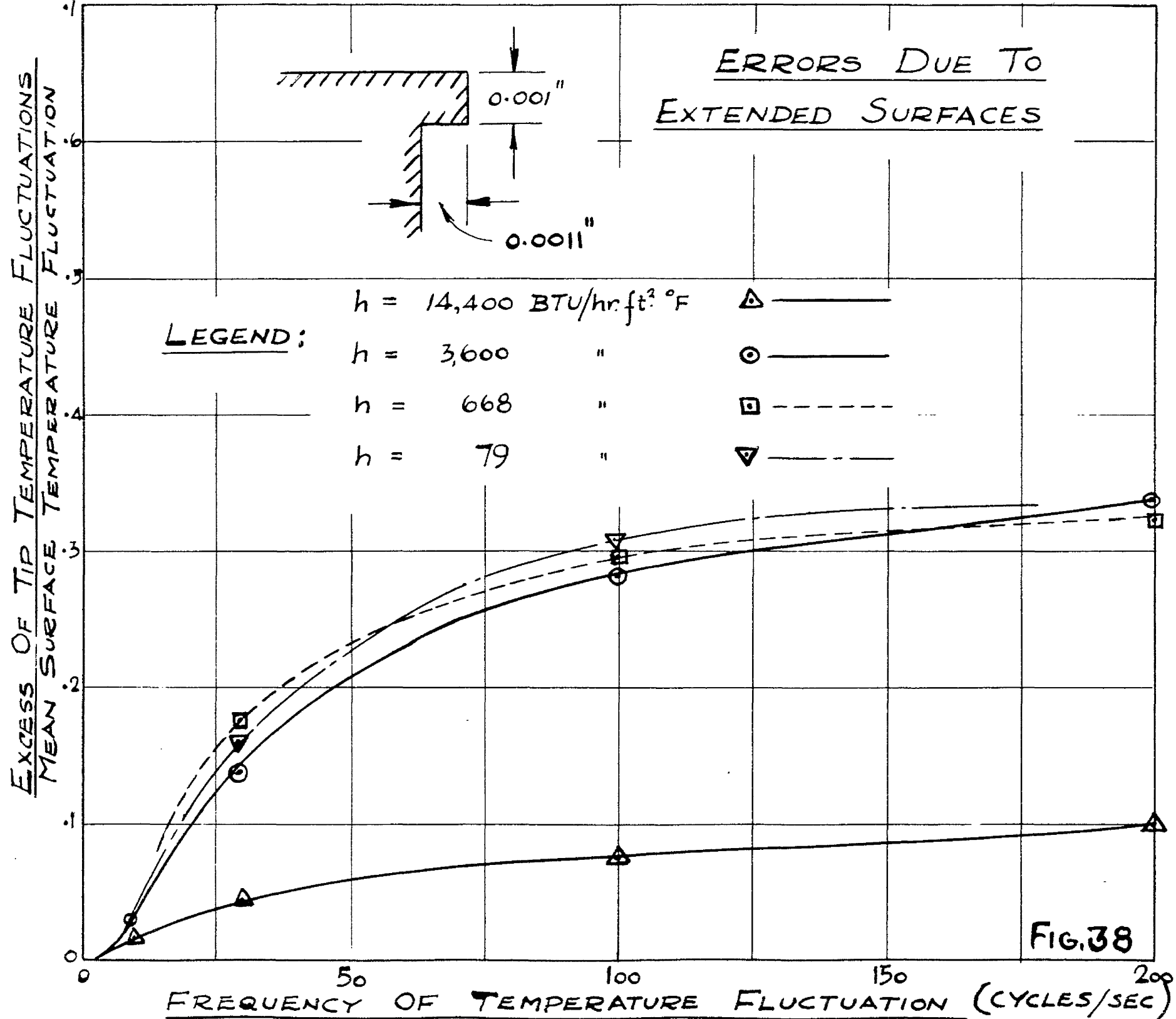
ERRORS DUE TO EXTENDED SURFACES
0.001"
0.0011"
LEGEND:
h = 14,400 BTU/hr ft² °F
h = 3,600 "
h = 668 "
h = 79 "
EXCESS OF TIP TEMPERATURE FLUCTUATIONS / MEAN SURFACE TEMPERATURE FLUCTUATION
0
.1
.2
.3
.4
.6
.7
0
50
100
150
200
FREQUENCY OF TEMPERATURE FLUCTUATION (CYCLES/SEC)
FIG. 38

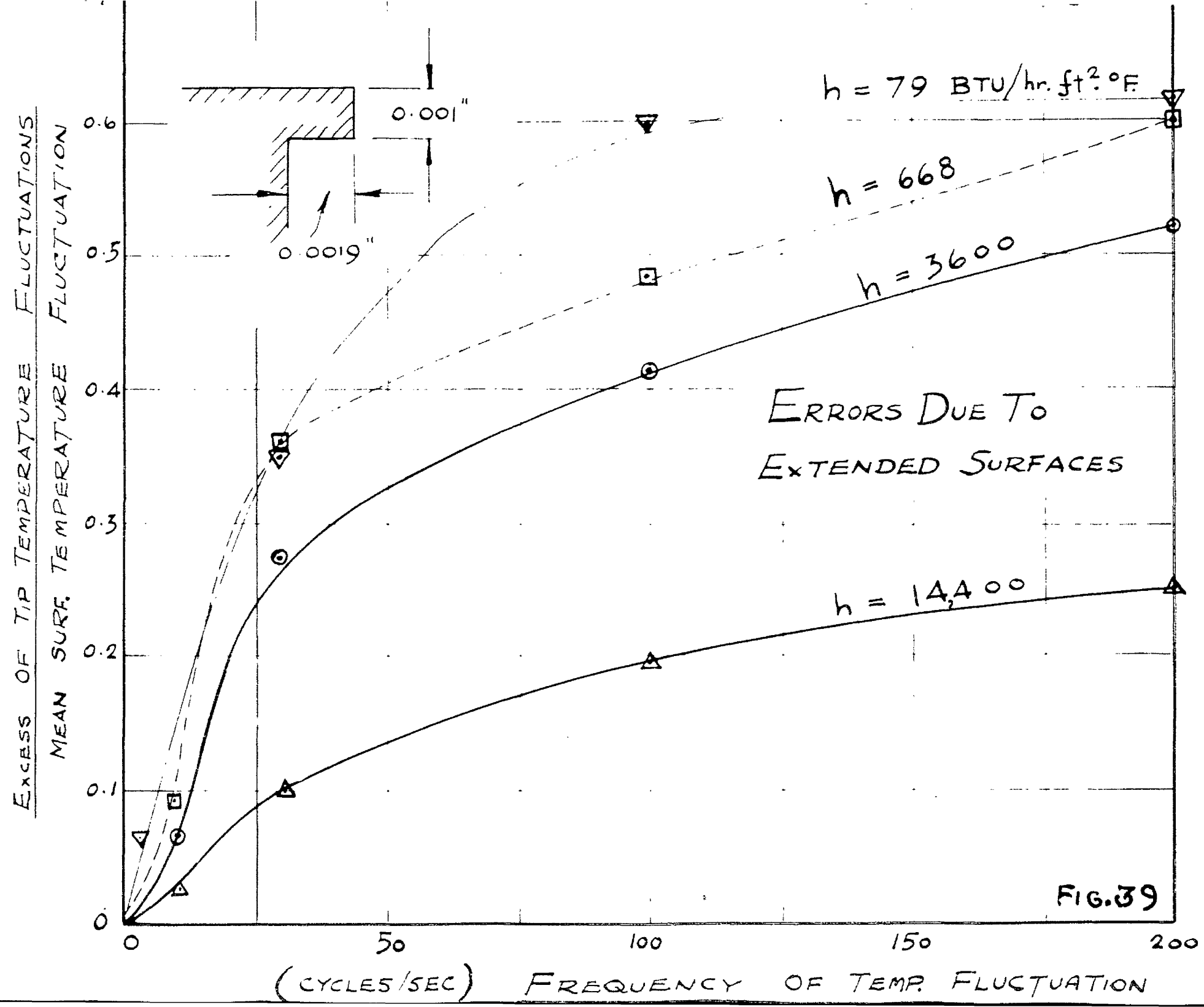
0.001"
0.0019"
h = 79 BTU/hr. ft². °F.
h = 668
h = 3600
h = 14,400
ERRORS DUE TO
EXTENDED SURFACES
FIG. 39
EXCESS OF TIP TEMPERATURE FLUCTUATIONS
MEAN SURF. TEMPERATURE FLUCTUATION
0
0.1
0.2
0.3
0.4
0.5
0.6
0
50
100
150
200
(CYCLES/SEC) FREQUENCY OF TEMP. FLUCTUATION

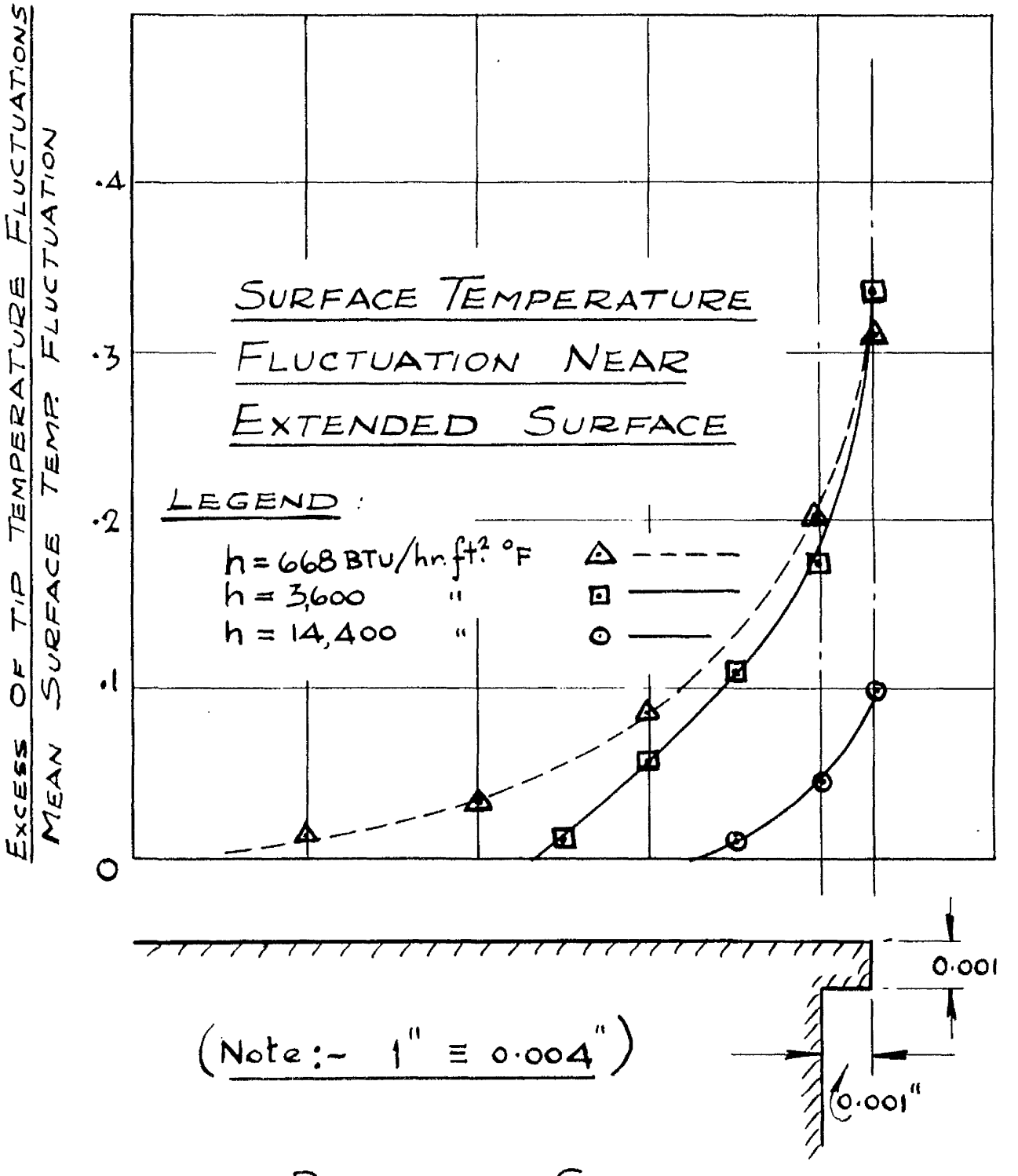
EXCESS OF TIP TEMPERATURE FLUCTUATIONS
MEAN SURFACE TEMP. FLUCTUATION
.4
.3
.2
.1
0
SURFACE TEMPERATURE
FLUCTUATION NEAR
EXTENDED SURFACE
LEGEND :
h = 668 BTU/hr.ft.² °F
h = 3,600 "
h = 14,400 "
0.001
(Note :- 1" ≡ 0.004")
0.001"
POSITION ON SURFACE

FIG.40

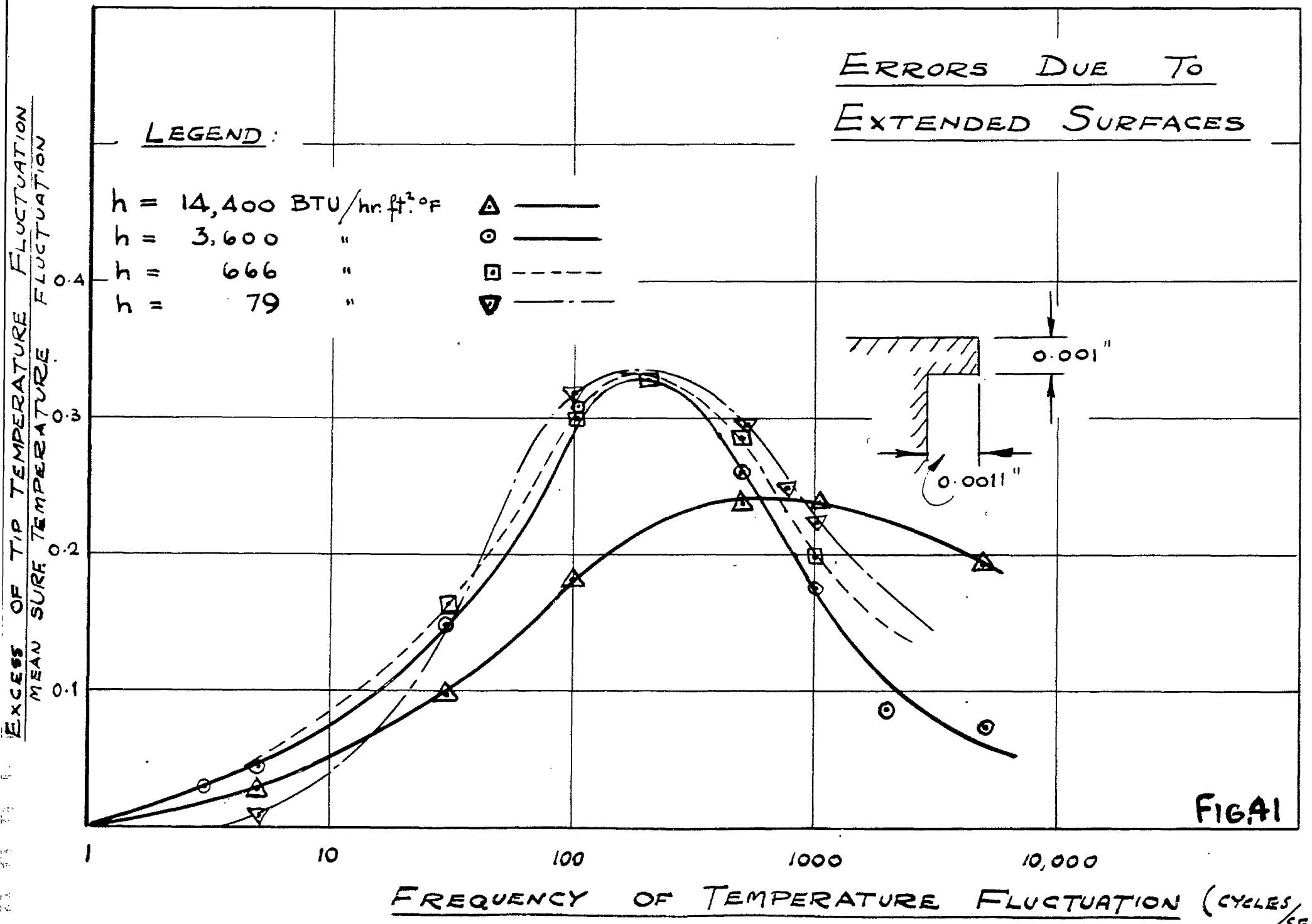
ERRORS DUE TO EXTENDED SURFACES
LEGEND:
h = 14,400 BTU/hr.ft².°F
h = 3,600 "
h = 666 "
h = 79 "
0.001"
0.0011"
EXCESS OF TIP TEMPERATURE FLUCTUATION / MEAN SURF. TEMPERATURE FLUCTUATION
0.4
0.3
0.2
0.1
1
10
100
1000
10,000
FREQUENCY OF TEMPERATURE FLUCTUATION (CYCLES/SEC)
FIG.41

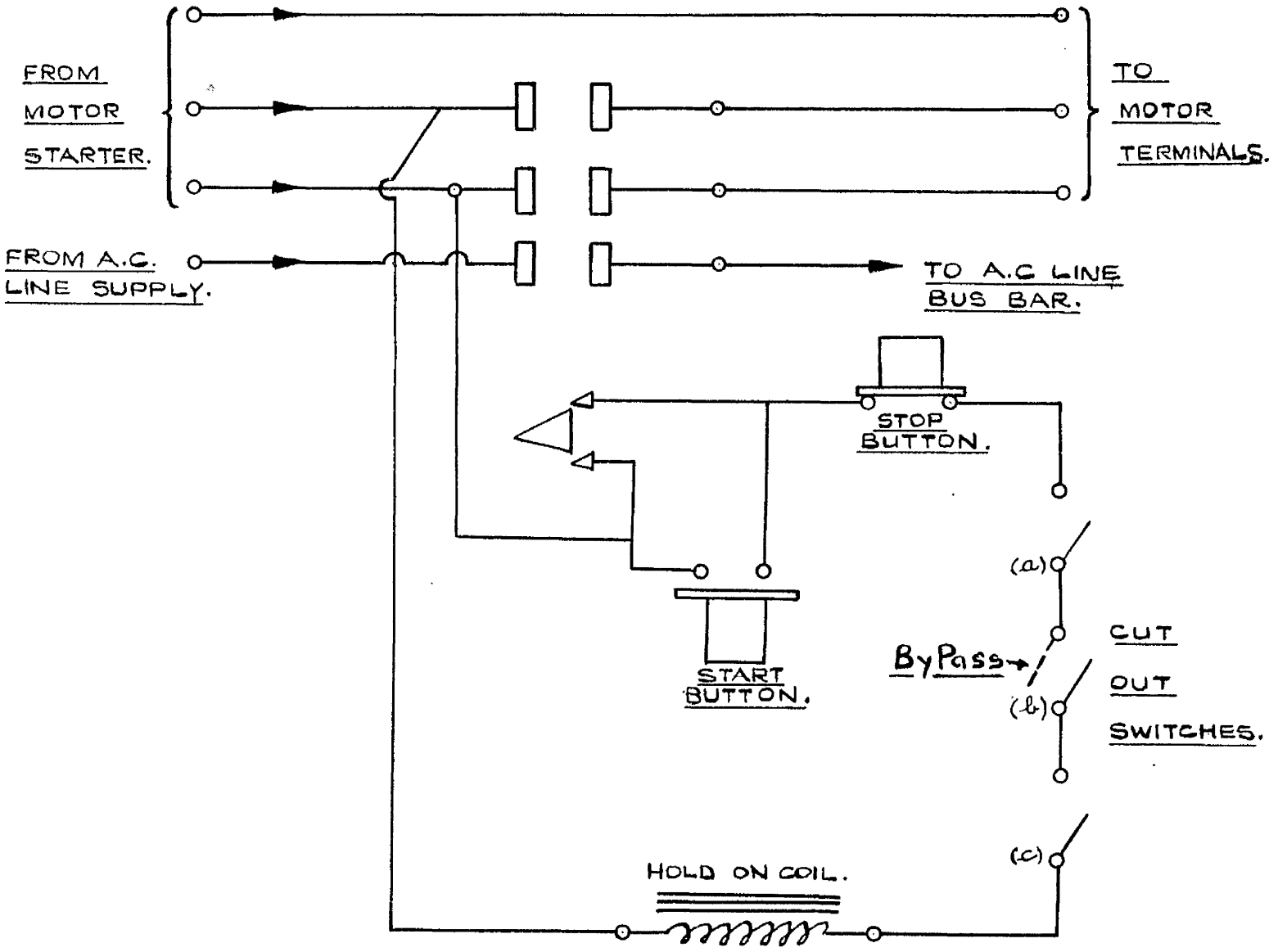

(a). CONDENSER H.P. CUT OUT.

(b). COMPRESSOR L.P. CUT OUT.

(c). CALORIMETER SHELL H.P. CUT OUT.

CUT OUT CIRCUIT.

FIG. No. 42

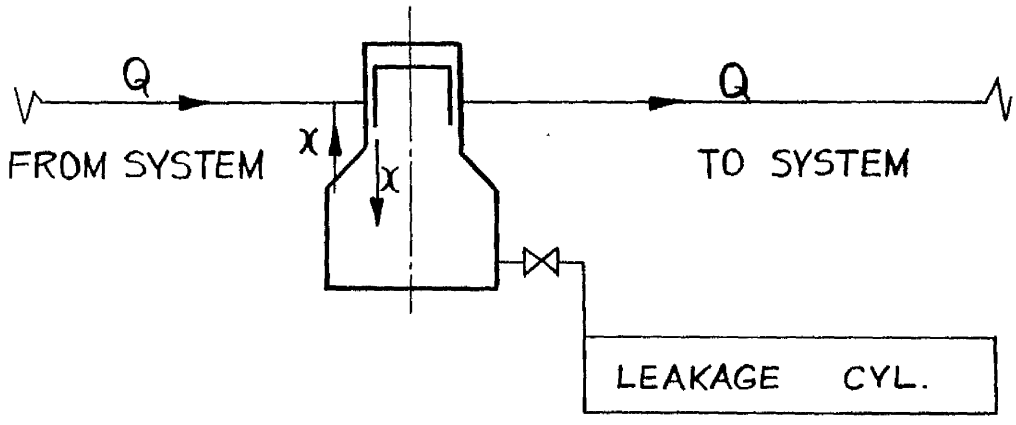

NORMAL RUNNING

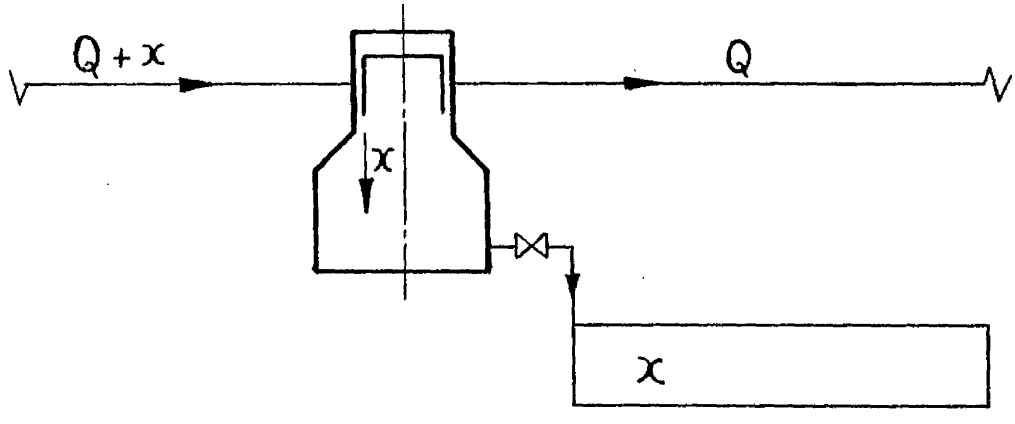

LEAKAGE TEST

PISTON LEAKAGE FLOW CHART

FIG.43

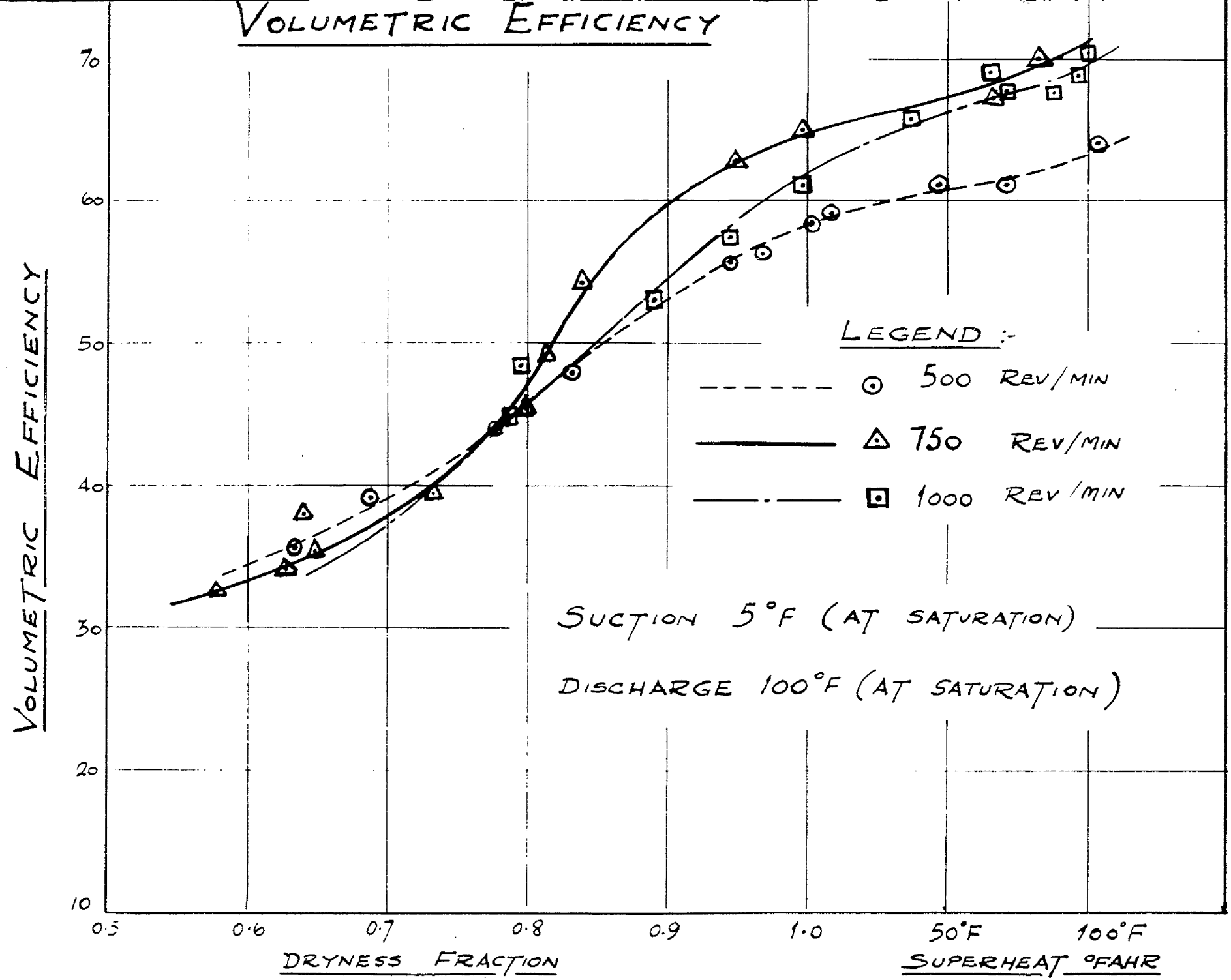

CONDITION AT COMPRESSOR SUCTION

FIG. 44

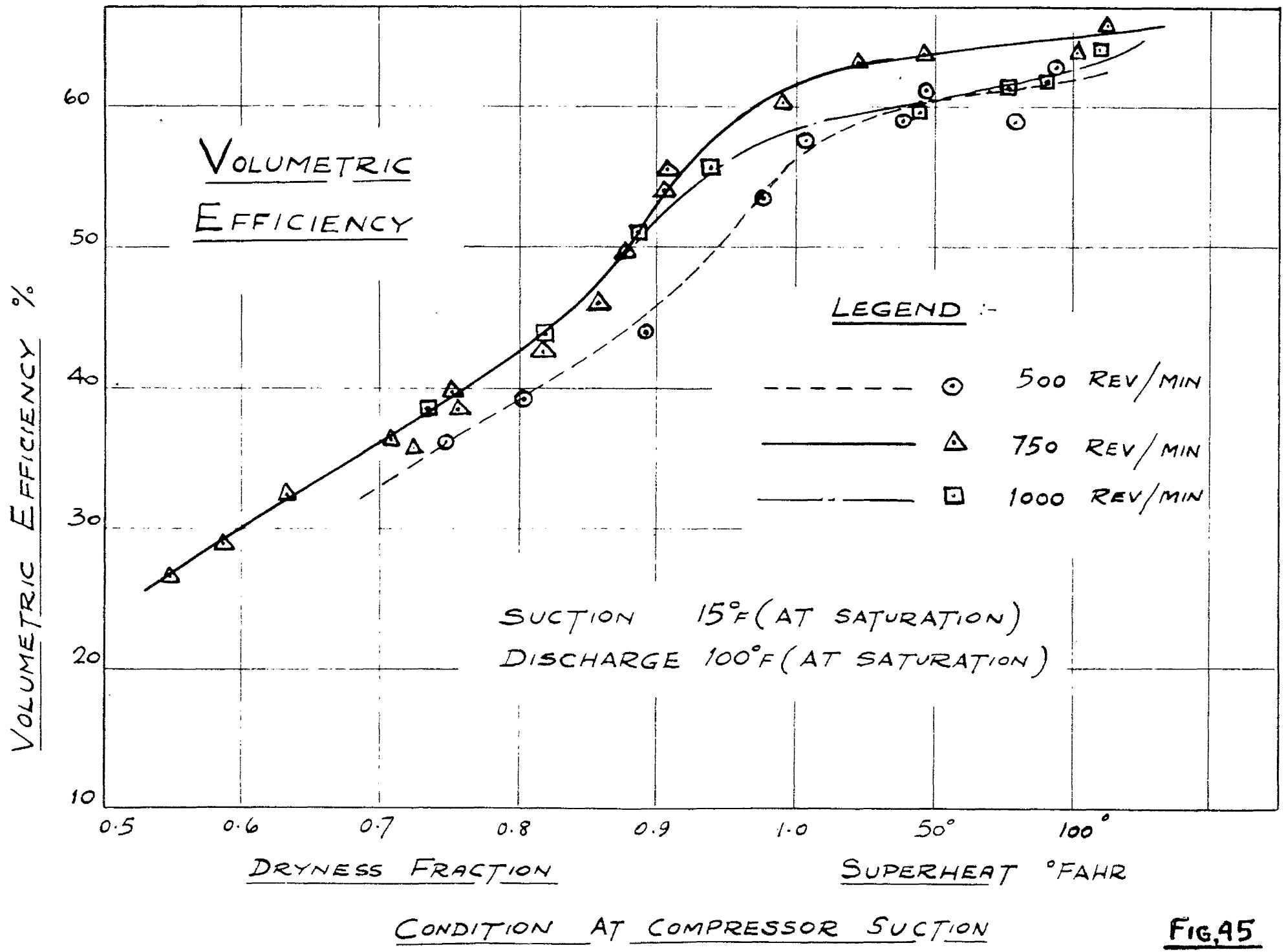

CONDITION AT COMPRESSOR SUCTION

FIG. 45

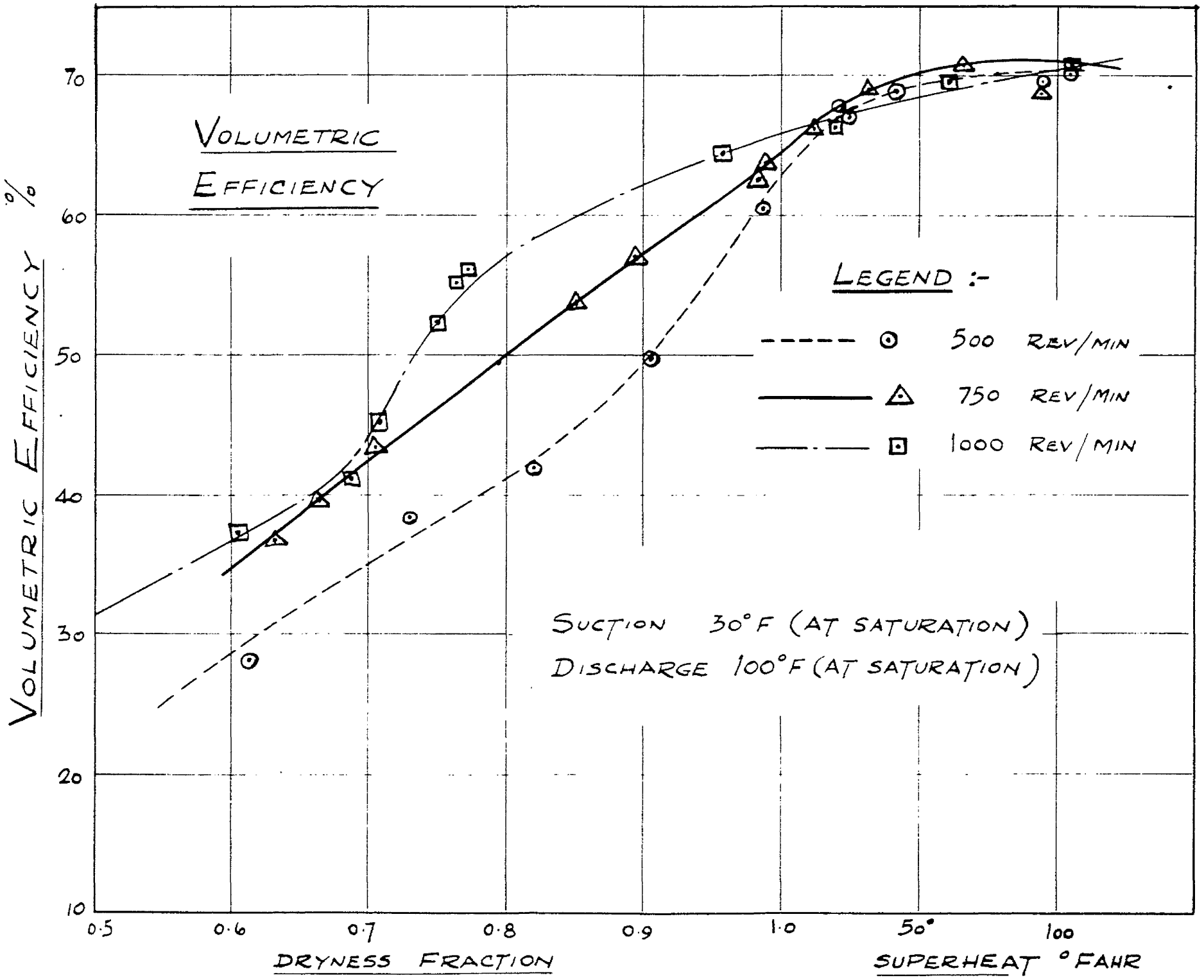

CONDITION AT COMPRESSOR SUCTION

FIG.46

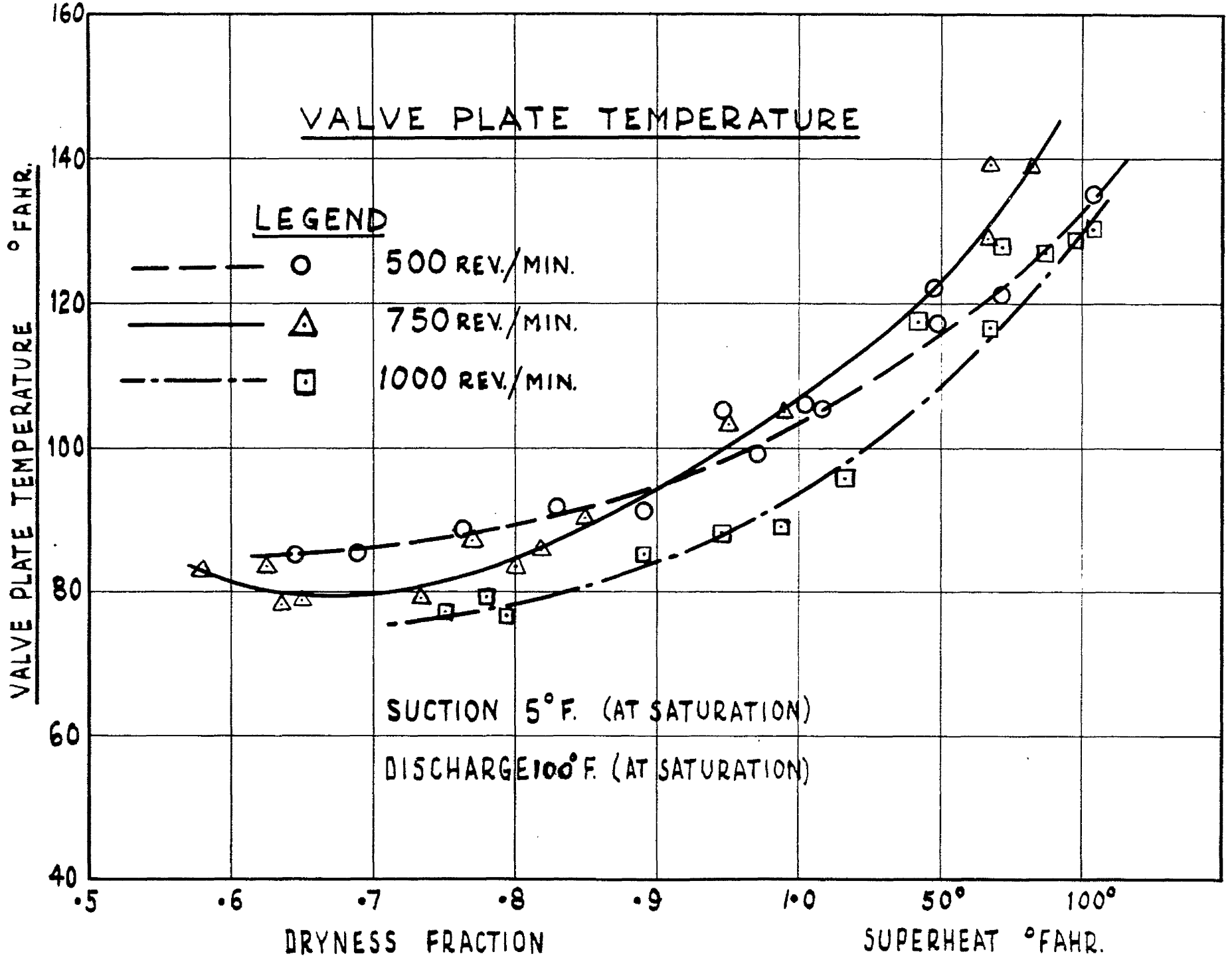

CONDITION AT COMPRESSOR SUCTION

FIG. 47

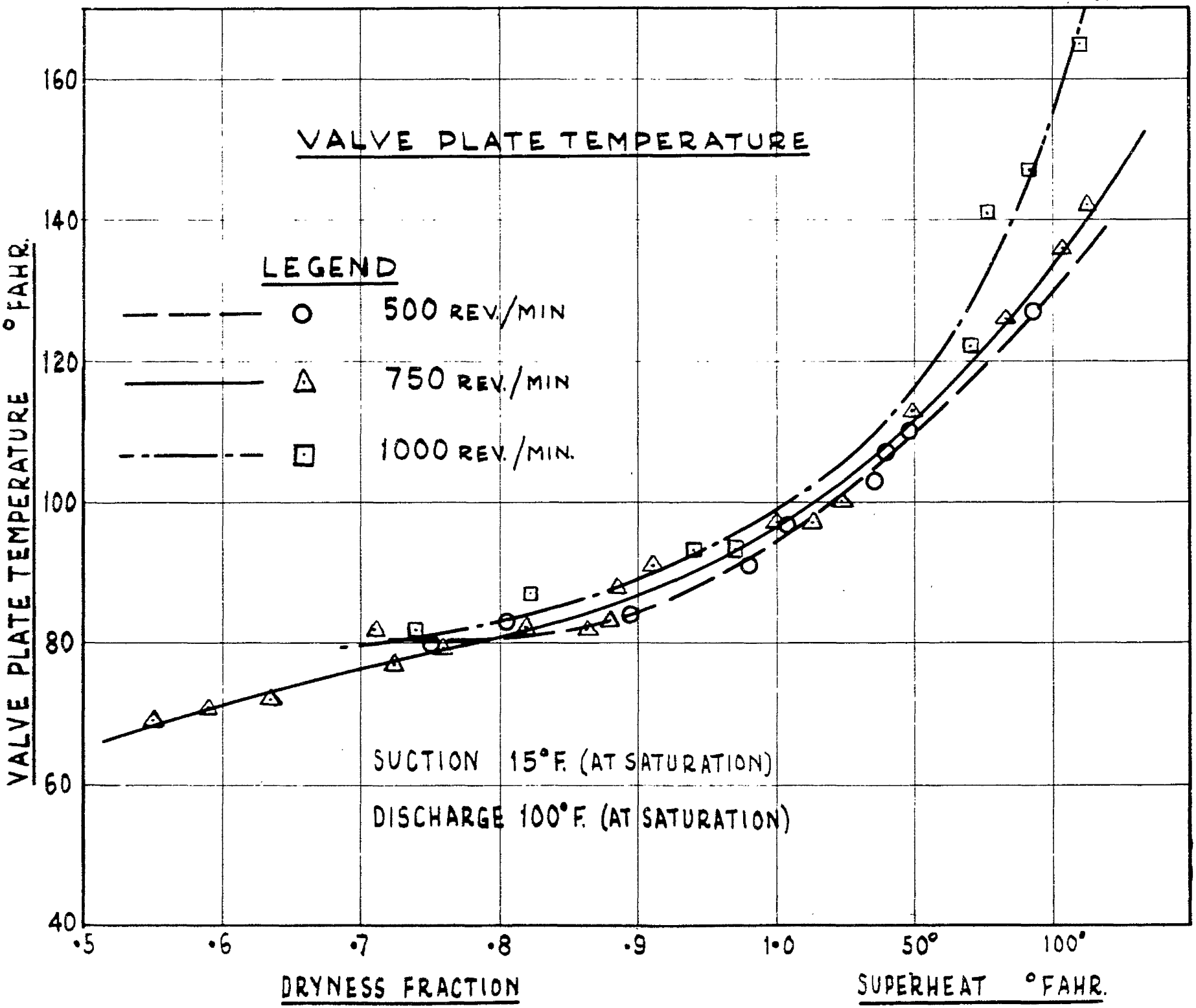

CONDITION AT COMPRESSOR SUCTION

FIG. 48

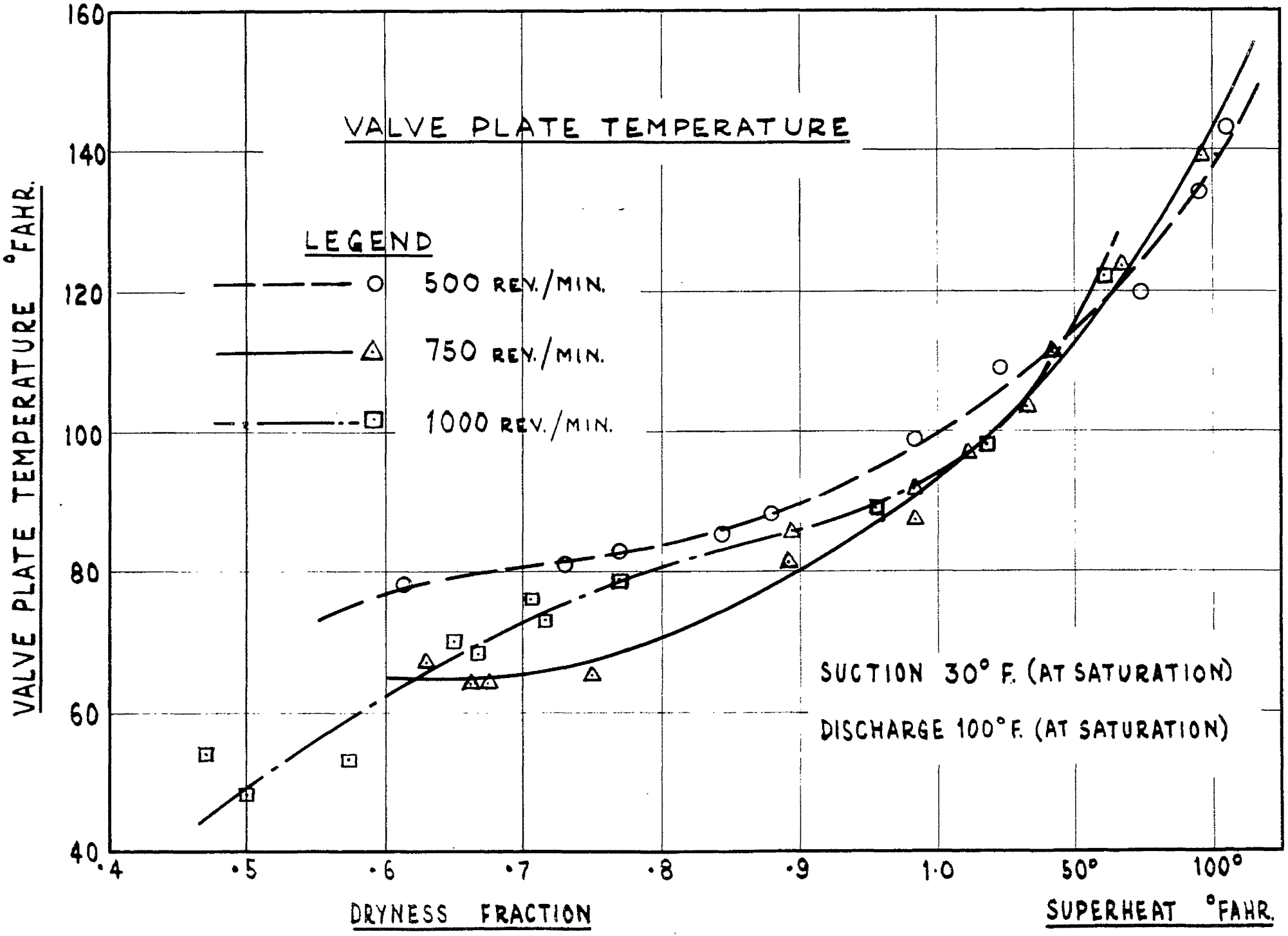

CONDITION AT COMPRESSOR SUCTION

FIG. 49

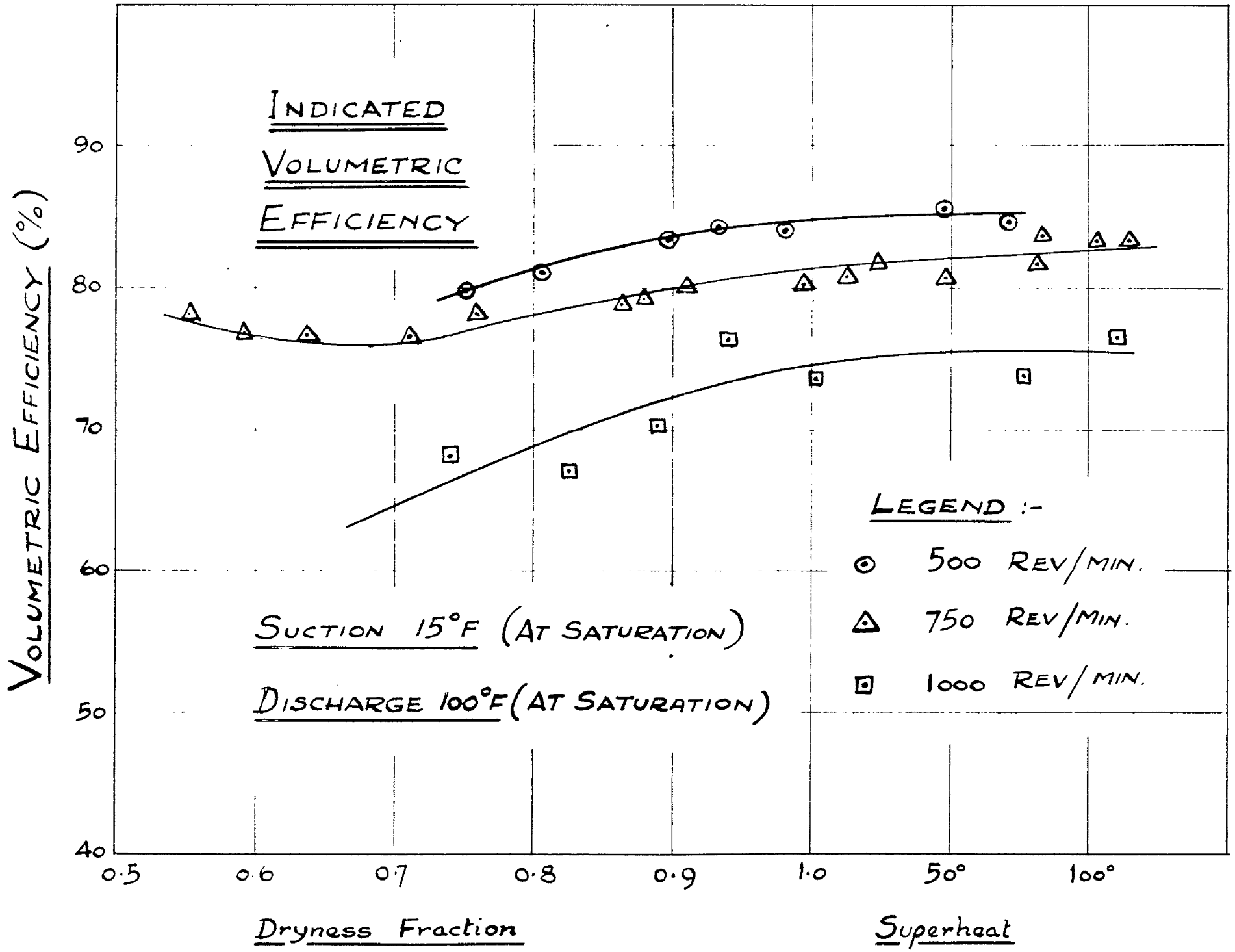

CONDITION AT SUCTION

FIG. 50

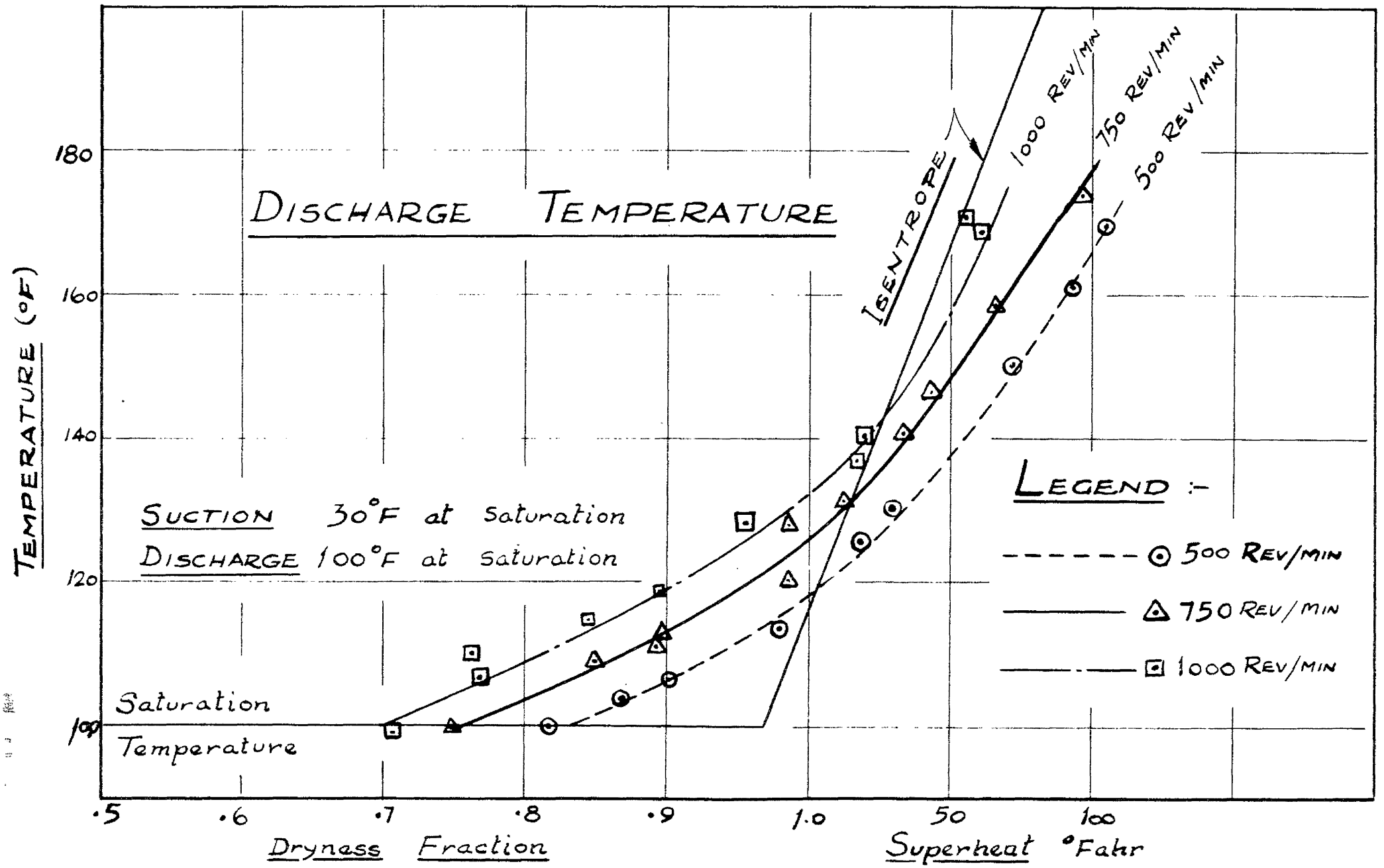

CONDITION AT COMPRESSOR SUCTION

FIG.51

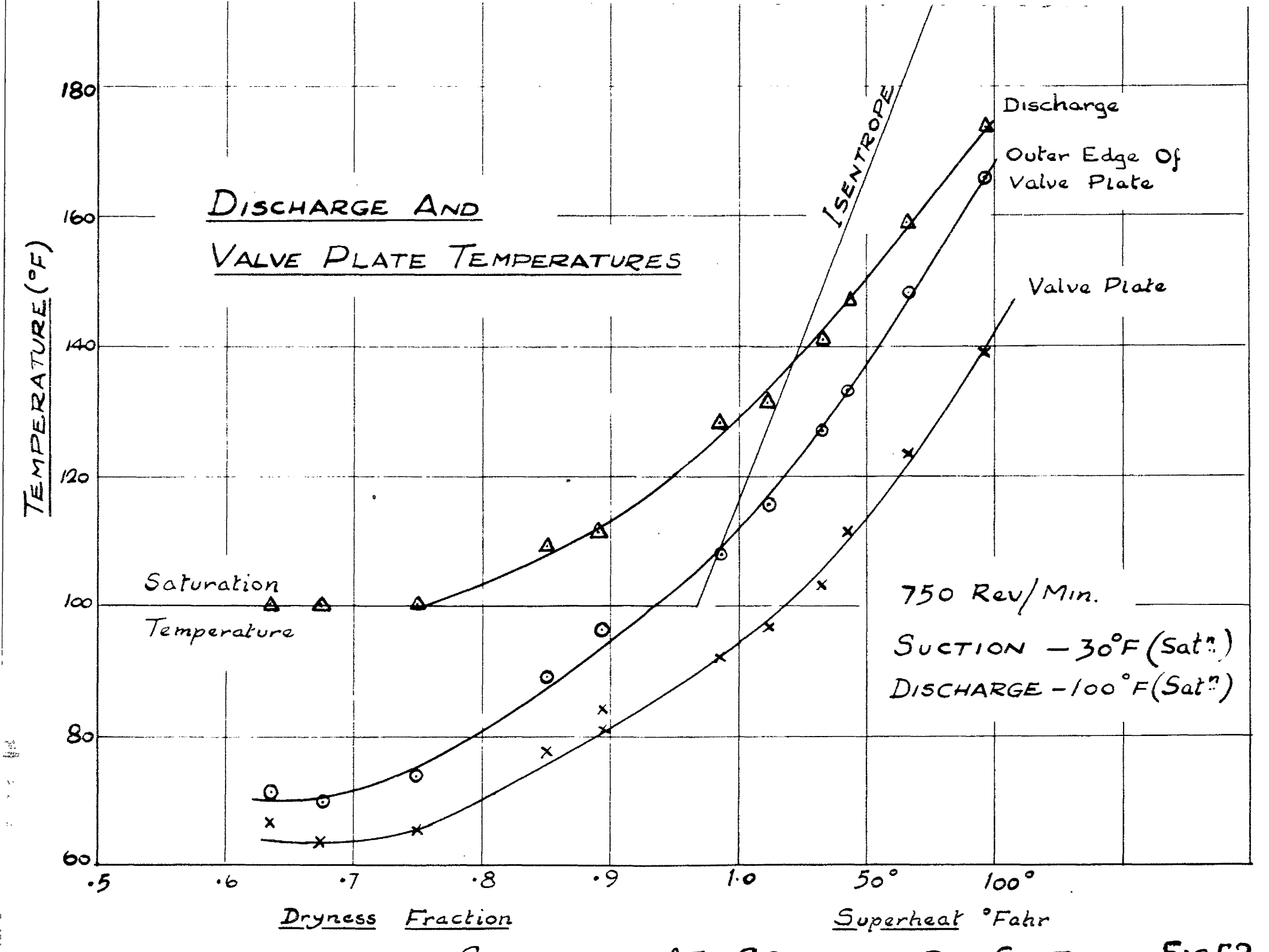

CONDITION AT COMPRESSOR SUCTION FIG.52

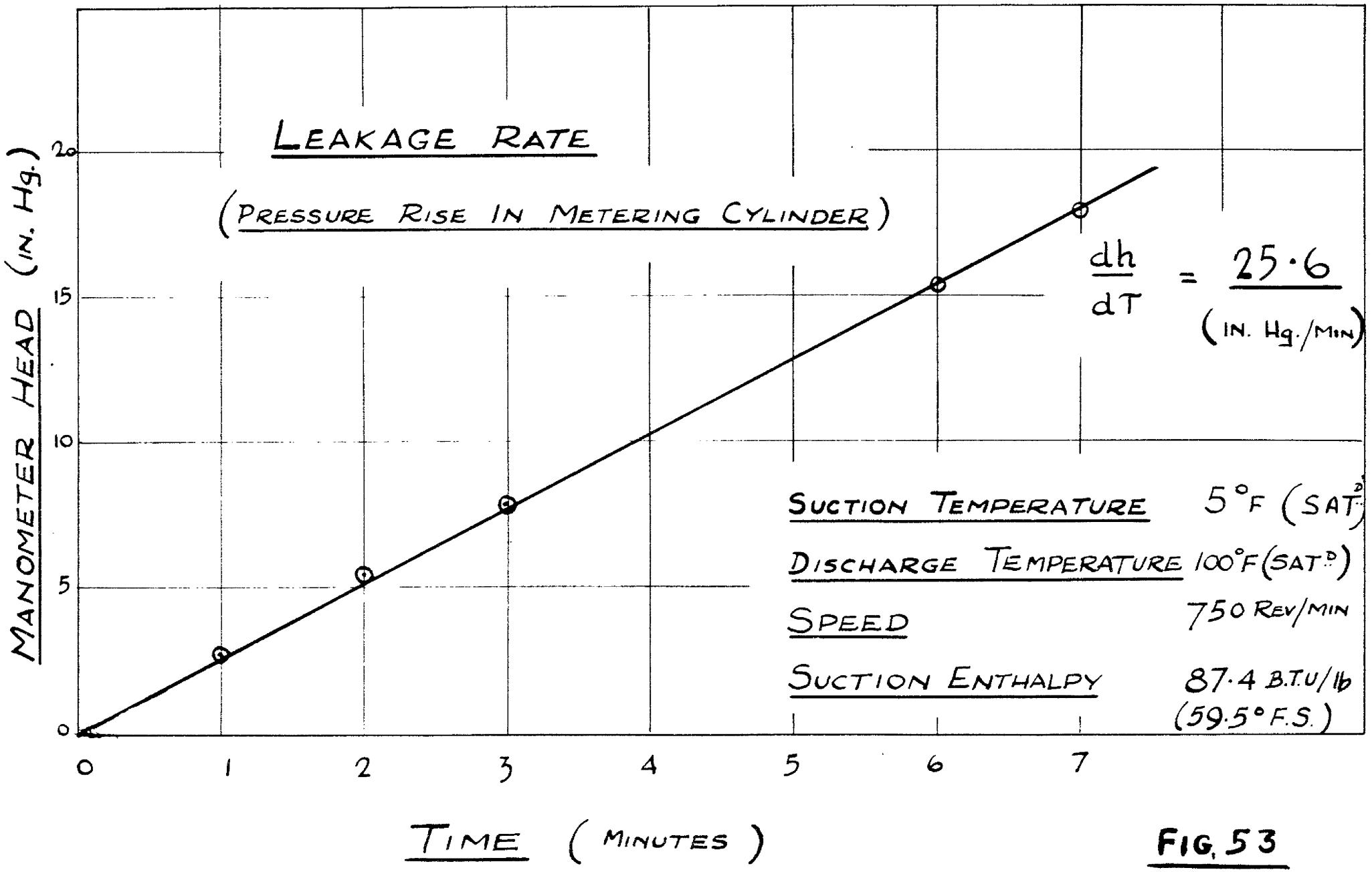
LEAKAGE RATE
(PRESSURE RISE IN METERING CYLINDER)
MANOMETER HEAD (IN. Hg.)
0
5
10
15
20
0
1
2
3
4
5
6
7
TIME (MINUTES)
dh/dT = 25·6 (IN. Hg./MIN)
SUCTION TEMPERATURE 5°F (SAT.D)
DISCHARGE TEMPERATURE 100°F (SAT.D)
SPEED 750 REV/MIN
SUCTION ENTHALPY 87·4 B.T.U/lb (59·5° F.S.)

FIG. 53

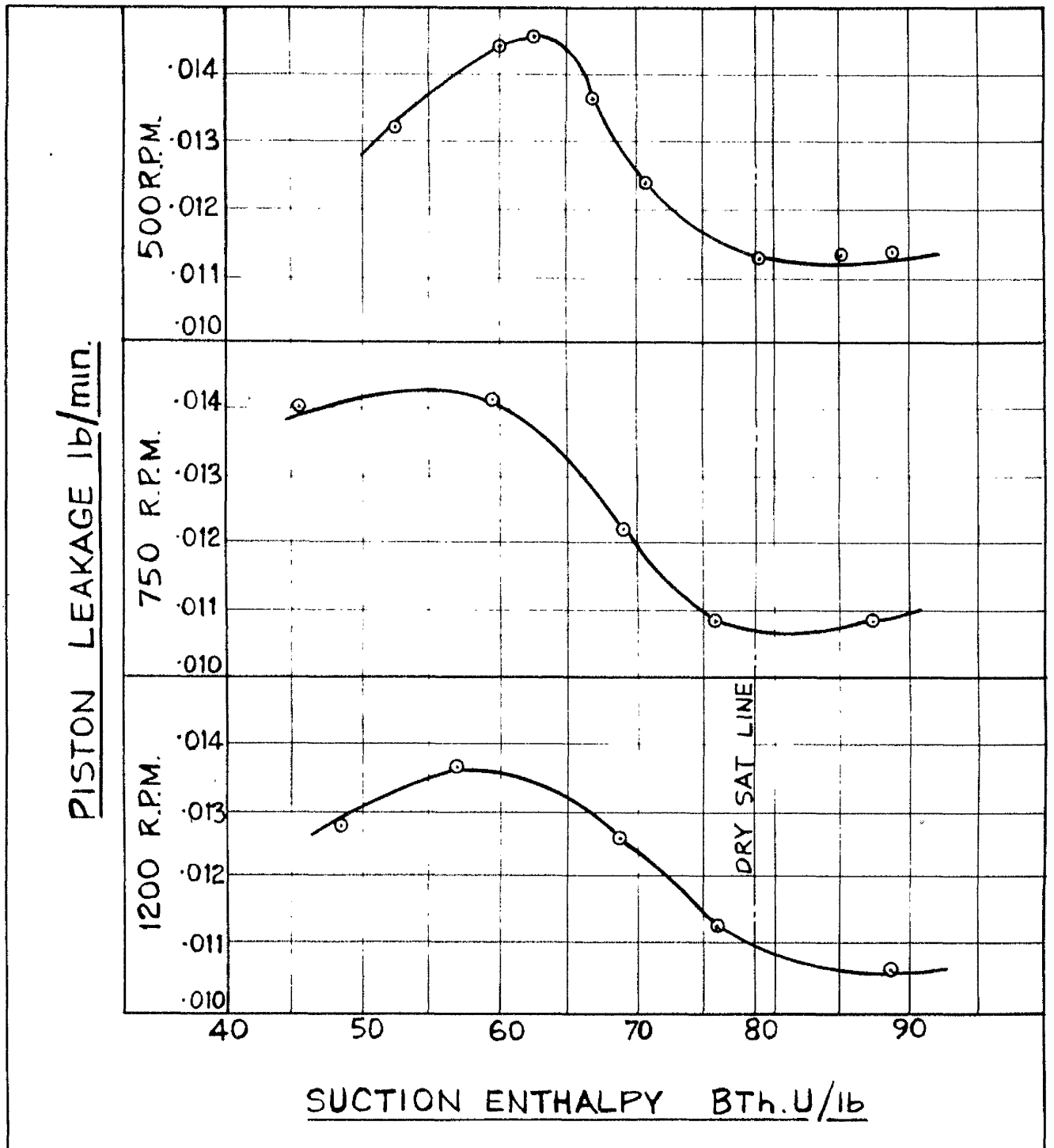

PISTON LEAKAGE RESULTS 5°F./100°F.

FIG. 54

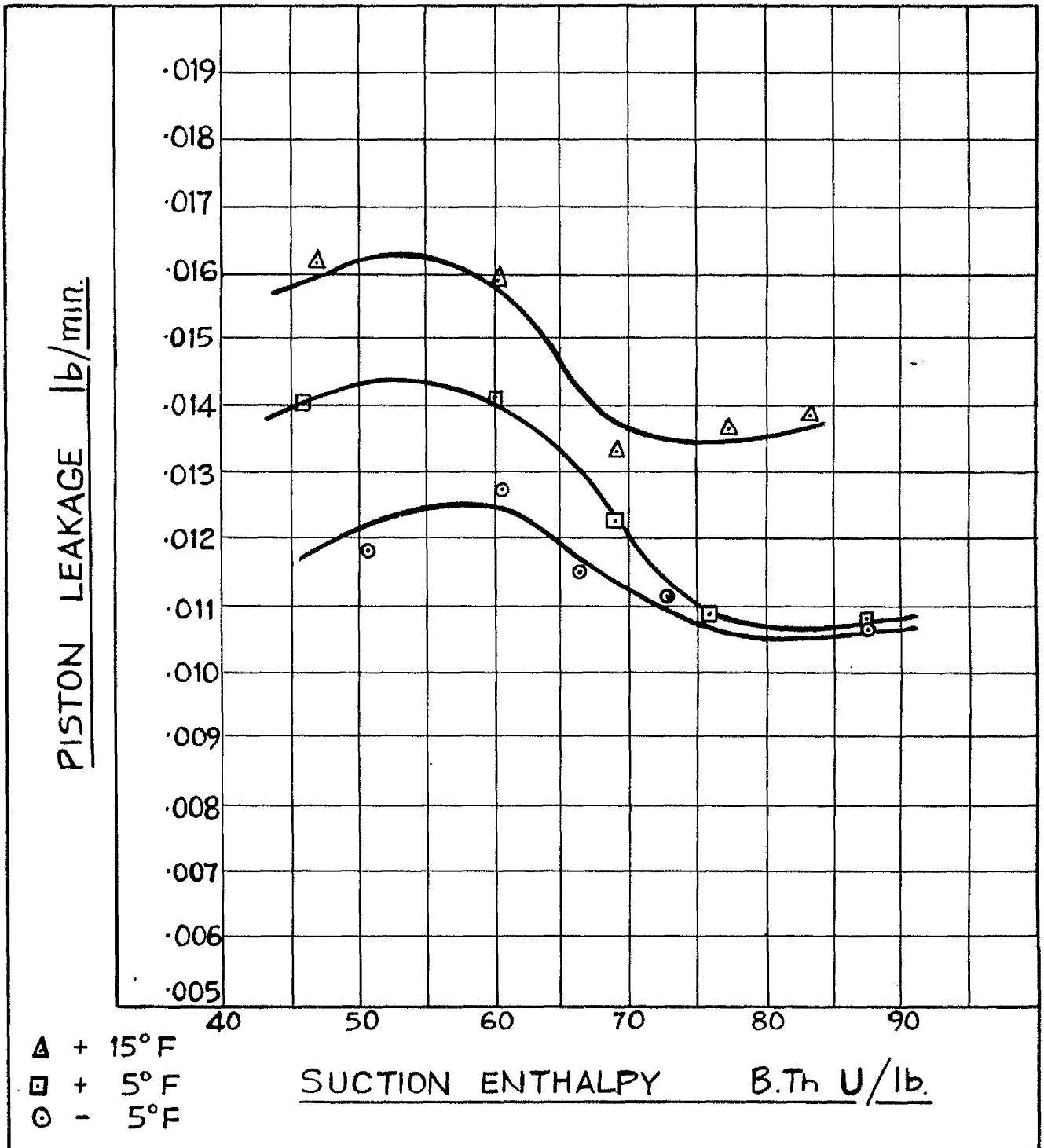

PISTON LEAKAGE RESULTS 750 R.P.M/100°F.

FIG. 55

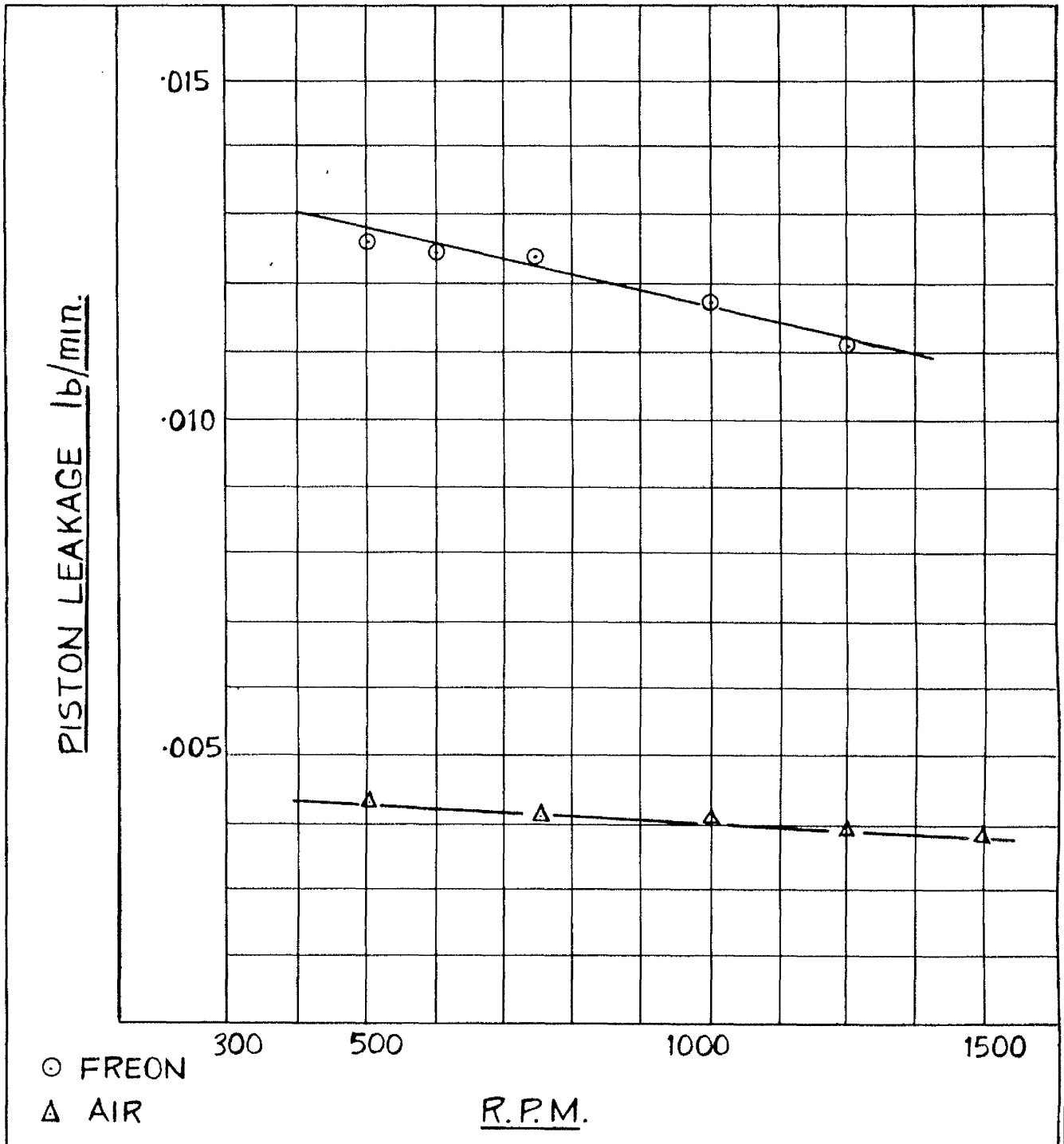

PISTON LEAKAGE RESULTS LEAKAGE/SPEED

FIG. 56

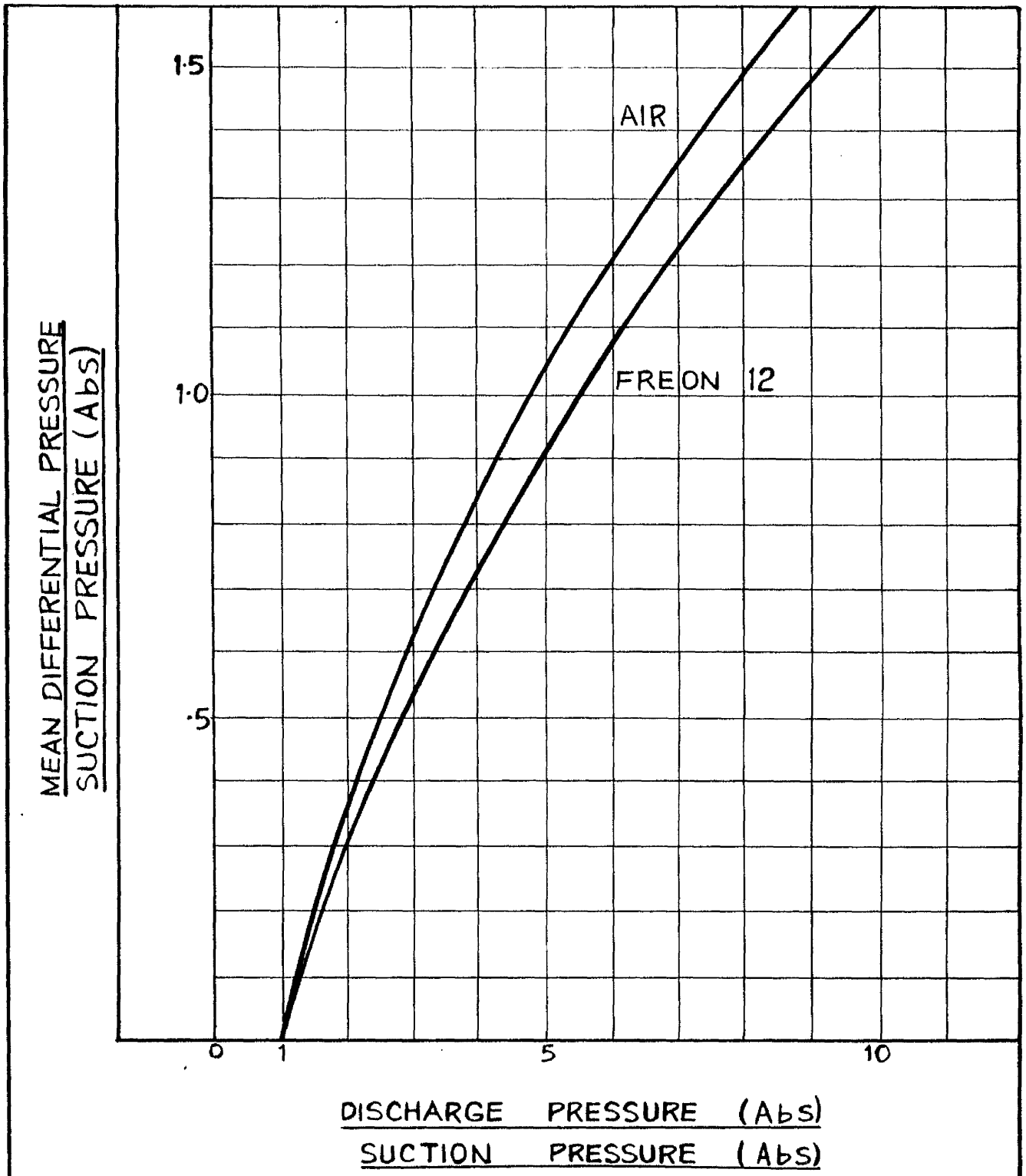

MEAN DIFFERENTIAL PRESSURE CURVES

FIG. 57

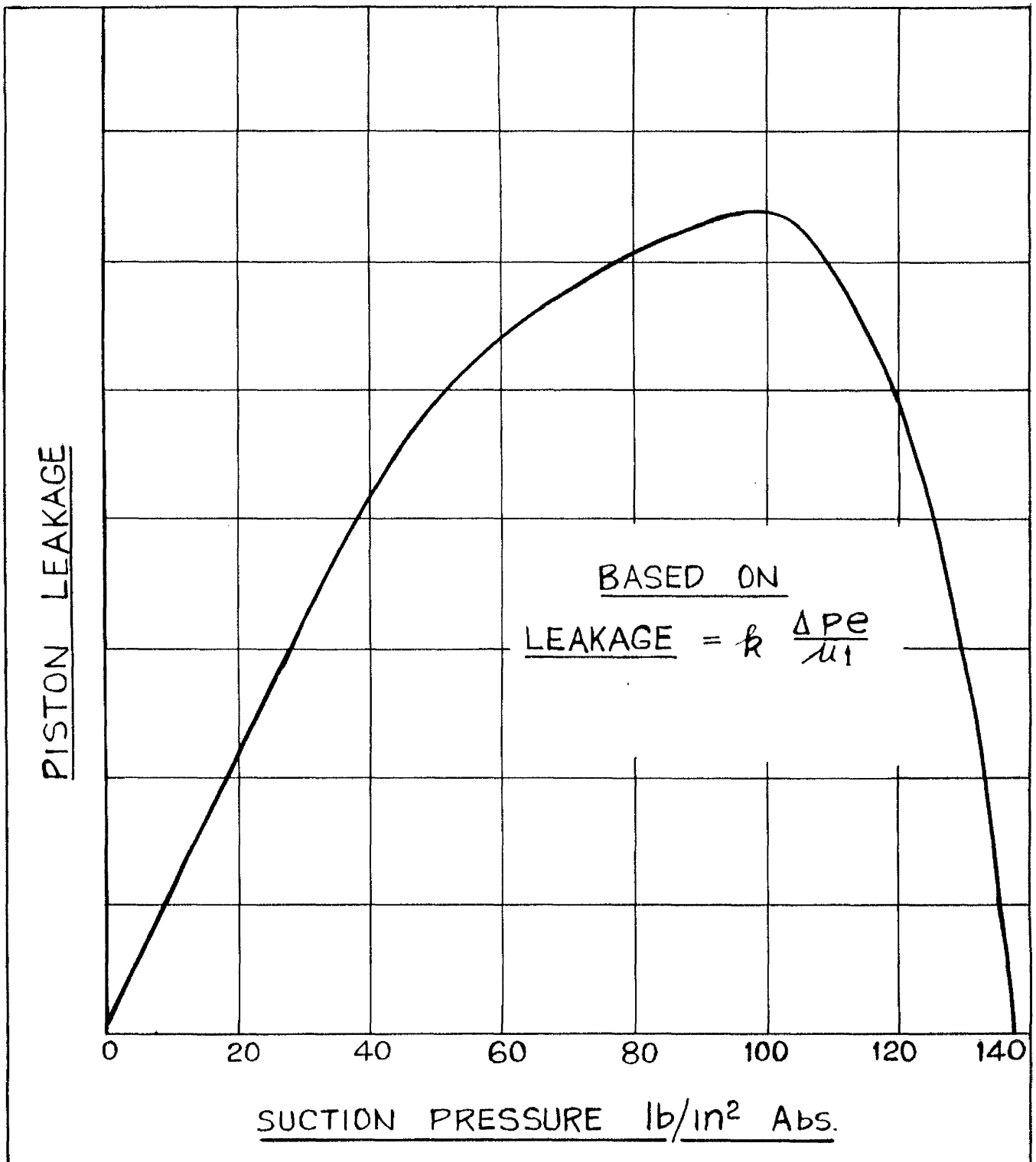

THEORETICAL PISTON LEAKAGE. (FREON 12)
CONDENSING PRESSURE 138 lb/in² abs.
SUCTION TEMPERATURE 120°F.

FIG. 58

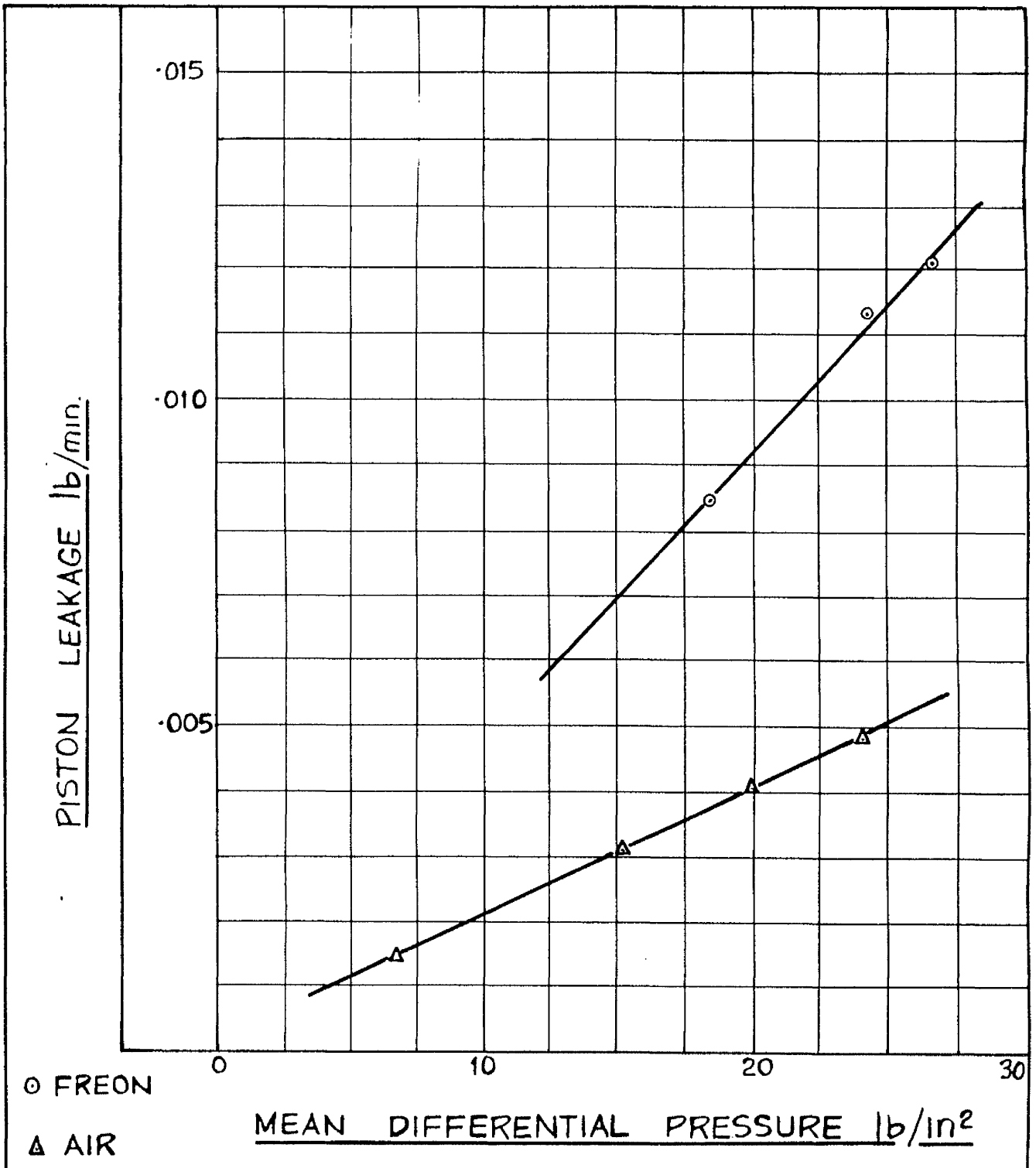

PISTON LEAKAGE RESULTS
VARIABLE DISCHARGE PRESSURE

Fig. 59.

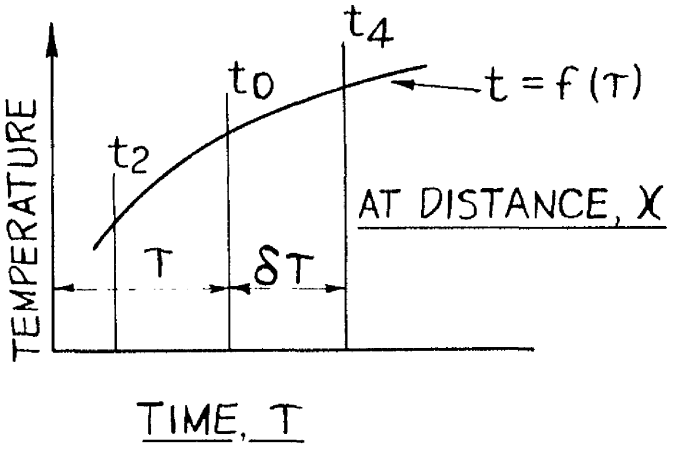

a.) TEMPERATURE GRADIENT WITH RESPECT TO TIME (τ) AT DISTANCE x.

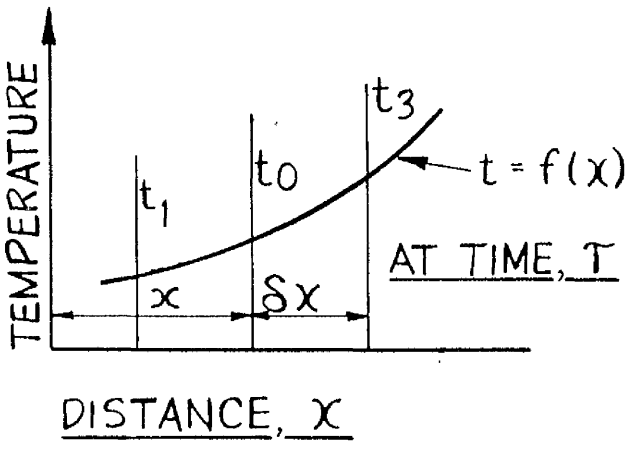

b.) TEMPERATURE GRADIENT WITH RESPECT TO DISTANCE (x) AT TIME T.

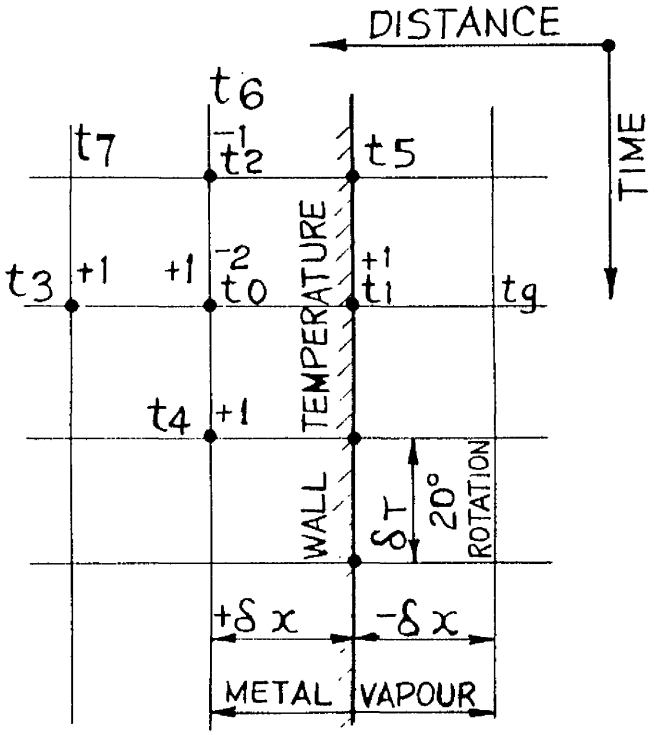

C. RELAXATION PATTERN FROM a AND b.

APPLICATION OF RELAXATION METHOD TO TEMPERATURE GRADIENT

FIG. 60

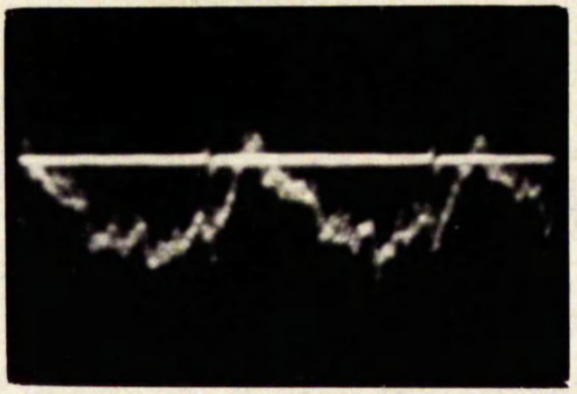

10°F. Supt.

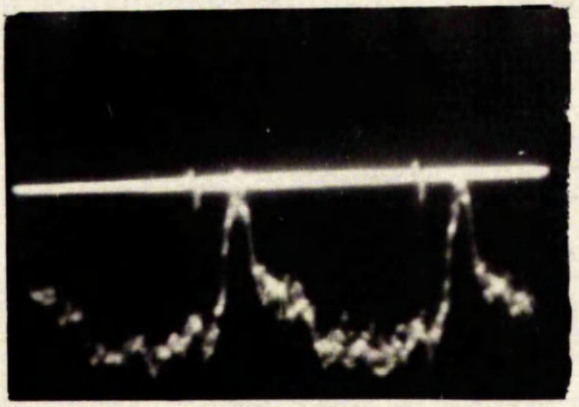

q = 0.817 dry.

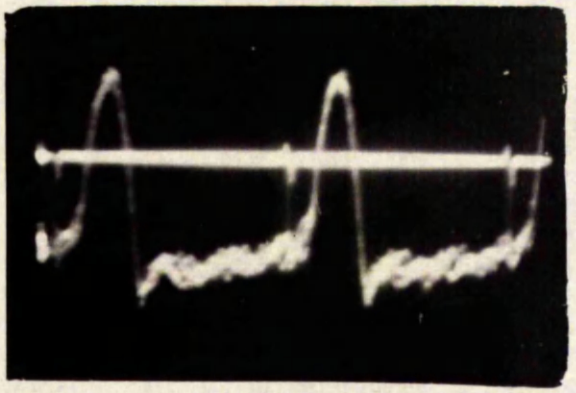

q = 0.64 dry.

CYCLICAL TEMPERATURE FLUCTUATION OSCILLOGRAMS Fig.61.

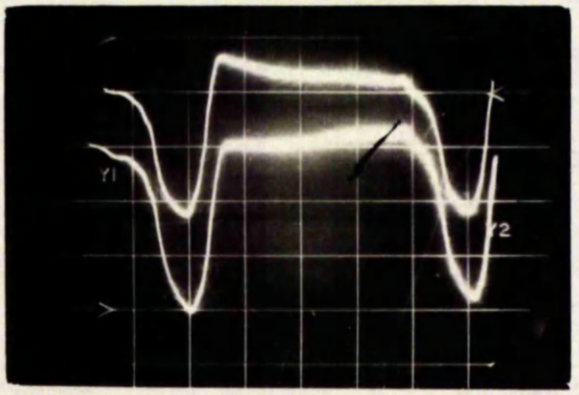

q = 0.64 dry.

CORRECTED TEMPERATURE FLUCTUATIONS Fig.62a

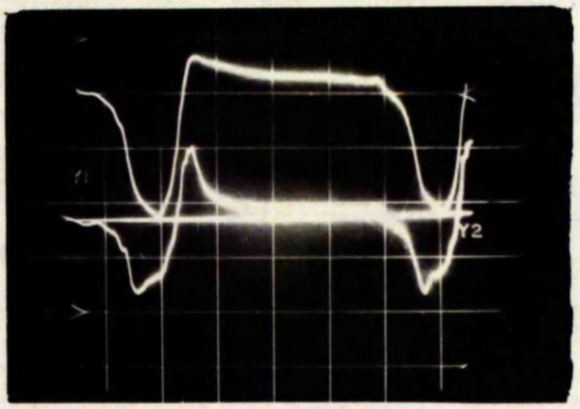

q = 0.64 dry.

TEMPERATURE GRADIENT CURVES, BY ANALOGUE Fig.62b.

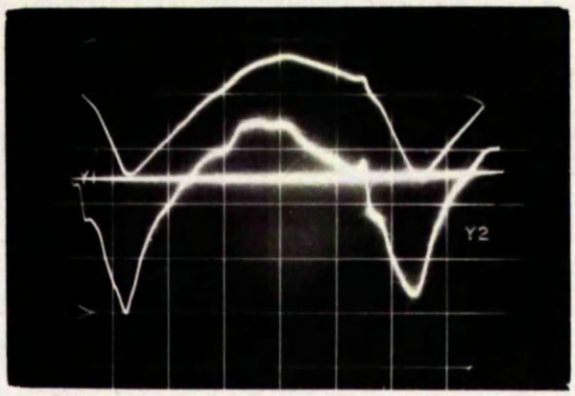

Temperature
Gradient
10°F. Supt.

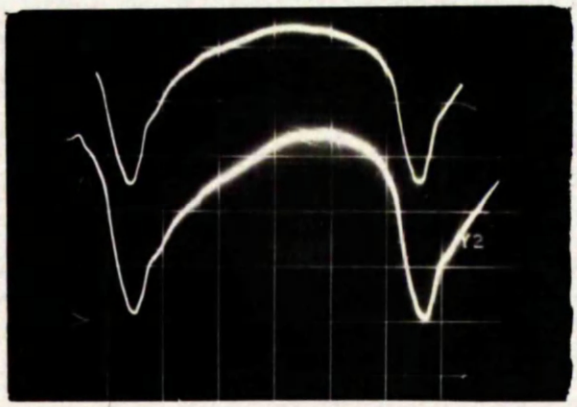

Corrected
Temperature
Fluctuation
q = 0.817 dry.

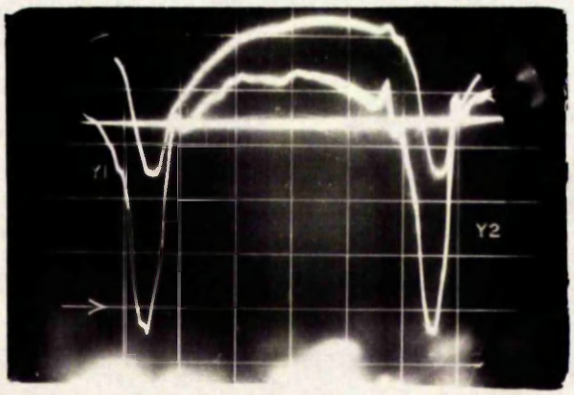

Temperature
Gradient
q = 0.817 dry.

TEMPERATURE GRADIENT CURVES, BY ANALOGUE, Fig.63.

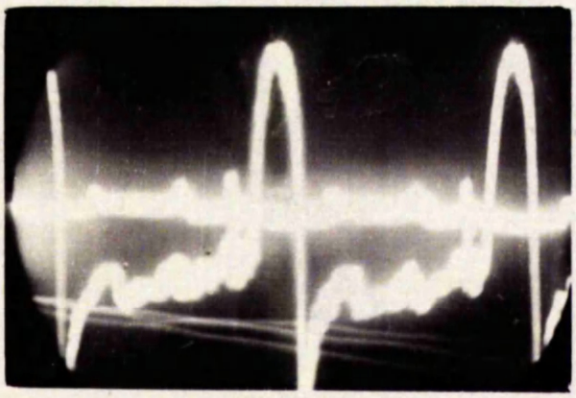

q = .695 dry.

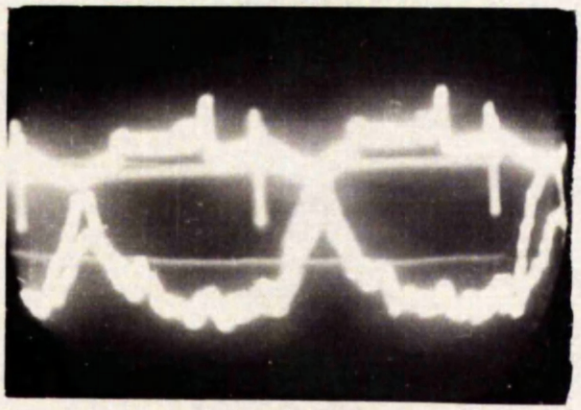

q = 0.582 dry.

EFFECT OF LOW SUCTION DRYNESS ON TEMPERATURE FLUCTUATION

Fig. 64.

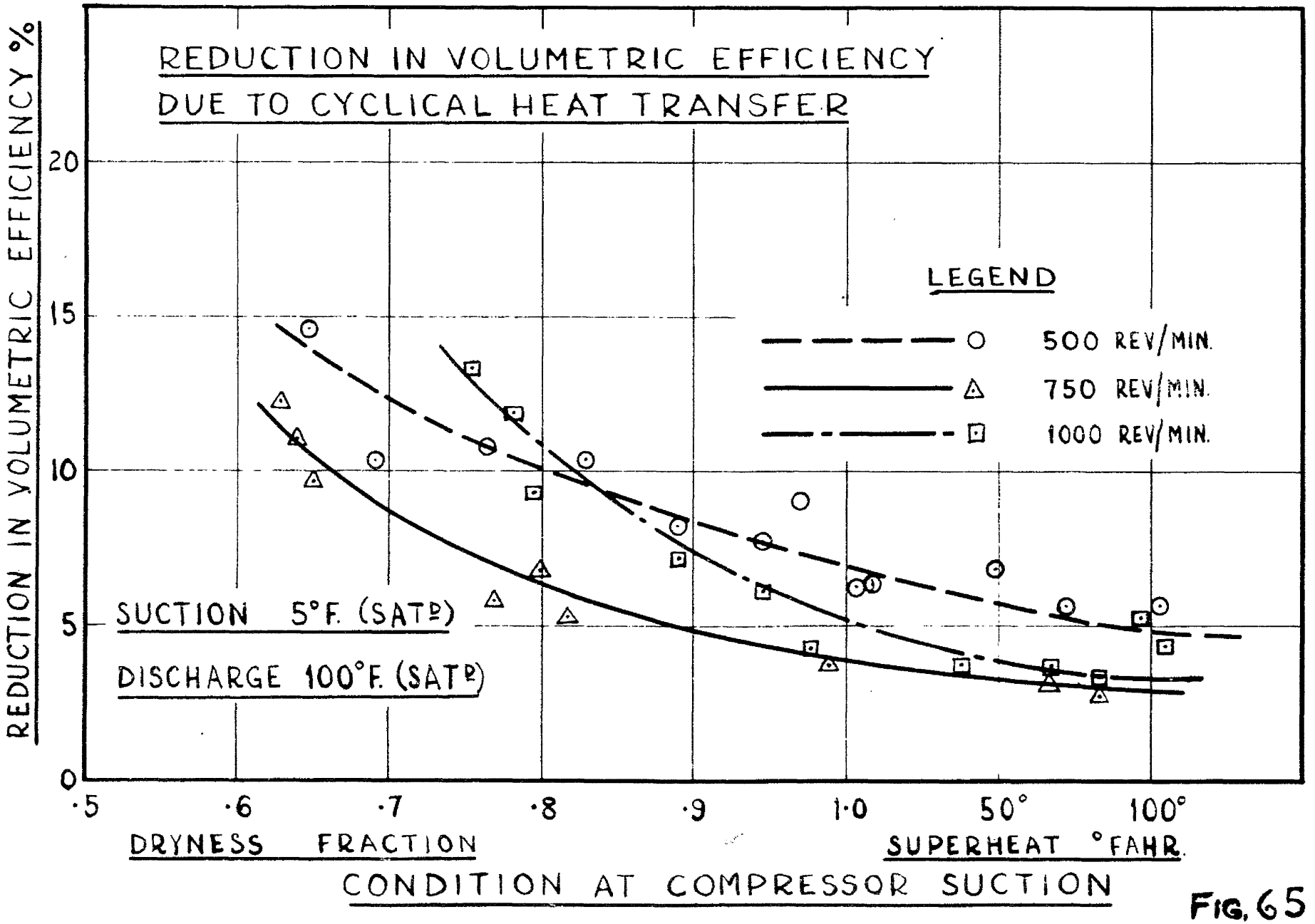
REDUCTION IN VOLUMETRIC EFFICIENCY
DUE TO CYCLICAL HEAT TRANSFER
REDUCTION IN VOLUMETRIC EFFICIENCY %
20
15
10
5
0
LEGEND
500 REV/MIN.
750 REV/MIN.
1000 REV/MIN.
SUCTION 5°F. (SATD)
DISCHARGE 100°F. (SATD)
·5
·6
·7
·8
·9
1·0
50°
100°
DRYNESS FRACTION
SUPERHEAT °FAHR.
CONDITION AT COMPRESSOR SUCTION

FIG. 65

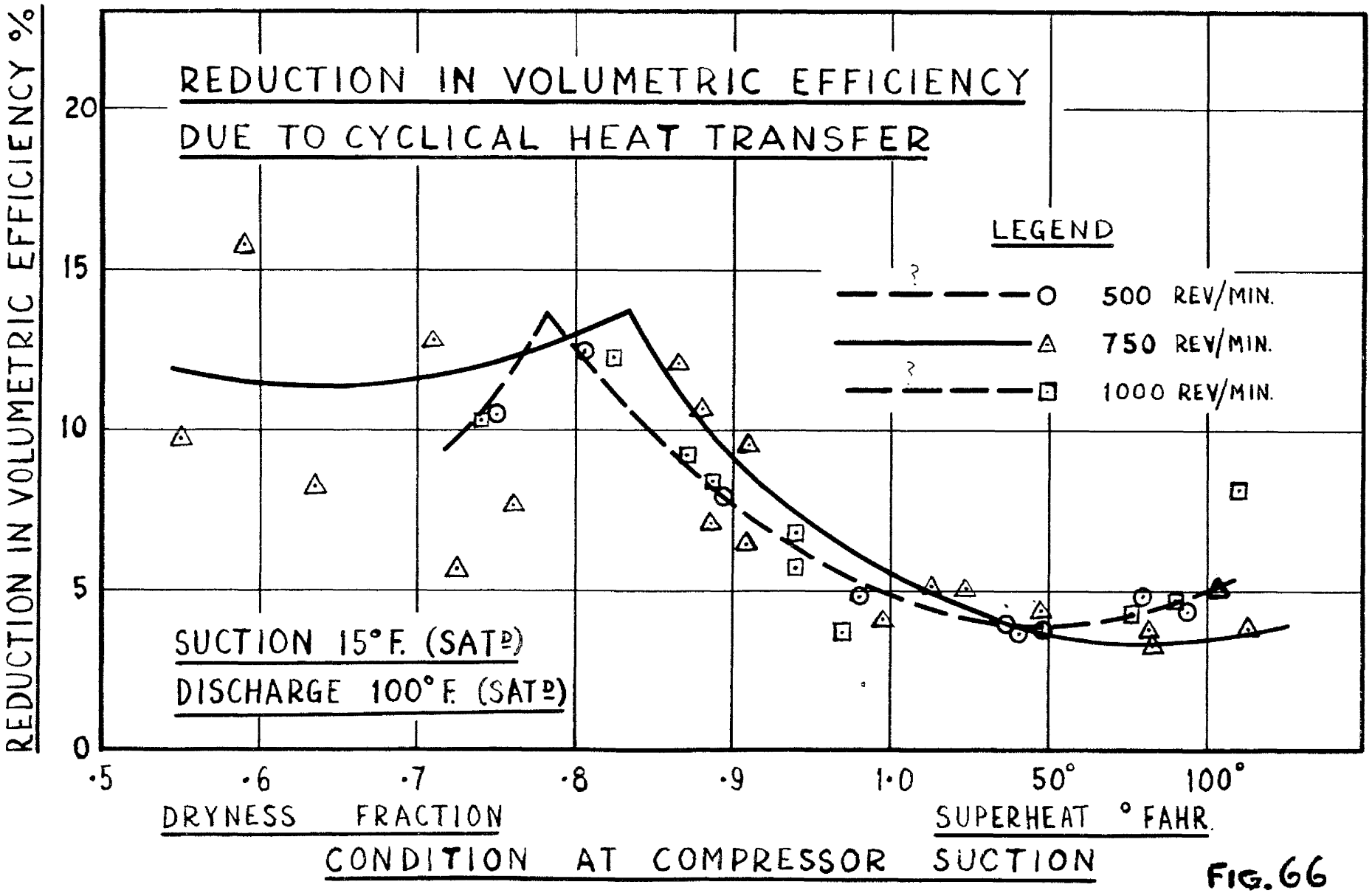
REDUCTION IN VOLUMETRIC EFFICIENCY
DUE TO CYCLICAL HEAT TRANSFER
LEGEND
500 REV/MIN.
750 REV/MIN.
1000 REV/MIN.
SUCTION 15° F. (SATD)
DISCHARGE 100° F. (SATD)
REDUCTION IN VOLUMETRIC EFFICIENCY %
0
5
10
15
20
·5
·6
·7
·8
·9
1·0
50°
100°
DRYNESS FRACTION
SUPERHEAT ° FAHR.
CONDITION AT COMPRESSOR SUCTION

FIG. 66

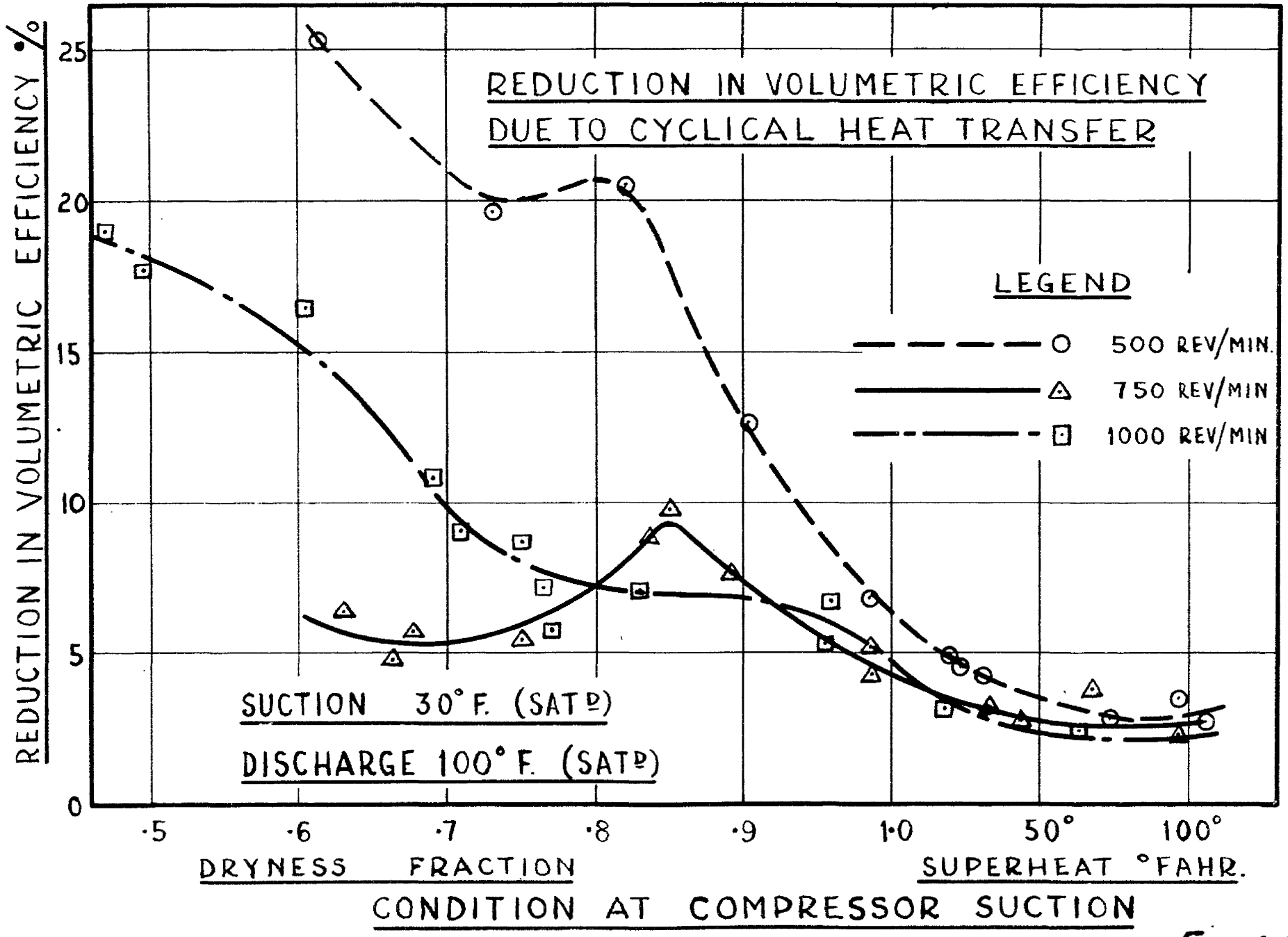
REDUCTION IN VOLUMETRIC EFFICIENCY %
25
20
15
10
5
0
REDUCTION IN VOLUMETRIC EFFICIENCY
DUE TO CYCLICAL HEAT TRANSFER
LEGEND
500 REV/MIN.
750 REV/MIN
1000 REV/MIN
SUCTION 30° F. (SAT P)
DISCHARGE 100° F. (SAT P)
·5
·6
·7
·8
·9
1·0
50°
100°
DRYNESS FRACTION
SUPERHEAT °FAHR.
CONDITION AT COMPRESSOR SUCTION

FIG. 67

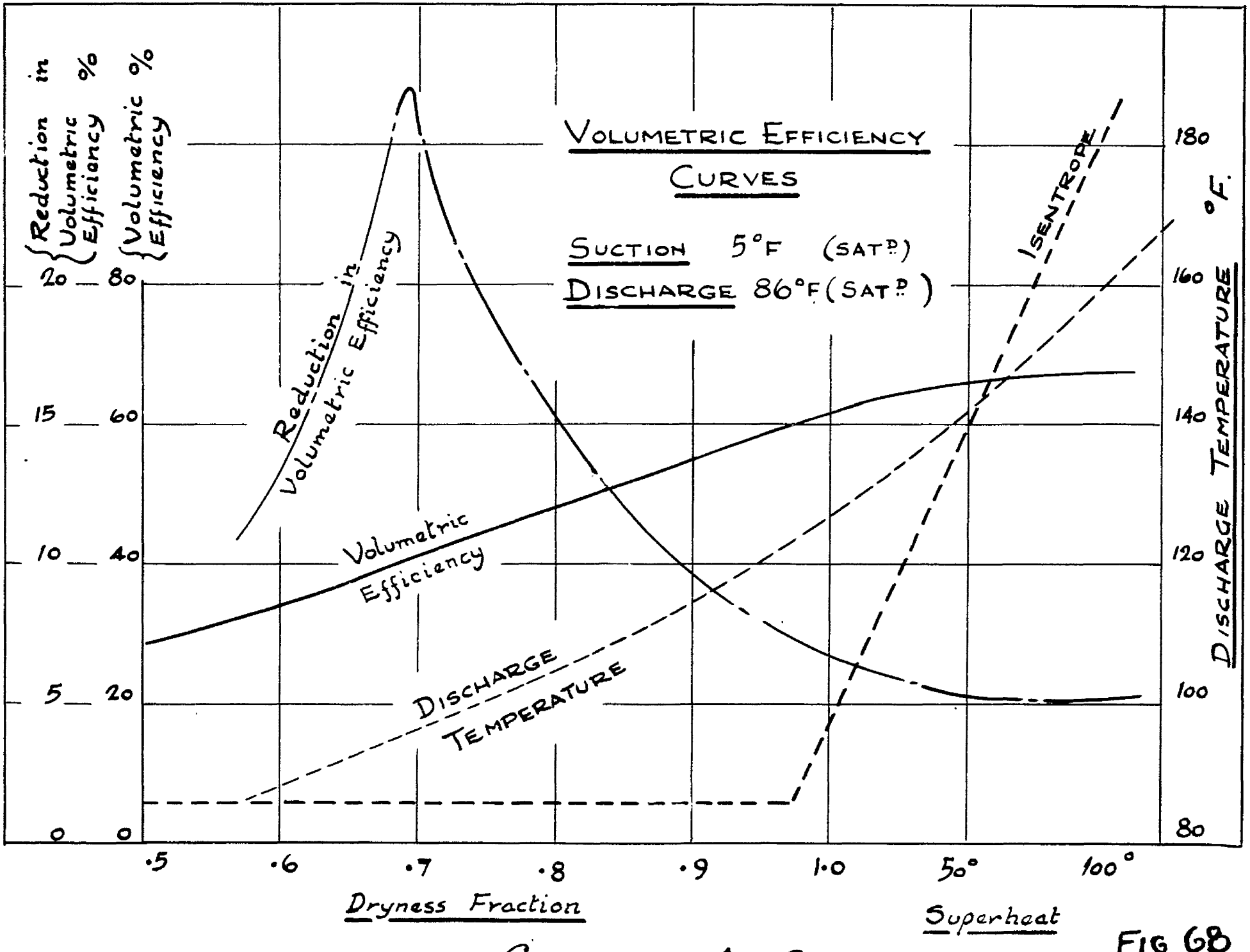
VOLUMETRIC EFFICIENCY
CURVES
SUCTION 5°F (SAT P)
DISCHARGE 86°F (SAT P)
Reduction in Volumetric Efficiency %
Volumetric Efficiency %
Reduction in Volumetric Efficiency
Volumetric Efficiency
Discharge Temperature
ISENTROPE
DISCHARGE TEMPERATURE °F.
20
15
10
5
0
80
60
40
20
0
180
160
140
120
100
80
·5
·6
·7
·8
·9
1·0
50°
100°
Dryness Fraction
Superheat
CONDITION AT SUCTION

FIG 68

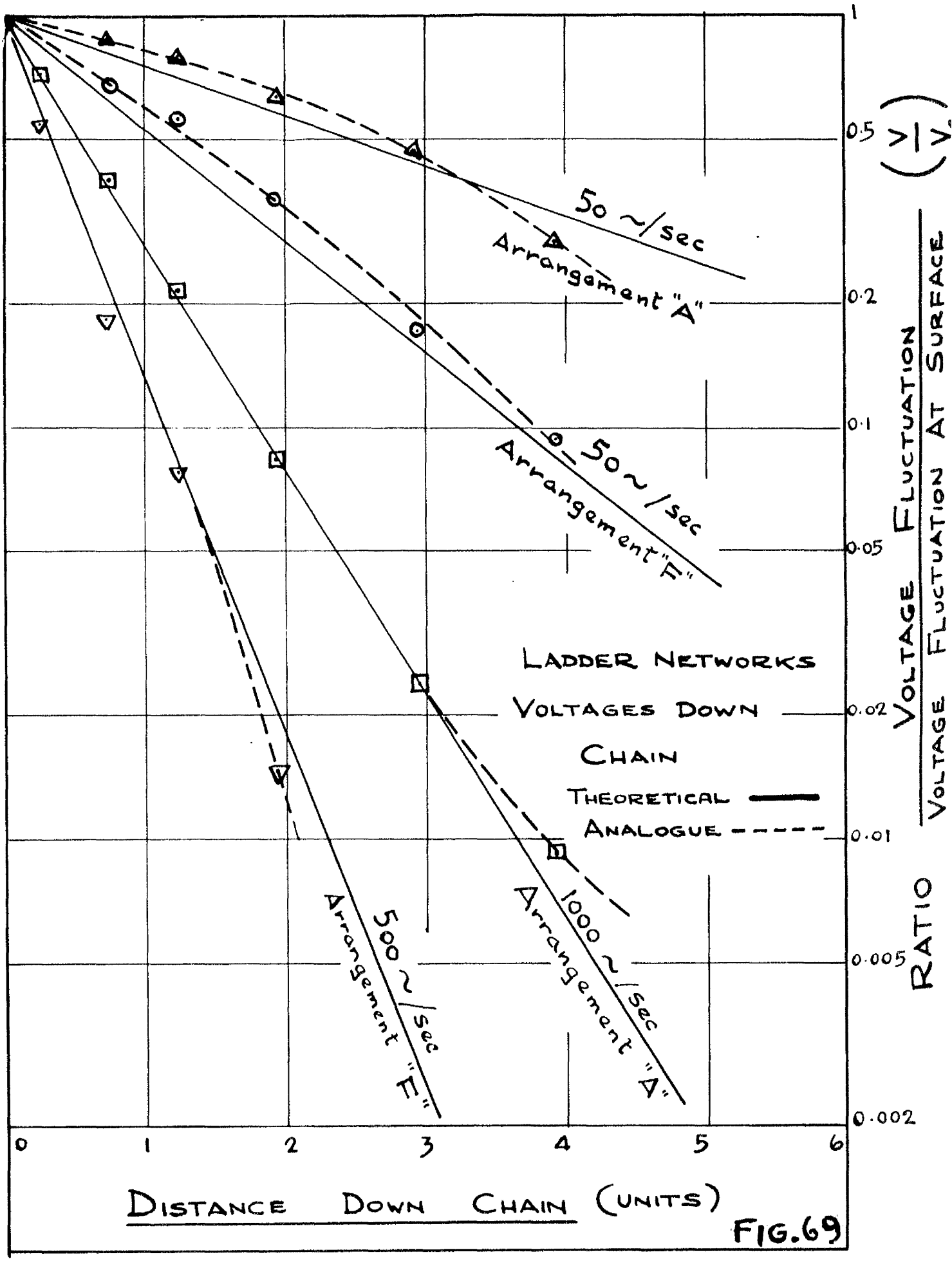
50 ~/sec
Arrangement "A"
50 ~/sec
Arrangement "F"
500 ~/sec
Arrangement "F"
1000 ~/sec
Arrangement "A"
LADDER NETWORKS
VOLTAGES DOWN CHAIN
THEORETICAL
ANALOGUE
1
0.5
0.2
0.1
0.05
0.02
0.01
0.005
0.002
VOLTAGE FLUCTUATION RATIO
VOLTAGE FLUCTUATION AT SURFACE / V
0
1
2
3
4
5
6
DISTANCE DOWN CHAIN (UNITS)

FIG.69

ELECTRICAL ANALOGUE

ONE-DIMENSIONAL LADDER NETWORKS

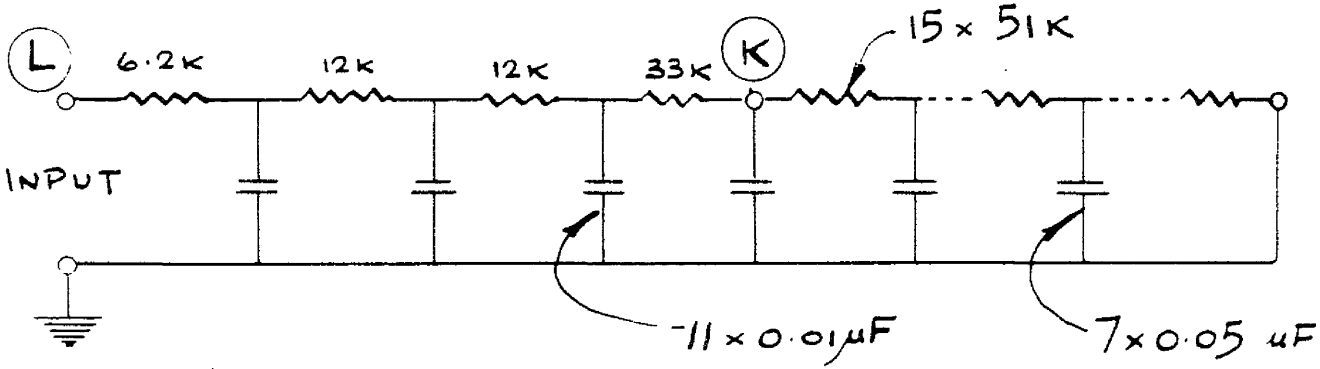

ARRANGEMENT "A"

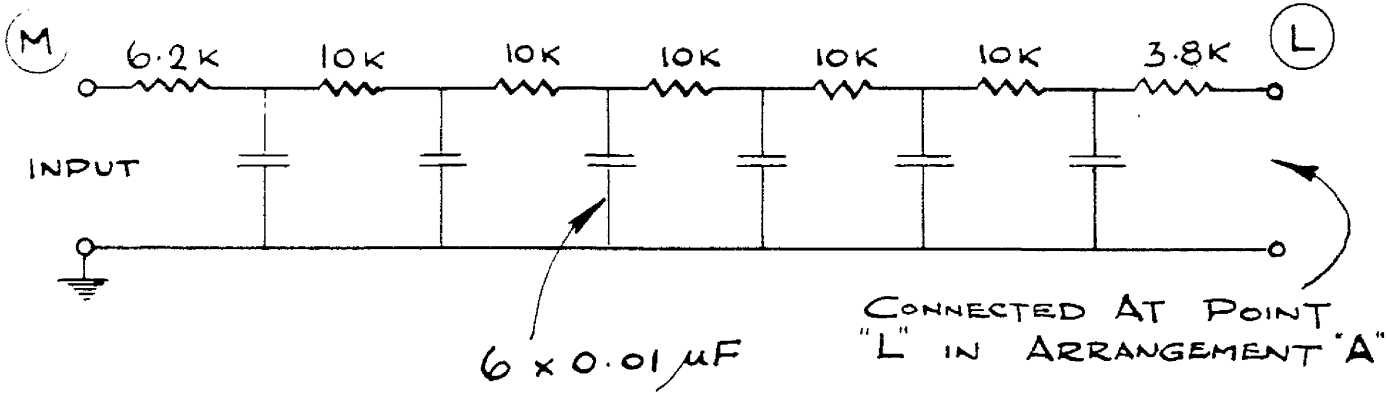

ARRANGEMENT "C"

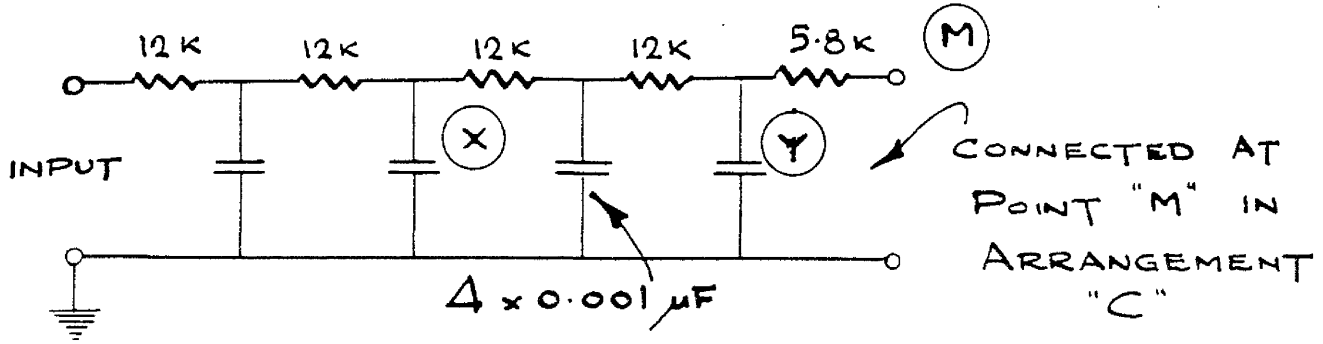

ARRANGEMENT "D"

ARRANGEMENT "B"

INPUT AT POINT "K" IN ARRANGEMENT "A"

ARRANGEMENT "E"

AS ARRANGEMENT "D" BUT WITH CONDENSERS "X" AND "Y" REMOVED

ARRANGEMENT "F"

AS ARRANGEMENT "A" BUT ALL CONDENSERS ARE 0·05 μF

FIG No 70

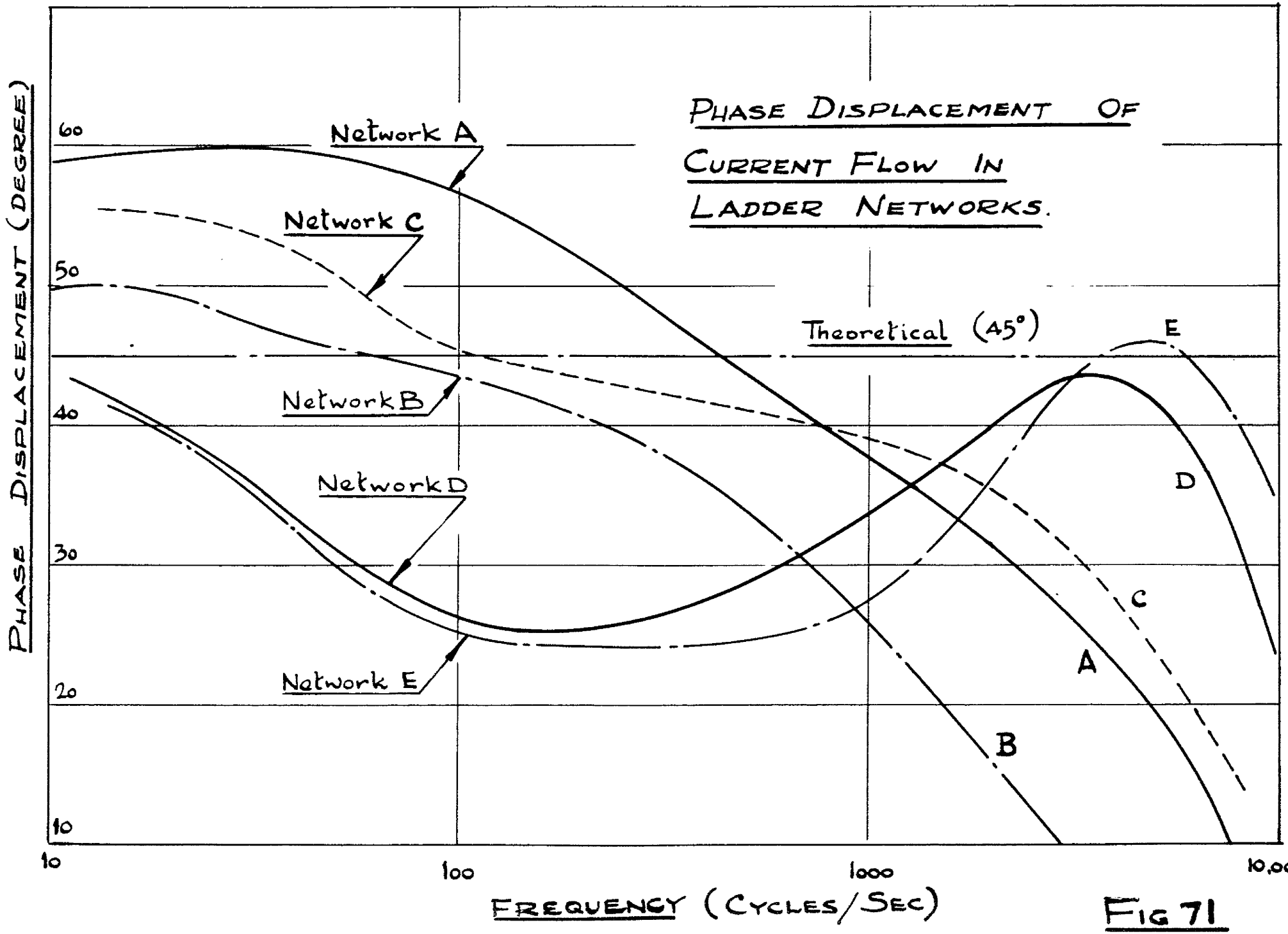
PHASE DISPLACEMENT OF CURRENT FLOW IN LADDER NETWORKS.
PHASE DISPLACEMENT (DEGREE)
60
50
40
30
20
10
Network A
Network C
Network B
Network D
Network E
Theoretical (45°)
A
B
C
D
E
10
100
1000
10,00
FREQUENCY (CYCLES/SEC)

FIG 71

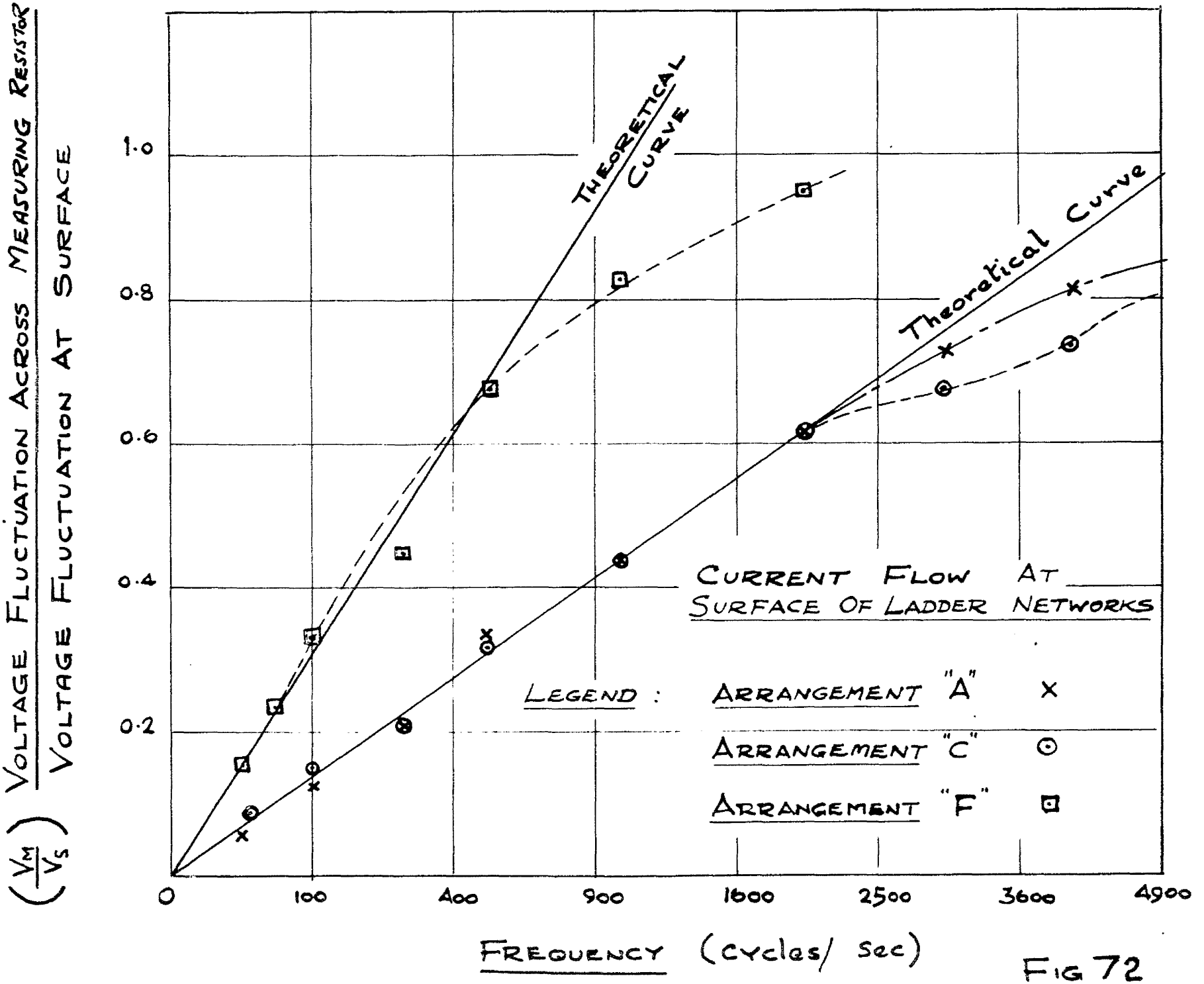
(VM/VS) Voltage Fluctuation Across Measuring Resistor / Voltage Fluctuation At Surface
1.0
0.8
0.6
0.4
0.2
0
100
400
900
1600
2500
3600
4900
Theoretical Curve
Theoretical Curve
Current Flow At Surface Of Ladder Networks
Legend :
Arrangement "A" ×
Arrangement "C" ⊙
Arrangement "F" ⊡
Frequency (cycles/ sec)

Fig 72

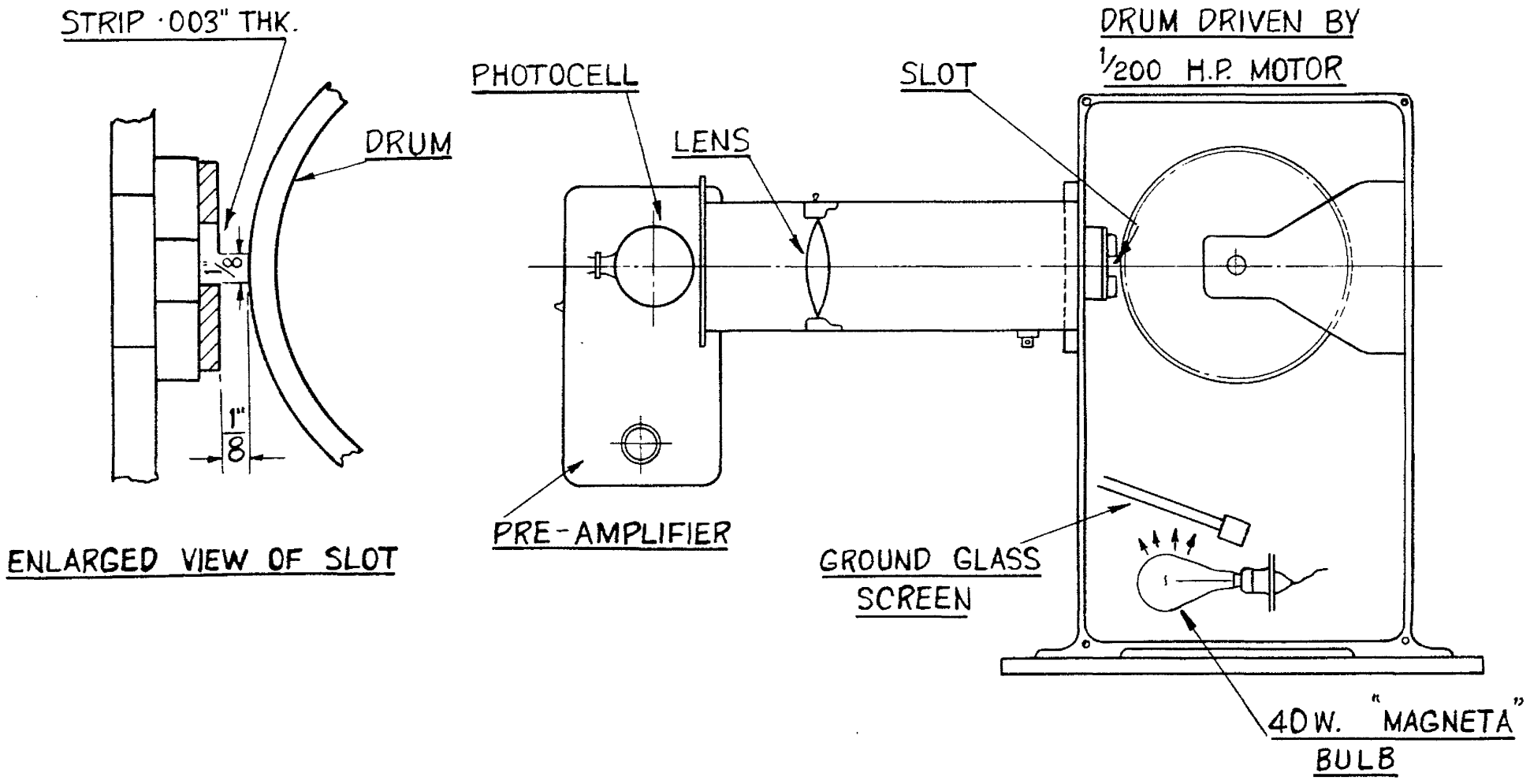

MODIFIED DRUM CAMERA

SCALE :- $\frac{1"}{4} = 1"$

FIG. 73

BLOCK DIAGRAM OF PHOTOFORMER

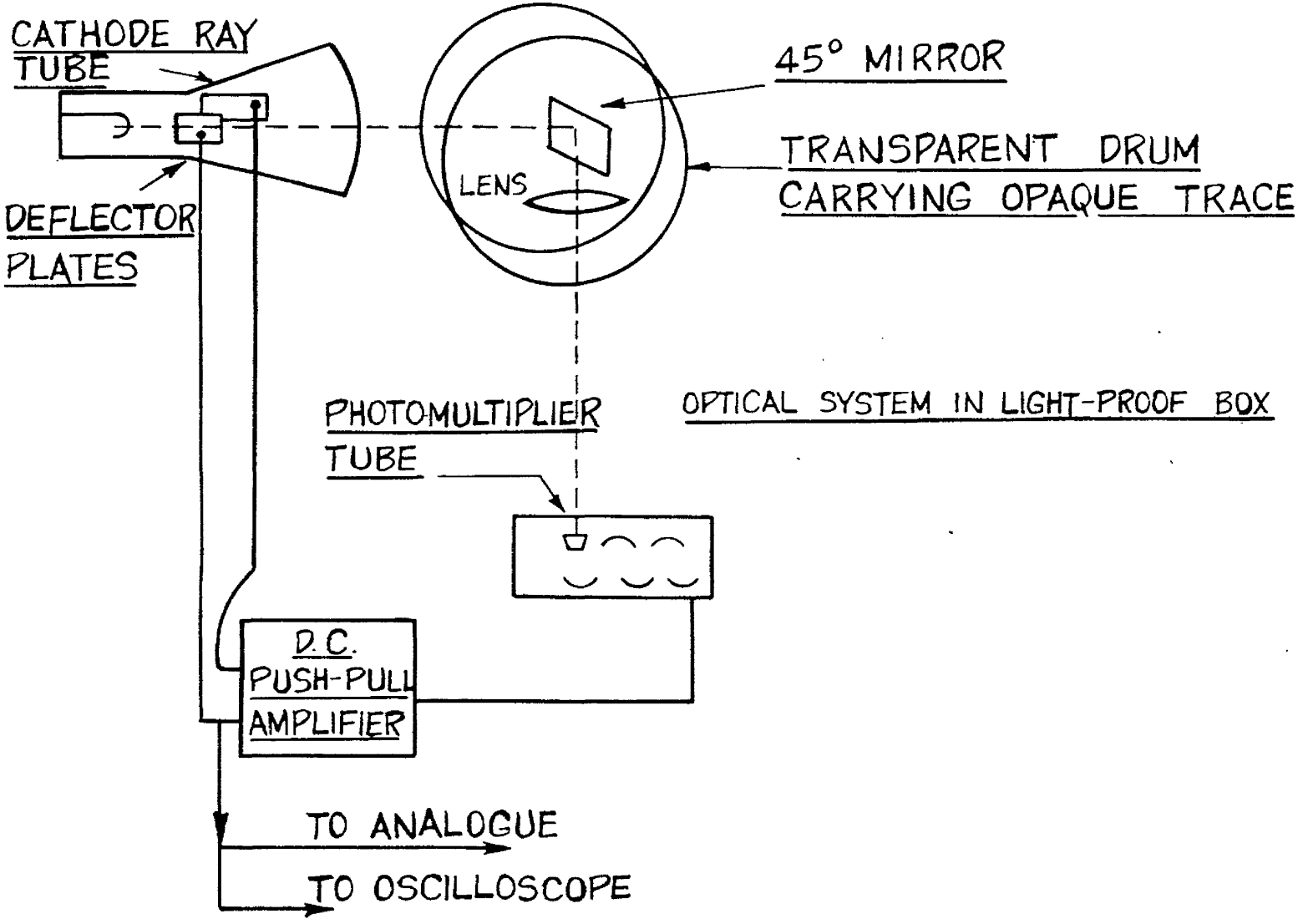

FIG.74

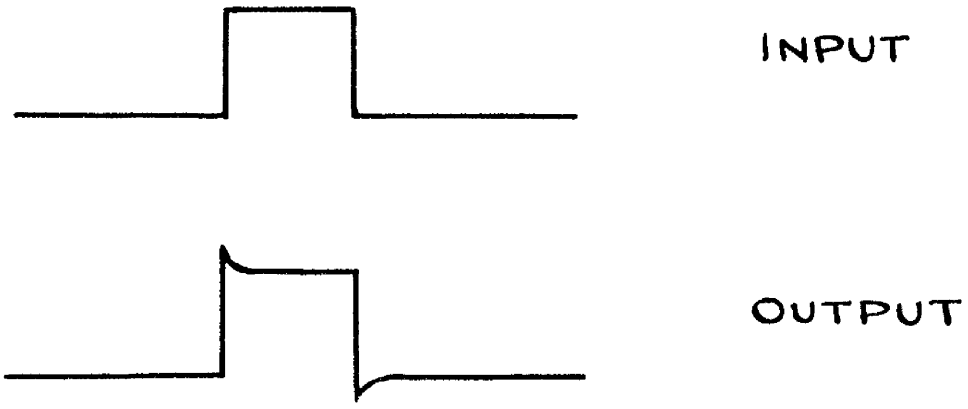

EFFECT OF EXCESSIVE GAIN

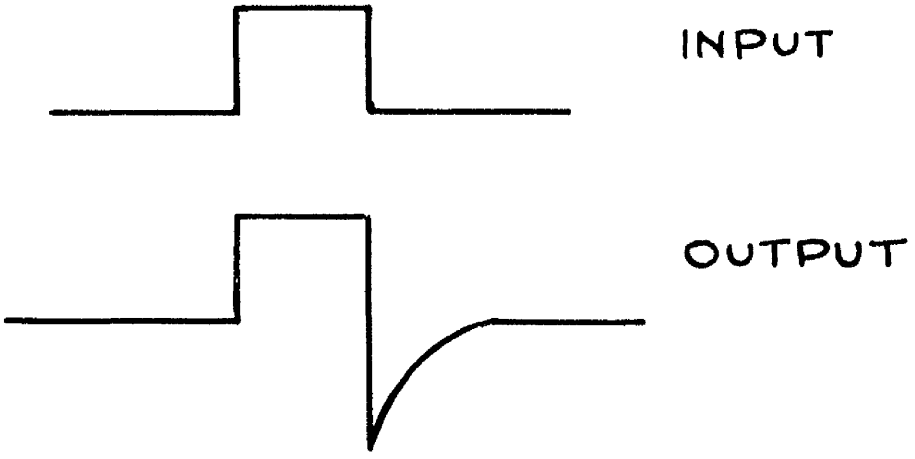

EFFECT OF TUBE AFTERGLOW

FIG 75

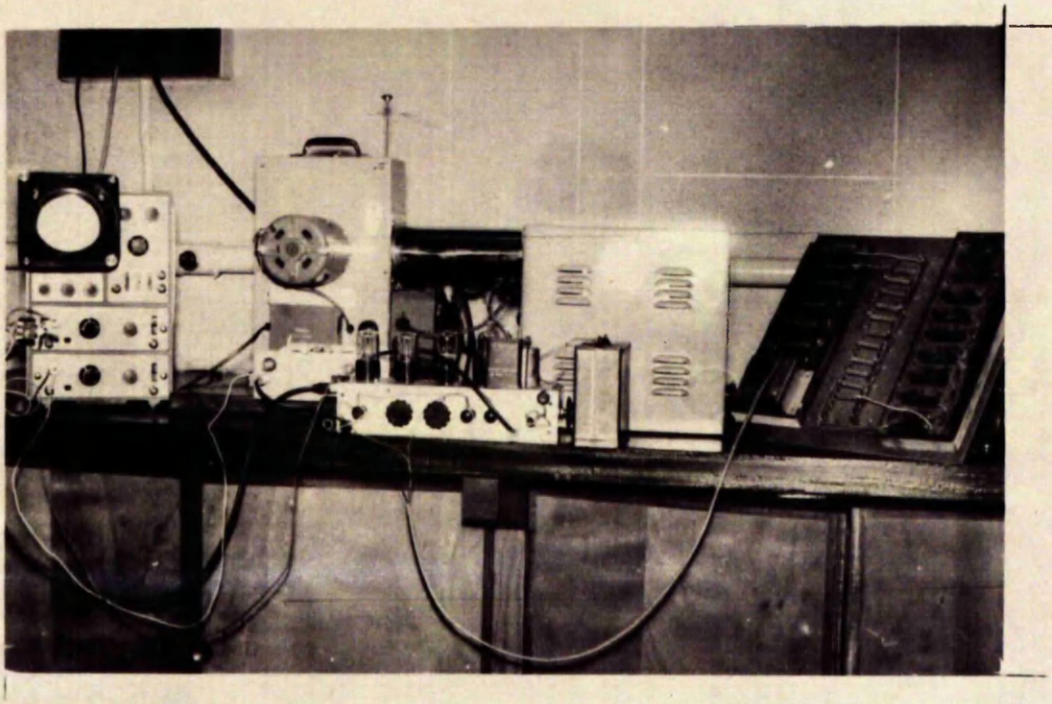

ELECTRICAL ANALOGUE APPARATUS Fig. 76a.

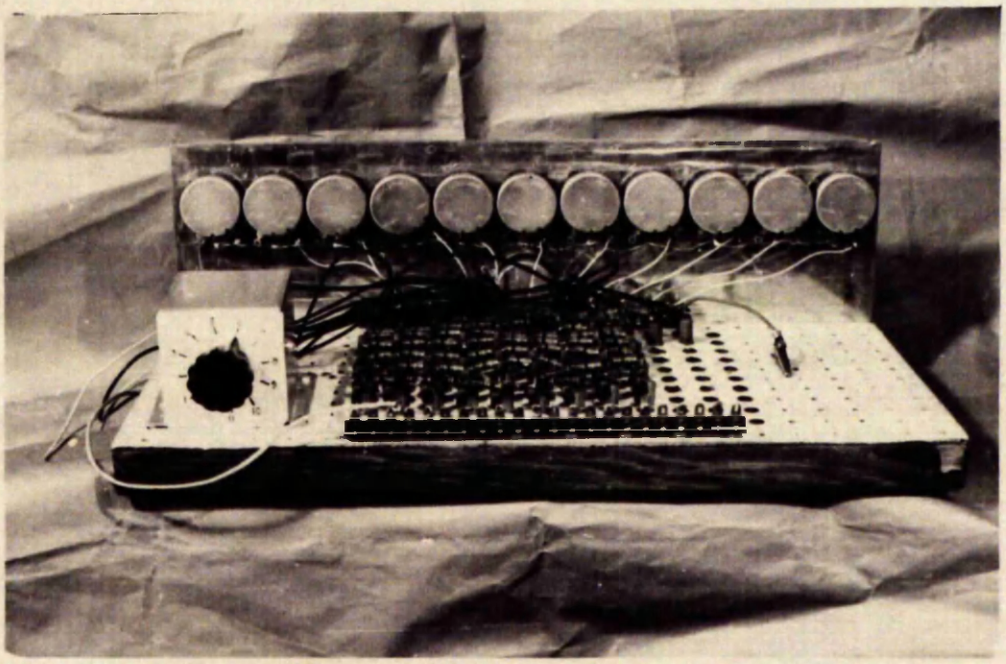

2-DIMENSIONAL ANALOGUE Fig. 76b.

PHOTOTUBE CIRCUIT DIAGRAM

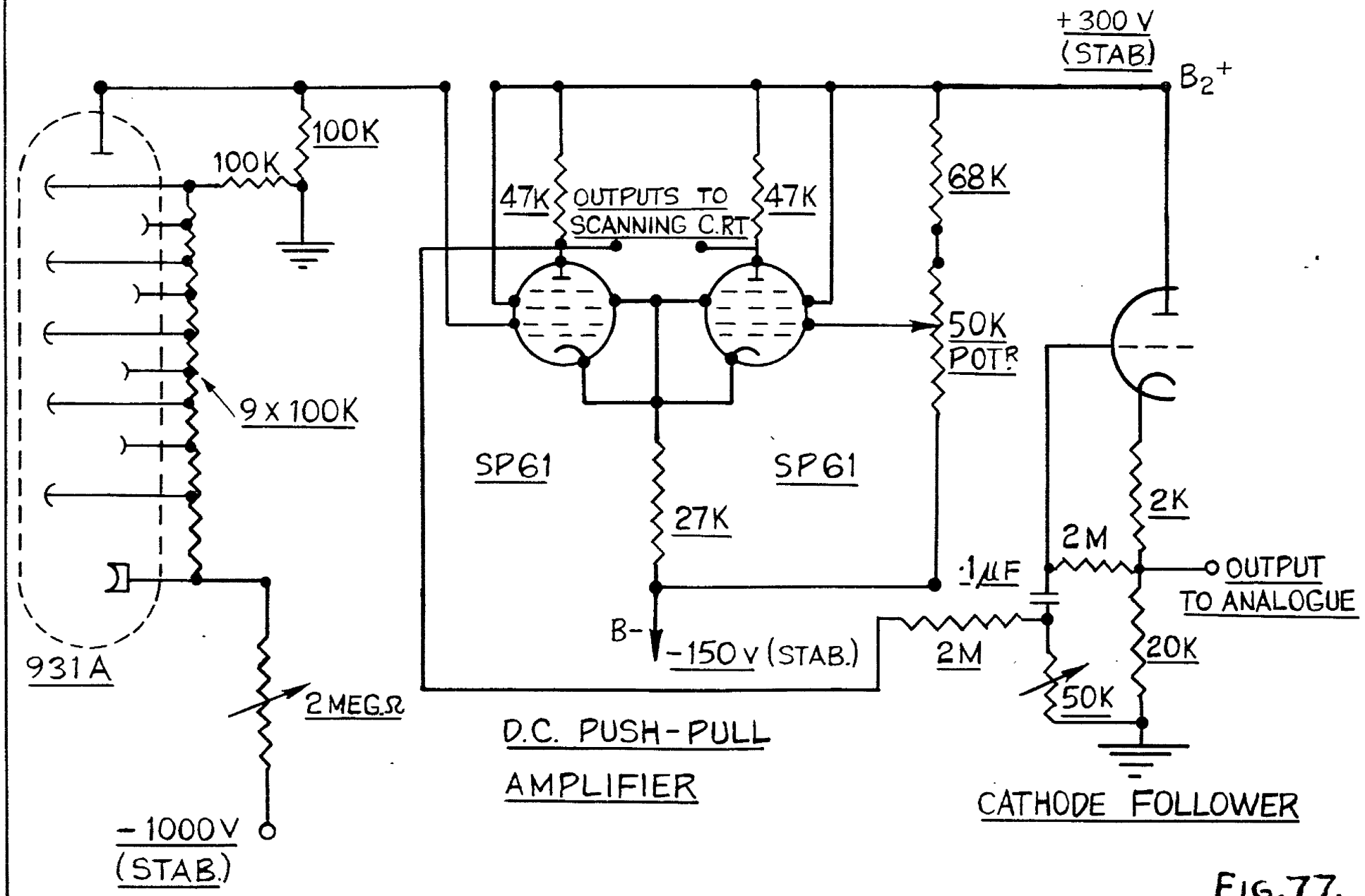

FIG. 77.

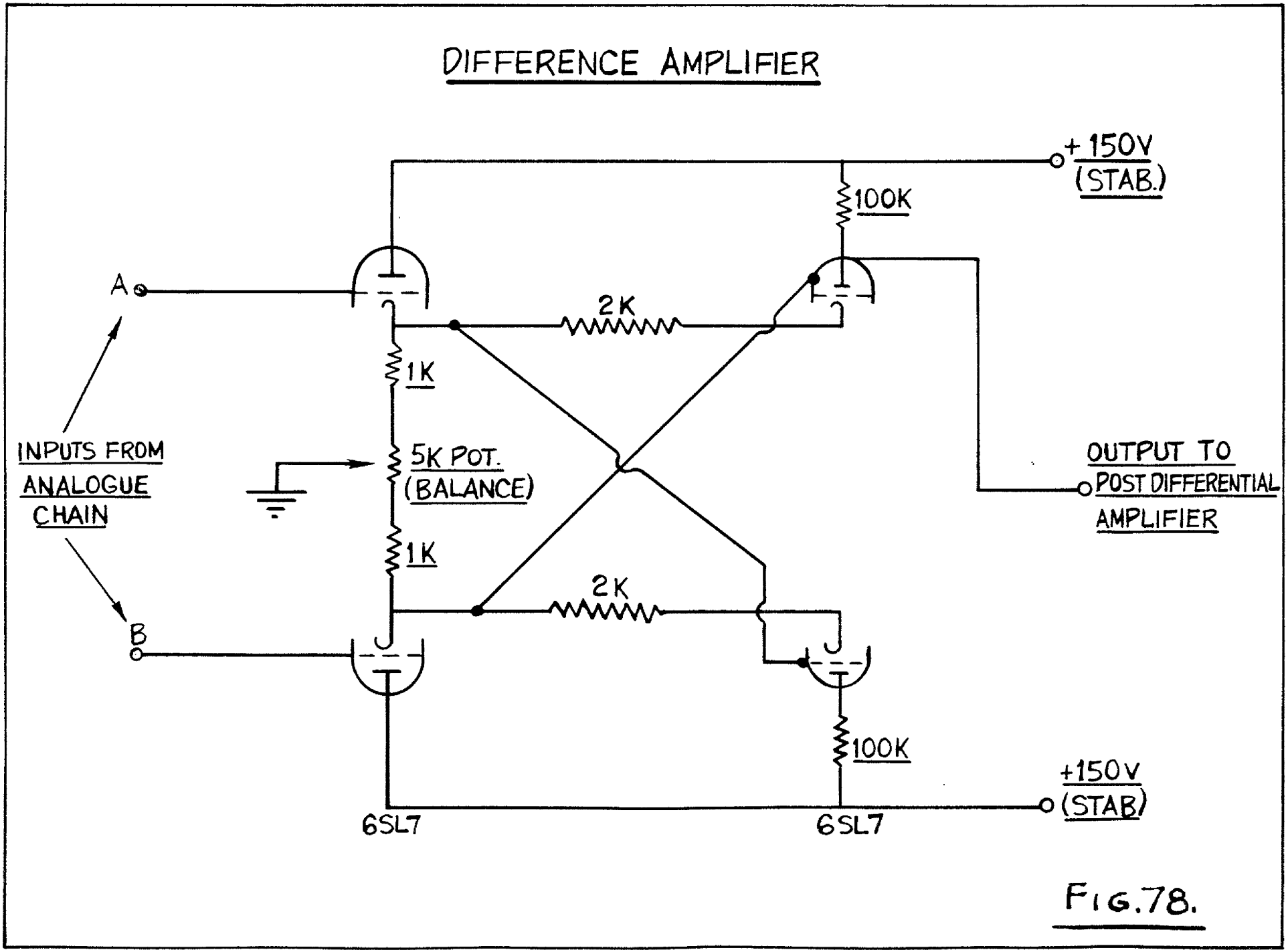
DIFFERENCE AMPLIFIER
+150V (STAB.)
100K
A
2K
1K
INPUTS FROM ANALOGUE CHAIN
5K POT. (BALANCE)
OUTPUT TO POST DIFFERENTIAL AMPLIFIER
1K
2K
B
100K
+150V (STAB)
6SL7
6SL7

FIG. 78.

ANALOGUE CHAIN FOR RADIAL FLOW IN SPHERES

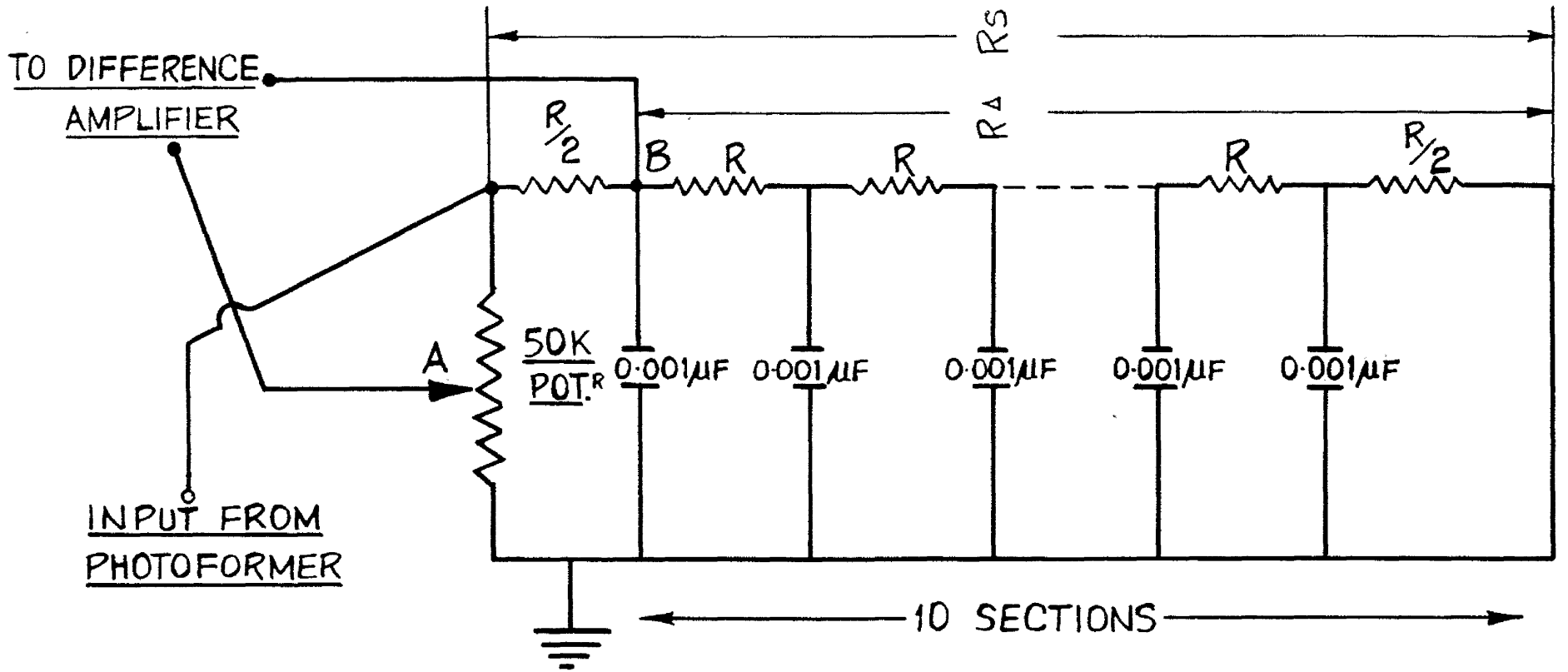

DROPLET DIAMETER	R
·001 IN.	5·1 K Ω
·002 IN.	22 K Ω
·003 IN.	51 K Ω

FIG. 79

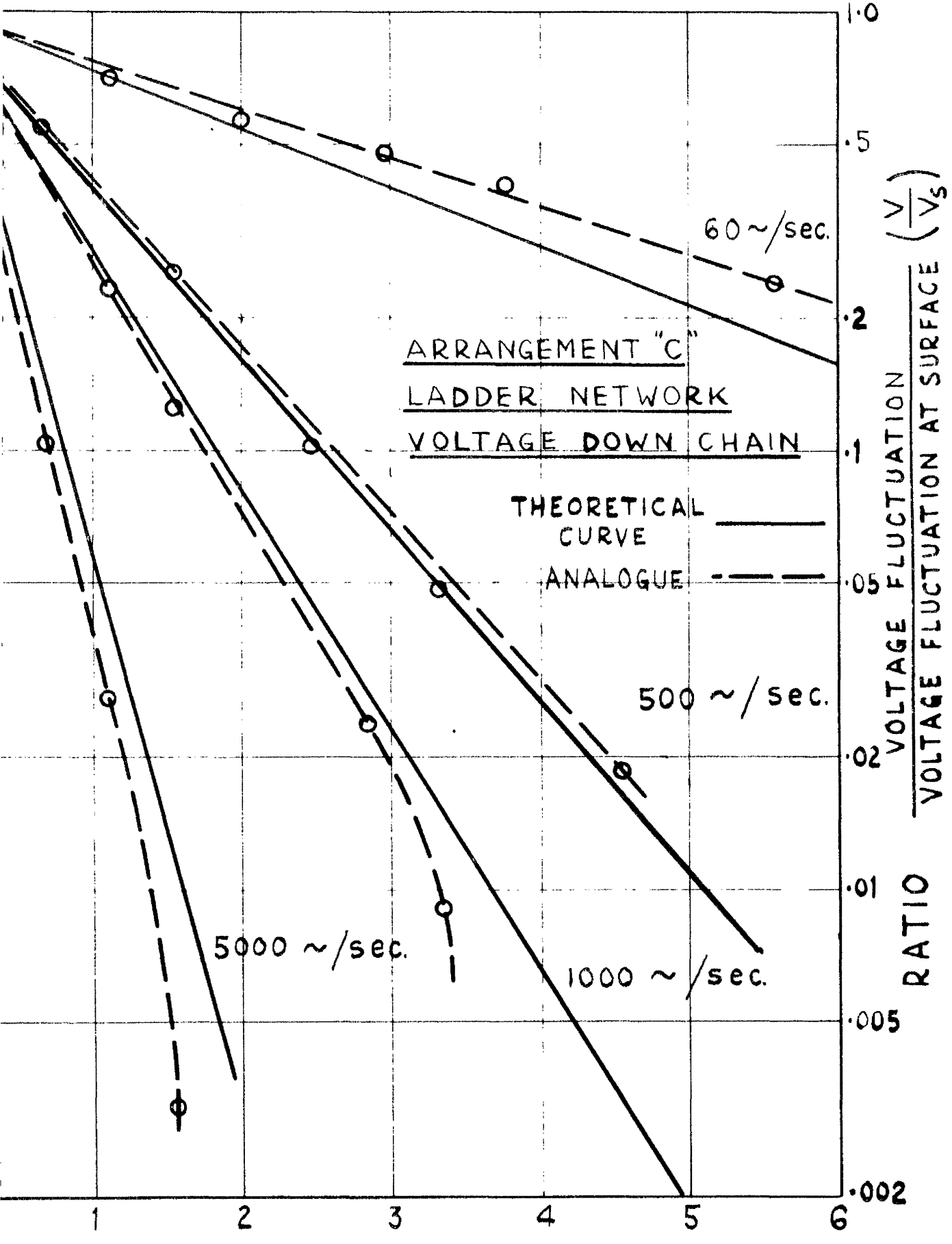
ARRANGEMENT "C"
LADDER NETWORK
VOLTAGE DOWN CHAIN
THEORETICAL CURVE
ANALOGUE
60 ~/sec.
500 ~/sec.
1000 ~/sec.
5000 ~/sec.
1·0
·5
·2
·1
·05
·02
·01
·005
·002
1
2
3
4
5
6
RATIO VOLTAGE FLUCTUATION / VOLTAGE FLUCTUATION AT SURFACE (V/Vs)
DISTANCE DOWN CHAIN (UNITS)

FIG. 80

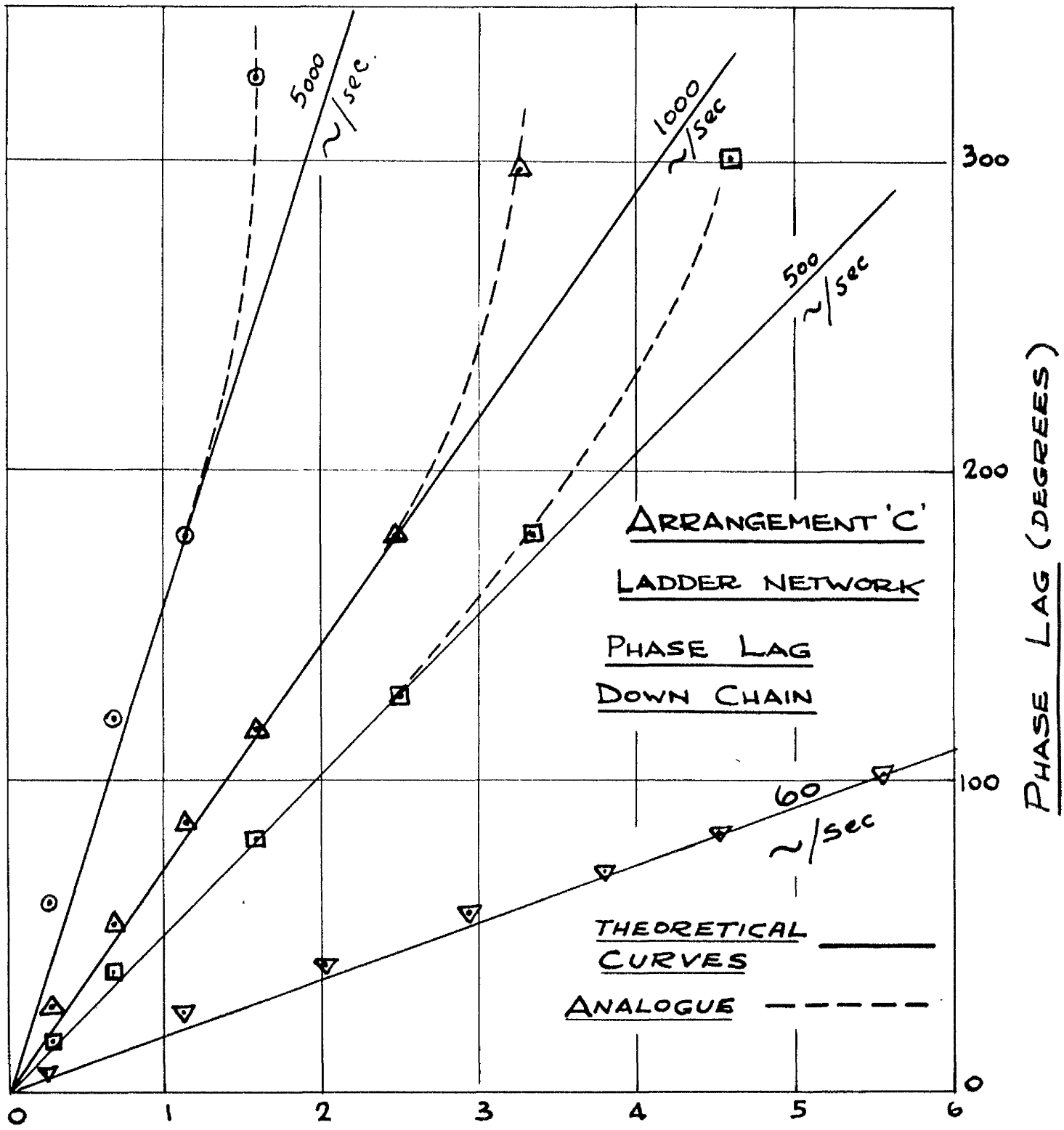
5000 ~/sec.
1000 ~/sec
500 ~/sec
60 ~/sec
ARRANGEMENT 'C'
LADDER NETWORK
PHASE LAG
DOWN CHAIN
THEORETICAL CURVES
ANALOGUE
0
100
200
300
PHASE LAG (DEGREES)
0
1
2
3
4
5
6
DISTANCE DOWN CHAIN (UNITS)

FIG. 81.

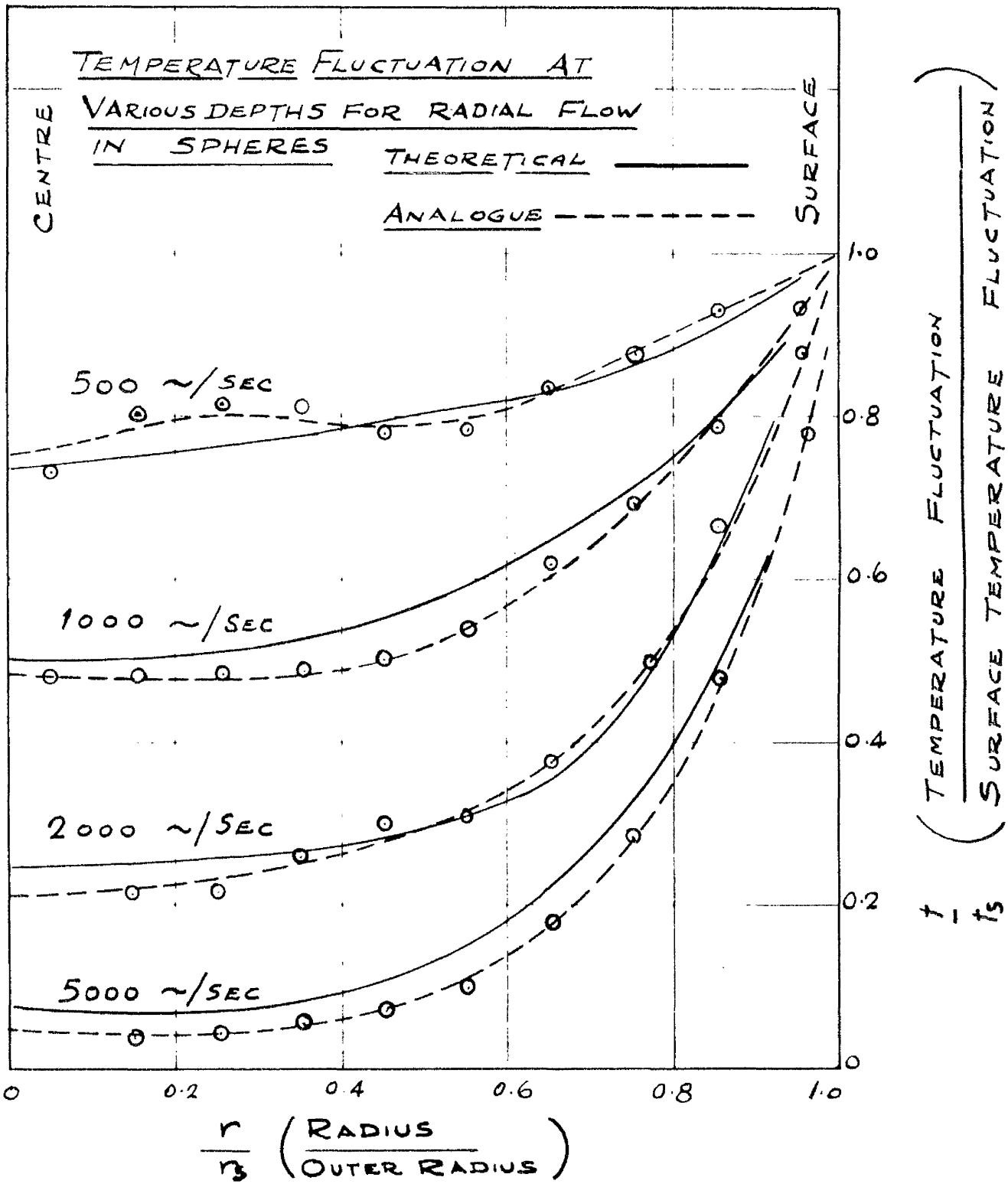
TEMPERATURE FLUCTUATION AT
VARIOUS DEPTHS FOR RADIAL FLOW
IN SPHERES
THEORETICAL
ANALOGUE
CENTRE
SURFACE
500 ~/SEC
1000 ~/SEC
2000 ~/SEC
5000 ~/SEC
0
0·2
0·4
0·6
0·8
1·0
r/r3 (RADIUS / OUTER RADIUS)
t − ts (TEMPERATURE FLUCTUATION / SURFACE TEMPERATURE FLUCTUATION)

FIG 82

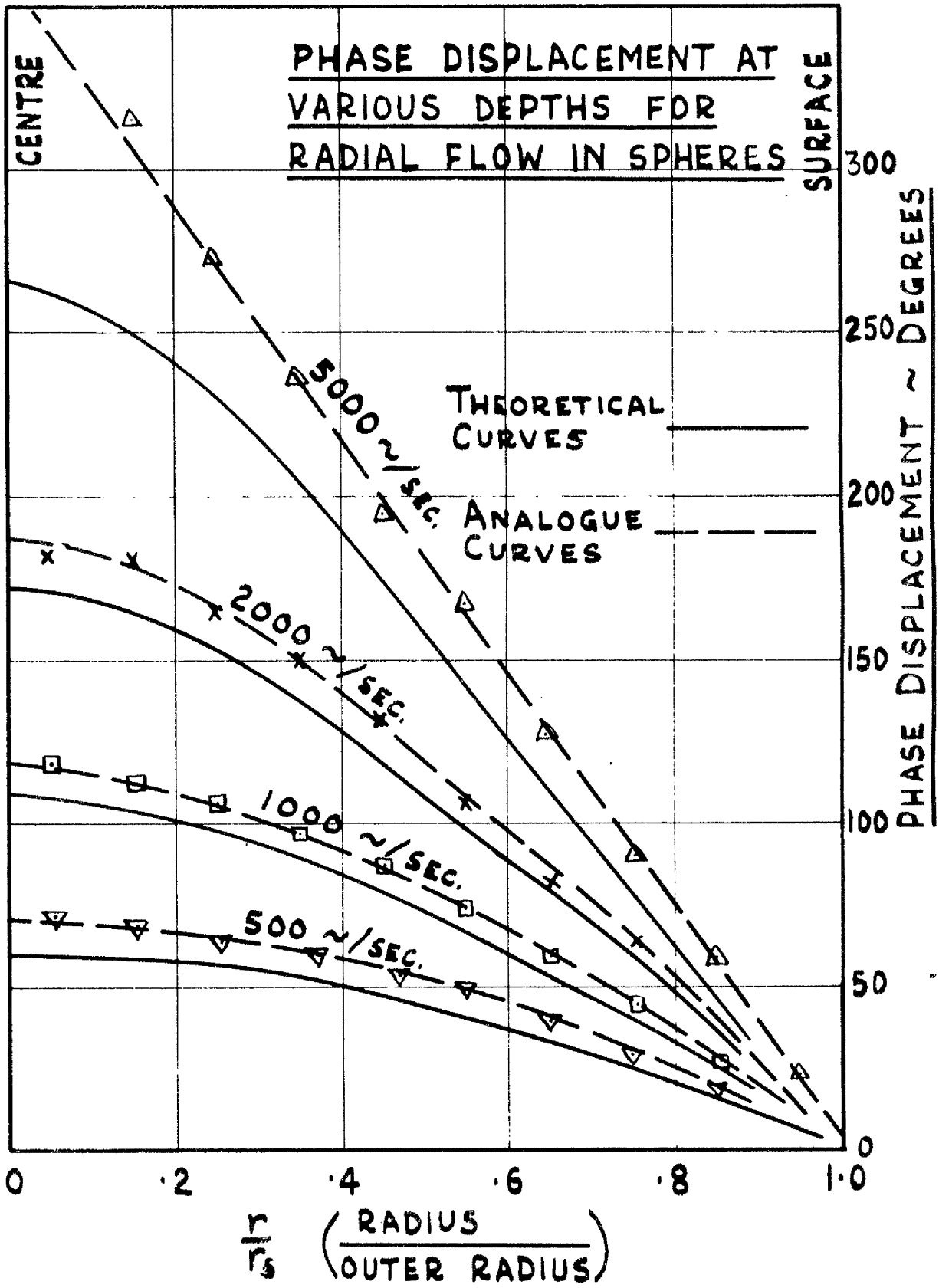
PHASE DISPLACEMENT AT VARIOUS DEPTHS FOR RADIAL FLOW IN SPHERES
CENTRE
SURFACE
THEORETICAL CURVES
ANALOGUE CURVES
5000 ~/SEC.
2000 ~/SEC.
1000 ~/SEC.
500 ~/SEC.
PHASE DISPLACEMENT ~ DEGREES
300
250
200
150
100
50
0
0
·2
·4
·6
·8
1·0
r/r₀ (RADIUS / OUTER RADIUS)

FIG. 83

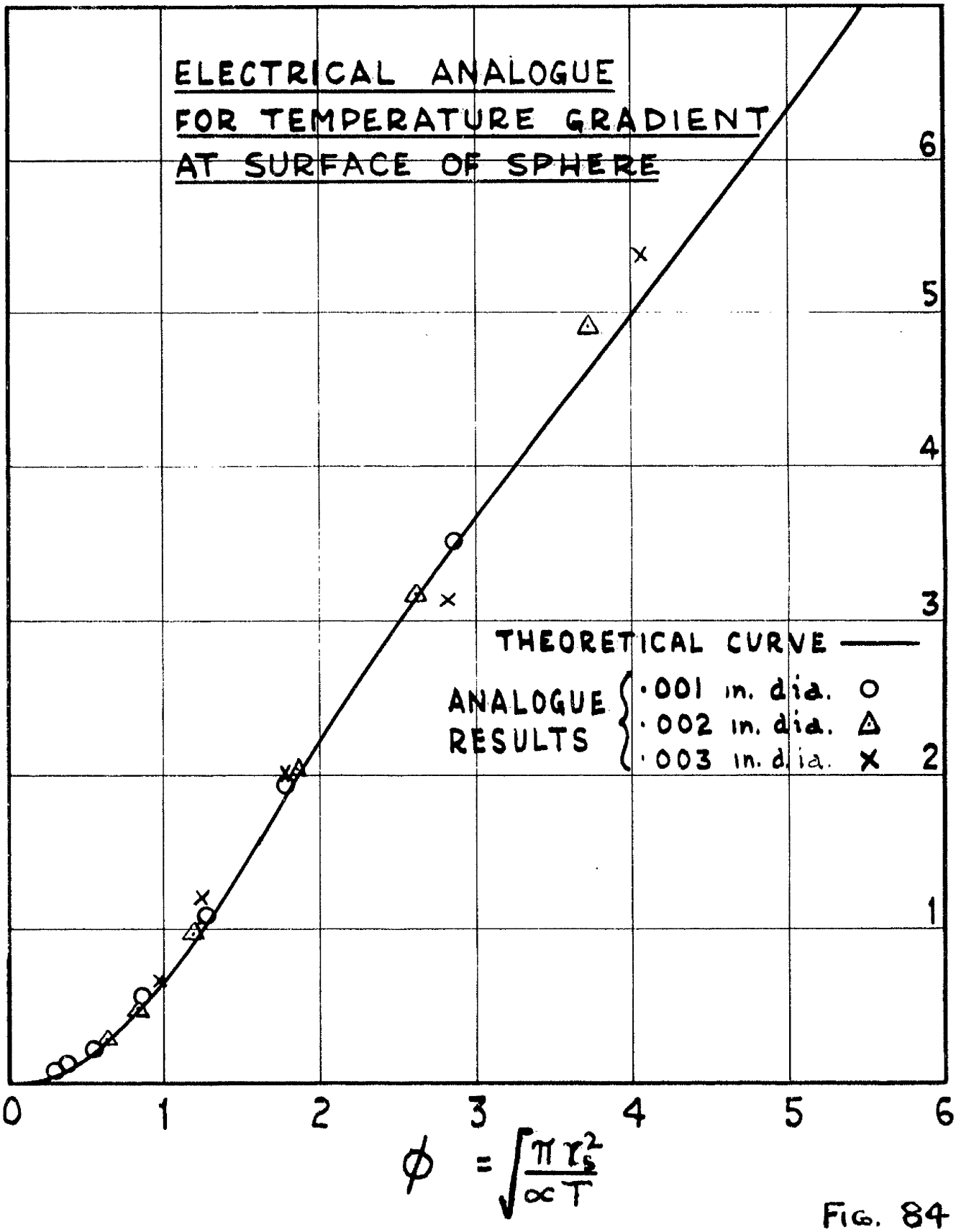
ELECTRICAL ANALOGUE
FOR TEMPERATURE GRADIENT
AT SURFACE OF SPHERE
THEORETICAL CURVE
ANALOGUE RESULTS
·001 in. dia. O
·002 in. dia. Δ
·003 in. dia. X
0
1
2
3
4
5
6
$\phi = \sqrt{\frac{\pi r_s^2}{\alpha T}}$
SURFACE TEMPERATURE GRADIENT X $\frac{\text{RADIUS}}{\text{SURFACE TEMP.}}$
$\left(\frac{dt}{dr}\right)_s \times \frac{r_s}{t_s}$

FIG. 84

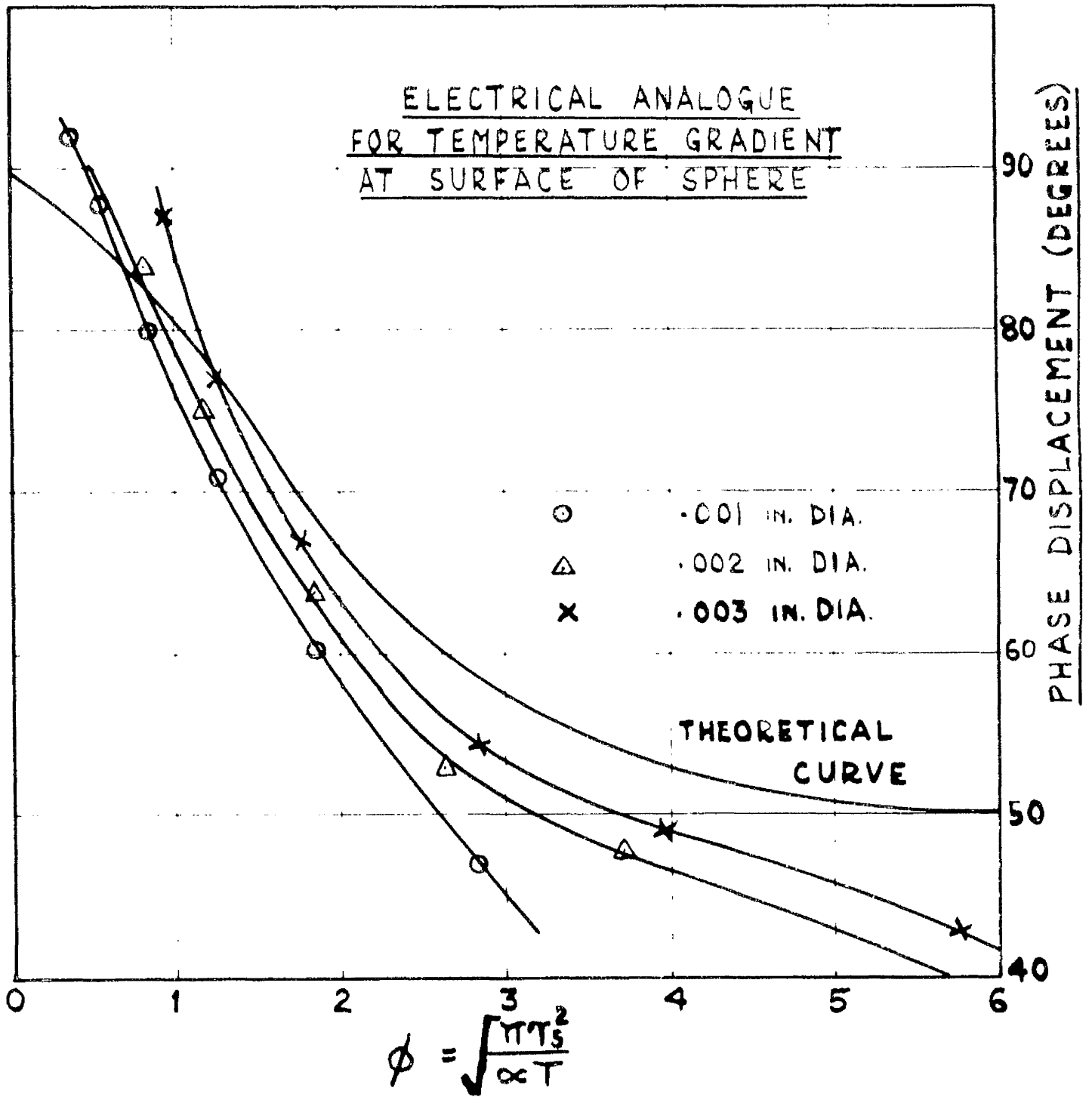
ELECTRICAL ANALOGUE
FOR TEMPERATURE GRADIENT
AT SURFACE OF SPHERE
PHASE DISPLACEMENT (DEGREES)
90
80
70
60
50
40
0
1
2
3
4
5
6
·001 IN. DIA.
·002 IN. DIA.
·003 IN. DIA.
THEORETICAL
CURVE
$\phi = \sqrt{\frac{\pi T_s^2}{\alpha T}}$

FIG. 85

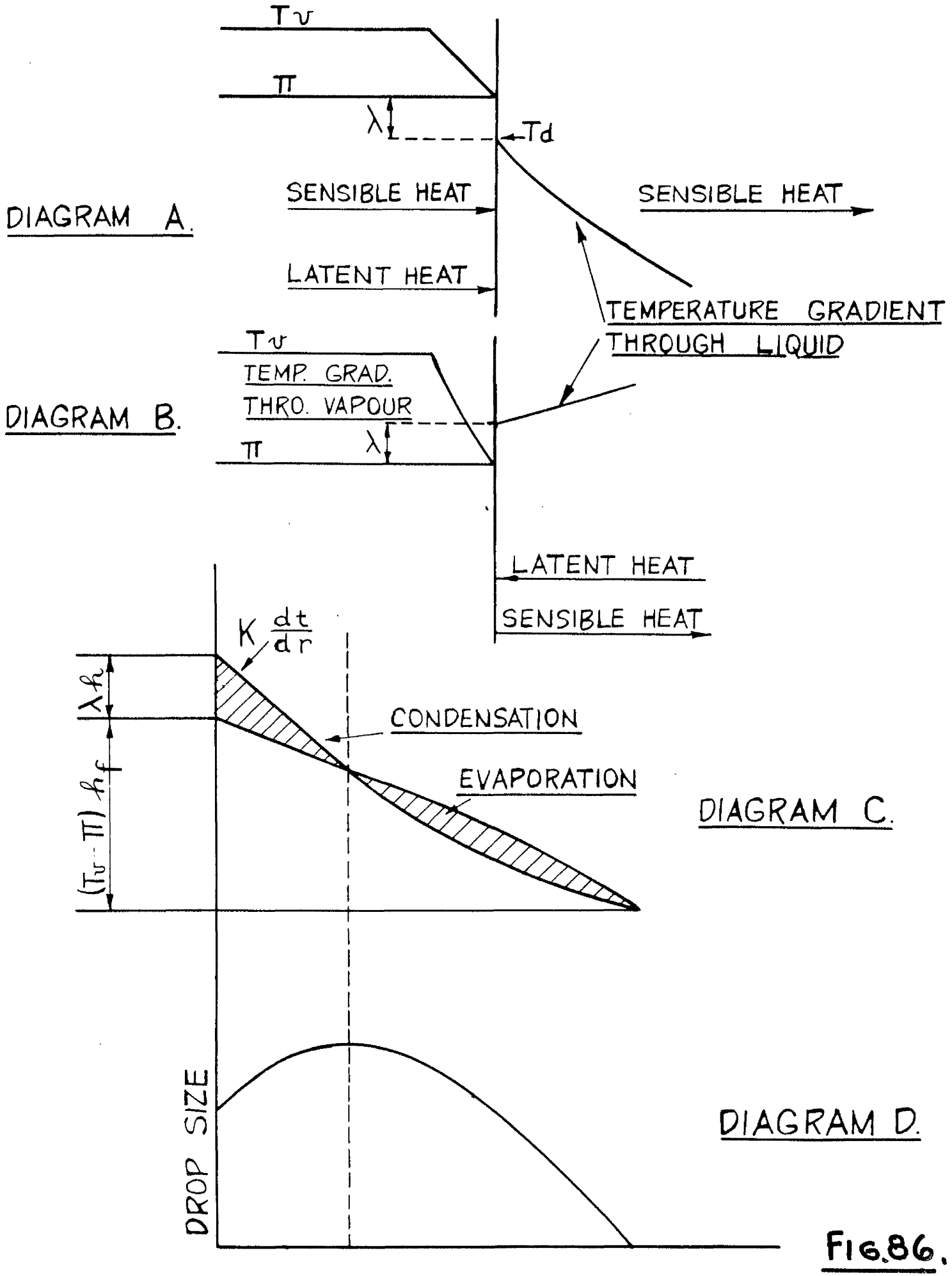

Fig.86.

HEAT FLOW BETWEEN DROPLET AND VAPOUR

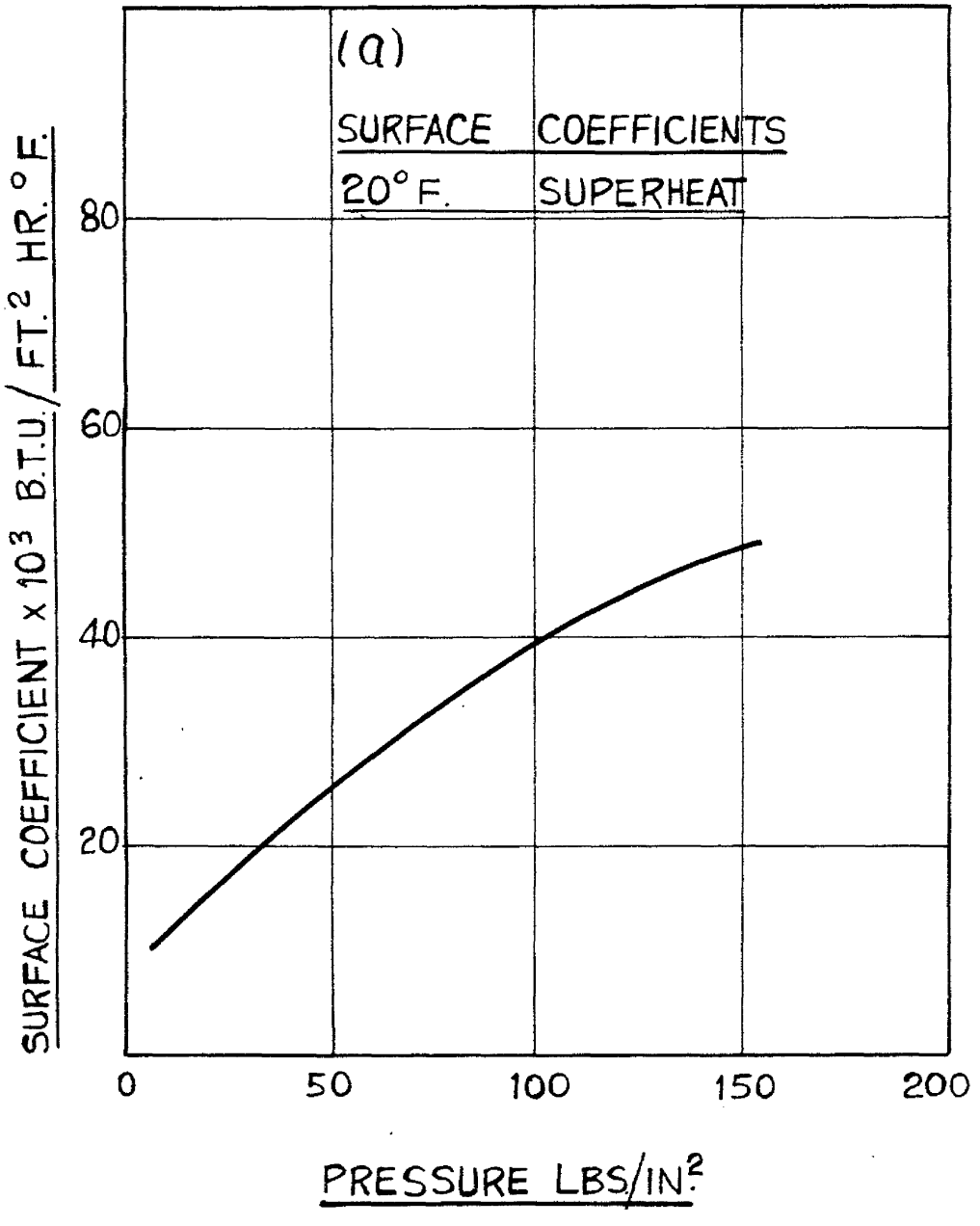

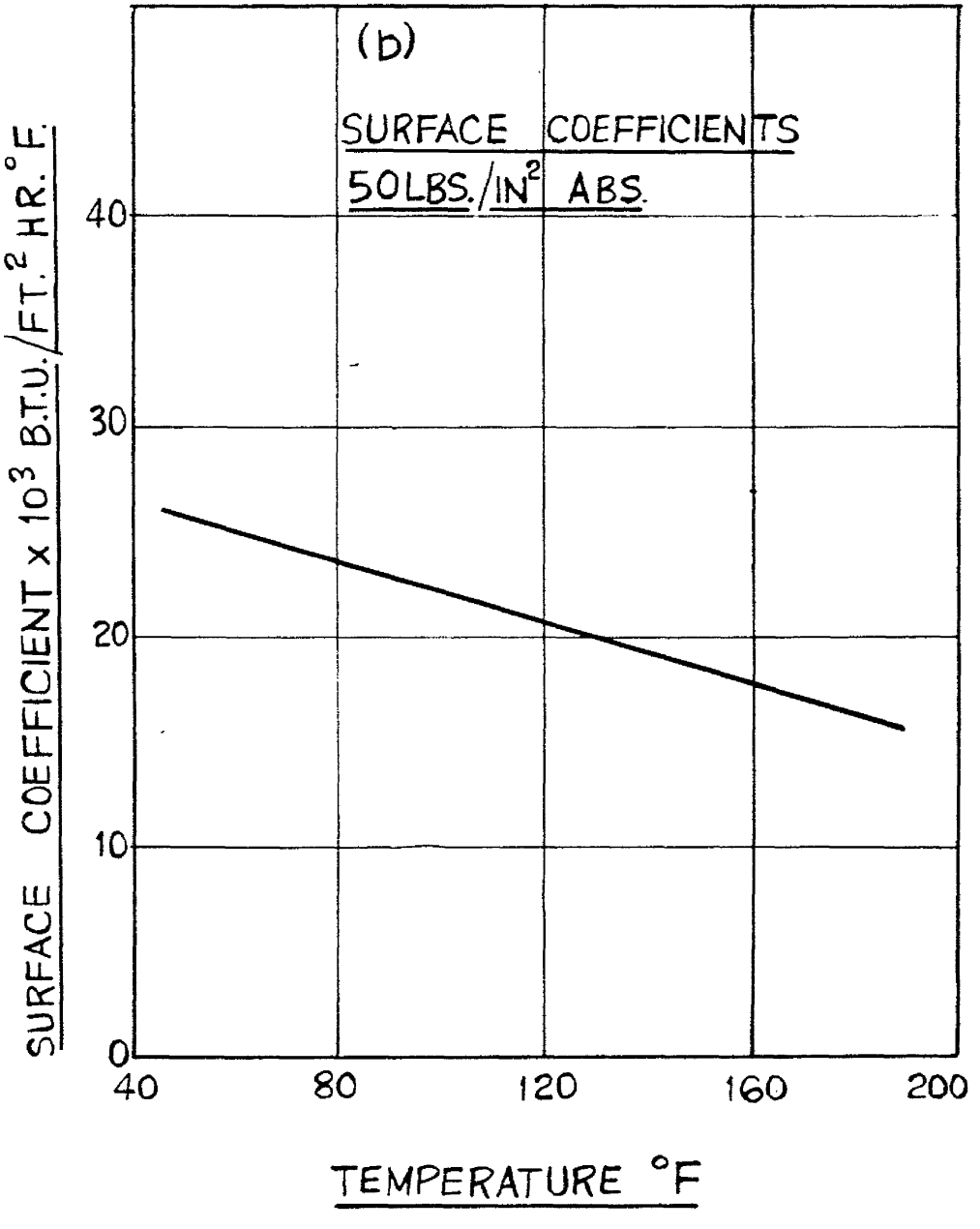

SURFACE COEFFICIENTS FOR F.12

FIG. 87

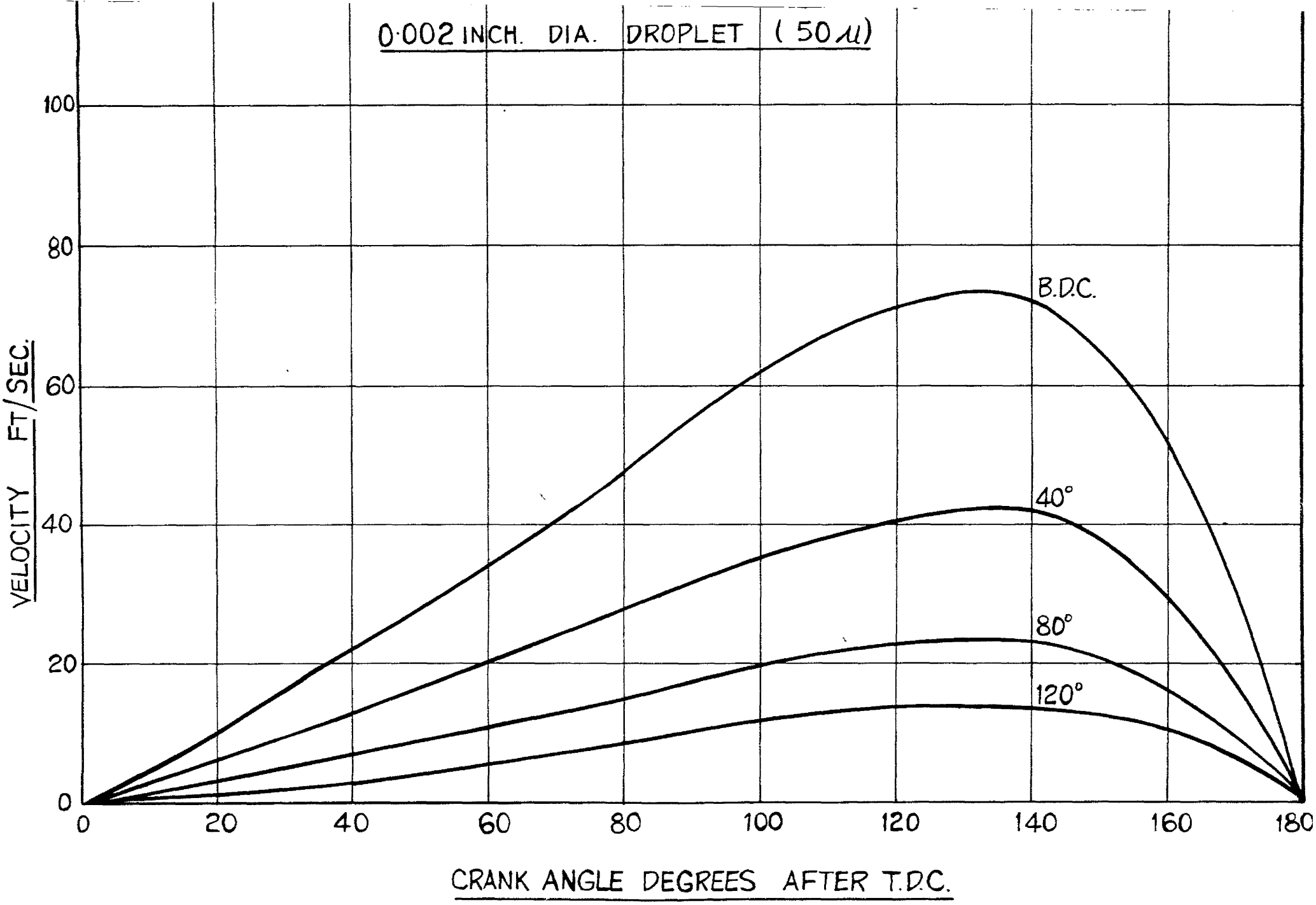

RELATIVE PARTICLE VELOCITY

FIG. 88

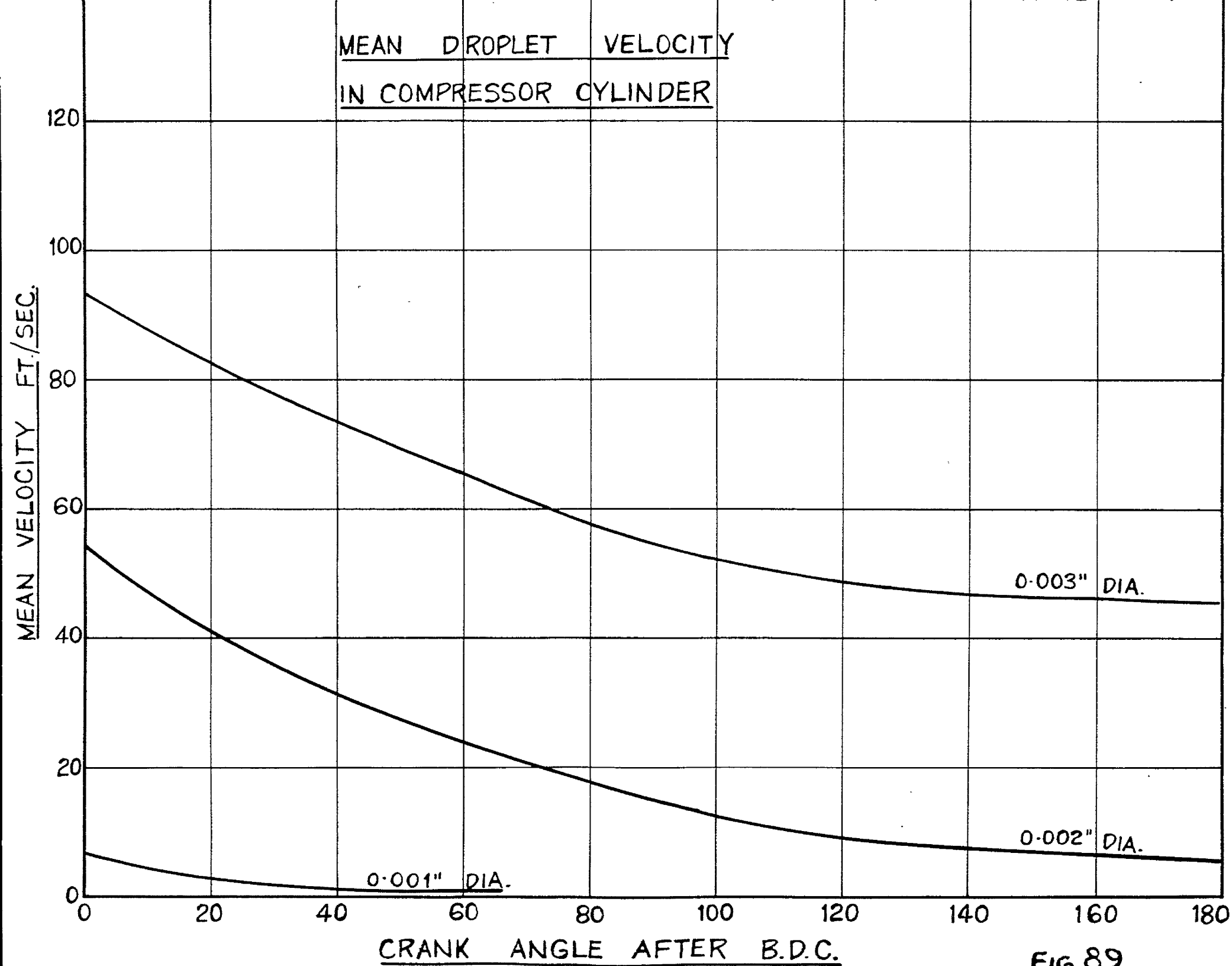
MEAN DROPLET VELOCITY
IN COMPRESSOR CYLINDER
MEAN VELOCITY FT./SEC.
0
20
40
60
80
100
120
0
20
40
60
80
100
120
140
160
180
0·003" DIA.
0·002" DIA.
0·001" DIA.
CRANK ANGLE AFTER B.D.C.

FIG 89

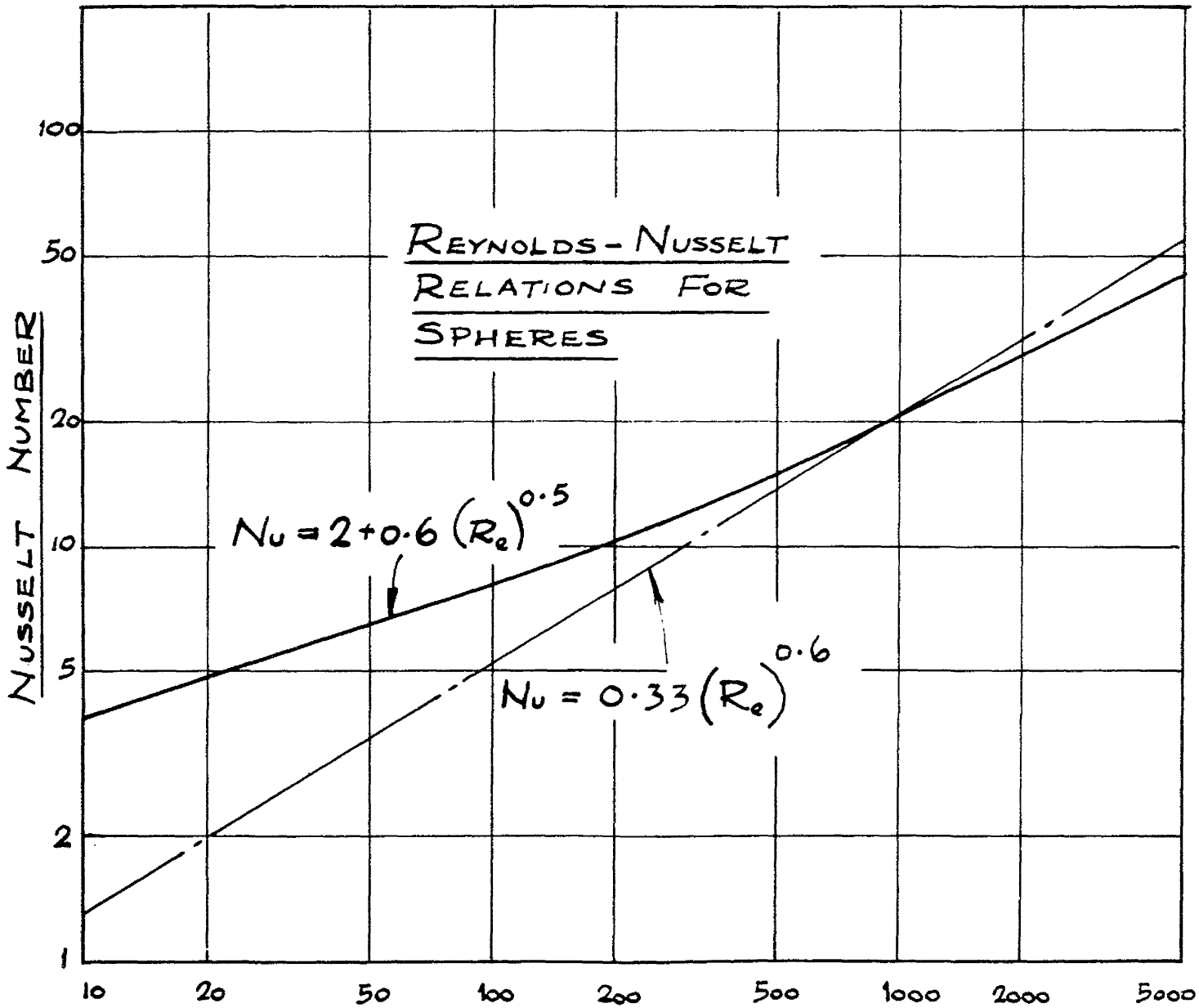
REYNOLDS - NUSSELT
RELATIONS FOR
SPHERES
NUSSELT NUMBER
100
50
20
10
5
2
1
$Nu = 2 + 0.6 (R_e)^{0.5}$
$Nu = 0.33 (R_e)^{0.6}$
10
20
50
100
200
500
1000
2000
5000
REYNOLDS NUMBER

FIG. NO. 90

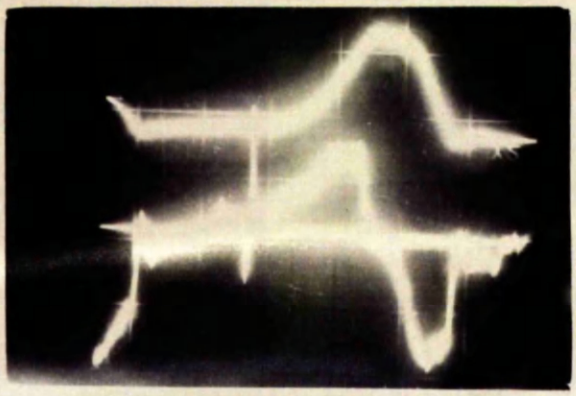

Successive
Cycles of
Temperature
Excursion.

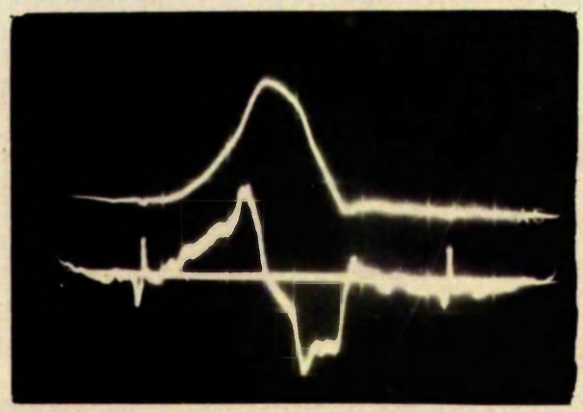

Uniform
Temperature
at beginning
of Compression.

COMPARISON OF SURFACE TEMPERATURE GRADIENTS ON DROPLETS.

Fig.91.

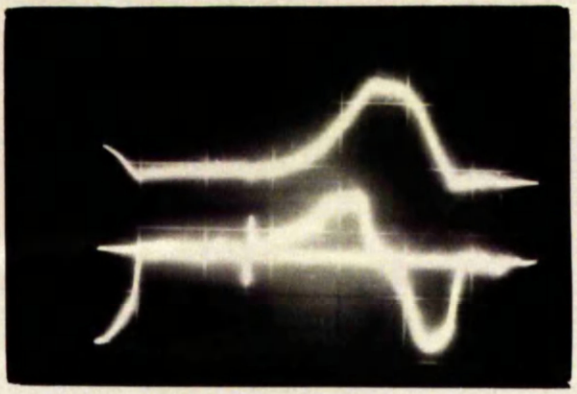

Droplet
.002" dia.

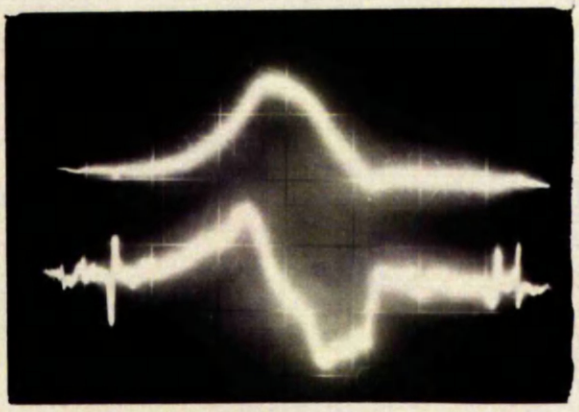

Droplet
.003" dia.

TEMPERATURE GRADIENTS FOR DROPLETS Fig. 92.

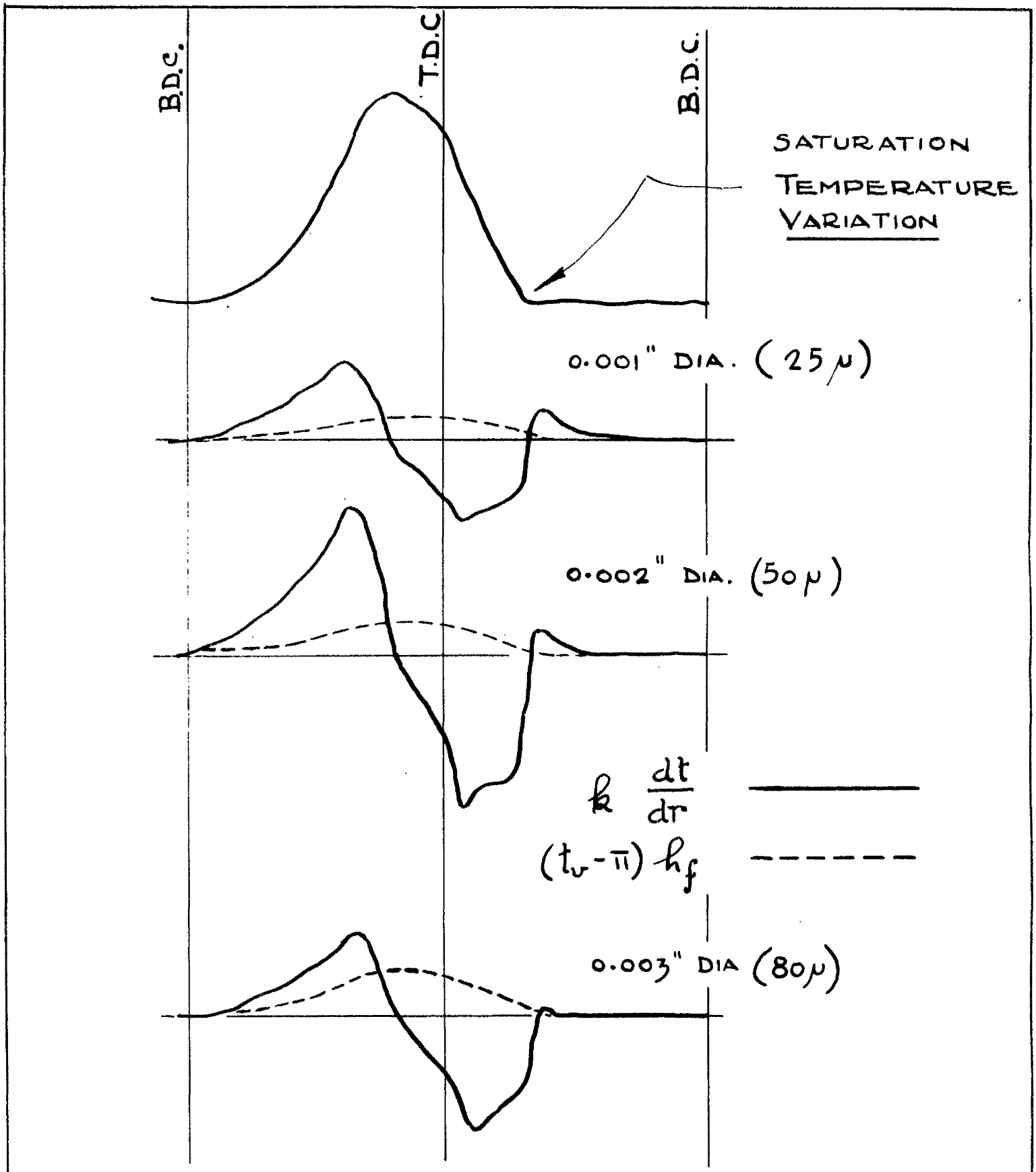

TEMPERATURE GRADIENTS AT SURFACE OF DROPLETS

FIG 93

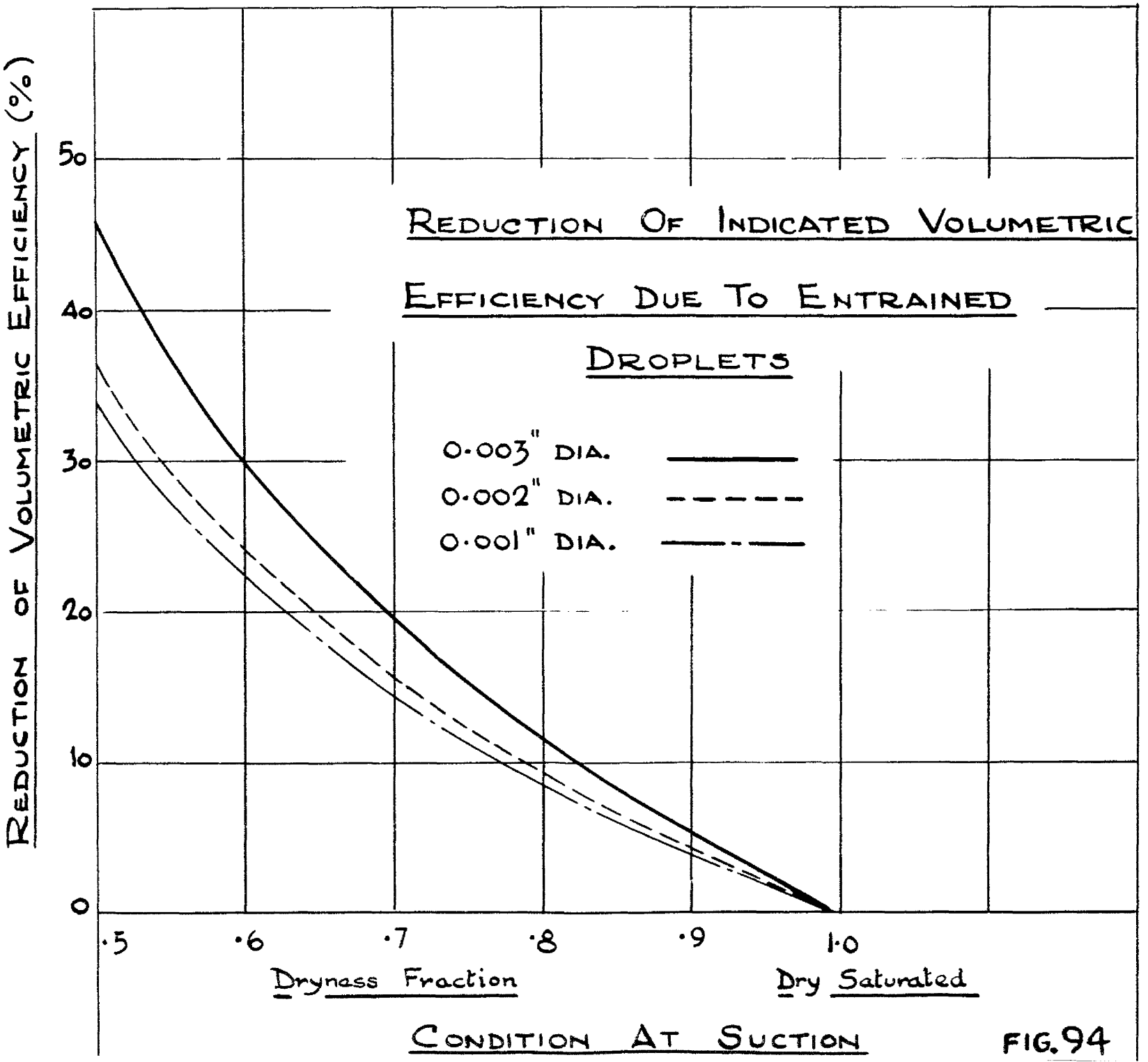
REDUCTION OF VOLUMETRIC EFFICIENCY (%)
50
40
30
20
10
0
REDUCTION OF INDICATED VOLUMETRIC EFFICIENCY DUE TO ENTRAINED DROPLETS
0·003" DIA.
0·002" DIA.
0·001" DIA.
·5
·6
·7
·8
·9
1·0
Dryness Fraction
Dry Saturated
CONDITION AT SUCTION

FIG. 94

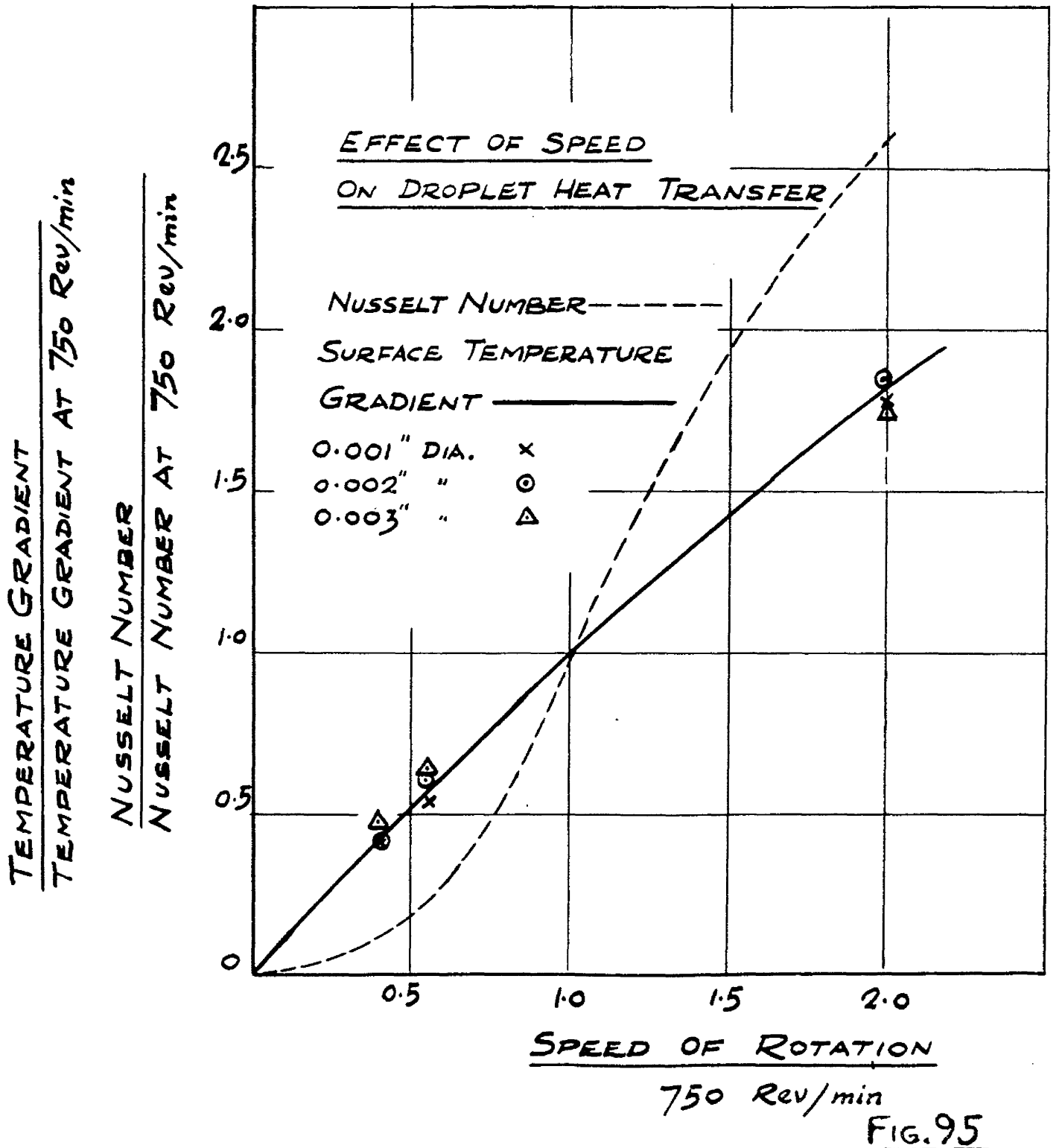
EFFECT OF SPEED
ON DROPLET HEAT TRANSFER
NUSSELT NUMBER
SURFACE TEMPERATURE
GRADIENT
0·001" DIA.
0·002" "
0·003" "
2·5
2·0
1·5
1·0
0·5
0
0·5
1·0
1·5
2·0
SPEED OF ROTATION
750 Rev/min
TEMPERATURE GRADIENT / TEMPERATURE GRADIENT AT 750 Rev/min
NUSSELT NUMBER / NUSSELT NUMBER AT 750 Rev/min

FIG. 95

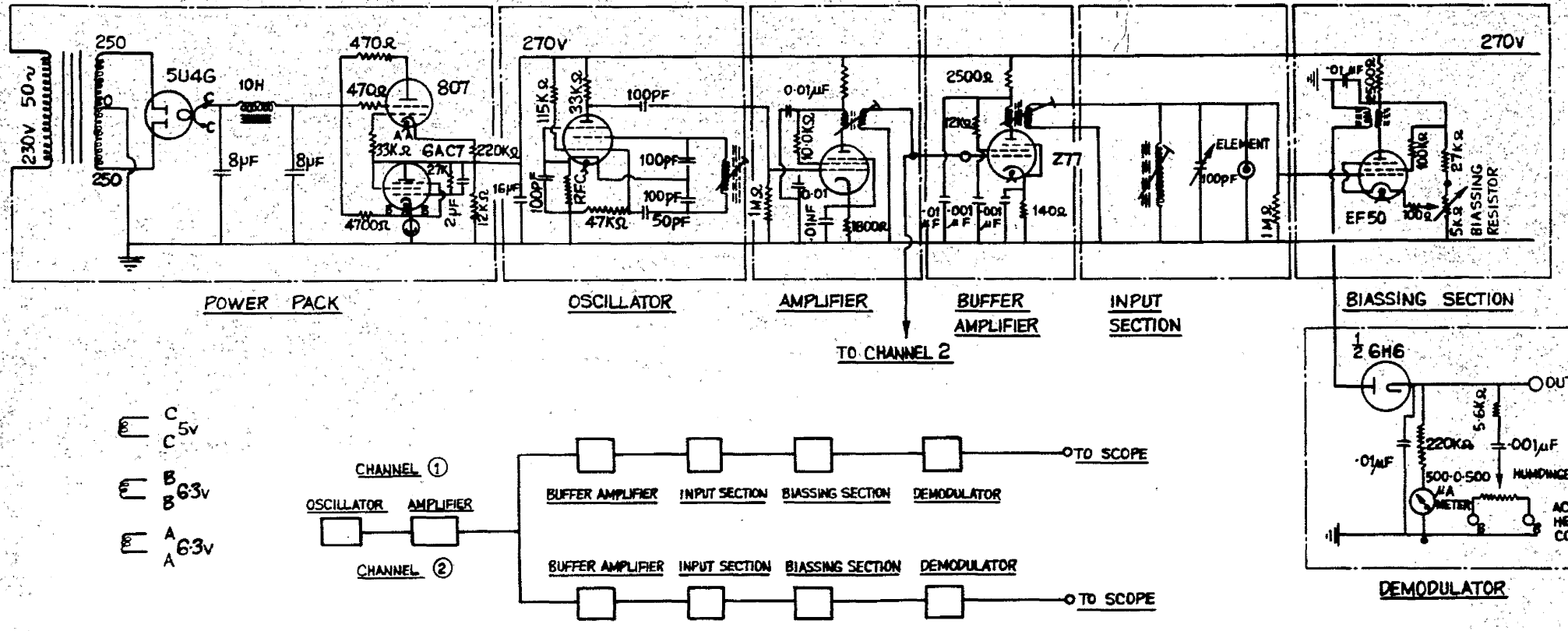

PICK – UP ELEMENT AMPLIFIER

FIG. 96.

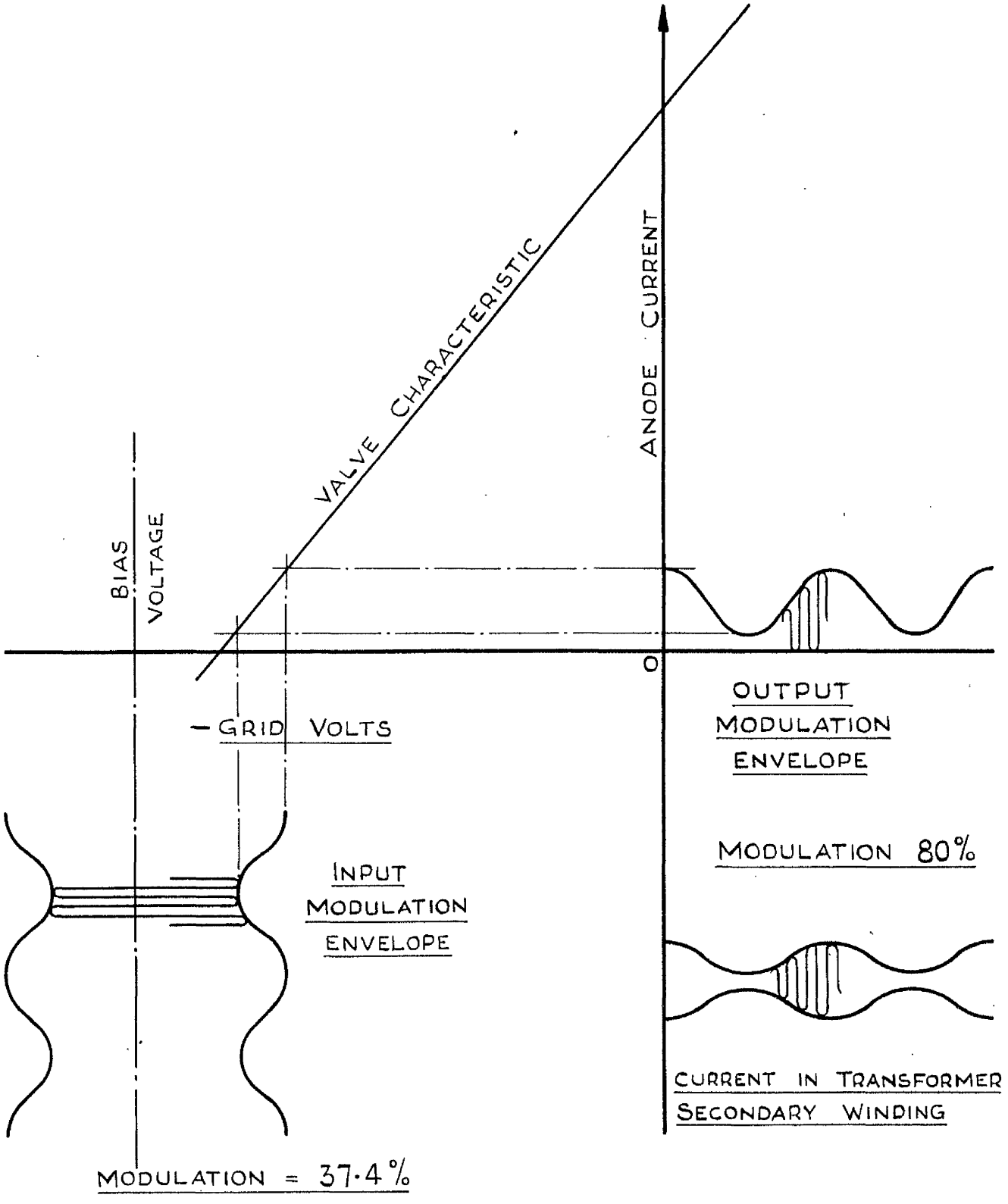

BIASSING SECTION VALVE OPERATION DIAGRAM

FIG. Nº 97

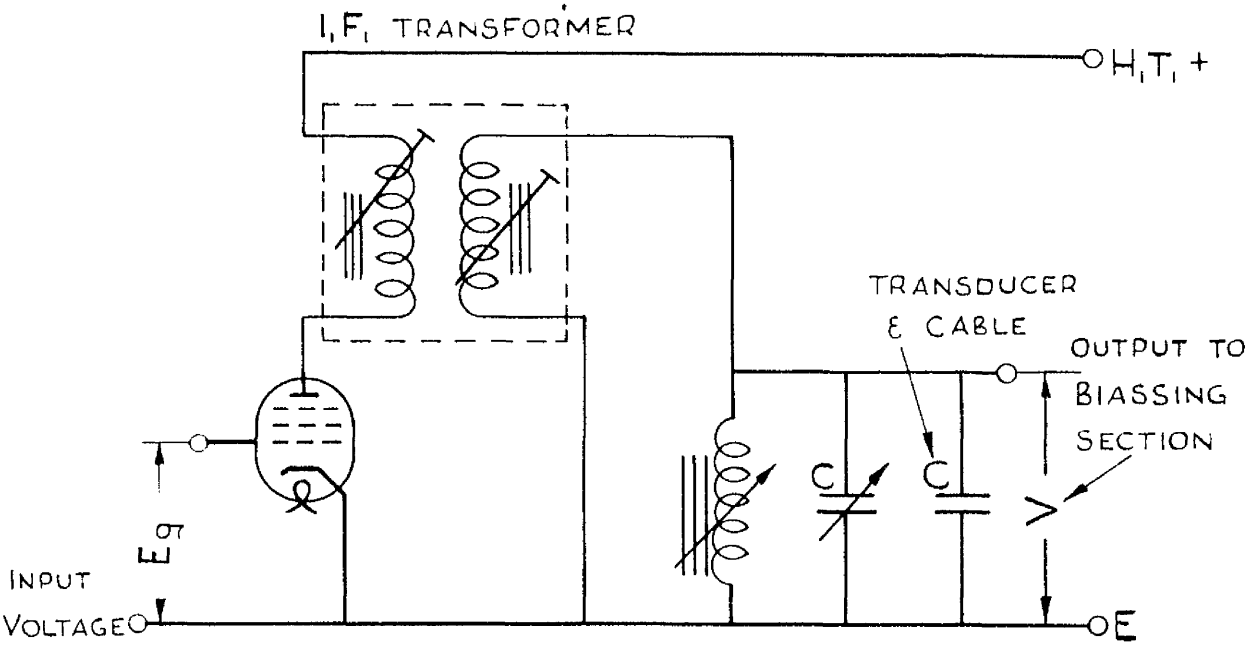

SKELETON CIRCUIT OF
BUFFER AMPLIER & INPUT SECTION

FIG. 98 (a)

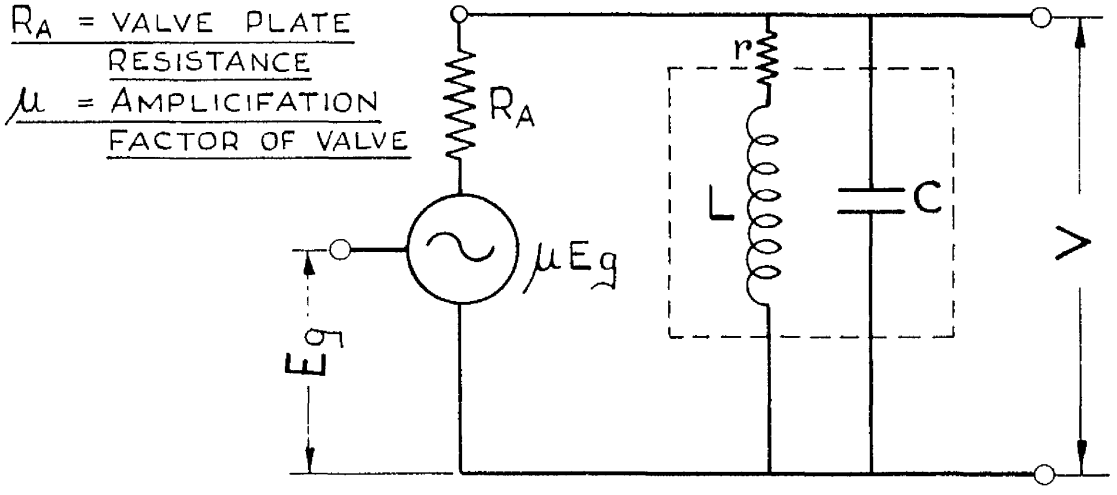

EQUIVALENT CIRCUIT OF
BUFFER AMPLIFIER & INPUT SECTION

FIG. 98 (b)

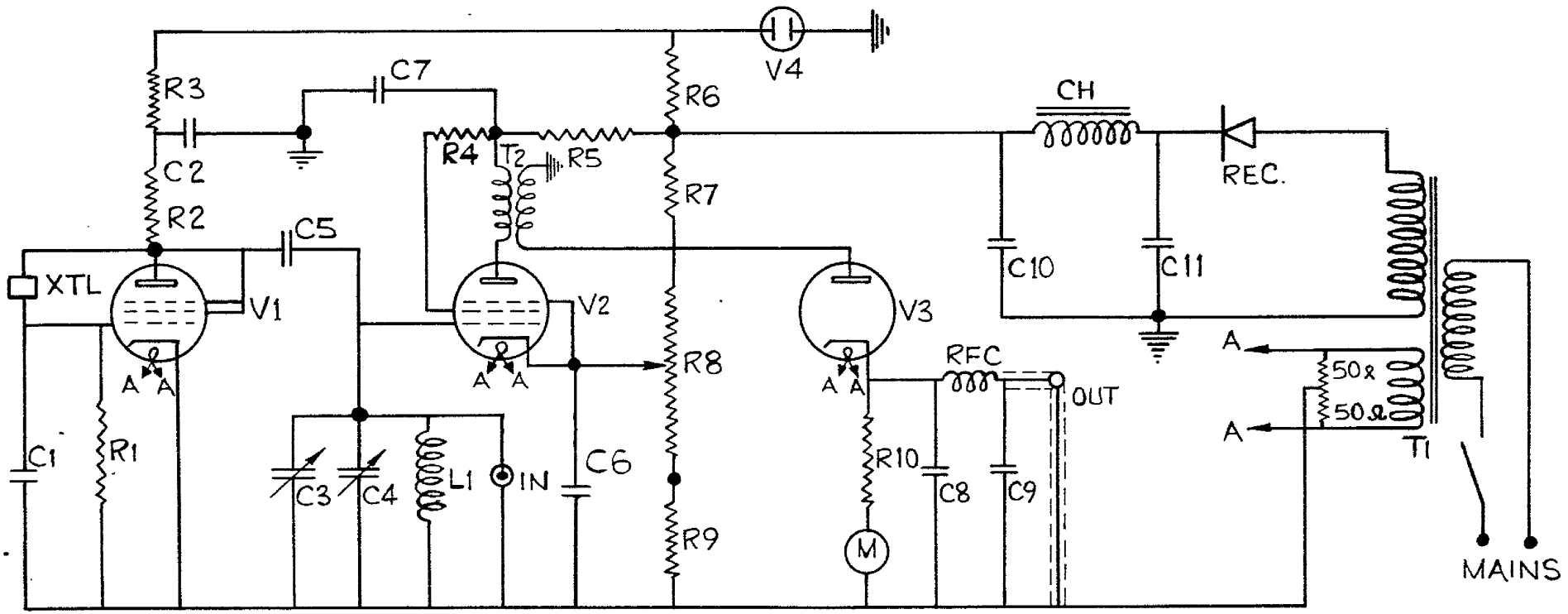

R1	47 K Ω
R2	47 K Ω
R3	10 K Ω
R4	100 K Ω
R5	10 K Ω
R6	47 K Ω
R7	10 K Ω
R8	1·2 K Ω
R9	150 K Ω
R10	4·7 K Ω
R11	50+50 Ω

C1	0·1 μ/d
C2	0·1 μ/d
C3	15 μμd
C4	100 μμd
C5	2 μμd
C6	·007 μF
C7	·01 μF
C8	100 μμd
C9	100 μμd
C10	200 MFd
C11	100 MFd

V1	EF 91
V2	EF 91
V3	6AL5
V4	0B2
REC	SIL. REC. 50.
T1	125·0·125V
T2	1·6 MC/S IFT.
L1	1·6 MC/S
XTL	1·6 MC/S
CH	5.H. MIN.

ELEMENT PICK-UP UNIT FIG 99

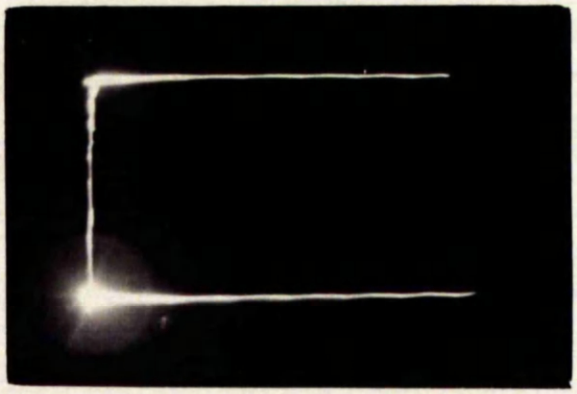

Response Curve.

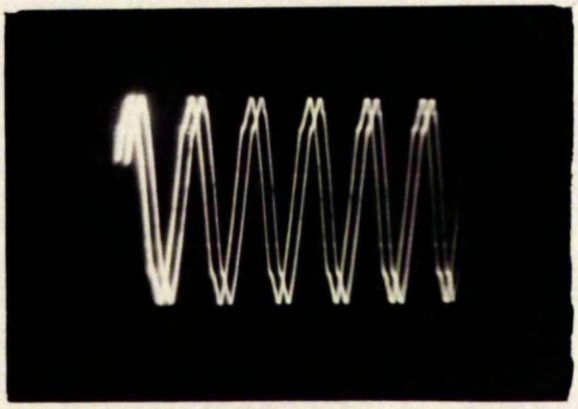

Timing Trace. (50 /sec.).

RESPONSE OF ELEMENT PICK-UP UNIT Fig. 100.

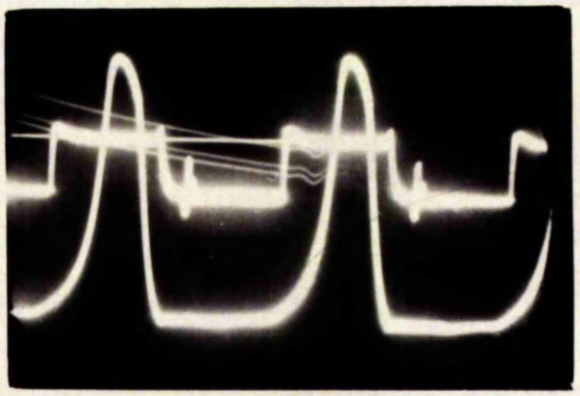

Pressure &
"Farnborough"
Diagram.

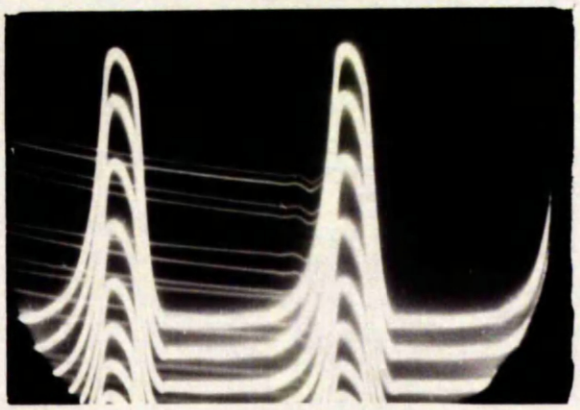

Calibration
Diagram.

TYPICAL PRESSURE & CALIBRATION DIAGRAMS. Fig.101.

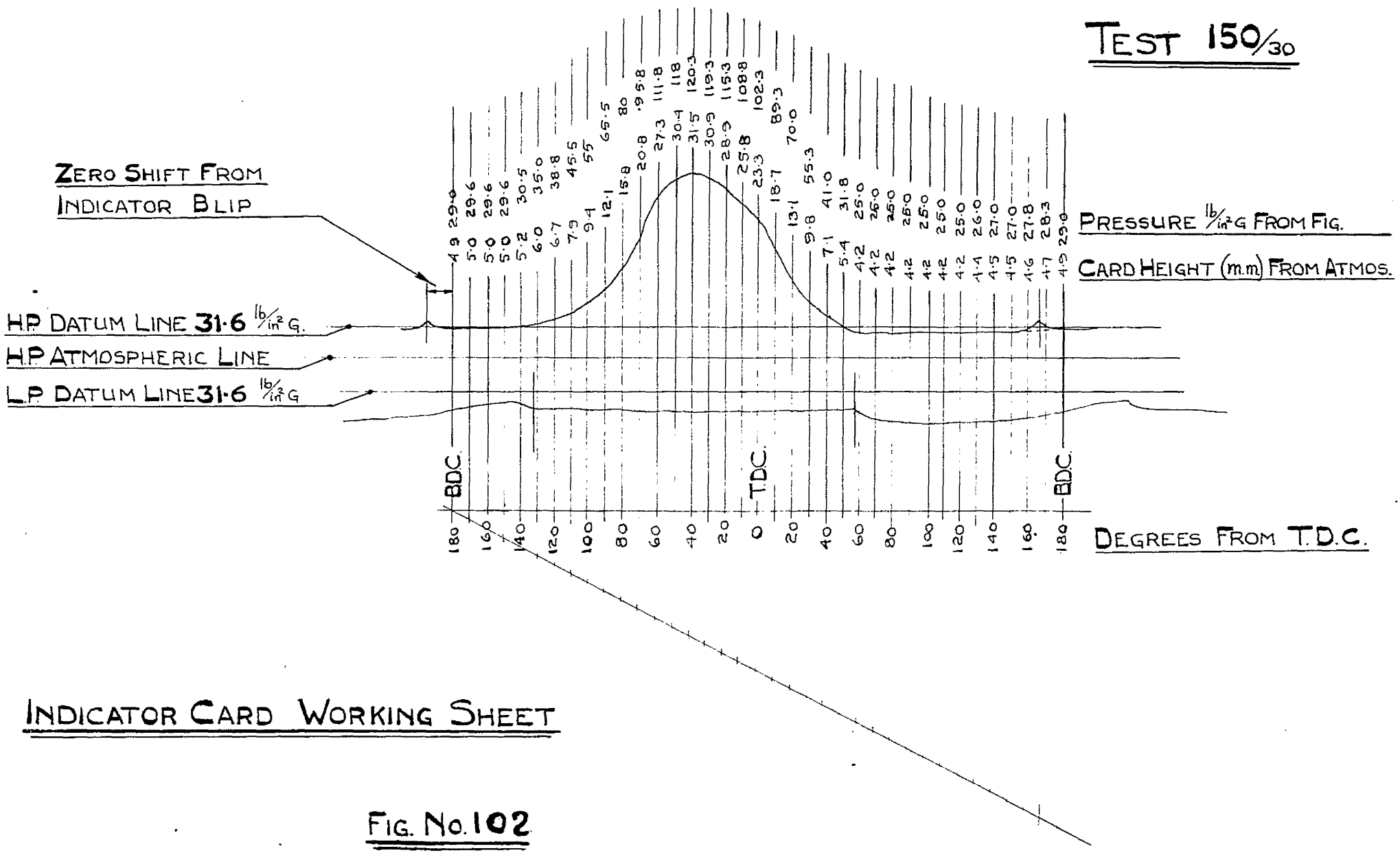

INDICATOR CARD WORKING SHEET

FIG. No. 102

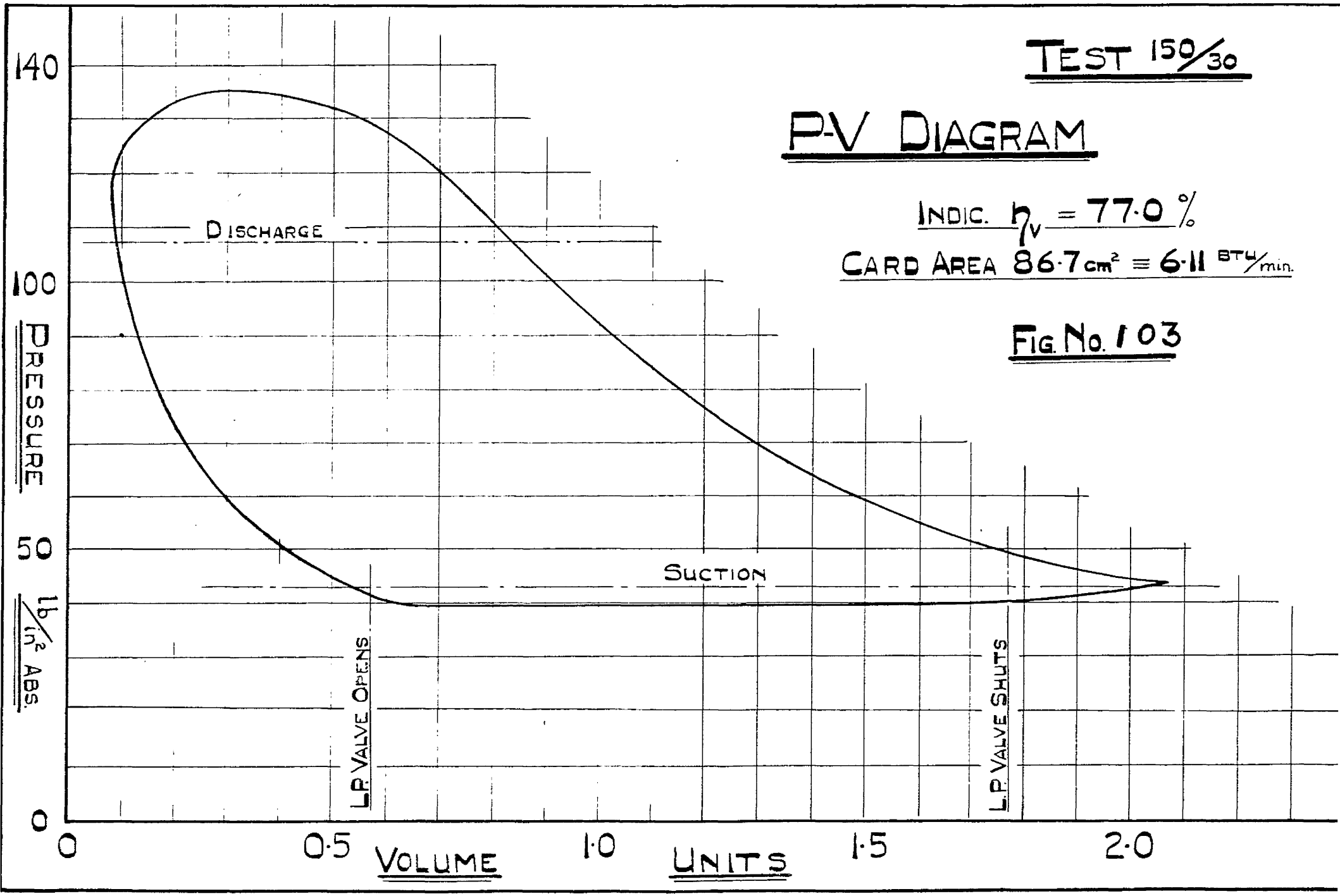
TEST 150/30
P-V DIAGRAM
INDIC. η_v = 77·0 %
CARD AREA 86·7 cm² ≡ 6·11 BTU/min.
FIG. No. 103
140
100
50
0
PRESSURE lb/in² ABS.
DISCHARGE
SUCTION
L.P. VALVE OPENS.
L.P. VALVE SHUTS
0
0·5
1·0
1·5
2·0
VOLUME UNITS

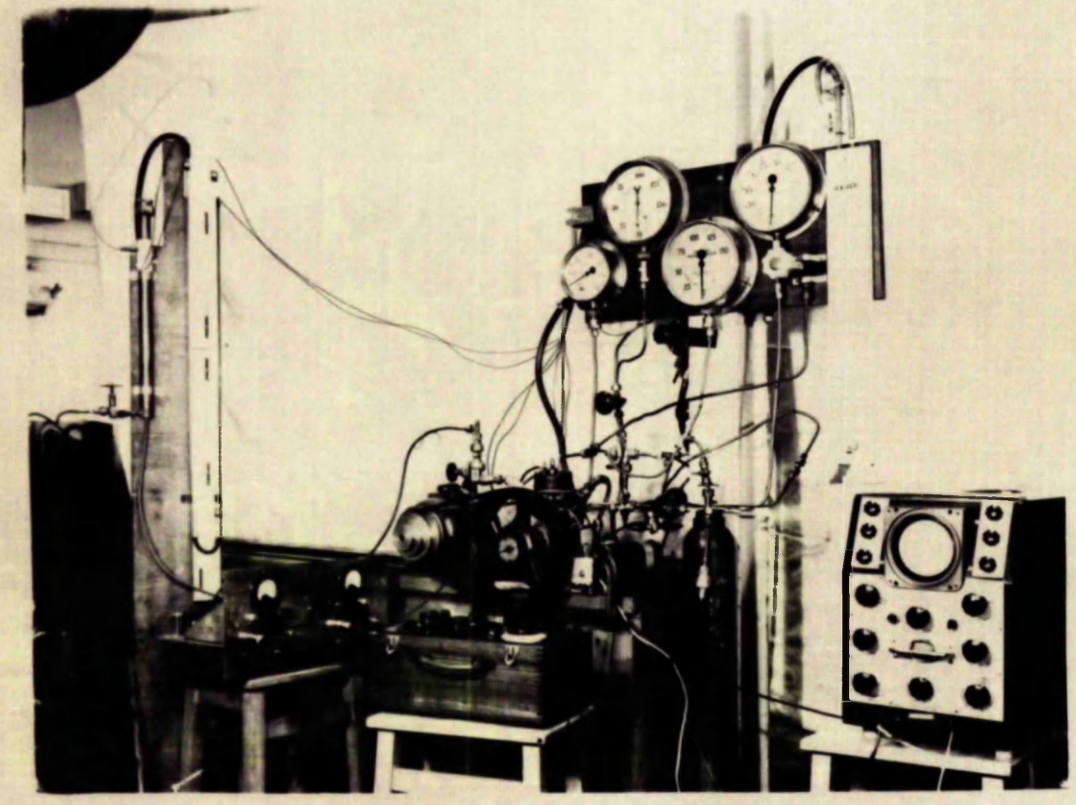

ARRANGEMENT OF AIR CIRCUIT Fig.104.

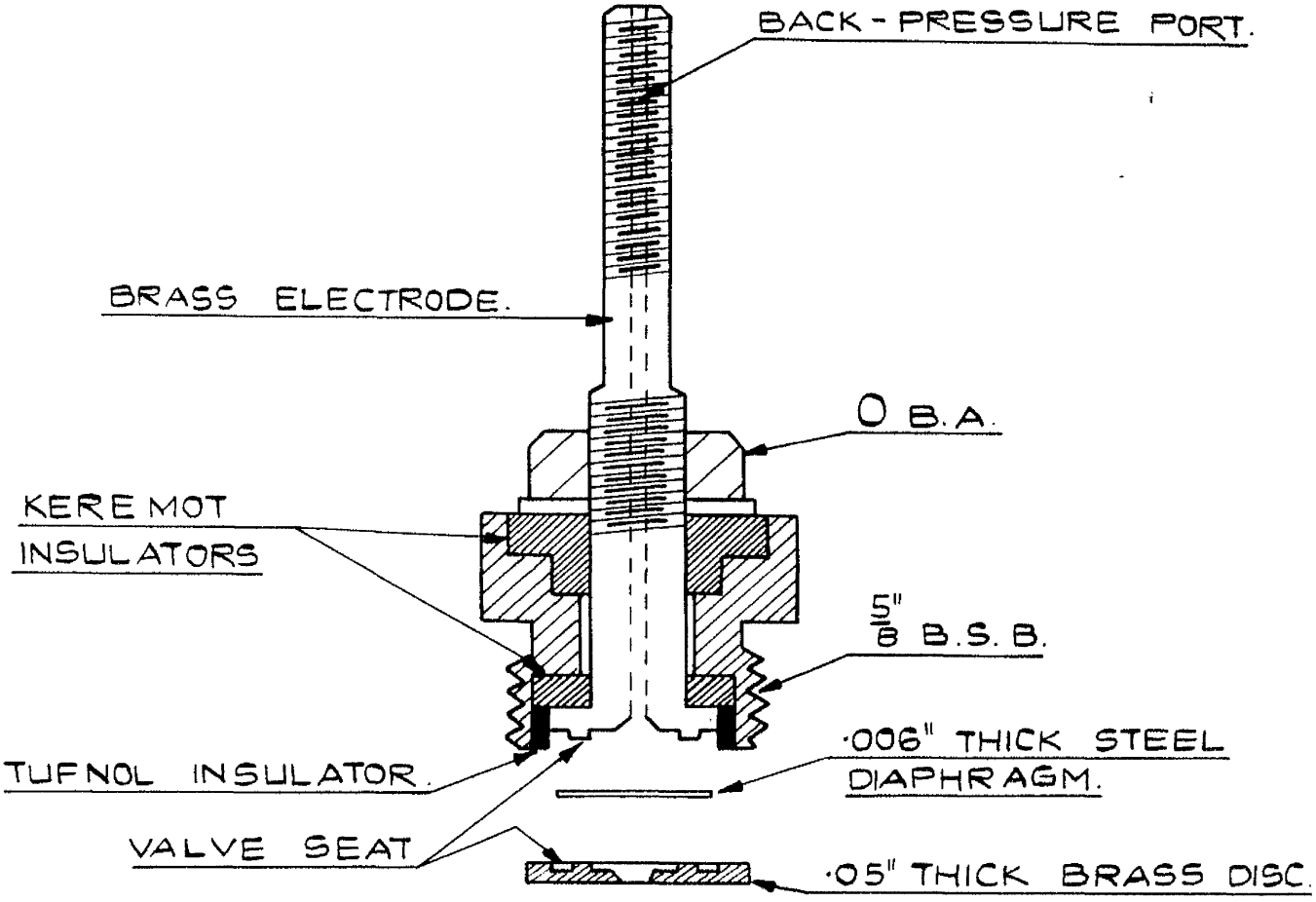

THE STEEL DIAPHRAM IS FREE TO MOVE ·003" BETWEEN BRASS DISC. AND CENTRAL DISC ENDED ELECTRODE.

DATUM PRESSURE ELEMENT

FARNBORO' - TYPE.

TWICE FULL SIZE.

FIG. Nº. 105

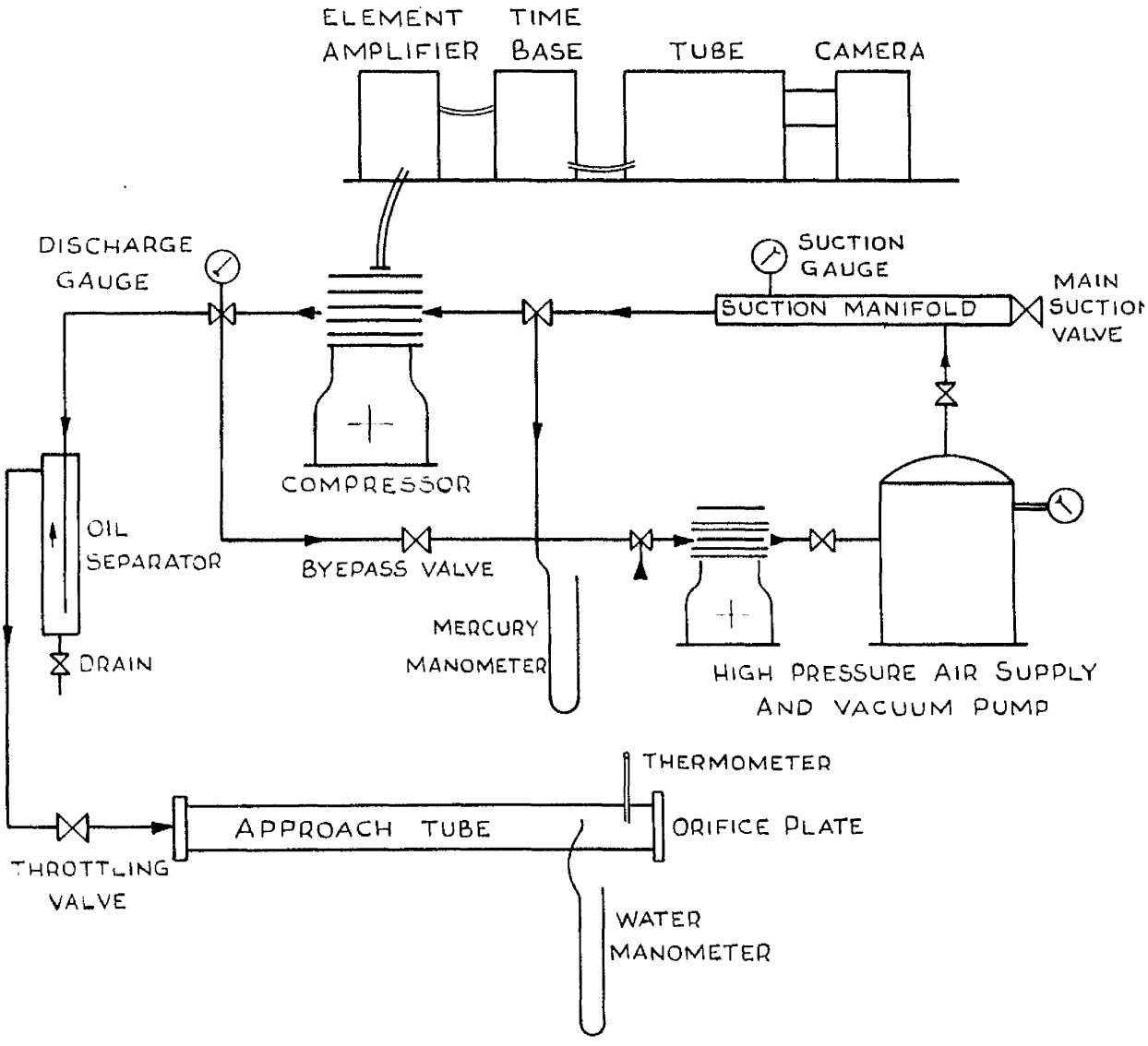

DIAGRAMMATIC ARRANGEMENT OF EXPERIMENTAL CIRCUIT

FIGURE No 106

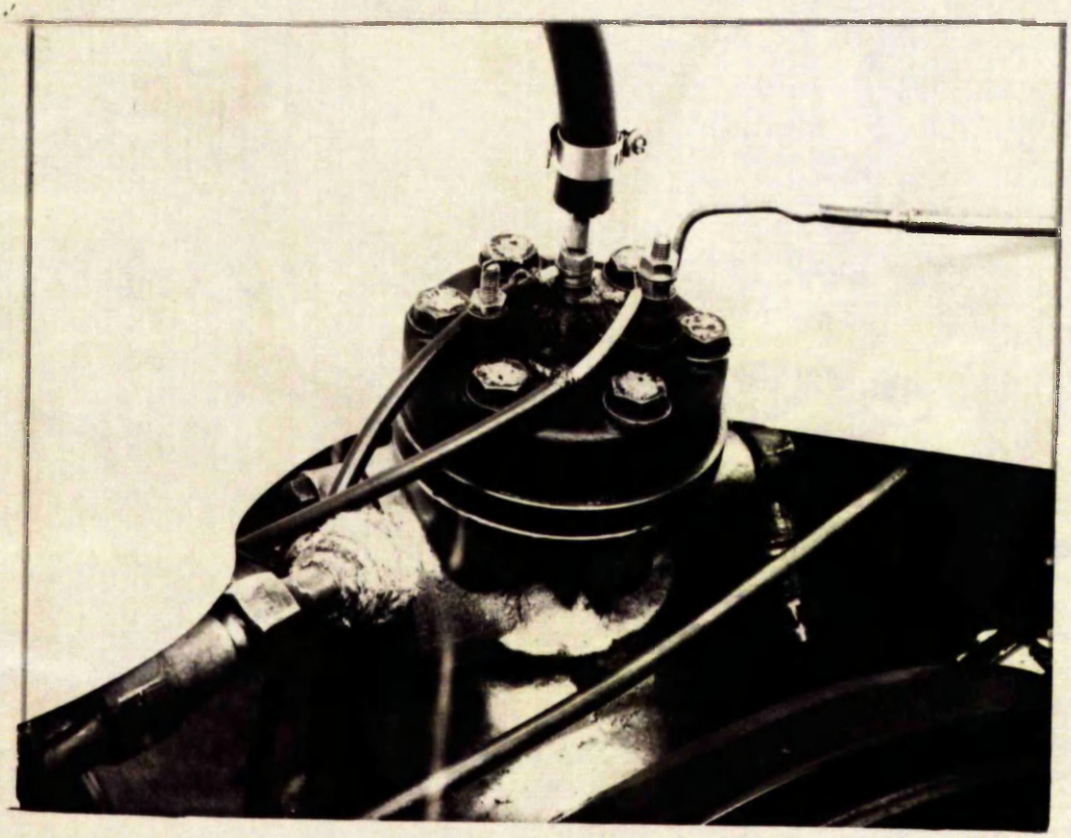

CLOSE-UP OF CYLINDER HEAD Fig. 107.

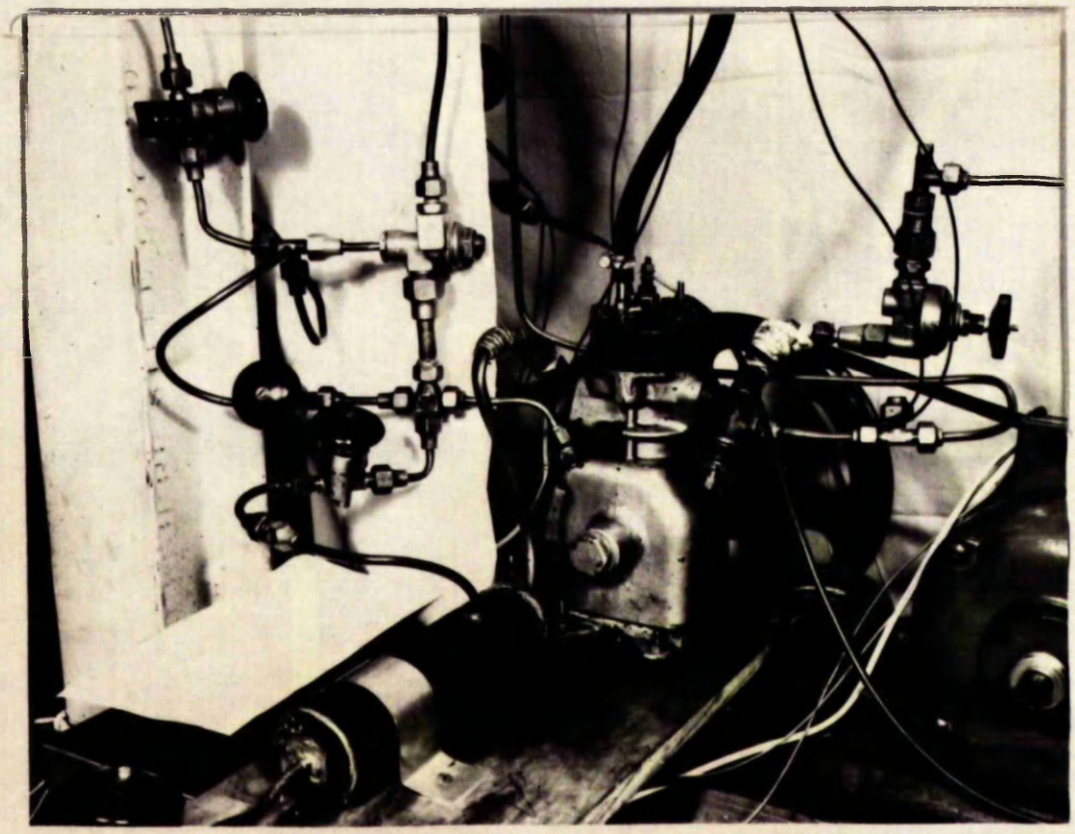

VIEW OF LEAKAGE MEASURING EQUIPMENT Fig.108.

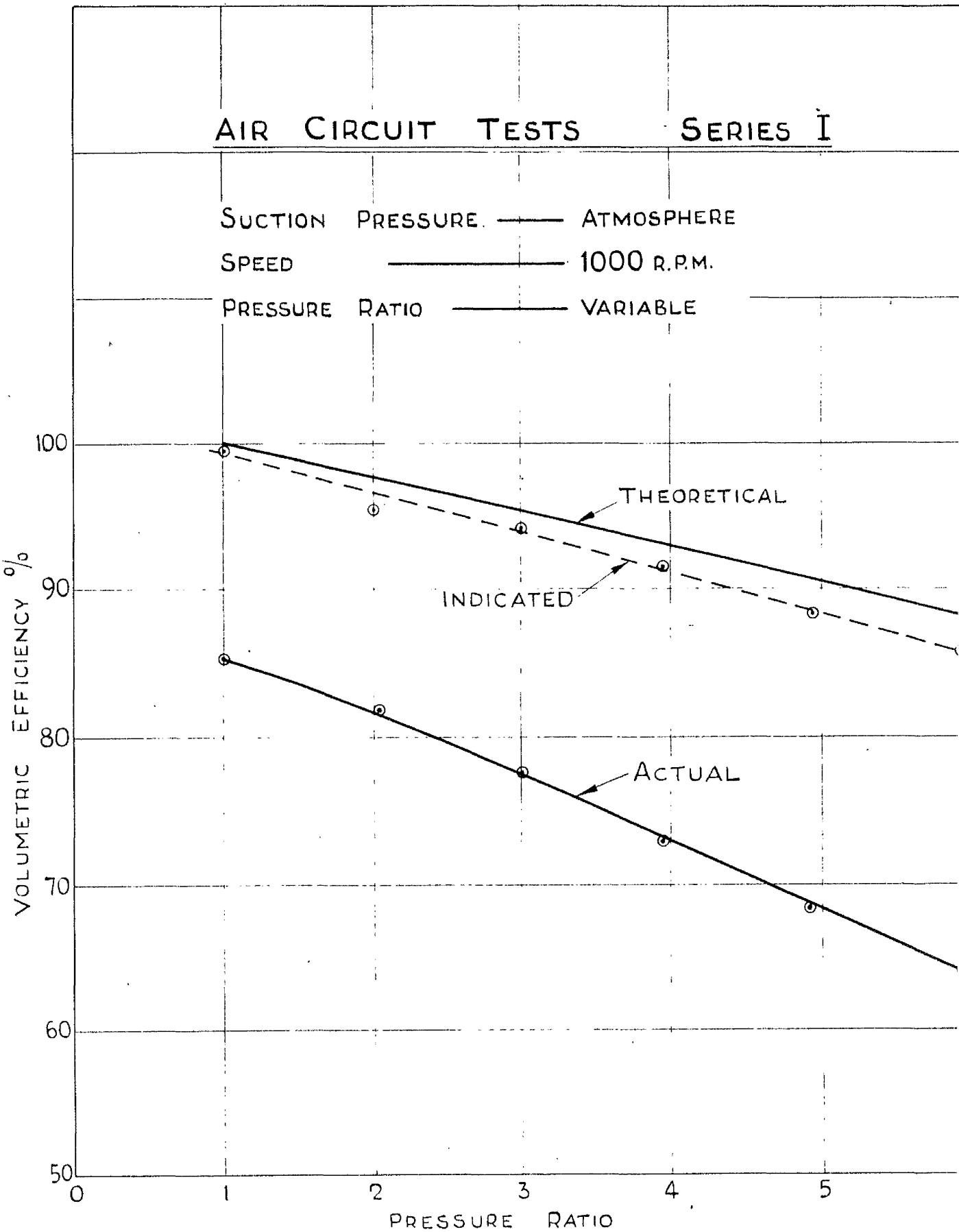

VOLUMETRIC EFFICIENCY CURVES

FIG. Nº 109

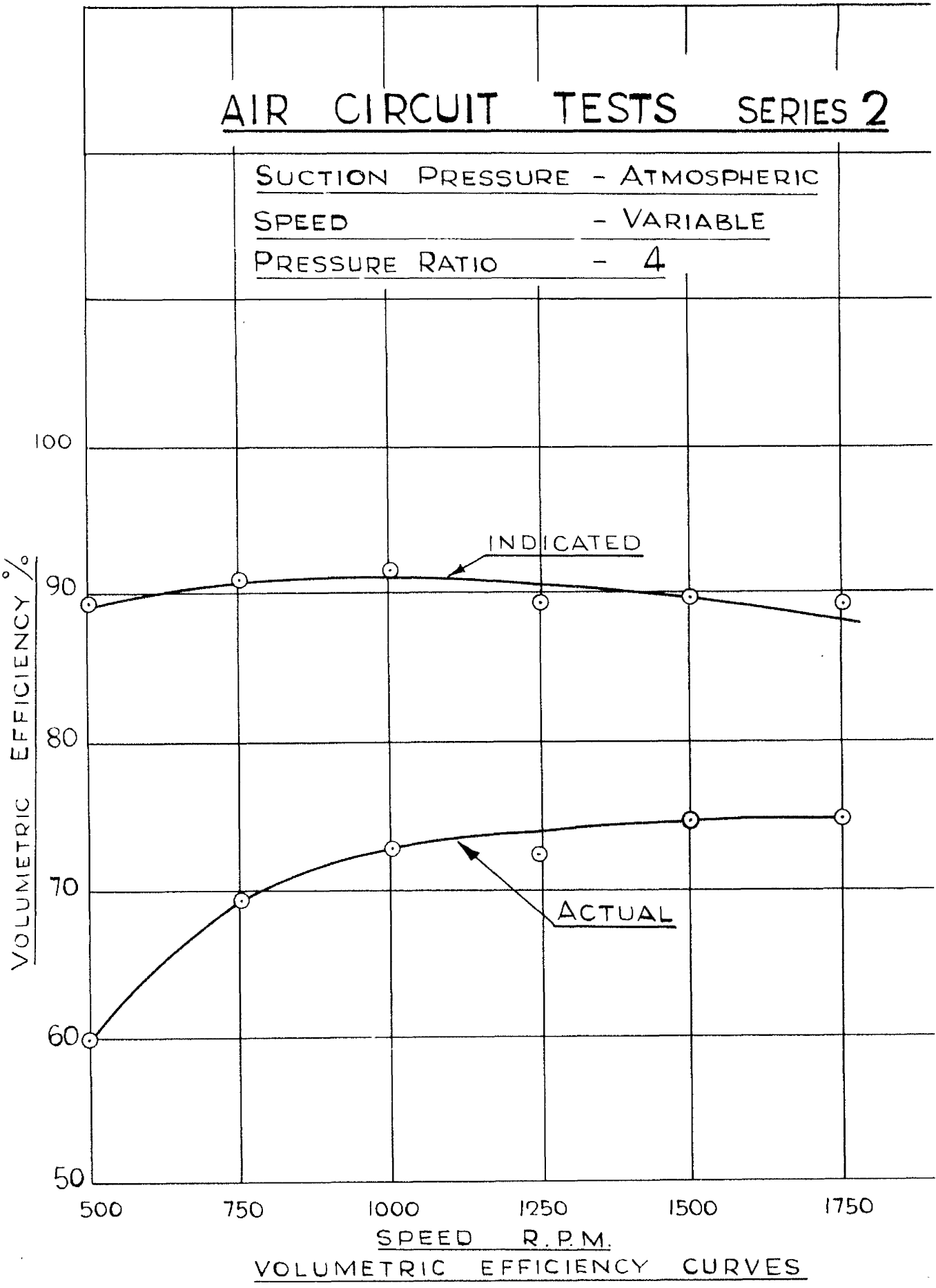

VOLUMETRIC EFFICIENCY CURVES

FIG. No. 11

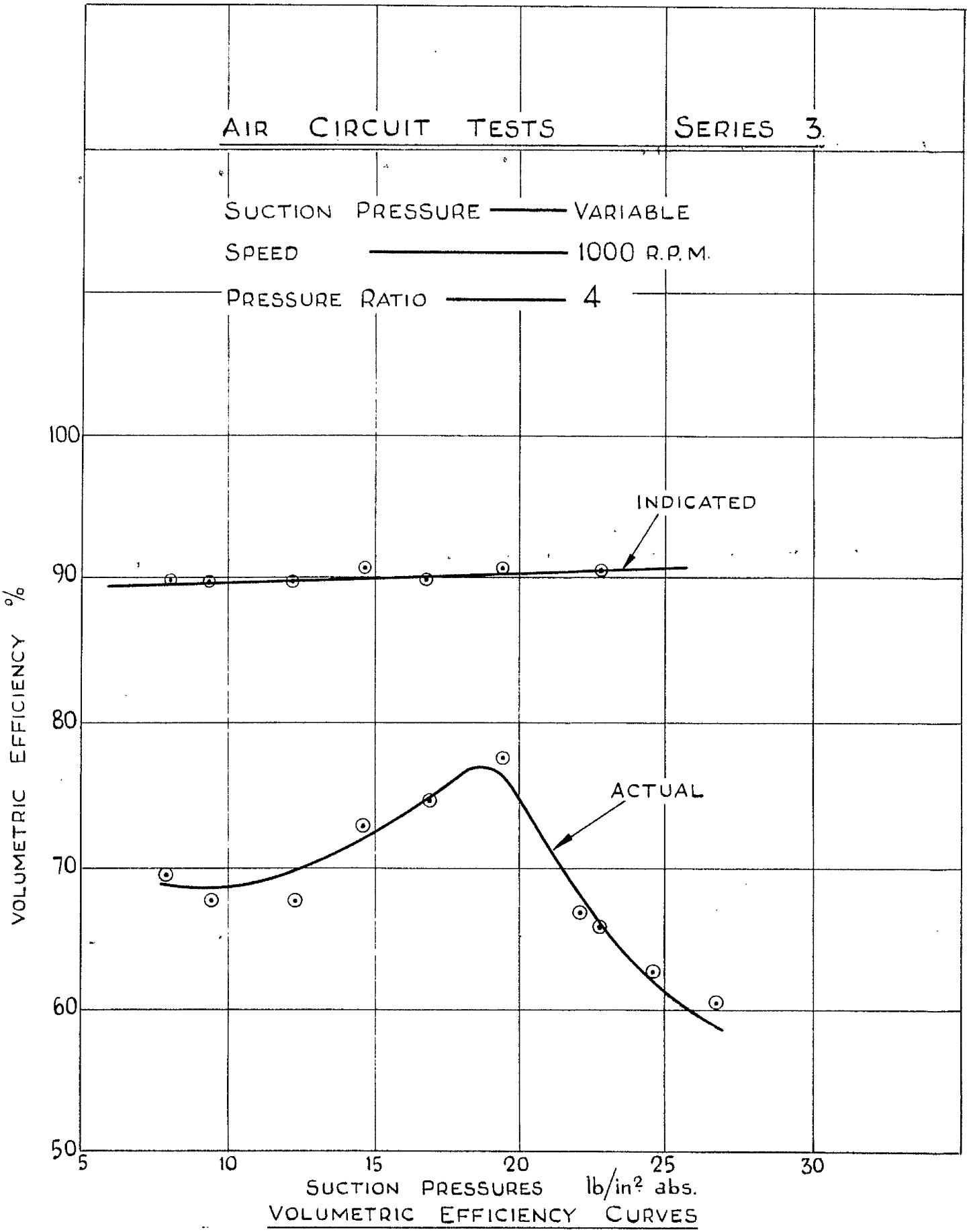

VOLUMETRIC EFFICIENCY CURVES

FIG. Nº 111

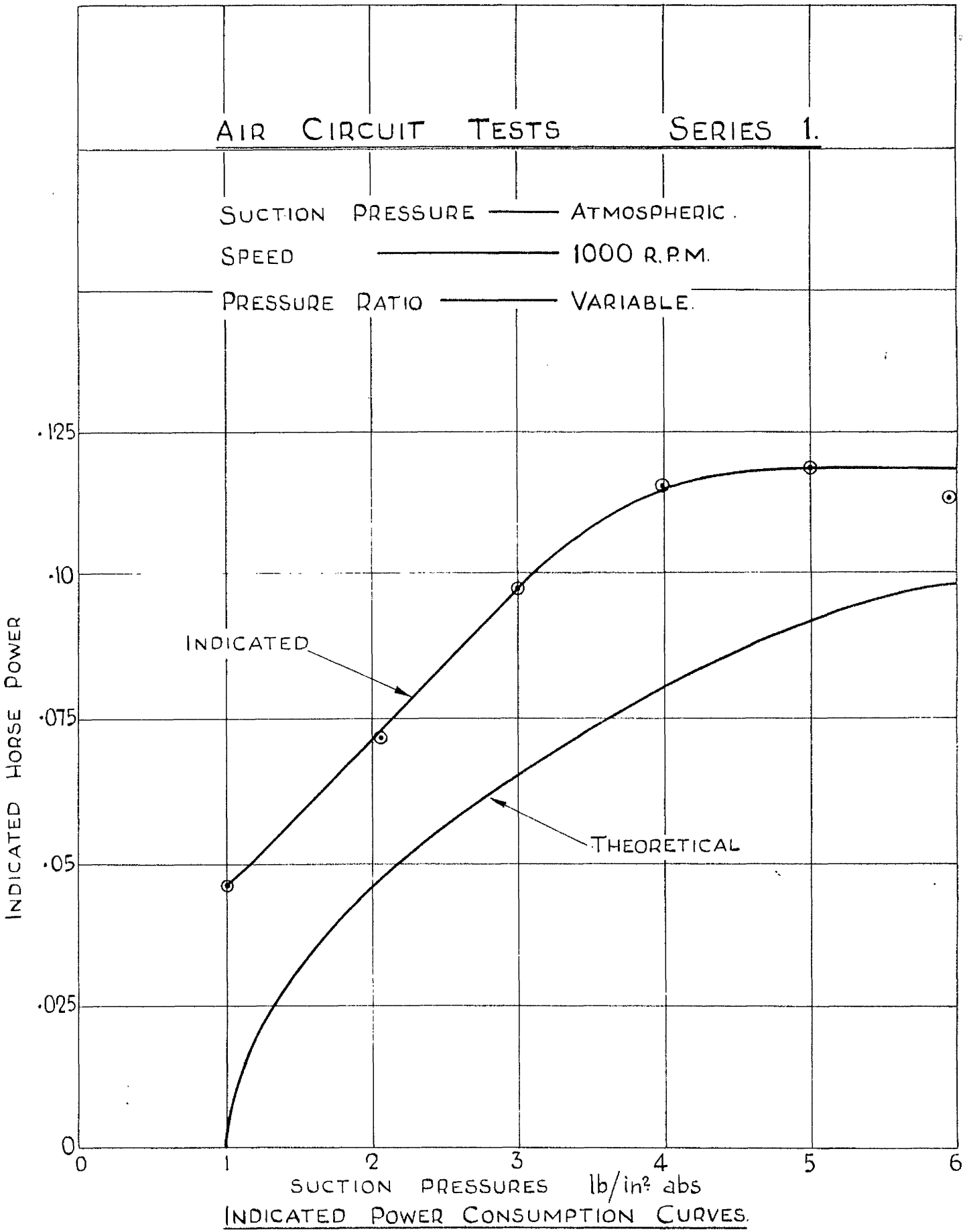

INDICATED POWER CONSUMPTION CURVES.

FIG. Nº 112

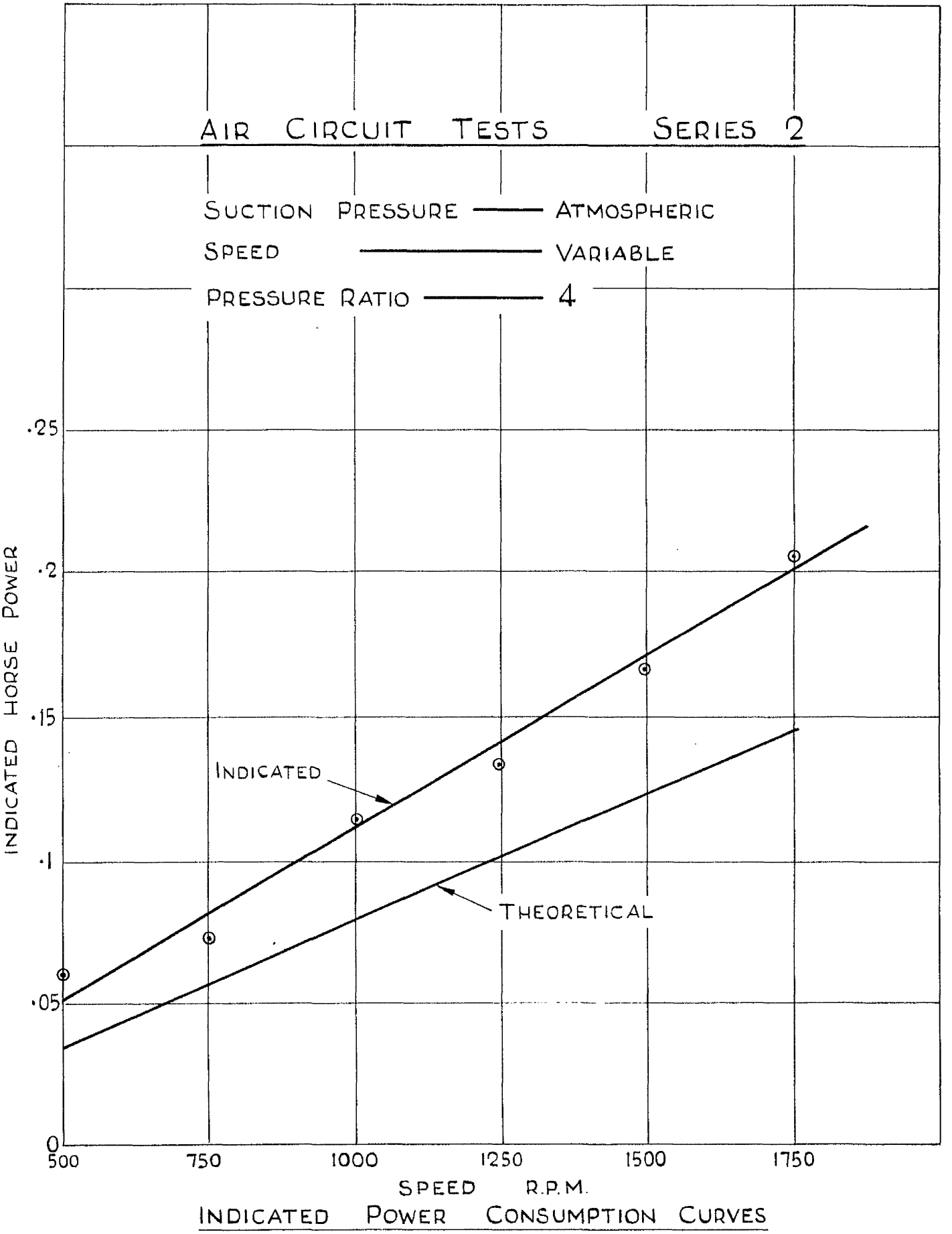

INDICATED POWER CONSUMPTION CURVES

FIG. Nº 113

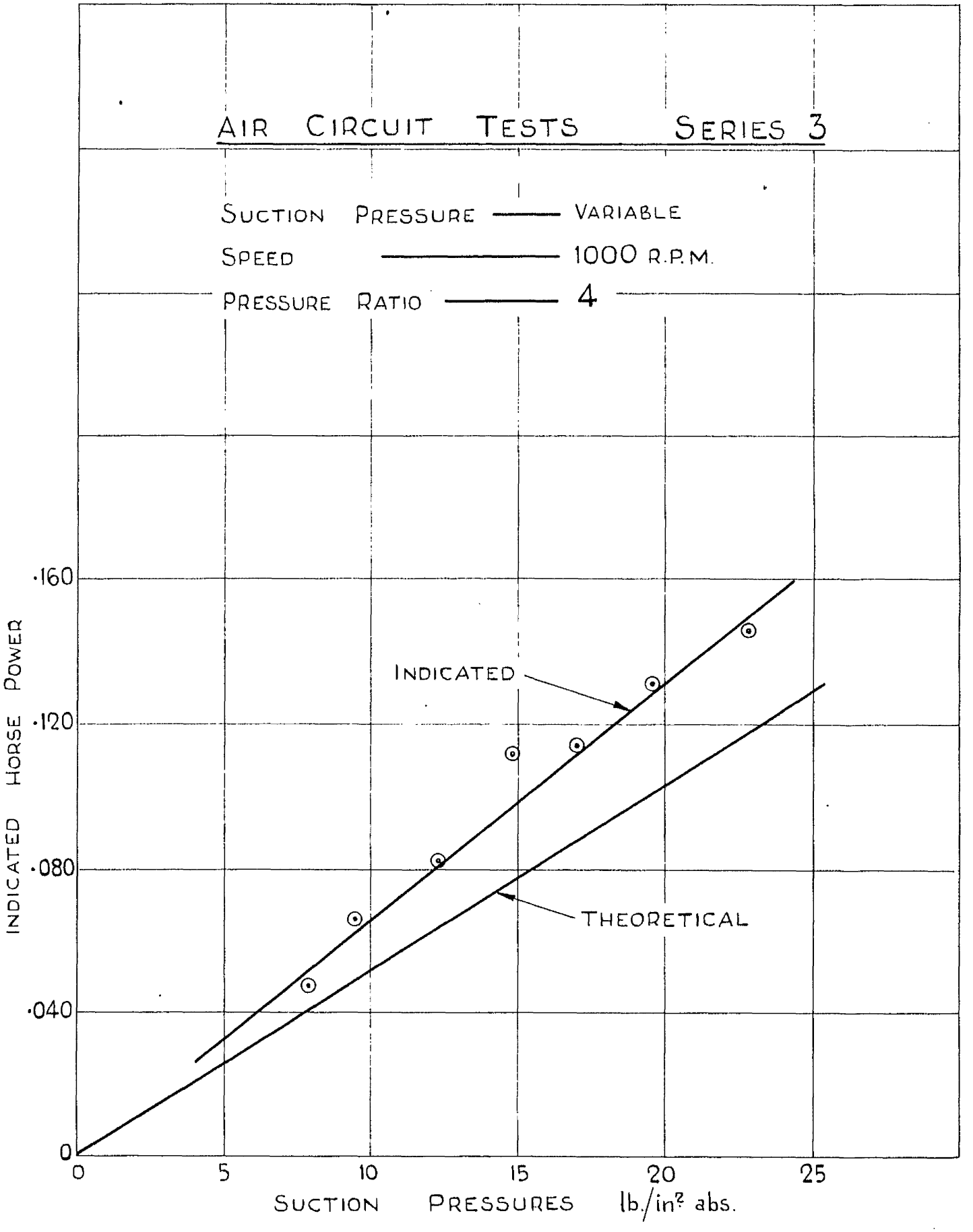

INDICATED POWER CONSUMPTION CURVES

FIG. Nº 114

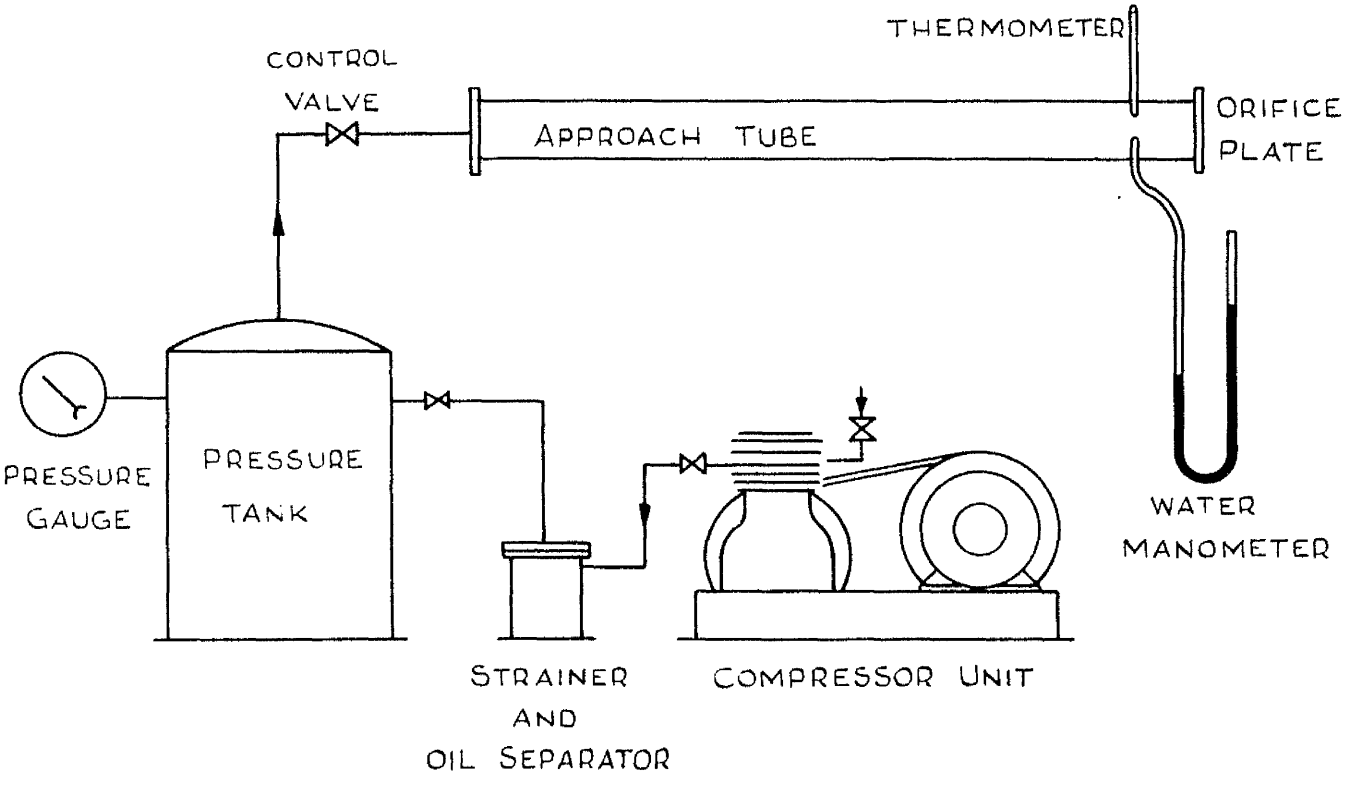

APPARATUS USED IN ORIFICE CALIBRATIONS

FIGURE Nº 115

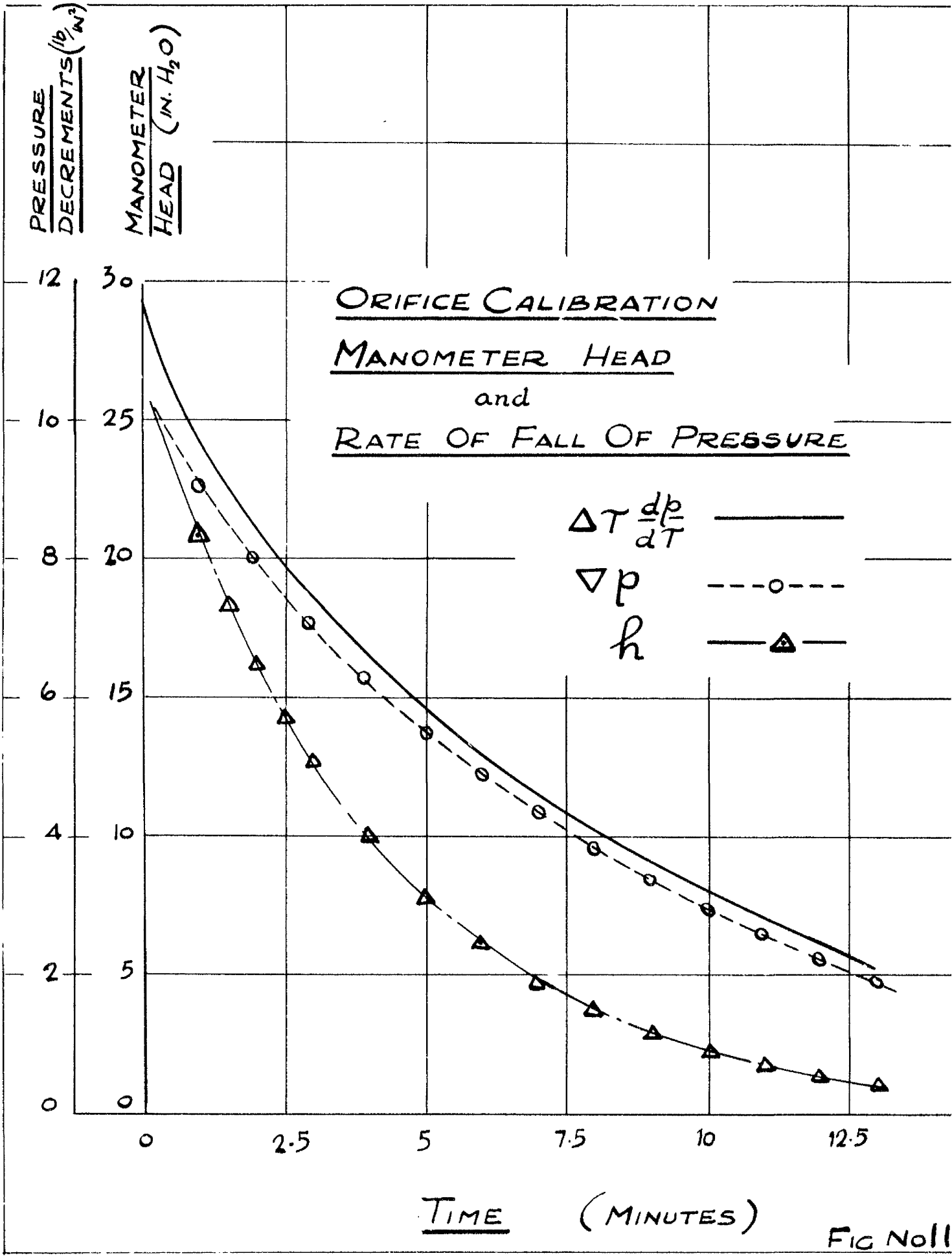
PRESSURE DECREMENTS (lb/in²)
MANOMETER HEAD (in. H₂O)
ORIFICE CALIBRATION
MANOMETER HEAD
and
RATE OF FALL OF PRESSURE
ΔT dp/dT
∇p
h
12
10
8
6
4
2
0
30
25
20
15
10
5
0
0
2·5
5
7·5
10
12·5
TIME (MINUTES)

FIG No 11

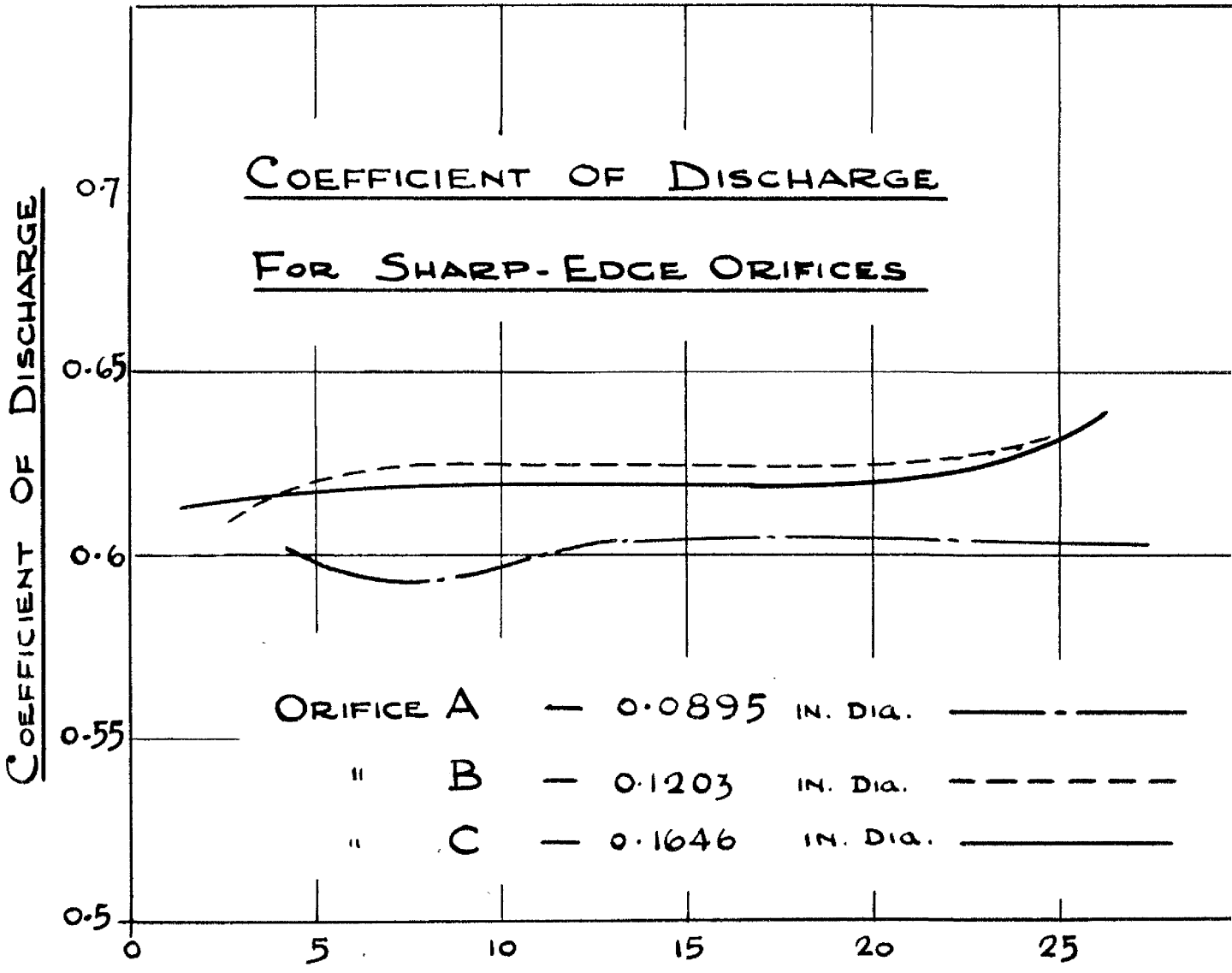
COEFFICIENT OF DISCHARGE
FOR SHARP-EDGE ORIFICES
COEFFICIENT OF DISCHARGE
0·7
0·65
0·6
0·55
0·5
0
5
10
15
20
25
ORIFICE A — 0·0895 IN. DIA.
" B — 0·1203 IN. DIA.
" C — 0·1646 IN. DIA.
ORIFICE HEAD (IN. H_2O)

FIG 117

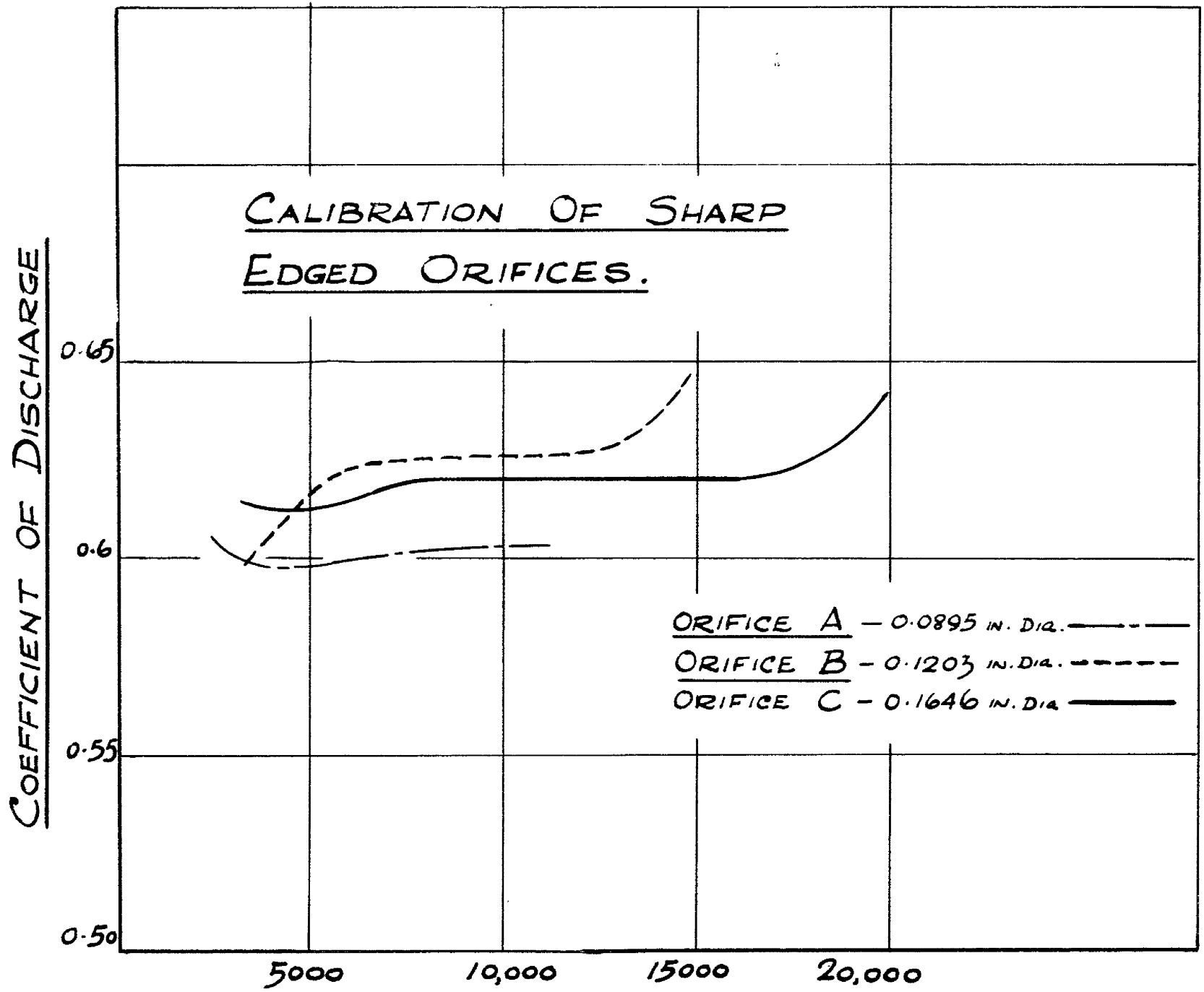
CALIBRATION OF SHARP EDGED ORIFICES.
COEFFICIENT OF DISCHARGE
0.65
0.6
0.55
0.50
5000
10,000
15000
20,000
REYNOLD'S NUMBER
ORIFICE A – 0.0895 IN. DIA.
ORIFICE B – 0.1203 IN. DIA.
ORIFICE C – 0.1646 IN. DIA

FIG. NO: 118

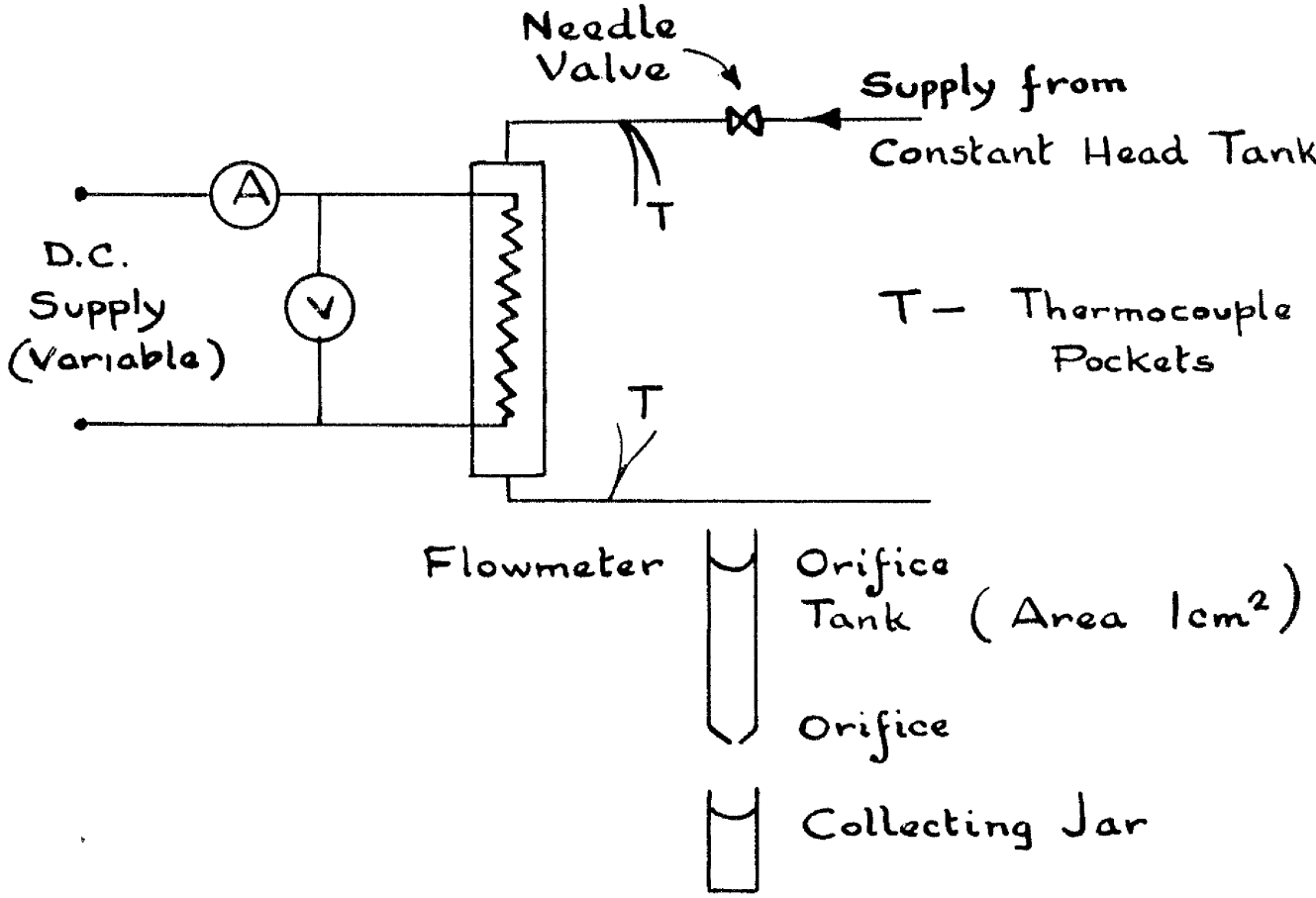

FLOWMETER CALIBRATION

FIG 119